Metolachlor and TCE Plume Characteristics in a Dolostone Aquifer Using a Transect

by

James H. Plett

A thesis
presented to the University of Waterloo
in fulfillment of the
thesis requirement for the degree of
Master of Science
in
Earth Sciences

Waterloo, Ontario, Canada, 2006

©James H. Plett, 2006

I hereby declare that I am the sole author of this thesis. This is a true copy of the thesis, including any required final revisions, as accepted by my examiners.

I understand that my thesis may be made electronically available to the public.

Abstract

Much is known about natural attenuation of contaminants in granular aquifers because many contaminant plumes in these aquifers have been intensively monitored with detailed sampling along cross sections positioned across the plumes (i.e. transects). However, little is known about natural attenuation of contaminant plumes in fractured rock. In this thesis study, strong natural attenuation of a persistent co-mingled plume of trichloroethylene (TCE) and an herbicide (metolachlor) in a 100 m thick dolostone aquifer used for municipal water supply in Cambridge, Ontario is shown based on detailed delineation of groundwater contaminant concentrations along a single transect located 150 m downgradient from the area where the metolachlor entered the dolostone and 300 m downgradient from the TCE source area. This delineation was accomplished using depth-discrete, multilevel groundwater monitoring systems in five cored holes and detailed analyses of contaminant concentration in rock cores. The maximum metolachlor concentration on the transect is a factor of 20 below the maximum concentration in the metolachlor source area and the maximum TCE concentration on the transect is lower by a factor of 100 from the TCE source area.

Matrix diffusion and strong temporal variability of the groundwater flow system caused by pumping of nearby municipal wells have likely caused strong natural attenuation of metolachlor and TCE and degradation has likely contributed to even stronger TCE attenuation. The transect shows rock core concentrations much higher than the groundwater concentrations in the multilevel systems at the same locations and in the conventional monitoring wells, which indicates that plume persistence is likely maintained by back dif-

fusion from the rock matrix, which has very low hydraulic conductivity but substantial porosity, into the active groundwater flow in the fractures.

Metolachlor has been observed at very low concentrations and has persisted at these concentrations in the nearest municipal pumping well located approximately 780 m down-gradient of the transect, however this well shows no detectable TCE. The relatively low concentrations along the transect and the replenishment of the plume by back diffusion suggests that a substantial increase of metolachlor or TCE in the municipal well is unlikely.

Acknowledgements

I would like to thank my supervisors Drs. Beth Parker and John Cherry for their support and guidance throughout my studies and for the valuable insight and comments during the writing process. Drs. Will Robertson and John Molson also provided valuable comments and suggestions as members of my committee. Syngenta Crop Protection Canada, Inc. has provided significant funding for this project, with site and data access arranged through Dr. Marian Stypa. Additional funding for this project was provided by the Natural Sciences and Engineering Research Council (NSERC), Canadian Foundation for Innovation (CFI), the Regional Municipality of Waterloo, Dillon Consulting Ltd., Flexible Liner Underground Technologies (FLUTe) Ltd. Co., Westbay Instruments Inc., and Solinst Canada Ltd.

Leanne Burns collaborated on field work and site characterization during the extent of her concurrent studies, which she completed in 2005. Special thanks go to Chris Turner for his assistance and feedback during the extent of my studies and Ray Carter of Dillon Consulting Ltd., who provided data from ongoing consulting at the Cambridge site as well as information from previous site investigations. Bob Ingleton and Paul Johnson provided essential technical support in the field. Rafael Jerez, Matt Whitney, Donna Kuntz, Ryan Kroeker, Dr. Jerome Perrin, and Jonathon Kennel also provided field assistance. All-Terrain Drilling Ltd., Geo-Environmental Drilling Inc., and Hopper Well Drilling Ltd., provided drilling support and borehole maintenance (which was needed more that I would have liked) during the course of this project. Jesse Ingleton assisted with the drilling of UW4 during the Fall of 2002 for Geo-Environmental Drilling Inc.; his memory lives on

in the hearts and minds of those that loved him. Laboratory analyses of VOC rock core, groundwater samples were performed at the University of Waterloo by Maria Gorecka, with lab assistance from Una Adamcic and Daisy Azadeh. Groundwater samples were also analysed by Wayne Noble at the University of Waterloo. Metolachlor rock core and water analyses were performed by Bryn Shurmer at the University of Guelph. Metolachlor and VOC groundwater analyses as well as geochemistry analyses were performed by Maxxam Analytics Inc. in Mississauga, Ontario. Isotope samples were analysed at the Environmental Isotope Laboratory at the University of Waterloo. Edison Amirthiraj performed the physical property analyses on rock core at the University of Waterloo. Carl Keller of FLUTe provided insight, advice, and assistance on the use and installation of all the FLUTe multilevel systems, blank liners and during hydraulic conductivity profiling. Scott Piggott of the University of Waterloo performed the neutron and gamma-gamma borehole logging. Peeter Pehme of Dillon Consulting Ltd. arranged and helped perform all the other geophysical logging and helped interpret and provide insight on the logs. Completion of the research would not have been possible without many co-op students who helped during the course of the site research. Co-op students include Aaron Vandenhoff, Cameron McNaughton, Shannon Robinson, Jennifer Russell, Scott Smits, Juliusz Gorecki, and Dave Fox. Office mates, Mandy Pierce, Jessi Meyer, Diane Austin, and Pat Quinn also provided assistance during my studies. Mary Anne Hardy and Chris Hanton-Fong provided administrative support during my research.

My fiancé, Khema Ablack, has provided field assistance and personal support throughout my studies. Without her continued support and advice I would not have been able

to accomplish my goals, I owe everything to her and look forward to our future together. My family has also served as an inspiration, and their support has been invaluable.

Contents

Abstract iii

Acknowledgements v

Table of Contents x

List of Tables xi

List of Figures xviii

1 Introduction 1

1.1 Scientific Background 1

1.2 Site Description 6

1.2.1 Site Location 6

1.2.2 Site Geology/Hydrogeology 6

2 Description of Methods 18

2.1 Drilling Methods 18

2.2 Rock Core Sampling . . . 21
2.2.1 Initial Core Assessment and Physical Property Sample Selection . . 21
2.2.2 Selection of Rock Samples for Contaminant Analysis . . . 22
2.2.3 Processing Rock Samples for Contaminant Analysis . . . 23
2.2.4 Decontamination Procedure . . . 25
2.2.5 Rock Core Analysis Methods: 2000-2003 . . . 25
2.2.5.1 Sample Collection and Analysis Procedures 2000 . . . 25
2.2.5.2 Sample Collection and Analysis Procedures: 2002 . . . 27
2.2.5.3 Sample Collection and Analysis Procedures: 2003 . . . 29
2.3 Data Validation . . . 30
2.4 Rock Core Conversions to Equivalent Porewater Concentrations . . . 31
2.5 Rock Matrix Physical Properties . . . 33
2.5.1 Matrix Porosity . . . 34
2.5.1.1 Imbibition Gravimetric Procedure . . . 34
2.5.2 Wet and Dry Bulk Density . . . 35
2.5.3 Solid Phase Organic Carbon (f_{oc}) . . . 35
2.6 Geophysical/Hydrophysical Logging . . . 36
2.6.1 Neutron and Gamma-Gamma Logs . . . 36
2.6.1.1 Neutron Log . . . 36
2.6.1.2 Gamma-Gamma Log . . . 37
2.6.2 Natural Gamma . . . 38
2.6.3 Borehole Video . . . 38

2.6.4 Acoustic Televiewer . . . 39
2.6.5 Detailed Temperature Profiling . . . 39
2.6.6 Heat-pulse Flow-metering . . . 40
2.6.7 Hydraulic Testing . . . 41
2.6.7.1 Straddle Packer Testing . . . 41
2.6.7.2 FLUTe Hydraulic Conductivity Profiling . . . 43
2.7 Multilevel Systems . . . 44
2.7.1 FLUTe Multilevel System . . . 44
2.7.2 Westbay Multilevel System . . . 45
2.7.3 Solinst Modified Waterloo Multilevel System . . . 46
2.8 Multilevel Groundwater Sampling . . . 47
2.8.1 Multilevel Sampling Procedures . . . 47
2.8.1.1 FLUTe Multilevel Sampling . . . 47
2.8.1.2 Westbay Multilevel Sampling . . . 48
2.8.2 Multilevel Groundwater Sample Analysis Procedures . . . 49
2.8.2.1 Aqueous VOC . . . 49
2.8.2.2 Aqueous Metolachlor . . . 51
2.8.2.3 Inorganic Hydrochemistry . . . 51
2.8.2.4 Environmental Isotopes . . . 52
2.9 Hydraulic Head Measurements . . . 53
2.9.1 Conventional Wells . . . 53
2.9.2 FLUTe . . . 54

2.9.3 Westbay 54

3 Results **62**

3.1 Geology 62

3.2 Hydraulic Conductivity 68

3.3 Hydraulic Head 70

3.4 Rock Core Concentrations 78

3.4.1 Metolachlor 78

3.4.2 TCE 79

3.4.3 Other VOCs 81

3.5 Multilevel Groundwater Monitoring 82

3.5.1 Metolachlor 82

3.5.2 TCE 85

3.5.3 Hydrochemistry 89

3.5.4 Isotopes 91

4 Discussion **166**

4.1 Evidence for Strong Natural Attenuation of Metolachlor and TCE 166

4.2 Evidence for TCE Degradation 171

4.3 Hydrogeologic Influences on Plume Position on the Transect 174

4.4 Inconsistencies between Plume and Potentiometric Surfaces 179

5 Conclusions **202**

References **206**

A Appendix A **216**

List of Tables

2.1 Drilling and completion details for UW Coreholes 56

2.2 Rock core analysis methods 57

2.3 Physical property measurements for the nine lithologic units 58

2.4 UW16B FLUTe multilevel system port locations 59

2.5 UW5 FLUTe multilevel system port locations 59

2.6 UW4 FLUTe multilevel system port locations 60

2.7 UW13 FLUTe multilevel system port locations 60

2.8 UW6 FLUTe multilevel system port locations 61

2.9 UW3 Westbay multilevel system zone locations 61

A.1 UW5 Rockcore porewater and multilevel concentrations comparison 216

A.2 UW4 Rockcore porewater and multilevel concentrations comparison 222

A.3 UW13 Rockcore porewater and multilevel concentrations comparison . . . 226

A.4 UW6 Rockcore porewater and multilevel concentrations comparison 229

A.5 UW3 Rockcore porewater and multilevel concentrations comparison 233

List of Figures

1.1 Site location in relation to municipal supply wells 10

1.2 General site hydrostratigraphy 11

1.3 A detailed monitoring network of wells at the study site 12

1.4 Timeline for events important to the study site, including contaminants release, supply well installations, average pumping rates 13

1.5 North-south cross section showing the potential plume locations within the dolostone aquifer 14

1.6 Three dimensional site view 15

1.7 Study site is located in Southern Ontario 16

1.8 Regional map showing site proximity to the Grand and Speed Rivers . . . 17

3.1 Cambridge porosity characteristics 93

3.2 Corelog Unit and Lithologic Unit descriptions 94

3.3 Corelogs across the transect 95

3.4 Lithology across the transect 96

3.5 UW5 Geology 97
3.6 UW4 Geology 98
3.7 UW13 Geology 99
3.8 UW6 Geology 100
3.9 UW3 Geology 101
3.10 Eramosa unit defined by gamma peak across the transect 102
3.11 Eramosa comparison for UW13 103
3.12 Evidence of karst features from borehole video 104
3.13 Hydraulic conductivity values obtained from straddle packer tests along the transect 105
3.14 FLUTe hydraulic conductivity results compared to straddle packer test data 106
3.15 Hydraulic head collected from the multilevel system in UW16B 107
3.16 Hydraulic head collected from the multilevel system in UW5 108
3.17 Hydraulic head collected from the multilevel system in UW4 109
3.18 Hydraulic head collected from the multilevel system in UW13 110
3.19 Hydraulic head collected from the multilevel system in UW6 111
3.20 Hydraulic head collected from the multilevel system in UW3 112
3.21 Composite vertical hydraulic head profiles from three overburden multilevels and multilevels in the dolostone 113
3.22 Comparison between vertical hydraulic head profile from a FLUTe multilevel and a Westbay multilevel system 114
3.23 UW16B hydrograph 115

3.24 UW5 and UW4 hydrograph . . . 116
3.25 UW13 and UW6 hydrograph . . . 117
3.26 UW3 hydrograph . . . 118
3.27 Hydraulic head contoured from multilevels and conventional wells along the transect in November 2005 . . . 119
3.28 Hydraulic head contoured from multilevels and conventional wells along the transect in December 2005 . . . 120
3.29 Potentiometric surface at 270 masl from November, 2005 . . . 121
3.30 Potentiometric surface at 270 masl from December, 2005 . . . 122
3.31 Potentiometric surfaces at 250 and 235 masl for November, 2005 . . . 123
3.32 Potentiometric surfaces at 250 and 235 masl for December, 2005 . . . 124
3.33 Regional potentiometric surfaces for the Upper Guelph Formation dolostone 125
3.34 Regional potentiometric surfaces for the Lockport Formation dolostone . . . 126
3.35 Total metolachlor rock concentrations along the transect . . . 127
3.36 Converted equivalent porewater metolachlor concentrations along the transect 128
3.37 Converted equivalent porewater metolachlor concentrations contoured along the transect . . . 129
3.38 Total TCE rock concentrations along the transect . . . 130
3.39 Converted equivalent porewater TCE concentrations along the transect . . . 131
3.40 Converted equivalent porewater TCE concentrations contoured along the transect . . . 132
3.41 Total PCE concentrations in rock core along the transect . . . 133

3.42 Total cDCE concentrations in rock core along the transect 134
3.43 Total tDCE concentrations in rock core along the transect 135
3.44 Metolachlor concentration profiles from multilevels in the source area and on the transect 136
3.45 Metolachlor concentration results from UW16B over a three month period 137
3.46 Metolachlor concentration results from UW5 over a three month period . . 138
3.47 Metolachlor concentration results from UW4 over a three month period . . 139
3.48 Metolachlor concentration results from UW13 over a three month period . 140
3.49 Metolachlor concentration results from UW6 over a three month period . . 141
3.50 Metolachlor concentration results from UW3 over a three month period . . 142
3.51 Metolachlor concentration versus time in UW5 multilevel ports. 143
3.52 Metolachlor concentration versus time in UW4 multilevel ports. 144
3.53 Metolachlor concentration versus time in UW13 multilevel ports. 145
3.54 Concentrations of metolachlor and TCE versus time for UW6 146
3.55 Concentrations of metolachlor and TCE versus time for UW3 147
3.56 Metolachlor concentration contours along the transect 148
3.57 TCE concentration with depth profiles for the source area and the transect 149
3.58 TCE concentration results from UW16B over a three month period 150
3.59 TCE concentration results from UW5 over a three month period 151
3.60 TCE concentration results from UW4 over a three month period 152
3.61 TCE concentration results from UW13 over a three month period 153
3.62 TCE concentration results from UW6 over a three month period 154

3.63 TCE concentration results from UW3 over a three month period 155
3.64 TCE results versus time from multilevel UW5 156
3.65 TCE results versus time from multilevel UW4 157
3.66 TCE concentration data contoured from multilevels along the transect . . . 158
3.67 Metolachlor and TCE concentration data from multilevels along the transect 159
3.68 Inorganic hydrochemistry results collected from multilevel UW16B in February, 2005 160
3.69 Comparison between UW16B inorganic hydrochemistry results collected from 2001 and 2005 161
3.70 Inorganic hydrochemistry results collected from multilevel UW13 in February, 2005 162
3.71 Comparison between tritium and ^{18}O results collected in UW16B from 2001 and 2005 163
3.72 Isotope results collected from UW16B and UW13 in February 2005 164
3.73 Isotopic comparison between $\delta^{18}O$ and $\delta^{2}H$ along with the Canadian Meteoric Water Line (CMWL) as a reference 165

4.1 North-south line along conventional monitoring wells towards pumping well G6 181
4.2 Metolachlor concentrations versus time in bedrock conventional wells along north-south line 182
4.3 Metolachlor concentration data from conventional wells OW16 (source area), OW13 and OW42 (transect), and G6 from 2001-present. 183

4.4 Metolachlor concentrations contoured from the source area to the multilevels along the transect . . . 184
4.5 TCE concentrations versus time in bedrock conventional wells along north-south line . . . 185
4.6 TCE concentrations contoured from the source area to the multilevels along the transect . . . 186
4.7 Metolachlor concentration contours along the transect related to the corelogs . . . 187
4.8 TCE concentration contours along the transect related to the corelogs . . . 188
4.9 UW16B TCE degradation products . . . 189
4.10 UW5 TCE degradation products . . . 190
4.11 UW4 TCE degradation products . . . 191
4.12 UW13 TCE degradation products . . . 192
4.13 UW6 TCE degradation products . . . 193
4.14 UW3 TCE degradation products . . . 194
4.15 UW16B comprehensive data set . . . 195
4.16 UW5 comprehensive data set . . . 196
4.17 UW4 comprehensive data set . . . 197
4.18 UW13 comprehensive data set . . . 198
4.19 UW6 comprehensive data set . . . 199
4.20 UW3 comprehensive data set . . . 200

4.21 Fracture rose diagrams obtained from fracture analyses on acoustic televiewer logs 201

Chapter 1

Introduction

1.1 Scientific Background

The nature and extent of many groundwater contaminant plumes emanating from industrial sites on granular aquifers (i.e. sand/gravel) has been determined from intensive field studies in North America and Europe. These studies have been complemented by tracer experiments and mathematical models during the past three decades and the behaviour of plumes in these geologic media is now well understood. This understanding of contaminant behaviour in granular aquifers has been enhanced by several long-term natural gradient tracer experiments, such as those at the Borden site (Mackay et al., 1986) and the Cape Cod site (LeBlanc et al., 1991). However, in comparison, knowledge concerning contaminant plumes in fractured rock is minimal, as indicated by a recent review paper (Berkowitz, 2002). The literature concerning contaminant behaviour in groundwater in fractured rock derives primarily from studies of crystalline rock such as granite, that has received research emphasis because of its selection as potential host rock for deep burial

of radioactive waste (Bear et al., 1993; Hadermann and Heer, 1996) in several countries (e.g. in Canada, Sweden, Switzerland and France), however, these investigations do not involve actual contaminant plumes because the waste has not yet been buried in the rock.

Sedimentary rock forms the bedrock in most of the industrialized regions of North America (Back et al., 1988) and yet there is minimal information on the nature and extent of these plumes in such rock. A literature review revealed no detailed descriptions of such plumes except for a plume in Wisconsin studied by a fellow M.Sc. student at the University of Waterloo (Meyer, 2005) and publications concerning only one natural gradient tracer test were found (Lapcevic et al., 1999b).

The University of Waterloo initiated a research program in 1997 concerning the nature and extent of organic contaminant plumes in fractured sedimentary rock at industrial sites. This research is directed at the development and field verification of a general conceptual model for organic contaminant behavior in fractured sedimentary rock with emphasis on organic plumes originating at industrial sites where Dense Nonaqueous Phase Liquids (DNAPLs) were the initial cause of the groundwater contamination. This research program now involves five fractured sedimentary rock sites where comprehensive field studies are being conducted (Parker, 2006). This thesis concerns one of the five sites, located in Cambridge, Ontario where an herbicide (metolachlor) and a cleaning solvent (trichloroethylene) form a co-mingled plume in a fractured dolostone aquifer used for municipal water supply (Figure 1.1). The co-mingled plume occurs in fractured dolostone of the Silurian Guelph and Lockport Formations overlain by approximately 20-40 m of Quaternary deposits and underlain by the Rochester Formation shale (Figure 1.2).

Investigations of the bedrock contamination at this site began in 1992 immediately following the discovery of herbicides in shallow soil exposed during renovation activities at an agrochemical formulating and packaging facility. These studies conducted during 1992-1993 by the consultants commissioned by the site owner indicated that, of the many herbicides found in the soil, only one (metolachlor) was found at levels of concern in the dolostone aquifer (Carter et al., 1994, 1995). These studies resulted in a network of conventional monitoring wells in the Quaternary deposits and in the upper part of the dolostone aquifer and these wells have served for annual or more frequent monitoring since their installation (Figure 1.3). These wells initially established the persistent presence of metolachlor in the dolostone aquifer, however no metolachlor was found in the nearby municipal water supply wells. These monitoring wells also resulted in the discovery of trichloroethylene (TCE) in the Quaternary deposits and the dolostone aquifer. Dames and Moore (1998) determined that the TCE entered the subsurface on an industrial property upgradient from the metolachlor source area.

The first phase of the site study by the University of Waterloo began in 1998, represented by the M.Sc. thesis by Turner (2001) who investigated the site hydrogeology and characteristics of the metolachlor and TCE contaminant distribution using rock core and a detailed multilevel system in the bedrock source area and in the plume 150 m downgradient in the believed direction of groundwater flow. Najiya (2003) described the bedrock geology and stratigraphy based on the continuous rock core obtained by Turner (2001). Turner (2001) concluded that the metolachlor and TCE contamination in the dolostone aquifer was caused by migration of metolachlor and TCE as DNAPLs through the Qua-

ternary deposits down into and throughout the dolostone. Parker et al. (2006b) provides support for this conclusion.

In the second phase of site studies by the University of Waterloo, the M.Sc. thesis by Burns (2005) determined, more thoroughly using three coreholes within a $10m^2$ area, the hydrogeologic conditions of fractures and fracture network interconnectivity in the dolostone in the area where the metolachlor DNAPL moved from the Quaternary deposits down into the dolostone, referred to as the metolachlor source area. The current M.Sc. thesis presented herein, is also part of this second phase, and concerns quantification of the groundwater plume direction of transport and the extent of natural attenuation of the co-mingled plume as it migrates away from the source area. The goal of this thesis is to determine, by intensive groundwater monitoring and other measurements along a vertical cross section (i.e. transect), the width and internal characteristics of the plume 150 m downgradient from the metolachlor source area. The premise of this thesis is that the metolachlor plume in the dolostone originates at or near the former agrochemical facility and that the plume migrates generally southeastward to municipal well G6, as shown in Figure 1.1. This was initially proposed by Carter et al. (1994, 1995), however, proof that the plume or at least part of the plume is migrating toward well G6 did not exist until 2001 when metolachlor was first detected in this well at low but persistent concentrations (Figure 1.4). However, given the Turner (2001) thesis results for deep bedrock aquifer contamination, there was interest in determining plume characteristics and flow directions throughout the entire aquifer thickness.

The transect approach for determining the nature of contaminant plumes and particularly for examining natural attenuation is well established for investigations in granular aquifers (Guilbeault et al., 2005; National Research Council, 2004; Einarson and MacKay, 2001), but it has not been used previously for investigating plumes in bedrock.

In 1993, Dames and Moore installed three monitoring wells in the dolostone along a line situated 150 m southwest of the input area. These wells were referred to by Dames and Moore (1993) as sentry wells and they showed much lower metolachlor and TCE concentrations than those in the bedrock source area. These sentry well results and the fact that the metolachlor had not shown up (as of 1993) in any of the municipal pumping wells, was the basis for the conclusion by Dames and Moore (1993) that physical processes such as dispersion were strongly attenuating the plume in the shallow part of the aquifer. However, all of these monitoring wells are screened in only the upper third of the dolostone aquifer and therefore they could not exclude the possibility of higher concentration zones of metolachlor deeper in the aquifer. It is also uncertain how much of the plume is being captured by G6, since the well is not installed throughout the entire vertical extent of the aquifer, it is possible that contaminants may be migrating below the completion depth of G6 (Figure 1.5).

Therefore, in this thesis, there is an emphasis on comprehensive monitoring throughout the full vertical thickness of the dolostone aquifer along the transect. The transect includes the sentry wells established by Dames and Moore (1993) and therefore this thesis is founded on a combination of long term and more recent and spatially intensive monitoring results. A conceptual representation of the transect and the metolachlor source area can be seen

in Figure 1.6. This thesis attempts to evaluate which of the various mechanisms for plume attenuation is prevalent as well as improve the estimate and certainty for the extent of plume attenuation within such a hydraulically active (variably pumped) aquifer with matrix and fracture transport.

1.2 Site Description

1.2.1 Site Location

The study site is located in southwestern Ontario, in an industrialized area of the city of Cambridge within the Regional Municipality of Waterloo (Figure 1.7). Situated in the Grand River Valley, the study site is near the confluence of the Grand and Speed Rivers which are to the southwest and northwest, respectively (Figure 1.8).

1.2.2 Site Geology/Hydrogeology

The Quaternary deposits overlying the Guelph and Lockport Formation dolostone, were characterized by Dames and Moore (1993) and divided into 4 units. These Quaternary deposits are dominated by ice-contact and glacio-fluvial outwash deposits of the Grand River Valley spillway and the Galt Moraine (Golder Associates, 1991). The outwash deposits are comprised of sand and gravel and the Galt Moraine is comprised of silty to sandy glacial till. The four Quaternary deposit units are further described by Lotowater Ltd. (1997) based on work completed by Karrow (1987). Units 1-4 (Figure 1.2) are described from the deepest unit (4) to the shallowest unit (1) as Catfish Creek Till, Port Stanley

Till, Wentworth Till and, sand and gravel deposits. Units 2 and 4 are considered laterally discontinuous aquitards by Dames and Moore (1993).

The bedrock beneath the Cambridge study area is comprised of the upper Guelph Formation and the lower Lockport Formation dolostone. These rock formations form the aquifer system and are underlain by the Rochester Formation shale which is considered as the bottom unit and aquitard for the study site. The dolostone formations were deposited during the Silurian Period approximately 400 million years ago and transformed from limestone by diagenetic processes at some stage during the subsequent time period (Lotowater Ltd., 1997).

The Rochester Formation shale is described as a dark grey, brown grey to blue grey, calcareous shale with carbonate interbeds (Johnson et al., 1992). Lotowater Ltd. (1997) identifies that the Cabot Head Formation and Rochester Formation shales may interfinger along the Algonquin Arch which forms the margin of the Michigan and Appalachian sedimentary basins and where this site is located. For the purposes of this study, the shale aquitard is referred to as the Rochester Formation.

The dolostone formation above the Rochester Formation shale is considered the Lockport Formation for the current study. The Lockport Formation is described as a blueish grey to light creamy grey, fine to medium grained, thickly bedded to massive, variably non-porous, dolostone with crinoid and tabulate coral fossils (Golder Associates, 1991). Lotowater Ltd. (1997) considered this unit to be the Amabel formation which has the same lithology as the Lockport Formation, however the Goat Island Member is considered integral to the Lockport Formation (Sanford, 1969; Johnson et al., 1992), and since Lotowater

Ltd. (1997) did not describe the Goat Island Member, they referred to the unit above the Rochester Formation as the Amabel Formation. The use of the Lockport Formation is consistent with Najiya (2003) and Burns (2005) and a unit above the Rochester Formation shale observed during drilling for the current study is similar to the Goat Island Member, described by Johnson et al. (1992) as dark to light grey, very fine to microcrystalline dolostone.

The Eramosa Member is considered the top unit of the Lockport Formation for this study to remain consistent with previous studies (Golder Associates, 1991; Najiya, 2003), however the Eramosa Member is considered the bottom unit of the Guelph Formation by Johnson et al. (1992) and Lotowater Ltd. (1997). The Eramosa Member is described by Golder Associates (1991) as a medium brownish grey, fine grained, thin to medium bedded, argillaceous dolostone with occasional dark grey to black shaley beds. This unit was not considered lithologically distinct during coring for the current study, however gamma logs performed after coring allowed identification of this unit based on a distinct peak found in the majority of the logs.

The upper dolostone unit in the study site is the Guelph Formation. The total thickness for this unit is approximately 50-60 m depending on the depth of the bedrock surface. The Guelph Formation is described as a light brownish grey to creamy grey, fine to medium grained, non-porous to porous, thin to thickly bedded dolostone with occasional vugs and fossils comprised largely of tabulate corals and brachiopods (Golder Associates, 1991). Golder Associates (1991) also describes an upper Guelph Formation unit approximately 15 m thick comprising of fine to medium grained, faintly porous, thinly to medium bed-

ded dolostone with some porous and vuggy interbeds, which was moderately to highly weathered on bedding partings.

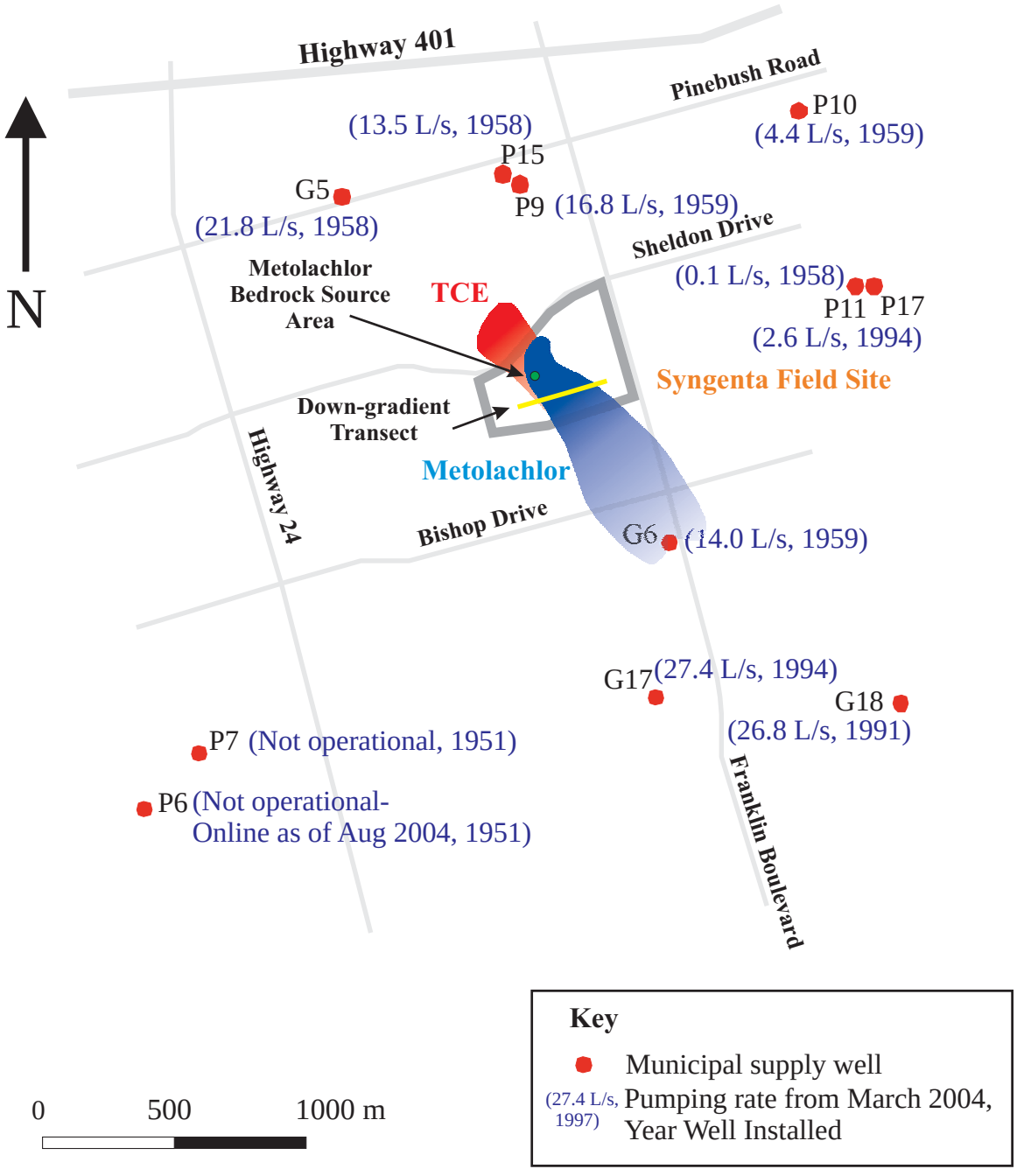


Figure 1.1: Plan view of site area and locations of municipal supply wells around the study site. Municipal supply well G6 initially detected metolachlor in 2001. Adapted from Turner (2001).

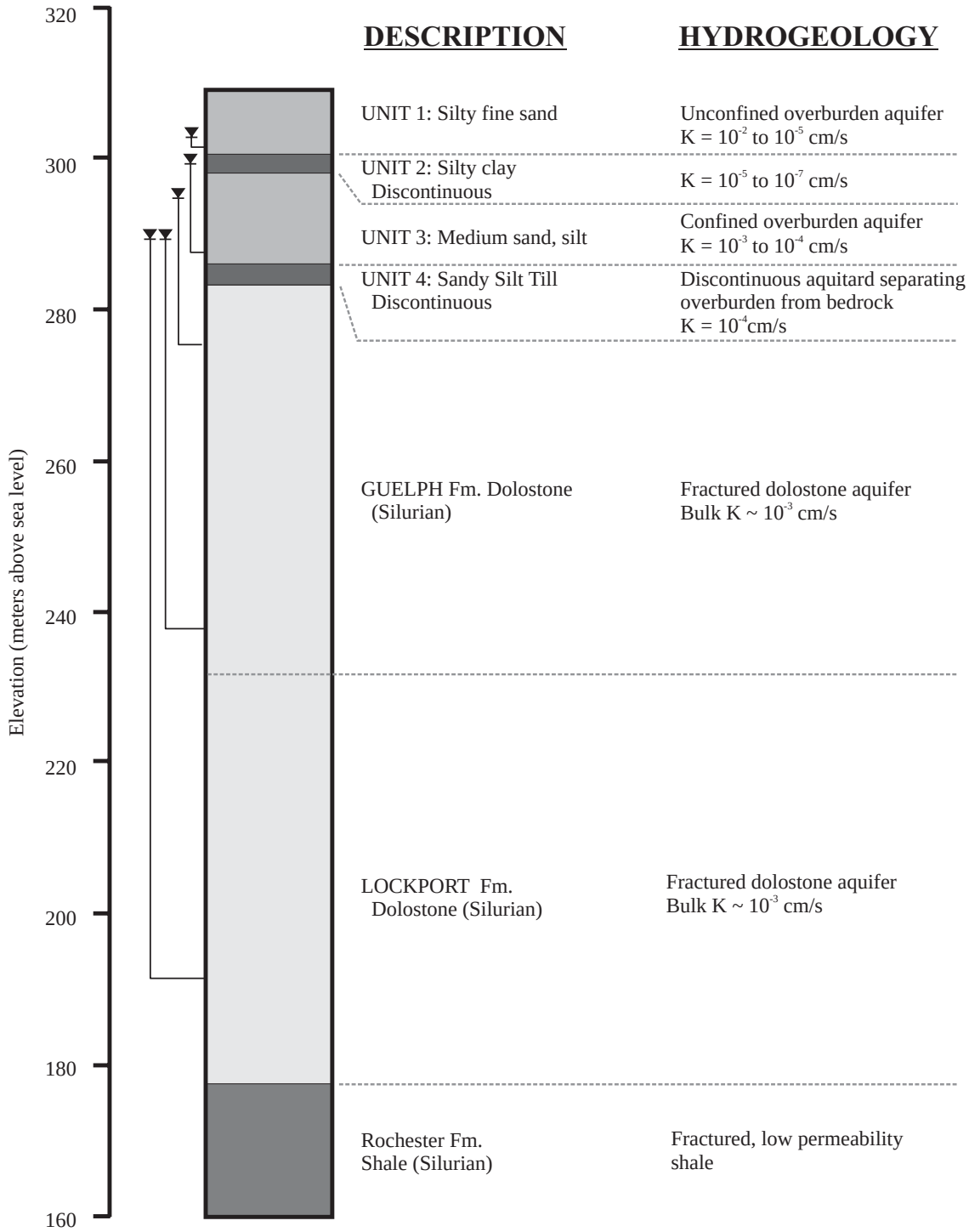


Figure 1.2: A general hydrostratigraphic column for the overburden and dolostone aquifer on site. The overburden is divided into four aquifer/aquitard units and the dolostone above the underlying Rochester Formation shale can be divided into the upper Guelph Formation and the lower Lockport Formation Silurian dolostone. Adapted from Turner (2001).

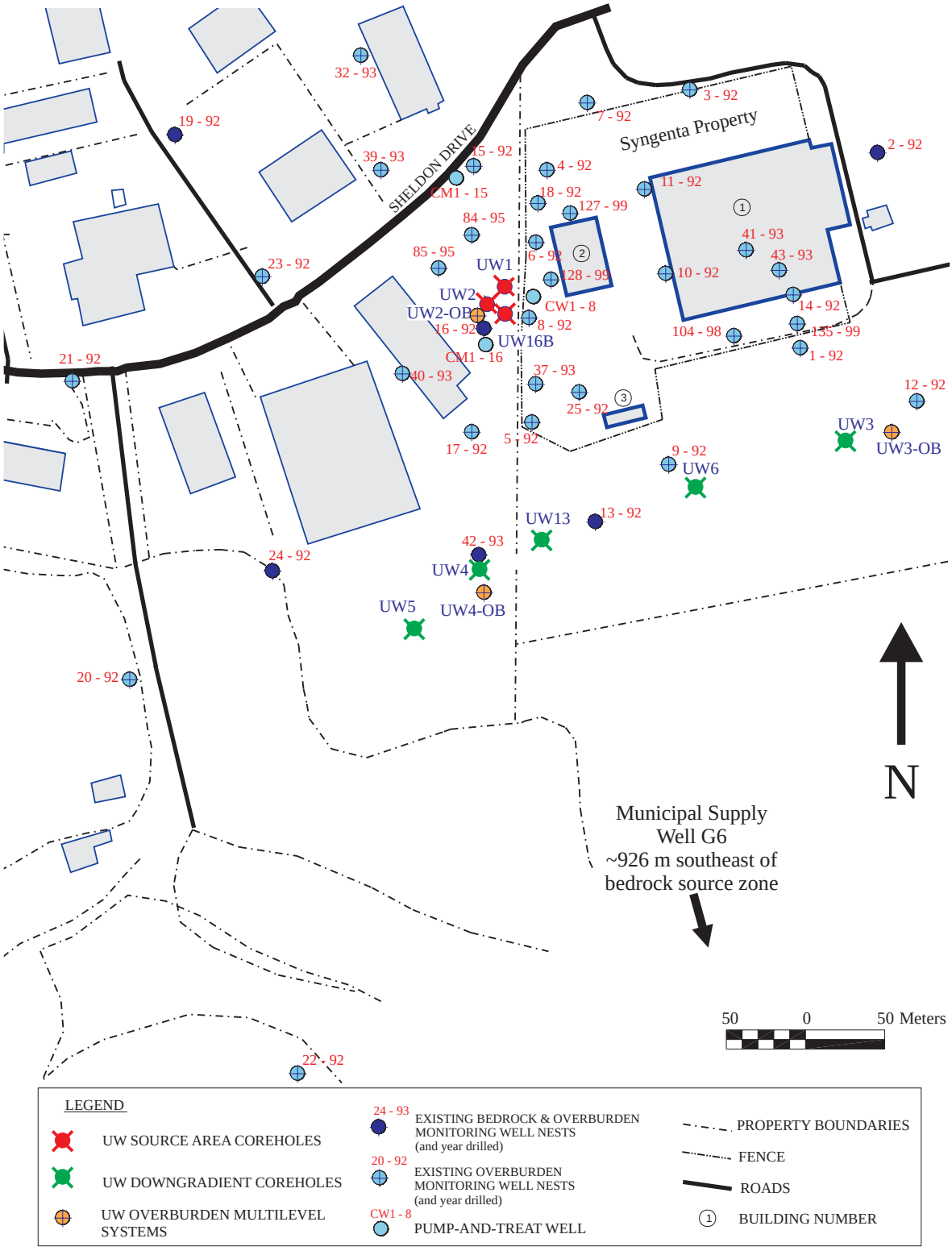


Figure 1.3: Location of monitoring wells. A detailed network of monitoring wells was initiated by consultants prior to the University of Waterloo involvement. Monitoring wells in the overburden and in the shallow bedrock determined the location of the downgradient transect. Adapted from Turner (2001).

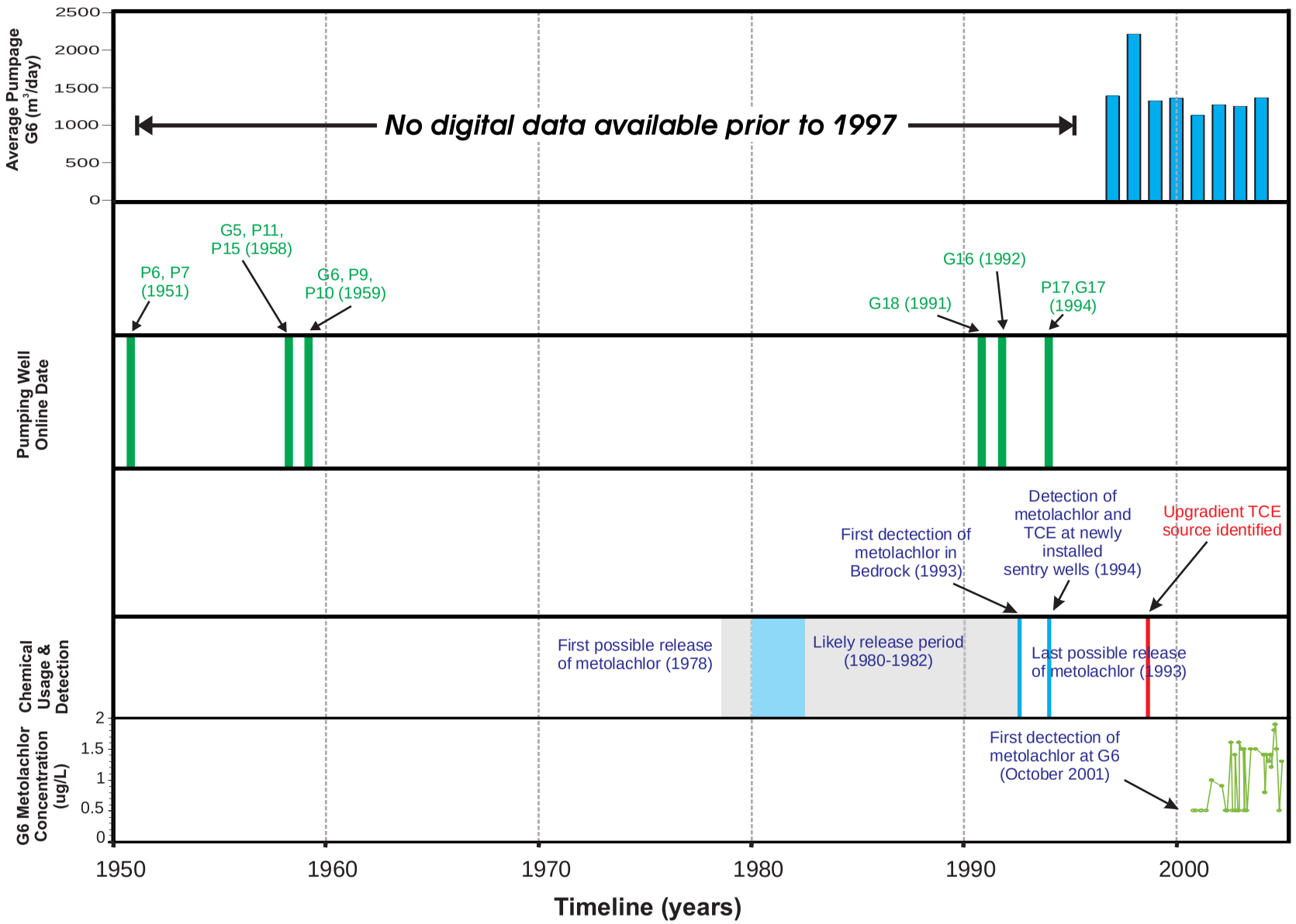


Figure 1.4: Timeline for events important to the study site, including contaminants release, supply well installations, average pumping rates, and concentrations of metolachlor in G6.

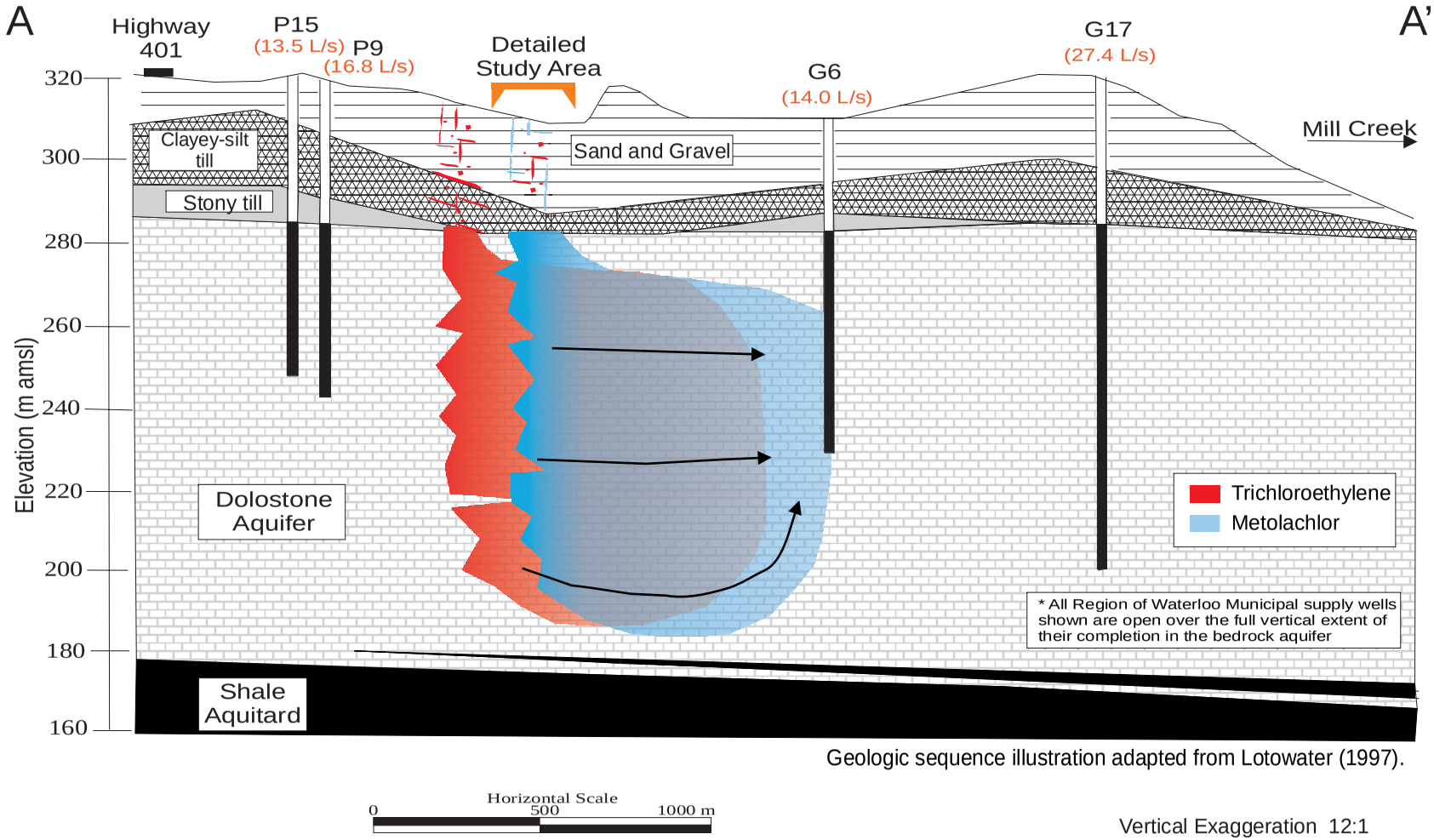


Figure 1.5: Conceptual model of co-mingled plume migration. Metolachlor was detected in supply well G6 in 2001 but it is unknown if the entire plume is captured or if some part of it is migrating beneath the well screen. TCE has not been detected in G6. Adapted from Burns (2005).

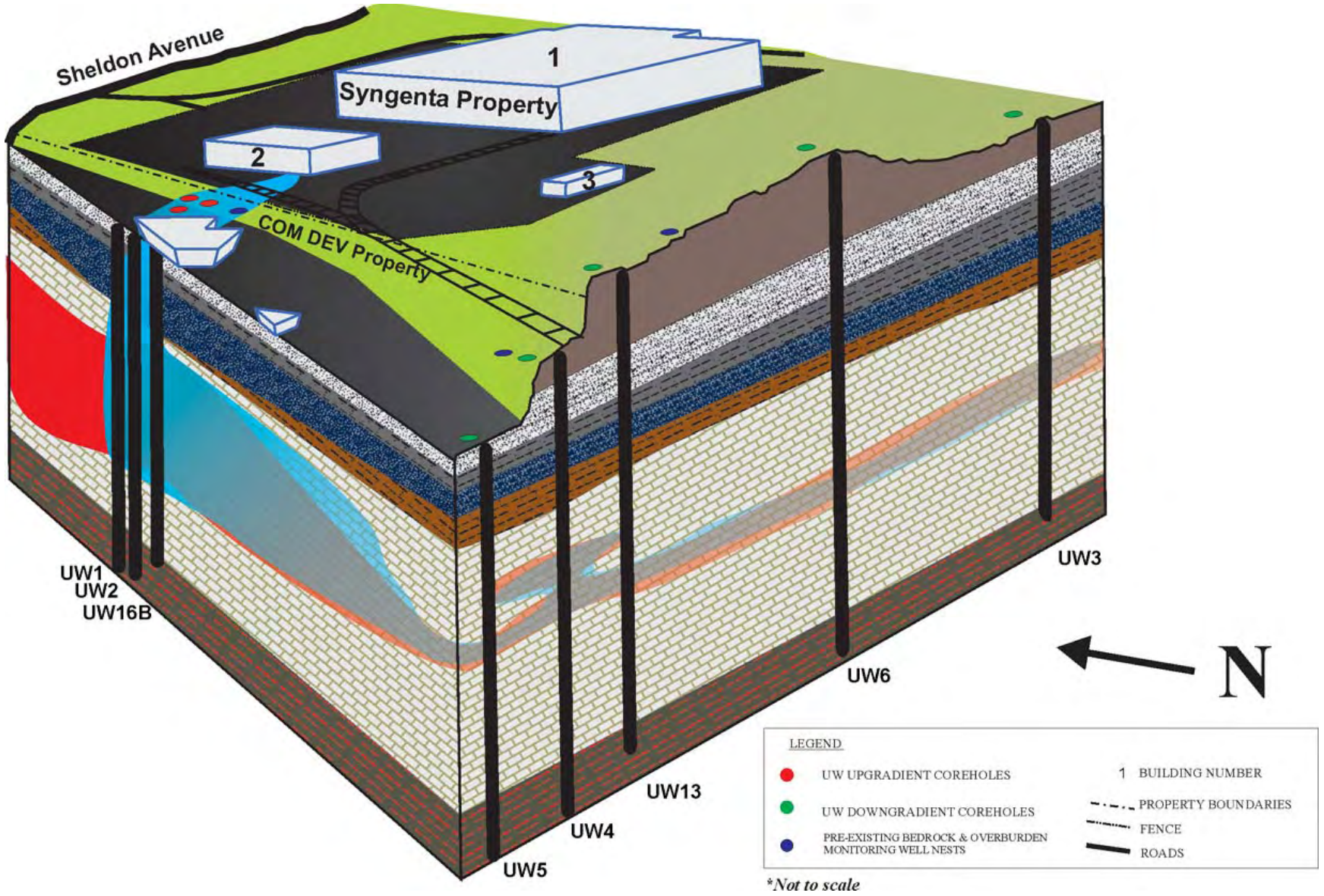


Figure 1.6: Site conceptual view illustrating the metolachlor source area (UW16B) and the transect. The metolachlor and TCE plumes are located in the middle of the aquifer along the transect based on monitoring of a detailed multilevel network installed along the transect .

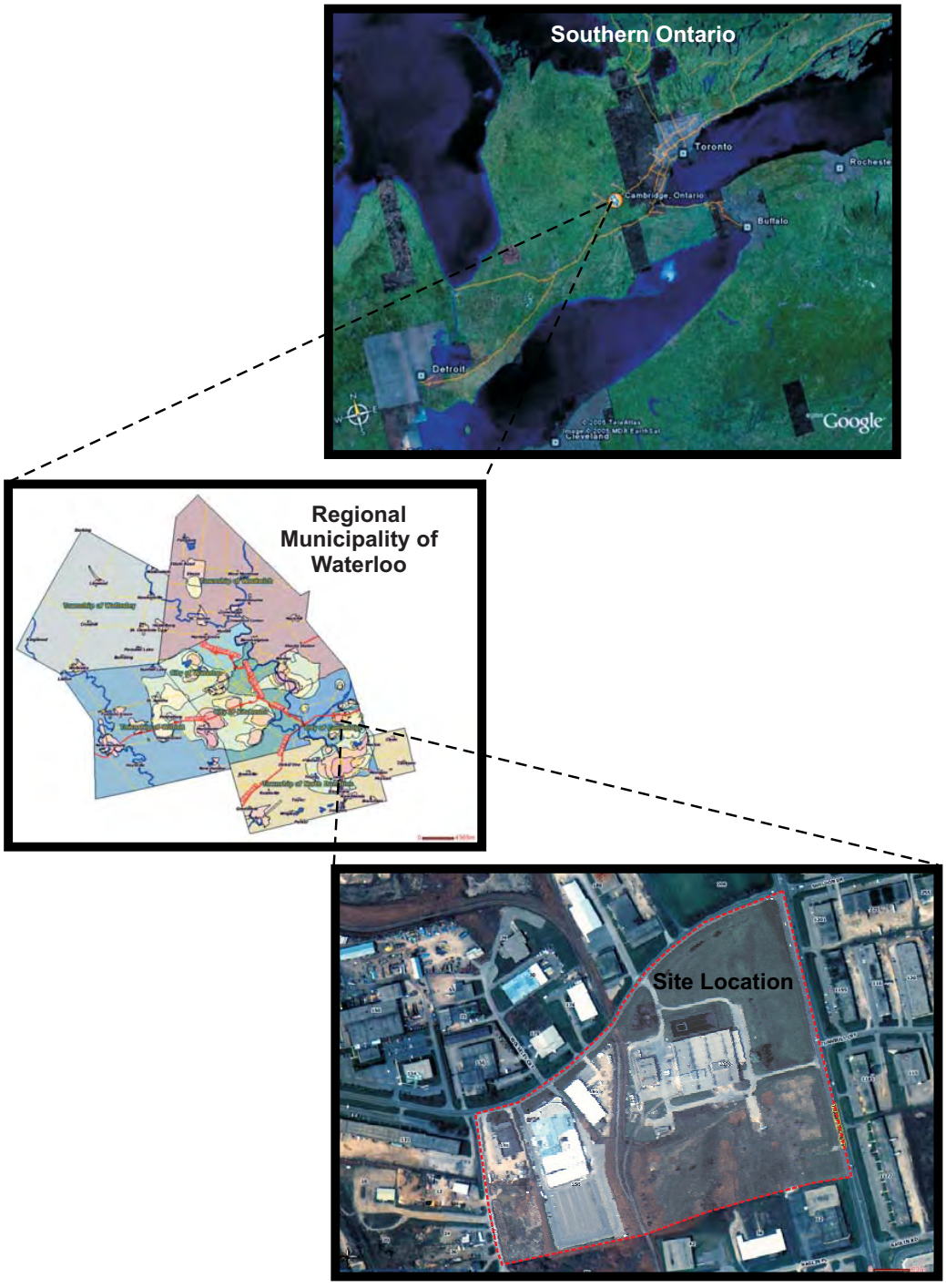


Figure 1.7: Plan views of study area location. The study site is located in Southern Ontario, approximately 100 km west of Toronto. Situated within the Regional Municipality of Waterloo, the study site in Cambridge is in a highly industrialized area.

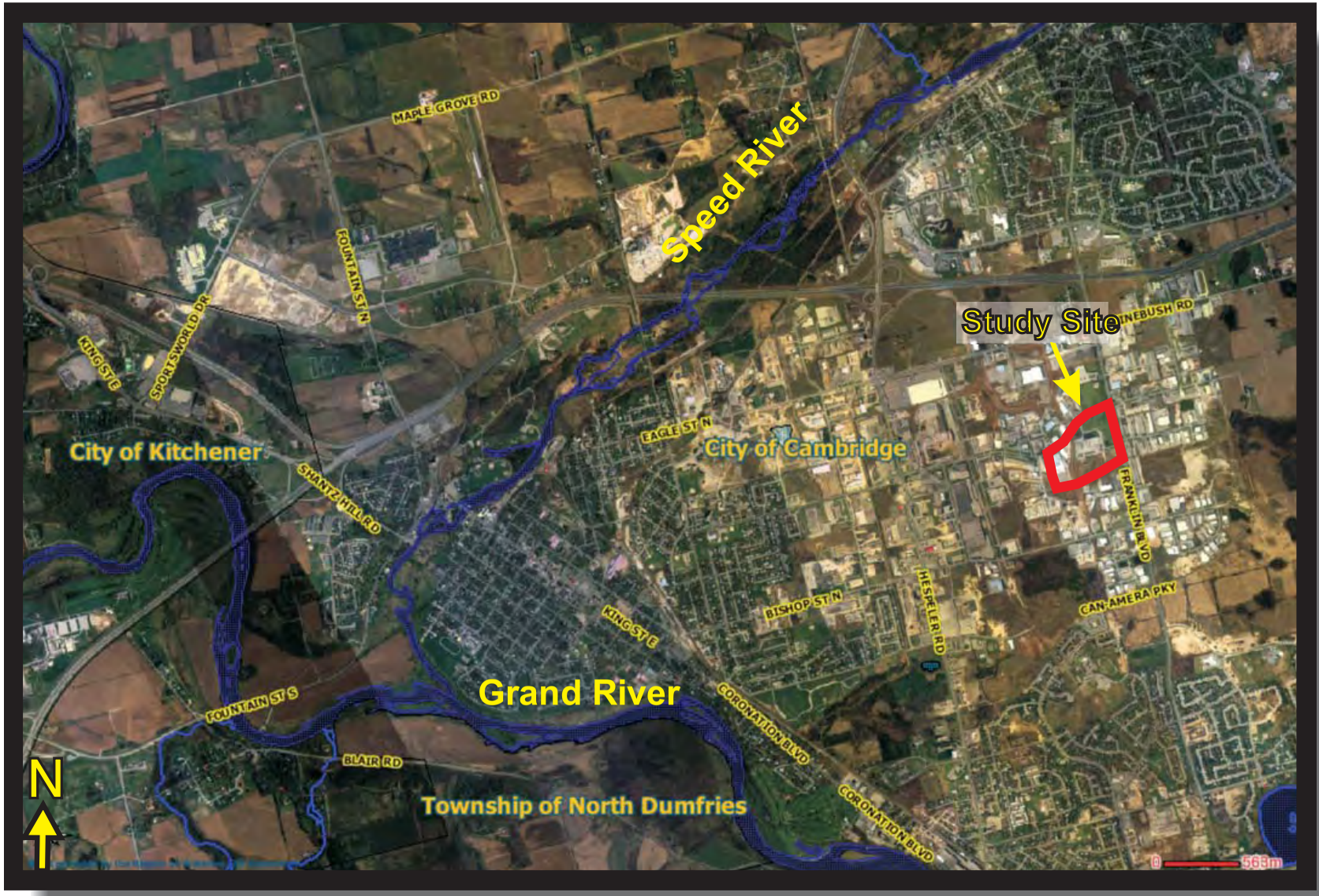


Figure 1.8: Areal photograph of site area. The study site is located near the Grand River to the southwest and the Speed River to the northwest.

Chapter 2

Description of Methods

2.1 Drilling Methods

Bedrock drilling by the University of Waterloo was initially started for a previous study by Turner (2001), and included UW16B and UW13. Table 2.1 provides detailed information on all University of Waterloo (UW) coreholes. The first corehole, UW16B, was drilled to a depth of 100 m below ground surface (bgs) in January 2000, and was the deepest corehole onsite at the time, extending three-quarters of the way through the dolostone aquifer. Since TCE and metolachlor were detected to the bottom of the corehole in both the rockcore porewater and groundwater samples collected from a multilevel system, the next corehole, UW13 (drilled in August 2000) was extended through the full extent of the aquifer into the underlying shale, approximately 150 $mbgs$. Davidson Well Drilling Ltd. drilled UW16B with a nominal hole diameter of 14.3 cm (5.63 in). All-Terrain Drilling Ltd., drilled UW13 approximately 153 m down gradient of UW16B and along an existing sentry transect of conventional wells installed by consultants as part of the initial

investigation (Dames and Moore, 1993). UW13 was drilled using a diamond impregnated PQ sized drill bit and a Christensen wireline solid core barrel which created a nominal 12.7 cm (5.0 in) corehole (Turner, 2001).

After the completion of the thesis of Turner (2001) and before the start of the current study, two more coreholes were drilled in 2002 along the transect, UW3 on the far eastern end of the transect, and UW4, 58 m west of UW13. UW3 was drilled in February 2002 by All-Terrain Drilling Ltd., to a depth of approximately 147 $mbgs$. A 17.46 cm (6.88 in) diameter mud rotary bit was used to drill through the overburden and 11 feet into the top of bedrock. A 10.2 cm (4 in) steel casing was then installed and the annular space between the casing and the rock was filled with cement to the surface. Once the casing had set, drilling continued using an HQ sized diamond impregnated bit creating a nominal 9.6 cm (3.78 in) borehole. At approximately 79 $mbgs$ (260 $ft\ bgs$), drilling was interrupted because the drill rods were stuck in the hole due to a wash-out from approximately 64 $mbgs$ to 74 $mbgs$. In order to clear debris from the drill rods, an 800-psi pump was used to blow debris to surface, however due to a pressure build-up in the rods up to 1500 psi, and then a sudden release back to 0 psi, hydro fracturing could have been possible which could have allowed the washout zone to cave-in substantially. The hole was then reamed out with a smaller diameter tri-cone bit to clear out any excess debris before drilling could continue.

Geo-Environmental Drilling Ltd. drilled UW4 in November 2002 to a depth of approximately 150 $mbgs$. Continuous core was collected using a diamond impregnated, HQ sized bit, producing a nominal 9.6 cm (3.78 in) borehole. Water from a private hydrant

connected to regional water supply was used to cool and lubricate the bit during drilling. The hydrant water was analysed for metolachlor and TCE, which was below the detection limit of 1 $\mu g/L$ for both metolachlor and TCE. A triple-tube core barrel system was used in order to maintain the highest integrity of core to allow for detailed fracture and lithology characteristics to be logged. The triple-tube system includes an outer core barrel, standard inner tube, and a third inner tube that is divided in half lengthwise within the standard inner tube. As the core is retrieved and lifted to the surface using a wire-line system, the core is contained within the core barrel and is insulated from the formation water as well as from atmospheric effects once above the water table. At surface, the core barrel assembly is connected to a hydraulic hose and the inner tube is pushed out by an ejection piston. The split core barrel is then opened and the undisturbed core is placed on an aluminum foil-lined, PVC core tray and covered to minimize volatile organic compound (VOC) volatilization.

During the current study, which was concurrent to work by Burns (2005), two more holes were drilled along the down gradient transect, UW5 to the far western end of the transect and UW6, located between UW13 and UW3. Geo-Environmental Drilling Ltd. drilled UW5 and UW6 in November and December 2003, respectively, using a diamond impregnated HQ sized bit leaving a nominal 9.6 cm (3.78 in) borehole. The overburden sediments were drilled using a tri-cone bit and permanent steel casing was set at least 3 m (10 ft) into the top of bedrock or where competent rock was encountered (Table 2.1). The casing was set using concrete and was allowed to cure 24 hours before drilling continued. Drilling water was supplied in mobile tanks by Brethren Water Supply Ltd.

from a private supply well in Baden, Ontario. This water was analysed for metolachlor and TCE, however concentrations were below the detection limits for metolachlor and TCE. The procedure for continuously coring these wells is similar to the procedure described for UW4 above. UW5 and UW6 were drilled to a depth of approximately 150 $mbgs$ and 165 $mbgs$, respectively.

2.2 Rock Core Sampling

2.2.1 Initial Core Assessment and Physical Property Sample Selection

Immediately after the core was placed on the foil-lined PVC core tray, it was quickly walked over to the covered processing station where the 1.5 m (5 ft) core was photographed and visually inspected and logging of fractures and lithology characteristics. A hydrogeologist and a geologist logged the core simultaneously. The geologist was responsible for logging the core, noting core recovery, depth intervals of core samples, bedding locations, fracture locations, orientations and features, stylolite locations, and RQD. The hydrogeologist was responsible for differentiating between fractures and mechanical breaks, and then selecting rock samples using a hammer and chisel, for metolachlor, VOC analyses and physical property measurements. Where fractures were obvious, a 2.5 cm (1 in) sample was collected at either the top or bottom fracture surface and then 15 cm (6 in) above and below the fracture, and 30 cm (12 in) above and below the fracture surface; thus, for every single-fracture encountered, five samples were collected for analysis. Where multiple

fractures were closely spaced, the sample spacing was adjusted accordingly. When cores were not fractured, three samples were selected, one near the top and bottom of the core and one in the middle.

Rock core was also collected for physical property analyses. These samples were selected, on average, every 3 m (10 ft) or where changes in lithology occurred and were approximately 30 cm (12 in) in length. Once the sample was selected and the description noted by the geologist, the sample was then wrapped in aluminum foil, plastic wrap and then paraffin wrap to prevent any atmospheric alterations of the sample. The cores were labeled by depth and corehole ID and the top and bottom of the core section was noted. The core sample was then stored in a cooler until it was brought back to the University of Waterloo where it was stored at a constant temperature of 4°C until analyses were performed. Wooden blocks were placed in the core boxes where samples were taken and were labeled with the sample ID and sample depth. The core boxes were then brought back to the University of Waterloo and stored in a warehouse in case future analyses were necessary.

2.2.2 Selection of Rock Samples for Contaminant Analysis

As noted in section 2.2.1, 2.5 cm (1 in) rock samples were collected based on fracture locations as well as at features that could be hydraulically active such as vugs, biomolds or a highly porous matrix, and lithology-change samples. After the samples were selected based on the sampling criteria, they were immediately wrapped in aluminum foil, labeled, placed in a resealable plastic bag, and then placed in a cooler at approximately 4°C

to prevent any volatile losses until they could be processed. A 5 *cm* (2 *in*) duplicate sample was taken every 20 samples or approximately 5% of the total samples, and was divided into quarters, two for VOC and two for metolachlor analyses. The next core run to be processed was not cored until only one or two samples remained to be processed to minimize disturbance times for the cores from time of coring to sample preservation in the sample containers described below.

2.2.3 Processing Rock Samples for Contaminant Analysis

The rock samples collected and temporarily stored in a cooler with ice containing a storage blank prior to being immediately processed on-site. Each sample was assigned a sample ID and that ID was then associated with a sample bottle number, each with a known mass, volume and mass of solvent for preservation and extraction. Samples being analyzed for VOCs used High-performance liquid chromatography (HPLC) grade methanol for the solvent whereas samples being analyzed for metolachlor used nanopure water, pentane, or hexane as the solvent, depending on the year of sample collection (Table 2.2). Although the sample size and solvent for metolachlor analyses differ, which will be outlined in section 2.2.5.1, the process for preparing samples for analyses are the same.

Once the sample is removed from the plastic bag and the foil is removed, it is placed into a trimming container where the 2.5 *cm* (1 *in*) sample is broken down to small pieces using a hammer and chisel. A portion of the broken sample is put immediately in a stainless steel crushing cell and crushed with a hydraulic cylinder using 5000-7000 *psi* to crush the sample into a fine-grained sample matrix. The remaining portion of broken sample is

re-wrapped in the foil and used for the metolachlor sample since it is less volatile than the VOC sample. Once the VOC sample is crushed, it is transferred to the pre-weighed sample bottle with a known volume of HPLC grade methanol. The metolachlor rock sample is immediately crushed thereafter in the same crushing cell without decontamination since it is essentially the same sample depth. Sample bottles are pre-filled with solvent, however due to possible volatile losses, the bottles are weighed just prior to filling with the crushed rock sample. The sample bottles are then weighed with the sample; the lid is sealed with Teflon^{TM} tape and placed in separate coolers for VOC and metolachlor analyses, at 4°C until they could be transported back to the University of Waterloo the same day as sampling. Equipment blanks were collected from all crushing equipment in contact with the sample by wiping down each surface with a wipe saturated with the respective solvent, and placed in the appropriate sample bottle. This procedure was repeated approximately every 20 samples in order to quantify the possible cross contamination associated with the sample collection. Each cooler contained a trip blank, which quantifies any cross-contamination within each cooler during shipping and storage. HPLC grade methanol and hexane solvent blanks were taken to ensure purity of solvents used for extraction or possible contamination. At UW, the trip and storage blanks were removed for immediate analysis and replaced with another blank during sample storage in constant temperature storage rooms (4°C) until extraction was complete.

2.2.4 Decontamination Procedure

All sampling equipment used in preparing the rock samples for analysis were decontaminated using a four-step process to prevent cross contamination. The decontaminated equipment included all items contacting the rock samples: crushing cells, piston heads, base plates, funnels, spatulas, trimming containers, and chisels. The first step used a phosphate free detergent to remove obvious debris from the equipment. The equipment was then immersed in a deionized water bath to remove any residual detergent. A thorough rinse using a wash bottle containing wash-grade methanol was then used followed by a rinse of deionized water from another wash bottle to remove all residual methanol from the equipment. The water and detergent baths were changed at least twice a day.

2.2.5 Rock Core Analysis Methods: 2000-2003

2.2.5.1 Sample Collection and Analysis Procedures 2000

Coreholes drilled during 2000 include UW16B and UW13. Drilled in January 2000, UW16B utilized a manual rock crusher described by Sterling (1999) to crush rock samples. This method used a manual rock crusher and several blows were required to crush a sample to an appropriate size. A hydraulic piston was used to crush samples for UW13, which allowed the sample to be crushed in one stroke and also minimized the potential volatile losses associated with multiple blows. Samples for TCE and metolachlor were placed in 125 ml glass jars with screw caps and Teflon^{TM}-lined septa. TCE samples were placed in a pre-weighed sample jar with approximately 60 ml of HPLC grade methanol. Before shipping back to the University of Waterloo, the 125 ml sample jars were placed

in 500 ml high density polyethylene (HDPE) jars filled with nanopure water to minimize volatile losses from the sample and help prevent cross contamination during transportation and storage of the samples. During storage of the samples at the University of Waterloo, the samples were shaken weekly to aid in the extraction of TCE into the methanol. UW16B samples were shaken approximately 17-18 times while samples for UW13 were shaken 10-11 times (Turner, 2001). As described by Gorecka et al. (2001), $1\mu L$ aliquots of methanol were analysed by direct injection into a Hewlett Packard (HP) gas chromatograph (GC) model# HP6890 equipped with a cool on-column injector and an HP-1, 30 m long, 0.32 mm ID, $5\mu m$ film-thickness column for separation and quantification using a micro-electron capture detector ($\mu - ECD$). The HP6890 GC was also equipped with a 6890 autosampler, a 6890 integrator and a GC autosampler controller. The GC oven temperature program was started at 55°C, held for 0.5 min and ramped at 10°C/min until the temperature reached 145°C. Detection limits for PCE, TCE, t-DCE, c-DCE, and 1,1-DCE, were determined to be 0.1, 0.1, 5.3, 3.5, and 6.5 $\mu g/L$ in methanol (MeOH) respectively. Nine-point calibration curves were created using methanolic standard solutions ranging in concentration from the detection limit of each compound to 3000 $\mu g/L$. The laboratory results are expressed as total TCE mass, which includes both the mass sorbed in the matrix and aqueous mass from the rock porewater, per L methanol. These data are then converted to total rock concentrations by multiplying the volume of methanol and dividing by the mass of rock in each sample, producing units of μg TCE/g wet rock.

Samples to be analysed for metolachlor were placed in pre-weighed 125 ml glass jars containing approximately 60 ml of nanopure water and 0.7 ml of 10% sodium azide solu-

tion to prevent biodegradation of metolachlor. Samples were shaken during storage time on a weekly basis to aid the extraction of metolachlor into the nanopure water. Samples for UW16B were shaken approximately 20-24 times whereas samples for UW13 were shaken 4 times since a laboratory study determined that rock-water metolachlor equilibrium is reached in less than 120 hours (Turner, 2001). According to Turner (2001), metolachlor samples were analysed at a lab in the Department of Chemistry at the University of Waterloo, using a Varian model 3400 GC equipped with a 30 m x 0.25 mm x 0.25 μm HP-5MS capillary column and a Varian ECD. The GC-ECD separation and detection conditions included a helium carrier gas flow rate of 1.4 mL/min, a total gas flow rate of 30mL/min at the detector end, and an injector temperature of 250°C. The GC oven temperature program was started at 100°C, held for 2 min and ramped at 10°C/min until the temperature reached 250°C. A 50 ml aliquot of water was removed from each sample and passed through 0.45 μm Acrodisc HT Tuffryn® filters to remove suspended solids. Metolachlor was extracted from aliquots using a Supelco solid phase microextraction (SPME) fibre with a 100 μm polydimethylsiloxane (PDMS) coating for 20 minutes at room temperature with magnetic stirring at 800 rpm. Calibration curves were determined using five standard metolachlor solutions with concentrations ranging from the method detection limit of 0.065 $\mu g/L$ to 39.6 $\mu g/L$.

2.2.5.2 Sample Collection and Analysis Procedures: 2002

Two coreholes were drilled in February and November 2002, UW3 and UW4, respectively. TCE samples collected at UW3 and UW4 were analysed using the same method described

in section 2.2.5.1.

Samples collected for metolachlor analysis were analysed using a different method than in section 2.2.5.1. Samples were crushed using the hydraulic piston, however the 125 ml glass sample jars contained approximately 60 ml of pentane. The sample bottles used for metolachlor contained a single layer Teflon^{TM} septa, and due to pentane's propensity to diffuse through Teflon^{TM}, the integrity of all samples collected for metolachlor in UW3 were compromised. The septa on the lids had been corrupted and the pentane was in direct contact with the nanopure water contained in the HDPE overjars, therefore none of the samples could be analysed and no metolachlor data were obtained from UW3. To correct for this problem, metolachlor samples from UW4 were analysed more rapidly to minimize the exposure of pentane to the Teflon^{TM} septa. Instead of using nanopure-water-filled overjars, high purity activated carbon was used to prevent cross contamination between samples. Samples were analysed at a University of Waterloo laboratory, using a method developed by Gorecka (2003). $1\mu L$ aliquots of pentane were analysed by direct injection into a Hewlett Packard (HP) gas chromatograph (GC) model# HP6890 equipped with a splitless injector and an HP-5, 30 m long, 0.32 mm ID, 0.25μm film-thickness column for separation and quantification using a micro-electron capture detector ($\mu - ECD$). The HP6890 GC was also equipped with a 6890 autosampler, a 6890 integrator and a GC autosampler controller. The GC oven temperature program was started at 35°C, held for 1 min and ramped at 15°C/min until the temperature reached 160°C. The temperature was then ramped at 10°C/min until the temperature was 290°C and then at 30°C/min until the temperature was 290°C and then held for 5 minutes. The detection limit for

metolachlor was determined to be $1\mu g/L$ in pentane. Calibration curves were created using pentane standard solutions ranging in concentration from the detection limit to 240 $\mu g/L$, using a 6 point calibration curve. The lab results were expressed as total metolachlor mass, which includes both the mass sorbed in the matrix and aqueous mass from the rock porewater, per L pentane. These data were then converted to total rock concentrations by multiplying by the volume of pentane and dividing by the mass of rock in each sample, producing units of μg metolachlor/g wet rock.

2.2.5.3 Sample Collection and Analysis Procedures: 2003

The final coreholes drilled along the down gradient transect were UW5 and UW6, drilled in November and December 2003, respectively. The sample collection process was the same as mentioned previously, however samples were collected in 40 ml glass volatile organic analysis (VOA) vials using a screw-cap top containing a 2-layer Teflon^{TM}/silica septa. Rock samples were collected in pre-weighed VOA vials containing approximately 18 ml of solvent, methanol for TCE analysis, and hexane for metolachlor analysis. TCE samples were analysed at the University of Waterloo using the method developed by Gorecka et al. (2001).

Analysis of metolachlor samples was performed at the University of Guelph Analytical Services Laboratory using the method described by Shurmer (2005). Following shaking of the metolachlor samples at the University of Waterloo, aliquots of the hexane extracted from the samples were sent to the University of Guelph for analysis. This procedure involved transferring 10 ml of the hexane extract into a 15 ml test tube and adding 0.5 ml

of iso-octane (trimethylpentane). The sample was then evaporated using a nitrogen blow-down apparatus, and reconstituted with 2.0 ml of hexane. The sample was then vortexed for twenty seconds, split in two GC vials and capped. One sample was refrigerated as a back-up while the other sample was analysed on the laboratory equipment. A 2 μL aliquot of the extract was then analyzed by direct manual injection onto a Restek Cl-pesticides column on a GC-μECD. The lab results were expressed as total metolachlor mass per litre hexane in original extract. The metolachlor detection limit was determined to be 0.7 $\mu g/L$ in hexane. This limit was determined by placing eight replicate spikes at approximately 2-5 times the anticipated detection limit in the GC-μECD under the same method as the sample analyses. The method detection limit was then determined by multiplying the standard deviation of these sample concentrations by three, thus obtaining the T-value for a 95% interval (Shurmer, 2005).

2.3 Data Validation

Once the data were back from the various laboratories, the data had to be reviewed based on concentrations in any of the blanks taken during sampling and associated with the specific sets of samples. This validation process is described by USEPA (1999). Samples analysed since 2003 used a flagging system described by USEPA (1999) and include six letter-flags used to qualify the sample concentration. ND was used for sample concentrations that were not detected, U means the analyte was not detected above the reporting limit (RL), J means the analyte was positively identified and an approximate concentration of the analyte is used, UJ means the concentration is less than the elevated RL due

to contamination of a blank or carryover, R means the sample results are rejected due to the presence of front-end interference, and E means the analyte concentration exceeds the calibration range; if no letter-flag was used, the concentration is quantifiable. If any sample concentration is less than 5 times the concentration in an associated blank, that sample is flagged J and treated similarly as samples with detected concentrations but below the limit of quantitation. The data are not changed, however the flag represents uncertainty in the data due to the strong possibility for cross-contamination in the sample blanks. If reported data did not include a limit of quantitation provided by the laboratory, a value of 3 times the method detection limit was used.

2.4 Rock Core Conversions to Equivalent Porewater Concentrations

Rock core data is reported by the laboratory in $\mu g/L$ MeOH. These data are then converted to $\mu g/g$ of wet rock. The conversion from extract concentration to wet rock concentration is as follows:

$$m_a = C_e \cdot V_e \tag{2.1}$$

$$C_t = \frac{m_a}{m_t} \tag{2.2}$$

where m_a (μg) is the calculated mass of analyte in the sample, C_e $(\mu g/L)$ is the concentration of the contaminant in the extract reported by the laboratory, V_e (L) is the volume

of extract in the sample, C_t $(\mu g/g)$ is the total contaminant mass per mass of wet rock, and m_t (g) is the mass of wet rock.

To convert from total contaminant concentration in wet rock $(\mu g/g)$ to equivalent porewater concentrations $(\mu g/L)$, the method adapted from Pankow and Cherry (1996) must be used:

$$C_w = C_t \frac{\rho_{b,wet}}{R \cdot \phi_m} \tag{2.3}$$

$$R = 1 + \frac{\rho_{b,dry}}{\phi_m} K_d \tag{2.4}$$

$$K_d = K_{oc} \cdot f_{oc} \tag{2.5}$$

where C_w $(\mu g/L)$ is the porewater concentration, ϕ_m is the matrix porosity, $\rho_{b,wet}$ (g/cm^3) and $\rho_{b,dry}$ (g/cm^3) are the bulk wet and bulk dry densities, R is the retardation factor accounting for sorption of the respective chemical to the rock solids, K_d (cm^3/g) is the partition coefficient between the rock matrix material and porewater that can be measured in the laboratory or estimated using the $K_{oc} \cdot f_{oc}$ correlation for hydrophobic organic contaminants, K_{oc} (cm^3/g) is the organic carbon partition coefficient, and f_{oc} is the fraction of organic carbon in the rock sample.

Olsen and Davis (1990) report that K_{oc} can be determined by the relation:

$$K_{oc} = 1.724 \cdot K_{om} \tag{2.6}$$

where K_{om} (mL/g) is the partition coefficient between organic matter and water.

According to Schwarzenbach et al. (1993), K_{om} can be estimated for certain organic molecules using:

$$logK_{om} = -a \cdot logC_{sat} + b \tag{2.7}$$

where a and b are the linear free energy relationships which equal 0.70 and 0.35, respectively for chlorinated hydrocarbons, and C_{sat} (mol/L) is the solubility of the chemical in water.

2.5 Rock Matrix Physical Properties

During drilling in 2003, 134 samples were collected from coreholes for Burns (2005) and from UW5 and UW6 for the current study for physical property analyses including, porosity, wet and dry bulk densities, permeability, and f_{oc}. The samples were collected after the core had been logged by the geologist and hydrogeologist and were approximately 30.5 cm (12 in) in length and were spaced at least 3.0 m (10 ft) apart. The samples were wrapped in aluminum foil, Parafilm^{TM}, and plastic wrap to preserve the porewater content. The samples were labeled with the corehole name, date, depth of sample interval and the top and bottom of the sample. They were then placed in a cooler and transported back to the University of Waterloo at the end of the day, and stored at 4 °C in a constant temperature room until analyses were initiated.

A subset of 43 rock samples was selected for physical property analyses. These samples were selected to represent the 9 matrix lithology classifications determined concurrently

with Burns (2005), and were selected from all of the coreholes drilled in 2003 (UW1, UW2, UW5, UW6). At least 4 samples were selected for each classification in order to calculate simple statistical variables. Porosity, wet and dry bulk densities and matrix permeability were measured using the methods used by Amirtharaj (2003) and f_{oc} samples were measured using the method described by Churcher and Dickhout (1987). The results from these methods can be found in Table 2.3.

2.5.1 Matrix Porosity

2.5.1.1 Imbibition Gravimetric Procedure

This procedure determines the connected pore space, known as the effective porosity, as the wetting fluid (brine) must imbibe through interconnected pathways (Amirtharaj, 2003).

First, the samples were sub-cored using a diamond core barrel producing a sample measuring 3.85 *cm* in diameter and approximately 4 *cm* long. The samples were then oven-dried at 100 °C for 24 hours, removed, weighed and placed in a desiccator. The samples were placed 4 to 6 at a time in a stainless steel chamber connected to a vacuum pump and a vessel located above the chamber containing brine or water controlled by an access valve. The chamber was then evacuated of air and filled with brine at 100 *psi* using nitrogen and left for 10-15 minutes. Once complete, the samples are re-weighed and the matrix porosity can be determined using the following formula described by Collins (1961) and Dullien (1992):

$$\phi_m = \frac{m_{wet} - m_{dry}}{V_b} \cdot \frac{1}{\rho_f} \tag{2.8}$$

where m_{wet} (g) and m_{dry} (g) are the masses of the saturated and dried samples respectively, V_b (cm^3) is the bulk volume of the sample, and ρ_f (g/cm^3) is the imbibing fluid density.

2.5.2 Wet and Dry Bulk Density

The bulk density of a porous medium is a ratio of the mass to the total volume (Craig, 1997). Wet and dry bulk densities were calculated from the data collected in section 2.5.1.1 using the following equations:

$$\rho_{b,wet} = \frac{m_{wet}}{V_b} \tag{2.9}$$

$$\rho_{b,dry} = \frac{m_{dry}}{V_b} \tag{2.10}$$

where $\rho_{b,wet}$ and $\rho_{b,dry}$ are the wet and dry bulk densities (g/cm^3), respectively, m_{wet} and m_{dry} are the wet and dry masses (g) of the samples respectively, and V_b is the bulk volume of the sample (cm^3) measured from sample dimensions based on an average of 3-4 measurements using a Vernier Caliper.

2.5.3 Solid Phase Organic Carbon (f_{oc})

Samples analysed for solid phase organic carbon (f_{oc}) were first pulverized into a powder using an alumina ceramic grinding container and a large shaking device. The device was cleaned between samples using carbon-free silica sand and then blown clean with an air compressor. Approximately 10 ml of rock powder was placed in a 40 ml glass vial and sent to the University of Waterloo Organic Geochemistry Laboratory for analysis. The

samples were analysed using the method developed by Churcher and Dickhout (1987), and the current method detection limit is 0.01%.

2.6 Geophysical/Hydrophysical Logging

In order to gain additional insight into the subsurface and to aid in the design of the multilevel systems, various geophysical and hydrophysical logs were employed down either a lined or open corehole. Each of the logs provided unique and valuable information towards a better understanding of the stratigraphy/lithology, flow system, and chemical distribution within the dolostone aquifer.

2.6.1 Neutron and Gamma-Gamma Logs

Both of these logs were conducted by the Environmental Geophysics Group at the University of Waterloo and were performed inside blank FLUTe-lined holes. Since these two probes use a radioactive source, it is valuable to perform the logs with the liner; in case the probe was dropped, it could be retrieved easily. The nylon fabric liner does not interfere with the logging and it recreates natural flow conditions in the aquifer by preventing cross-connection typically resulting from open corehole conditions.

2.6.1.1 Neutron Log

The neutron log was performed using a Comprobe^{TM} (Model# 2136) dual-spaced neutron probe which emits the neutrons and bombards non-radioactive elements stimulating them to emit gamma rays which provide information on moisture content and therefore porosity

in a water-saturated environment (Kearey and Brooks, 1991). The neutrons are emitted from a 3 curie Americium-Beryllium source with a 458 year half-life, reaching on average, 20-30 m into the corehole wall. According to Kearey and Brooks (1991), the neutrons collide with atomic nuclei in the corehole wall, and since a single hydrogen atom has almost the same mass as a neutron, the collision transfers considerable kinetic energy and slows the neutron to the point where it can be absorbed by a larger nucleus. This neutron capture gives rise to gamma radiation and the intensity of the radiation is controlled by how far it has traveled from the point of neutron capture, hence, the farther the radiation travels the higher the porosity and the lower the count rate.

2.6.1.2 Gamma-Gamma Log

Gamma-ray density or Gamma-Gamma logging was performed with the Mineral Logging Systems^{TM} bulk density probe. This probe is a decentralized, side-collimated tool that is forced against one side of the corehole with a centralizer spring. Gamma rays are emitted approximately 10 to 15 cm into the corehole wall using a Cesium-137 (Cs^{137}) source, which has a 30-year half-life. Gamma-ray photons collide elastically with electrons and are reduced in energy which is known as Compton Scattering. The number of collisions over any particular interval of time depends on the abundance of electrons present, which in turn is a function of the formation density (Kearey and Brooks, 1991). A detector approximately 40 cm from the source intercepts scattered gamma rays and displays the result as a count rate. Higher density formations (i.e. lower porosity) cause fewer gamma rays to reach the detector which therefore causes a lower count rate.

2.6.2 Natural Gamma

The natural gamma log is a representation of the clay content in the formation being tested. According to Kearey and Brooks (1991), shales and clays contain small quantities of radioactive elements, specifically K^{40}, which occurs in micas, alkali feldspars, and clay minerals and trace amounts of U^{238} and Th^{232}. These produce gamma radiation which is detected with the Geonics^{TM} EM39 tool with a sodium iodide detector. This log is typically useful for determining shale horizons and can provide an estimate of clay mineral content within the Guelph-Lockport Formations, as well as potassium-rich evaporites such as Gypsum, which was found in cores logged for this study, as very thin layers.

2.6.3 Borehole Video

The borehole video comprises an Image Systems^{TM} downward facing analog camera with a halogen light source below the camera lens. The camera is lowered in the hole over a depth counter connected to the video recorder attached using a teflon reinforced video cable that provides real-time imaging of the borehole wall. The video is recorded on a VHS tape with the depth counter visible during playback so features such as fractures or large vugs can be identified at the appropriate depth. If the corehole has been disturbed, several days may be required before a clear picture can be achieved due to increases in turbidity in the water column.

2.6.4 Acoustic Televiewer

An Advance Logic Technology (ALT) FAC40 televiewer was used to provide a digital image of the corehole. According to Advanced Logic Technology (2002) the FAC40 televiewer produces images of the corehole wall that are based on the amplitude and time of travel of an ultrasonic beam reflected from the corehole wall. The ultrasonic energy wave is generated by a specially designed piezoelectric ceramic crystal and has a frequency of around 1.4 MHz. On triggering, an acoustic energy wave is emitted by the transducer and travels through the acoustic head and corehole fluid until it reaches the interface between the corehole fluid and the corehole wall. Here a part of the beam energy is reflected back to the sensor, the remainder continuing on into the formation at a changed velocity. By careful time sequencing, the piezoelectric transducer acts as both transmitter of the ultrasonic pulse and receiver of the reflected wave. The travel time for the energy wave is the period between transmission of the source energy pulse and the return of the reflected wave measured at the point of maximum wave amplitude. This amplitude is processed in real-time on a computer which displays the digital image of the corehole wall to a resolution of 50 μm.

2.6.5 Detailed Temperature Profiling

Detailed temperature profiling was done in the coreholes to detect temperature variations of a few $10,000ths$ of a degree Celsius (0.0001°C), which according to Greenhouse and Pehme (2002), that can used to identify hydraulically active fractures. Temperature profiling was done in FLUTe-lined holes to recreate natural flow conditions and in open holes,

using a temperature probe that can measure temperature variations to within 0.0001 °C. These data are then compared and information about the ambient flow in the formation can be assessed.

Another method used to asses the flow conditions in the formation was active temperature profiling. This is accomplished by heating the entire length of the corehole (lined or open) using a $50W$ line source for two hours. Heating the corehole fluid accentuates the temperature contrast and helps identify hydraulically active zones where colder water enters or leaves the corehole (Greenhouse and Pehme, 2002). The corehole is then logged using the sensitive temperature probe and the data are compared with the logs collected under ambient flow conditions.

2.6.6 Heat-pulse Flow-metering

Heat pulse flow-metering was performed in the open coreholes to obtain information on vertical hydraulically active zones in the corehole. An HFP-2293 Heat-pulse Flow-meter owned by the University of Waterloo was used for this purpose.

The tool is lowered into the borehole via a cable attached to a winch. When the tool is in position to take a flow measurement, the trigger assembly button is pressed. This sends a heat-pulse down the center conductor which, when detected by circuitry in the probe, fires the heat grid and signals the surface monitoring equipment and software to begin a flow measurement cycle. The grid heats a sheet of water that moves with the flow of the borehole water up or down to the upper or lower heat sensor. The difference in temperature between the sensors is detected by an amplifier. The output of this amplifier

is then converted to a frequency. This frequency is then driven up the cable line and monitored by the surface equipment. A complete flow measurement is made when the time has been accurately measured from when the heat grid was fired to when a peak temperature change, carried by the flow, is detected by either the sensor located above or below the heat grid (MSI, 2002). The coreholes were tested every metre and the data were manually qualified based on the heat-pulse signature of that test zone.

2.6.7 Hydraulic Testing

2.6.7.1 Straddle Packer Testing

Straddle packer testing involves sealing a zone in the formation between two packers and injecting water into the formation at a constant head to determine the formation transmissivity. The equipment used was borrowed from the National Water Research Institute, a division of Environment Canada, and the procedure is described by Lapcevic et al. (1999a). UW5, UW4, and UW6 were tested in the spring of 2004; UW13 was tested during work carried out by Turner (2001); and UW3 was not tested due to a $10m$ washout zone and the concern for equipment loss or damage in the corehole.

The testing apparatus consists of two sliding-head, nitrogen-inflated packers spaced approximately $2.2m$ apart. This design allows for the stiff rubber packer to inflate against the corehole wall which can withstand high pressures and ensures a proper corehole wall seal in deep flow systems.

Water was injected from one of five tanks, ranging in discharge rates from 3.64×10^{-7} to 8.29×10^{-4} m^3/cm through 1.59 cm (5/8 in) polyethylene tubing. A Druck model

PDCR-1830 300 *psig* transducer was used to monitor hydraulic head in the test zone prior to, and during each test. Using this set-up, it was possible to achieve transmissivity values between 1×10^{-10} and 1×10^{-4} m^2/s. The transmissivity is calculated using the flow rate and pressure change within the test zone using the Theim equation:

$$T = \frac{Q}{\Delta H 2\pi} \cdot ln(\frac{r_e}{r_w}) \tag{2.11}$$

where T is the transmissivity of the test zone (m^2/s), Q is the measured flow rate (m^3/s), ΔH is the change in head (m) from the equilibrium head in the zone and the head from each test, r_e is the radius of influence (m), and r_w is the well radius (m).

To determine bulk hydraulic conductivity (assumed to be horizontal), the transmissivity calculated from equation 2.11 is divided by the test interval spacing as follows:

$$K_b = \frac{T}{b} \tag{2.12}$$

where K_b is the bulk hydraulic conductivity (m/s), and b is the test interval length (m).

The radius of influence is assumed to be 10 m based on a study published by Bliss and Rushton (1984). Although the radius of influence is unknown, transmissivity is relatively insensitive to this term, resulting in small errors because it appears as a logarithmic term in equation 2.11.

It is possible to determine the hydraulic fracture aperture from these data using the Cubic Law, however this is not part of this thesis. The Cubic Law, derived by Snow (1968)

is as follows:

$$2b = (T \cdot \frac{12\mu}{\rho g})^{\frac{1}{3}} \tag{2.13}$$

where $2b$ is the equivalent hydraulic aperture (m), μ is the kinematic viscosity of water $(Pa \cdot s)$, ρ is the density of water (kg/m^3), and g is the gravitational acceleration constant (m/s^2).

2.6.7.2 FLUTe Hydraulic Conductivity Profiling

Hydraulic conductivity was also determined using the FLUTe hydraulic conductivity method. UW4, UW5, and UW6 were testing using this method which is described by Keller et al. (2006) as a method in which a continuous flexible cylindrical tube made of impervious urethane coated nylon is inserted down the open hole using water applied under constant hydraulic head while the descent rate down the hole is measured. The descending liner is a piston that pushes the borehole water out into the hydraulically open fractures intersecting the hole. The liner descent rate is governed by the transmissivity of the open segment of the hole remaining below the bottom of the liner. This open borehole segment below the liner continually decreases until the liner reaches the bottom of the hole or until the descent rate is determined too slow to continue monitoring. The descent velocity decreases markedly as the liner front passes and seals each hydraulically active fracture, which thereby identifies each fracture or fracture zone. An analytical mathematical model was developed to calculate the hydraulic conductivity from the velocity change at each identified fracture, fracture zone, or permeable bed.

2.7 Multilevel Systems

Multilevel systems were installed in all of the wells along the transect; four FLUTe systems (UW4, UW5, UW6, UW13) and one Westbay system (UW3). Installations were completed after intensive logging was done in the coreholes and these data along with rock core data were used to determine the sampling intervals for each system. Detailed port locations for all of the multilevel systems can be found in Tables 2.4 to 2.9.

2.7.1 FLUTe Multilevel System

UW13 was the first down-gradient transect well to have a FLUTe multilevel installation. The diameter of this borehole is 12.7cm (5 in) and therefore the FLUTe was be designed with 10 sampling ports and 10 dedicated pressure transducers (2.7). The system was installed in February 2004 through the full extent of the aquifer and into the underlying shale, with the bottom port installed in the shale. Sampling ports were placed based on data from rock core concentrations and various geophysical and hydrophysical logs described in section 2.6. Sampling is achieved by injecting compressed nitrogen into a 1.59cm (5/8 in) Polyvinylidene Difluoride (PVDF) tube at the surface to drive water through two check valves and out of a second 0.64cm (1/4 in) PVDF tube at the surface.

UW5 was the next down-gradient corehole to be fitted with a FLUTe multilevel system (Table 2.5). The 12-port multilevel system was installed in May 2005 and due to installation difficulties, was not installed to the bottom of the corehole but stopped just above the shale, part way through port 11 installation. The corehole was drilled with HQ sized (9.6cm) drill rods, and due to the small diameter, the FLUTe design had to be

altered to allow for 12 sampling ports. These modifications were used for FLUTe systems installed in UW4 and UW6 also. The nitrogen injection PVDF tubing was reduced from 1.59cm (5/8 in) diameter to 1.27cm (1/2 in) diameter. To save space and increase the number of monitoring ports, only 6 pressure transducers were used instead of one for every sampling port, and more flexible tubing connecting to the sampling port was used to allow for easier installation into the corehole.

Both of the FLUTe multilevel systems for UW4 and UW6 were installed in August 2005, and both were installed through the entire extent of the aquifer and into the underlying shale (Tables **??**). After the multilevel installation in UW4 was complete, it was discovered that 3 of the 12 ports did not produce water, which was likely due to a kinked sampling port tube, and one of the pressure transducers did not function properly. All of the ports and pressure transducers in UW6 functioned properly.

2.7.2 Westbay Multilevel System

A 25-zone Westbay multilevel system was designed and installed in UW3 on September 15, 2005 (Table 2.9). The zone locations were predetermined and the components were pieced together at the time of installation with the assistance of a Westbay technician. Each monitoring zone contained at least one sampling port and one pumping port. HQ sized drill rods were reinserted in the well by a drilling contractor to a depth of approximately 91$mbgs$ (300 ft bgs) to ensure that a large washout zone would not collapse and potentially lodge the system in the hole before installation was complete. During installation of the Westbay multilevel system, the connection between components (i.e. ports, PVC casing)

were pressure tested to ensure a water tight seal throughout the entire length of the system. After the system was assembled and positioned at the bottom of the corehole, the packers were inflated with water starting from the bottom packer and moving sequentially up the string of packers. The first 11 packers were inflated and then the drill rods were pulled to allow the remaining 19 packers to be inflated. During the drill rod retrieval process the rods unscrewed and approximately $90m$ (295 ft) of rod dropped onto an inflated packer at a depth of 93.8 $mbgs$ (307.7 ft). Upon trying to retrieve the dropped drill rods, the Westbay casing detached at $95.9mbgs$ (314.6 ft) and was pulled to the surface. The components were disconnected and cleaned and then a reinstallation was attempted, however, attempts to reconnect to the installed section left in the bottom of the hole were unsuccessful and the new system was installed with only the remaining 14 zones. All packer pressures during inflation and QAQC checks performed during installation can be found in Westbay (2005).

After installation, all 14 zones were purged via the pumping ports and volumes equivalent to three times the sample zone volume plus the volume in the 100 metres of Watera^{TM} tubing was purged.

2.7.3 Solinst Modified Waterloo Multilevel System

Three, fifteen port modified Waterloo multilevel systems were installed in the overburden near existing multilevel systems installed in the bedrock. The systems were installed using a rotosonic rig in order to minimize disturbance of the corehole wall. Sand and bentonite were used to create the monitoring intervals and the seals between 15 monitoring ports.

The details of the systems and the detailed installation procedures are discussed in Parker et al. (2006a).

2.8 Multilevel Groundwater Sampling

Groundwater sampling was conducted on a monthly basis for metolachlor and VOC analyses from all multilevel systems after installation. Metolachlor samples were initially analysed by the University of Guelph Analytical Services Laboratory but was switched to Maxxam Analytics after four months. Analysis of the VOC samples was initially done by a University of Waterloo laboratory and then by Maxxam Analytics. Sub-samples were sent to the Institute for Groundwater Research Laboratory at the University of Waterloo to analyse for TCE degradation products.

2.8.1 Multilevel Sampling Procedures

2.8.1.1 FLUTe Multilevel Sampling

Groundwater samples were collected after initially purging the system. Two complete pump strokes of the nitrogen displacement system were completed and then sampling commenced on the third pump stroke after the initial purge water that was mixed with nitrogen from the previous pump stroke was discarded. All of the FLUTe ports were purged at the same time and were allowed to recover before the following pump stroke commenced. Sampling of all the FLUTe multilevel systems could be completed within one day. Samples were placed in coolers at 4°C and transported back to the University of

Waterloo and then delivered to the respective laboratories for analyses. Trip blanks and sample duplicates were collected for quality control and quality assurance purposes.

2.8.1.2 Westbay Multilevel Sampling

Sampling a Westbay multilevel system involves lowering a sampling probe and pressurized $250ml$ sample containers connected in series down the inside of the Westbay PVC casing using a motorized winch. Once the probe is lowered to the appropriate sample zone depth, commands are sent to the probe from a control panel at surface to open the port and retrieve the groundwater sample. A pressure transducer built into the probe monitors the pressure within the sample containers and once the containers are filled, they are sealed and raised to the surface and sample bottles are filled for the various analyses being performed. For volatile samples, the containers are left pressurized and the samples are retrieved from a spout at the end of the series so the samples are not exposed to the atmosphere. Semi-volatile or non-volatile samples are collected from the sample container by unscrewing one end of the container and pouring the sample out. Depending on the number of samples collected and the volume required for analysis, sampling of the Westbay system usually required two days to complete. All of the equipment was decontaminated between sample zones using a rinse of wash-grade methanol and a rinse of de-ionized water from wash bottles. The samples were stored in coolers at 4°C and transported back to the University of Waterloo and then delivered to the respective laboratories for analyses. Trip blanks, sample duplicates, and equipment blanks were collected for quality control and quality assurance purposes.

2.8.2 Multilevel Groundwater Sample Analysis Procedures

Various laboratories were used for analysing the groundwater samples collected from the multilevel systems. Each laboratory uses a different method which usually results in a different method detection limit (mdl). The methods will be discussed in the following sections.

2.8.2.1 Aqueous VOC

From March 2004 until September 2005 samples were analysed at a University of Waterloo laboratory using the method described by (Guilbeault et al., 2005). Samples were collected in $40ml$ VOA vials with no head space and were analyzed within 7 days.

Prior to analysis, the samples are prepared with $2ml$ of sample and $2ml$ of capillary GC-grade pentane, which is mixed with 500 $\mu g/L$ of 1,2-dibromoethane as an internal standard. The mixture is then shaken on an orbital shaker at 300 rpm for 15 minutes. The pentane is then extracted and split into two samples. One is analyzed on a gas chromatograph and the other is refrigerated and used if necessary to dilute and re-run the sample. The Hewlett Packard (HP) gas chromatograph (GC) model# HP6890 is equipped with a cool on-column injector and an HP-1, 30 m long, 0.32 mm ID, $1.8\mu m$ film-thickness column for separation and quantification using a micro-electron capture detector ($\mu - ECD$). The HP6890 GC was also equipped with a 6890 autosampler, a 6890 integrator and a GC autosampler controller. The GC oven temperature program was started at 35°C, held for 4 minutes and ramped at 10°C/min until a temperature of 60°C is reached. The temperature is then ramped again at 30°C/min until a temperature

of 105°C is reached and then it is held for 2.5 minutes. Detection limits for PCE, TCE, t-DCE, c-DCE, 1,1-DCE, and CF were determined to be 1.0, 1.0, 125, 100, 100 and 1.0 $\mu g/L$, respectively. Laboratory controls were run every 40 samples or at the beginning and end of the sequence if appropriate.

Aliquots of each sample were sent to the Institute for Groundwater Research Laboratory at the University of Waterloo for analysis of TCE degradation products, until October 2005 when Maxxam Analytics was used for VOC analysis. The method developed by Noble (2004) provides much lower detection limits than those listed above. The samples are analyzed by creating headspace at a ratio of 6.0ml headspace to 4.0ml aqueous sample. The samples are shaken for 15 minutes to promote equilibration between gaseous and liquid phases. The samples are then placed on a headspace autosampler and a 1ml sample is injected into a GC with a Hnu photoionization detector (PID) using a Hnu NSE-plot capillary column with a 6:1 split injector. Method detection limits for vinyl chloride, 1,1-DCE, t-DCE, and c-DCE are 1.3, 3.9, 2.3, and 1.9 $\mu g/L$, respectively.

Samples collected between October and December 2005 were analysed at Maxxam Analytics in Mississauga, Ontario. Three, 40ml Volatile Organic Analyte (VOA) vials containing 1.0ml of 50% hydrochloric acid (HCL) as a preservative were required for analysis in case of high concentrations requiring dilution. The samples were analysed using the standard US EPA SW846 method 8260B (USEPA, 1996b). This method reported concentrations for 38 compounds including PCE, TCE, 1,1-DCE, c-DCE, and t-DCE with method detection limits reported as 0.1 $\mu g/L$.

2.8.2.2 Aqueous Metolachlor

Samples collected between March and November 2004 were analysed by the Guelph Analytical Services Laboratory at the University of Guelph. The method required a $40ml$ sample and the method described by (Burns, 2005), a Master's Thesis completed concurrently with this study, is outlined as follows. Sample volumes of $20ml$ are combined with $2g$ of sodium chloride as a modifier. SPME extractions are performed using an $85\mu m$ polyacrylate fibre. The fibre was exposed to the headspace above the modified sample for 20 minutes while stirring at $900RPM$. A GC-μECD and a Restek Cl-Pesticides column was used to analyse the samples. The method detection limit was determined to be 1 $\mu g/L$, with a reporting limit of 5 $\mu g/L$.

Samples collected after December 2004 were analysed by Maxxam Analytics in Mississauga, Ontario. A $1L$ sample contained in an amber glass bottle was required. The samples were analysed using standard USEPA methods 0625, 8270B, 0525.1, and 3510C (USEPA, 2003, 1991, 1990, 1996a). This process involves transferring the water sample to a separatory funnel, and then fortifying the sample with surrogates to monitor the extraction process. The extraction uses an organic solvent and the subsequent organic extract is then concentrated and analyzed by the GC/MS. The method detection limit determined from this procedure was 0.5 $\mu g/L$.

2.8.2.3 Inorganic Hydrochemistry

Inorganic analyses were performed on wells UW13 and UW16B in February 2005. Samples were collected in $200ml$ polyethylene bottles and sent to Maxxam Analytics (formerly PSC

Analytical Services) in Bedford, Nova Scotia. No preservation or filtration was necessary in the field as it was done in the laboratory. The Rapid Chemical Analysis package (RCAp^{TM}) was used to analyse for thirty standard water quality variables which, when viewed collectively, give a broad and complete inorganic profile of the water. Dissolved metals analysis was also completed with the RCAp scan. All analyses are defined by USEPA or SM methods.

Field parameters were also collected including pH, temperature, and alkalinity. Alkalinity was determined in the field using a Hach Test Kit. This procedure involves collecting a 250 ml sample of groundwater and mixing in bromcresol green-methyl red indicator and then titrating the mixture using 1.6N sulphuric acid until the water is light pink in colour. The reading on the digital titrator equals the concentration of $CaCO_3$ in mg/L. pH was determined using an Orion 250A+ pH/mV/RmV/ORP meter and an Orion 9107BN triode with an Ag/AgCl internal reference system.

2.8.2.4 Environmental Isotopes

Environmental isotope samples, including tritium (^3H), deuterium (^2H), and ^{18}O, were collected from UW16B and UW13 in February 2005. The unfiltered groundwater samples were collected in $1L$ High Density Polyethylene (HDPE) Nalgene^{TM} bottles and sent to the Environmental Isotope Laboratory (EIL) at the University of Waterloo.

The method for tritium analysis developed by Drimmie et al. (1991a), uses liquid scintillation counting. The samples were enriched 15 times by electrolysis and then counted. The detection limit for enriched samples is 0.6 ± 0.8 tritium units (TU).

^{18}O samples were analysed using the method developed by Drimmie and Heemskerk (1993) which involves equilibrating the sample with CO_2. A VG MM 903 triple Faraday bucket collector mass spectrometer equipped with a 90^{o}, 9 cm radius magnet was used for analysis, with a method precision of $\pm 0.2‰$.

Deuterium analysis involved methods developed by Coleman et al. (1982) and Drimmie et al. (1991b). The analyses are performed on hydrogen gas produced from water reduced on hot manganese, with a method precision of $\pm 0.8‰$.

2.9 Hydraulic Head Measurements

2.9.1 Conventional Wells

Pressure transducers were installed in conventional wells to continuously monitor hydraulic head fluctuations around the site. Solinst^{TM} Model 3001 pressure transducers were installed in 8 conventional wells including holes installed in the overburden and holes installed in the bedrock. The Solinst^{TM} Leveloggers^{TM}, have a pressure range of 5 $psig$ with a maximum error of $\pm 0.2\%$ of the full scale or 0.7 cm. A Barologger^{TM} was also required to monitor changes in atmospheric pressure, this was installed in a conventional well above the water table; the error of the probe is $\pm 0.5cm$. All of the pressure transducers are connected to the surface with direct read cables so that the transducers do not need to be retrieved to download the data. Some direct read cables have malfunctioned and it is now necessary to retrieve some of the transducers manually to download the hydraulic head data.

2.9.2 FLUTe

In-situ^{TM} PXD-261 pressure transducers are integrated into the FLUTe multilevel system in order to continuously monitor the depth-discrete ports. All of the pressure transducers are connected to the surface by vented, kevlar reinforced quick connect cables connected to a Hermit 3000^{TM} data logger and all of the transducers recorded in 30 minute increments, synchronized across the site. T he pressure transducers have an error of $\pm 0.05\%$ of the full pressure scale (typically 100 *psia*) or 3.5 *cm*.

2.9.3 Westbay

The Westbay multilevel system does not contain built-in pressure transducers to monitor hydraulic head, instead, pressure transducers can be installed and continuously record and then be removed when needed. A string of 12 pressure transducers was installed in series for a period of two months from November 2005 to January 2006 in the Westbay system installed in UW3. This string of pressure transducers is referred to as a Modular Subsurface Data Acquisition (MOSDAX) system. The MOSDAX string is lowered inside the Westbay multilevel system and each transducer is secured manually at each monitoring port. The system is connected to a data logger and the hydraulic head was monitored continuously in 30 minute increments for the two month period.

The two shallowest zones (1 and 2) in the Westbay multilevel system had pressure transducers with a pressure range of 100 *psig* with an accuracy of $\pm 0.1\%$ of the full scale. The transducers installed in monitoring zones 3 to 14 have pressure ranges of 250 *psig*

which also have an accuracy of $\pm 0.1\%$ of the full scale. The resolution for both the 100 *psig* and the 250 *psig* pressure transducers is $\pm 0.025\%$ of the full scale.

Table 2.1: Drilling and completion details for the eight University of Waterloo (UW) coreholes on the study site. UW1, UW2 and UW16B are in the metolachlor source area and were used by Burns (2005)

Corehole ID	Drilling Start Date (dd/mm/yy)	Drilling End Date (dd/mm/yy)	Drilling Company	Drill Rod Size	Corehole Diameter (in)	Total Depth (mbgs)	Top of Rock (mbgs)	Casing Depth (mbgs)	Casing Diameter (in)	Ground Surface Elevation (masl)	Completion Status	Multilevel Installation Date
UW1	24/09/03	09/10/03	Geo-Environmental	HQ	3.78	157	26	29	4	309.22	blank FLUTe lined	*na*
UW2	23/10/03	04/11/03	Geo-Environmental	HQ	3.78	156	26	31	4	309.00	blank FLUTe lined	*na*
UW3	22/02/02	12/03/02	All-Terrain	HQ	3.78	144	30	34	4	313.89	14-zone Westbay	Oct-05
UW4	05/11/02	21/11/02	Geo-Environmental	HQ	3.78	149	23	25	4	307.18	9-port FLUTe	Aug-05
UW5	06/11/03	20/11/03	Geo-Environmental	HQ	3.78	151	22	26	4	306.74	11-port FLUTe	May-05
UW6	25/11/03	11/12/03	Geo-Environmental	HQ	3.78	165	34	37	4	320.84	12-port FLUTe	Aug-05
UW13	24/08/00	07/09/00	All-Terrain	PQ	5.00	150	35	38	5	319.27	10-port FLUTe	Feb-04
UW16B	02/03/00	15/03/00	Davidson Well Drilling	*na*	5.63	100	29	36	6	309.13	15-port FLUTe	July-00[a]
UW16B (Deep)	10/10/03	16/10/03	Geo-Environmental	HQ	3.78	135	*na*	*na*	*na*	*na*	*na*	*na*

[a]Removed in December, 2001 and re-installed in June, 2004 with In-Situ^{TM} pressure transducers.

Table 2.2: Different rock core analysis methods used for different drilling years. Adapted from Burns (2005).

Parameter	MDL ($\mu g/L$) in extract			Extractant (HPLC Grade)			Bottle Volume (ml)			Extractant Volume (ml)			Analysis Technique[a b]		
	2000	2002	2003	2000	2002	2003	2000	2002	2003	2000	2002	2003	2000	2002	2003
Metolachlor	0.07	1.0	0.7	Water	Pentane	Hexane	125	125	40	60	60	18	SPME	GC with ECD detector[c]	GC with ECD detector[d]
TCE	0.1	0.1	0.1	Methanol	Methanol	Methanol	125	125	40	60	60	18	GC with ECD detector	GC with ECD detector	GC with ECD detector
PCE	0.1	0.1	0.1	Methanol	Methanol	Methanol	125	125	40	60	60	18	GC with ECD detector	GC with ECD detector	GC with ECD detector
c-DCE	3.5	3.5	3.5	Methanol	Methanol	Methanol	125	125	40	60	60	18	GC with ECD detector	GC with ECD detector	GC with ECD detector
t-DCE	5.3	5.3	5.3	Methanol	Methanol	Methanol	125	125	40	60	60	18	GC with ECD detector	GC with ECD detector	GC with ECD detector

[a]GC: direct on-column injection unless otherwise stated.
[b]UW Lab used for analyses unless otherwise stated.
[c]splitless injection.
[d]University of Guelph Laboratory used for analysis.

Table 2.3: Physical property measurements, which include matrix porosity, matrix permeability,and wet and dry bulk densities, for the nine lithologic units. Adapted from Burns (2005).

Unit ID		**Number of Samples Analysed**	**Lab-Measured Physical Properties**									
			Matrix Porosity (%)		**Permeability (cm^2)**		**Wet Bulk Density (g/cm^3)**		**Dry Bulk Density (g/cm^3)**		f_{oc} (%)	
Plett (2006)	Burns (2005)		*Range*	*Average*	*Range*[a]	*Average*	*Range*	*Average*	*Range*	*Average*	*Range*	*Average*
a	G	5	4.1–12.0	8.0	8.4E-13–1.1E-10	2.5E-11	2.62–2.69	2.66	2.53–2.62	2.58	0.005–0.030	0.014
b	E	8	2.5–10.1	5.5	9.9E-15–9.8E-10	1.6E-10	2.33–2.79	2.62	2.26–2.78	2.56	0.003–0.030	0.010
c	A	4	3.6–15.3	6.7	9.9E-15–5.0E-11	1.5E-11	2.55–2.72	2.64	2.40–2.67	2.54	0.005–0.014	0.008
d	B	7	5.8–12.5	9.0	9.9E-15–4.3E-12	9.7E-13	2.58–2.75	2.68	2.46–2.70	2.61	0.006–0.018	0.012
e	I	4	5.5–10.4	8.6	9.9E-15–9.6E-11	2.5E-11	2.59–2.92	2.69	2.47–2.82	2.59	0.003–0.015	0.010
f	C	5	1.2–7.4	4.7	9.9E-15–1.2E-11	4.9E-12	2.20–2.74	2.60	2.15–2.70	2.52	0.003–0.027	0.013
g	F	4	4.1–11.0	6.1	9.9E-15–1.3E-9	3.3E-10	2.61–2.75	2.67	2.52–2.70	2.61	0.005–0.017	0.012
h	H	4	0.8–4.2	2.6	9.9E-15–2.8E-12	7.1E-13	2.66–2.82	2.75	2.56–2.78	2.69	0.023–0.125	0.056
i	D	5	2.3–16.7	9.7	9.9E-15–1.3E-9	1.5E-11	2.39–2.78	2.65	2.43–2.67	2.60	0.059–0.132	0.089
DOLOSTONE			0.8–15.3	6.8	9.9E-15–1.3E-9	1.6E-10	2.20–2.92	2.67	2.15–2.82	2.59	0.003–0.125	0.017
SHALE			2.3–16.7	9.7	9.9E-15–1.3E-9	1.5E-11	2.39–2.78	2.65	2.43–2.67	2.60	0.059–0.132	0.089

[a]The indicated low-end detection limit of the permeability equipment is 9.9E-15 cm^2.

Table 2.4: UW16B FLUTe multilevel system port locations.

Port ID	Top Elevation (masl)	Bottom Elevation (masl)	Port Length (m)	Transducer
1	273.7	272.2	1.5	Y
2	270.4	268.8	1.6	Y
3	266.4	264.9	1.5	Y
4	262.5	260.6	1.9	Y
5	256.4	254.9	1.5	Y
6	250.5	248.9	1.6	Y
7	246.3	244.8	1.5	Y
8	243.0	240.9	2.1	N
9	239.9	237.6	2.3	Y
10	234.0	232.5	1.5	Y
11	230.8	229.1	1.7	Y
12	226.7	225.2	1.5	Y
13	224.3	220.9	3.4	Y
14	216.8	215.3	1.5	Y
15	211.1	209.6	1.5	Y

Table 2.5: UW5 FLUTe multilevel system port locations.

Port ID	Top Elevation (masl)	Bottom Elevation (masl)	Port Length (m)	Transducer
1	280.64	273.40	7.2	Y
2	264.00	261.15	2.8	N
3	253.55	250.93	2.6	Y
4	248.57	246.12	2.4	N
5	243.66	240.20	3.5	N
6	238.91	234.57	4.3	Y
7	232.92	229.00	3.9	Y
8	217.73	214.06	3.7	N
9	212.24	210.86	1.4	N
10	193.00	185.76	7.2	N
11	176.44	173.90	2.5	Y
12	166.21	160.92	5.3	Y

Table 2.6: UW4 FLUTe multilevel system port locations.

Port ID	Top Elevation (masl)	Bottom Elevation (masl)	Port Length (m)	Transducer
1	281.56	274.96	6.6	Y
2	270.50	267.43	3.1	N
3	264.48	262.03	2.4	N
4	257.18	253.95	3.2	Y
5	248.17	246.08	2.1	N
6	244.64	242.67	2.0	N
7	238.41	235.12	3.3	Y
8	216.77	213.30	3.5	Y
9	206.46	202.08	4.4	N
10	195.25	190.73	4.5	N
11	178.91	173.42	5.5	Y
12	164.65	161.88	2.8	Y

Table 2.7: UW13 FLUTe multilevel system port locations.

Port ID	Top Elevation (masl)	Bottom Elevation (masl)	Port Length (m)	Transducer
1	279.17	276.97	2.2	Y
2	273.87	271.67	2.2	Y
3	266.77	261.67	5.1	Y
4	249.27	243.37	5.9	Y
5	232.77	227.47	5.3	Y
6	223.77	220.27	3.5	Y
7	211.77	209.77	2.0	Y
8	202.77	199.17	3.6	Y
9	185.77	184.27	1.5	Y
10	173.67	172.27	1.4	Y

Table 2.8: UW6 FLUTe multilevel system port locations.

Port ID	Top Elevation (masl)	Bottom Elevation (masl)	Port Length (m)	Transducer
1	283.74	279.18	4.6	Y
2	269.53	267.16	2.4	N
3	263.82	260.48	3.3	N
4	249.90	248.60	1.3	N
5	243.76	241.36	2.4	N
6	236.59	234.68	1.9	Y
7	232.79	230.60	2.2	Y
8	227.97	223.39	4.6	N
9	208.05	204.93	3.1	Y
10	189.99	186.90	3.1	N
11	175.53	172.57	3.0	Y
12	166.70	163.70	3.0	Y

Table 2.9: UW3 Westbay multilevel system zone locations.

Zone ID	Top Elevation (masl)	Bottom Elevation (masl)	Zone Length (m)	Transducer
1	282.57	278.29	4.3	Y
2	277.09	274.94	2.2	Y
3	274.04	271.59	2.5	Y
4	270.69	269.48	1.2	Y
5	265.51	262.75	2.8	Y
6	261.85	260.64	1.2	Y
7	256.36	255.15	1.2	Y
8	254.23	251.49	2.7	N
9	250.57	239.30	11.3	Y
10	238.38	235.95	2.4	Y
11	235.02	232.26	2.8	Y
12	231.36	229.55	1.8	Y
13	228.62	226.50	2.1	N
14	225.57	223.75	1.8	Y

Chapter 3

Results

3.1 Geology

Various forms of porosity exist in the cores obtained from Cambridge, Ontario. Matrix porosity consists of pinpoint and vuggy porosities. Figure 3.1 illustrates the various forms of porosity seen in core taken from the Cambridge site. These forms exist together as well as separately and are described by Najiya (2003) as pores less than or equal to $3mm$ and pores greater than $3mm$, respectively. Fracture porosity is significant in its relation to contaminant flow and distribution throughout the aquifer. Both vertical and more prominently, horizontal fractures were identified in the core. Some fracture surfaces were stained with iron or manganese oxides and these fractures were likely hydraulically active at some point in the past and are possibly still active. Stylolites represent a form of fracture porosity. These features are similar to bedding planes and were seen throughout the core. According to Langer (1999); Langer et al. (1999), the term stylolite is generic and does not imply a specific composition. Stylolites are produced by pressure dissolution

due to loading or tectonically related stress, which causes carbonates to become mobilized therefore concentrating relatively insoluble residual phases such as organic matter in these internal discontinuities (Langer, 1999).

Corelog Units were defined on the transect based on porosity, fracture frequency, stylolite abundance, and other features such as fossils. Figure 3.2 shows the 24 Corelog Units and the nine lithologic units based on matrix characteristics. Figure 3.3 shows the corelog correlation along the transect. Correlation between coreholes was accomplished based on visual description corelogs from the various coreholes. Each of the corelogs was analysed and divided into Corelog Units, the units that had similar characteristics were then visually correlated across the transect. The overburden was not analysed in this study and therefore only a very general representation is shown in Figure 3.3; the overburden data were obtained from work by Turner (2001). The corelogs are variable over the extent of the transect and some units are only found in one or two coreholes.

The overburden-bedrock interface unit, which is the uppermost bedrock unit, ranges in thickness from approximately 0.5 m to 2 m, and is very weathered and usually broken-up and fractured with iron staining visible on most fracture surfaces. This unit was observed in all coreholes along the transect and due to its lack of competence, casing was installed approximately 3 m (10 ft) from the top of rock, through this unit and into the underlying competent rock. The top of rock occurs at approximately 285 m above sea level asl, with the range of top-of-bedrock elevations between 287 and 284 $masl$.

A unit in the middle of the dolostone aquifer at approximately 235 $masl$, labeled as Corelog Unit J, was found in all of the coreholes along the transect except at UW13. This

unit is similar to the Eramosa unit described in Najiya (2003), Lotowater Ltd. (1997), and Langer (1999); however, it did not contain the most typical form described by Sanford (1969) as dark greyish brown to black, bituminous dolostone, with localized limestone and shale. The Eramosa unit is described in this study as having moderate to low pinpoint porosity, abundant stylolites, few fractures and occasional fossils. UW13 has an unusual corelog relative to the other transect holes and shows transition zone units (Corelog Unit V) at elevations of approximately 235 $masl$ and 210 $masl$. Corelog Unit V is described in this study as massive dolostone with no fractures, no stylolites and abundant pyrite and glauconite and it is typically found at the boundary with the shale at 175 $masl$. This unit has a characteristic spike in the gamma log which defines the transition zone above the shale and the underlying shale. Shale values typically have greater than the maximum scale value of 100 counts per second (cps). Corelog Unit V and the shale were not clearly defined in the gamma log obtained from UW13.

The abundance of Corelog Units is related to the complex and highly variable fracture network in the dolostone aquifer on site. Lotowater Ltd. (1997) concluded that the hydrostratigraphic units are not well defined in the aquifer and that the development of a stratigraphic correlation of aquifer and aquitard zones within the dolostone aquifer is difficult. The Corelog Units were defined to identify zones of hydraulic activity within the aquifer. Therefore, units could have a similar description and only differ by fracture frequency or stylolite abundance. This classification scheme was also used to identify matrix properties which is discussed below. The underlying Rochester Formation shale characterized by Corelog Unit W and described as dark shale with interbedded dolostone,

is referred to as the bottom of the aquifer system for this study and is considered an aquitard. The data supporting this conclusion will be discussed further in section 4.

The twenty-four Corelog Units were subdivided into nine lithology units based on matrix characteristics. Figure 3.4 shows the correlation of matrix lithology along the transect which has much greater continuity than the Corelog Units. The matrix lithology continuity indicates the complexity of the fracture network and identifies the zones within the dolostone aquifer that may be more influenced by matrix diffusion and sorption. These matrix lithology units were classified concurrently with Burns (2005), however, Burns (2005) used a previous version of the classification (Table 2.3). Figure 3.4 represents the matrix characteristics which are essential in determining the rock's potential for chemical sorption. Rock units that contain higher organic carbon content (i.e. stylolites) potentially have a greater capacity for chemical sorption (Langer, 1999; Langer et al., 1999). This would suggest that lithology unit *b*, because it is densely stylolitic, could potentially retard the transport of contamination. Figure 3.3, conversely represents the Corelog Units based partly on fracture frequency. The units with abundant fractures likely offer a lower resistance to fluid flow and therefore could be active pathways for contaminant transport. Figures 3.3 and 3.4 represent the core log data from the coreholes along the transect from two different points of view, however they both play an important role in determining contaminant fate and transport through the dolostone aquifer.

Figures 3.5 to 3.9 show the detailed corelogs for each transect corehole along with the acoustic televiewer data and the gamma log collected from each corehole. Acoustic televiewer data were collected from UW13, however the resolution was poor and was

therefore not included in Figure 3.7. The Eramosa unit, which is evident when viewing the gamma log, is represented by a distinct peak in the log at approximately 235 *masl*. This is consistent with the description of the Eramosa unit by Lotowater Ltd. (1997), which states that the Eramosa Member has significantly higher gamma and lower (electrical) resistivity values on geophysical logs than the overlying Guelph Formation beds. Burns (2005) also shows the presence of a gamma log peak coincident with the Eramosa unit in the source area of the study site (i.e. UW16B, UW1, UW2). UW13 and UW3 are the only coreholes on the transect not to show a gamma peak at 235 *masl*. The Eramosa unit was not described in the corelog from UW13 (Turner, 2001), however it was described in the UW3 corelog. The weakened gamma signature is likely due to a large washout in that zone during drilling, affecting the corehole diameter and reducing the signal returning to the probe. Core was collected from this zone for analyses, however the corehole wall was not intact when the gamma log was performed and therefore produced a weak signal. Figure 3.10 shows the gamma logs in transect with the Eramosa unit highlighted. This gamma peak occurs at approximately the same elevation as Corelog Unit *J* in each corelog. Core logs for UW13 (Turner, 2001) did not describe the Eramosa unit (Corelog Unit *J*), and gamma logs did not detect the typical peak at this location, however the Eramosa unit was described by Najiya (2003) who logged the same core as Turner (2001) and found the Eramosa Member to be 20 *m* thick. Najiya (2003) described the Eramosa Member as a light-grey to dark-grey brachiopod-bryozoan wackestone, with biomold porosity. A simplified lithologic column, based on work completed by Najiya (2003), is presented next to the gamma log in Figure 3.11 to show the absence of the gamma signature at UW13

and therefore the absence of the Eramosa unit.

Karst features may be present in the aquifer as evidenced by Figure 3.12 which shows images from borehole videos collected in UW3, UW5, and UW6. The images from UW3 show the large washout zone at approximately 245 *masl* with debris and large pieces of rock. The image from UW5 show pebbles and cobbles that are rounded and smooth at approximately 245 *masl*. The images from UW6 are taken at two different elevations, one at 237 *masl* and the other at 280 *masl*. The image taken at 237 *masl* shows a large vug nearly the circumference of the corehole. Although the connection to the aquifer is uncertain the image taken at 280 *masl* shows rounded, smooth cobbles and in the video, flow velocities were very high as indicated by a "streamer" showing the flow. The first corehole drilled by Turner (2001) (UW16A), located approximately 7 *m* south of UW16B, was abandoned after the corehole continuously collapsed and at 41.8 *mbgs* (267.4 *masl*), drilling was stopped. The collapsing of the corehole may have been due to large voids (conduits) or highly rubblized rock zones and video logs performed by Turner (2001), acquired after drilling, showed large washout zones just below the casing at approximately 25 *mbgs* (284.3 *masl*), similar to what was observed in UW3. Lotowater Ltd. (1997) concluded that measurable groundwater flow intervals within the dolostone aquifer usually coincide with planar macropores. The planar macropores are interpreted to be solution-altered fractures and bedding planes (Lotowater Ltd., 1997) which can be considered to be karst features. These karst features may provide laterally continuous conduits for preferred groundwater flow pathways and chemical transport or they may be local features that are limited in lateral extent and interconnect with the fracture network, and observed

flow conditions in the corehole may be local effects enhanced by the corehole connection. Although the aquifer on a whole is not considered as typically karstic (Perrin et al., 2006), determining the presence and locations of these karst features may help in determining the controls on the characteristics of the contaminant plumes.

3.2 Hydraulic Conductivity

Hydraulic testing of the aquifer using straddle packers set at 2.2 m spacing with constant head injection determined the transmissivity variations with depth and the bulk hydraulic conductivity from transmissivity values is calculated using the Theim equation. The bulk hydraulic conductivity represents both matrix and fracture hydraulic conductivities, however it is the fracture hydraulic conductivity that is the most significant because groundwater flow occurs predominantly in the fracture network on site (Lotowater Ltd., 1997), and therefore contaminant transport will most likely occur in the hydraulically active fractures. Figure 3.13 shows hydraulic conductivity values from the corehole along the transect and from UW16B as a comparison for the source area. Although the upper measurement limit for hydraulic conductivity of the straddle packer system is reported by Turner (2001) to be 5×10^{-5} m/s some values were greater than this value. For each test interval the straddle packer procedure involved three test repetitions, each with a higher constant pressure; the first test was performed at 3-4 psi. A hydraulic pressure value was recorded for this test pressure increment, however when a second test was performed at a higher constant pressure, no head increase was recorded by the pressure transducer in the test zone and therefore could not be tested further. Values above 5×10^{-5} m/s are

presented in Figure 3.13, however these values should be taken as $\geq 5 \times 10^{-5}$ m/s. UW3 was not tested, however Figure 3.13 shows a hypothetical hydraulic conductivity for the washout zone which would likely be above the upper limits of the test system.

Each corehole along the transect has a highly variable bulk horizontal hydraulic conductivity versus depth profile with differences of up to 4 orders of magnitude occurring even between adjacent 2.2 m test zones. There is a thick zone with many relatively high hydraulic conductivity test intervals along the transect in the middle part of the dolostone aquifer at 250-230 $masl$. This elevation corresponds to the zone where karst features were observed in the borehole video (Figure 3.12) and is also positioned at or just above the Eramosa unit as defined by the gamma logs (Figure 3.10) and as Corelog Unit J in Figure 3.3.

The hydraulic conductivity profiles with depth gradually decrease near the dolostone shale interface (Figure 3.13). UW5 and UW4 are the only two coreholes to have tests performed in the shale and the values show very low hydraulic conductivity and some values lie below the lower limit of the test system at 5×10^{-11} m/s. These layered, very low horizontal hydraulic conductivity values for some intervals in the shale suggest that the vertical hydraulic conductivity of the shale is likely low as well. The vertical hydraulic connectivity in the shale will be discussed further in section 3.3.

The FLUTe hydraulic conductivity profiling method was used for determining formation hydraulic conductivity. Figure 3.14 shows the FLUTe profiling data compared to the straddle packer testing results. Data collected above 220 $masl$ for the FLUTe profiling method were not used due to problems associated with the measurements. Due to the

relatively small hole diameter (9.6 *cm*), and high permeability of the upper part of the aquifer, the rate of descent of the FLUTe liner was above the limit of the data encoder causing the data to be problematic above 220 *masl*. Frictional resistance and drag of the liner on itself as the liner was installed into the corehole also provided errors in the data and not until all of the liner material was beneath 220 *masl* did the data become usable (Keller, 2005). The FLUTe profiling method compared very well below 220 *masl* with the straddle packer data. The highest hydraulic conductivity intervals from straddle packer testing correspond closely in vertical position to the highest hydraulic conductivity values from FLUTe profiling. Although the magnitude of the changes in the respective logs are not everywhere similar, the general shape is similar as well as the maximum values from each method.

3.3 Hydraulic Head

Hydraulic head measurements were collected from all multilevels along the transect as well as the multilevel installed in the source area (UW16B). Vertical hydraulic head profiles shown on Figure 3.15 for UW16B provide results from the source area for comparison to the transect. Figure 3.15 shows vertical head profiles recorded at three representative times in the FLUTe multilevel system in UW16B. Ports 1-5 show a strong downward component of gradient and below port 5 no dominant trend in the vertical component of gradient exists but there is a minor gradient reversal between ports 10 and 13. There does not appear to be any stratigraphic or lithologic correlation which coincides with this minor gradient reversal, however a slight decrease in hydraulic head does occur where

the gamma peak of the Eramosa unit occurs suggesting that at this location this zone has lower vertical hydraulic conductivity. The vertical hydraulic profiles for UW5 (Figure 3.16) shows a decreasing trend with depth. Port 1 has the highest head and there is a vertical gradient towards port 3. No strong vertical gradient exists between ports 3 and 6. The Eramosa unit, indicated by the thin gamma peak, coincides with a vertical head differential of 0.09 which divides the upper Guelph Formation dolostone from the underlying Lockport Formation dolostone. Also, the Eramosa unit at this location has a 3 orders of magnitude decrease across the Eramosa unit based on straddle packer test hydraulic conductivity (Figure 3.16).

The FLUTe multilevel system installation in UW5 was interrupted half way into the installation of port 11, and the installation was not completed to the bottom of the corehole. Therefore the hydraulic head from the bottom port (11) of UW5 is a blended head over the vertical interval from the port location to the bottom of the hole at approximately 150 *mbgs*. The hydraulic conductivity profile from Figure 3.16 shows that there is an interval of higher hydraulic conductivity at the top of port 11, therefore this zone may provide the largest influence on the hydraulic head value for port 11.

Figure 3.17 shows results from the 12-port FLUTe multilevel system installed in UW4. Of the 6 pressure transducers installed in UW4, one (port 8) malfunctioned. Unfortunately this transducer would have provided the head differential, if any, across the Eramosa unit. A large head drop is present in the shallowest port (1) and then a slight vertical component of gradient exists between ports 7 and 11. Port 12, located in a zone of highest hydraulic conductivity in the shale, shows a slightly higher hydraulic head that increased with time

over the three month period, suggesting slow recovery to equilibrium conditions. It is difficult to determine if there is any influence on the hydraulic head profile from the Eramosa unit at this location due to the malfunction of the transducer in port 8, however there does not appear to be any obvious stratigraphic influences other than in port 12 where there is a higher hydraulic head in the underlying Rochester Formation shale.

The vertical head profiles in Figure 3.18 are from the 10-port FLUTe multilevel system installed in UW13. A slight vertical gradient is present through the aquifer with the lowest head at the deepest aquifer port (9). What is notably distinct in UW13 is the lack of a steep vertical gradient at the top of the Guelph Formation and a large head differential in the Rochester Formation of almost 3 m. The head in port 6 is slightly higher than port 5, which coincides with the zone of highest horizontal hydraulic conductivity indicated by the straddle packer tests (Figure 3.18).

Figure 3.19 shows the vertical hydraulic head profile collected from the 12-port FLUTe multilevel system installed in UW6. There is a large vertical gradient between the top port situated near the top of the bedrock and port 6 which is positioned just above the Eramosa unit. These two ports (1 and 6) occur in zones of high hydraulic conductivity. Below port 6, ports 7, 9, 11, and 12 show no significant vertical gradient. Ports 6 and 7 bound the Eramosa unit and show no evidence of any stratigraphic influence, however there is a slight increase in head between ports 6 and 7 which is consistent with time (Figure 3.19). Port 12, situated in the shale, has a very similar hydraulic head value to port 11, therefore the shale appears to be hydraulically connected to the overlying dolostone aquifer at this location.

Corehole UW3, drilled on the eastern end of the transect and fitted with a 14-zone Westbay multilevel system, was monitored for a period of two months between November 2005 and January 2006 using a string of 12 pressure transducers referred to as the MOSDAX system. Figure 3.20 shows the data from November and December 2005 along with the detailed corelog and gamma log. The shallowest zone (1), installed at the top of bedrock, shows a very high hydraulic head and then a very large vertical hydraulic gradient (1.54) occurs between the next zone (2), approximately 2 m lower. This is the highest vertical gradient observed in all multilevel systems along the transect. The large vertical hydraulic gradient (1.54) occurs between the highly fractured and weathered Corelog Unit A and Corelog Unit B, which is much more competent. A gamma peak at approximately 277 $masl$ shows Corelog Unit B has a higher clay content than the overlying unit which could also contribute to the vertical head differential. From zone 2 to zone 3, there is a slight head loss and then below zone 3 there are no vertical gradients between zones. Although zone 9 is situated over a large washout zone, described as the Eramosa unit in corelogs, no vertical head differential is present across that unit.

The highest hydraulic head values in each profile occur at approximately 280 $masl$ at the top of rock and this top-of-rock head value is relatively high compared to the next lowest (adjacent) port along the transect. This shows the influence of a vertical flow restrictor shallow in the Guelph Formation except UW13 and to a lesser extent in UW5. There is some vertical hydraulic head influence due to the Eramosa unit, however it is discontinuous laterally across the transect. The vertical hydraulic head influence from the Eramosa unit is only strongly observed in UW5 and with much less effect in UW6 and

UW13. The influence of the Eramosa unit on the vertical head profile of UW4 is uncertain due to a pressure transducer malfunction. There does not appear to be a substantial difference in hydraulic head between the Guelph and Lockport formation dolostone, however UW5 did show a distinct vertical head differential between the formations; the shallower Guelph Formation has the higher hydraulic head. Of the three coreholes with monitoring ports in the shale (UW13, UW4, UW6), two (UW13 and UW4) showed a distinct vertical gradient from the shale to the overlying dolostone aquifer.

Three holes were installed in the overburden using a rotosonic rig. These holes were fitted with modified 15-port Waterloo multilevel systems, for monitoring hydraulic head in the Quaternary overburden deposits; these systems and the instillation methods are described by Parker et al. (2006a). Multilevel systems were installed near UW16B in the source area, UW4 on the western end of the transect and UW3 on the eastern end of the transect. By combining the vertical hydraulic head profiles from these overburden multilevel systems with the vertical hydraulic head profiles from the bedrock multilevel systems, a better understanding of the vertical head distribution can be seen for the entire system. Figure 3.21 shows these composite profiles of the overburden head and the bedrock head. The data from the overburden were acquired in July 2004 and the bedrock data were taken on November 2005. Although these data were collected at different times, the bedrock profiles are very consistent as can be seen in Figures 3.15 to 3.20, and therefore these profiles are likely representative of the site conditions. Each composite hydraulic head profile shows a large head loss between the top of the groundwater zone to approximately 296 *masl*, below which the vertical gradient is nearly absent. The profile

for the source area (UW2-OB/UW16B, Figure 3.21), shows a neutral downward gradient above the bedrock boundary which is related to the zone of increased hydraulic connection between the overburden and the bedrock where it is believed the initial contaminants were able to reach the bedrock. The hydraulic head drops at the top of bedrock and the gradient persists through the top 10 m of rock and then no vertical gradient is present. The profile at UW4 (Figure 3.21), shows a slight decrease in hydraulic head at the overburden-dolostone interface, and then a head drop in the top 10 m of bedrock. UW3 (Figure 3.21), shows a significant head drop just above the overburden-dolostone interface, however the vertical gradient is neutral into the bedrock and then there is a strong vertical gradient from 278 to 276 $masl$, below which is a neutral vertical gradient. Therefore it is apparent that there is a greater hydraulic connection between the overburden and the dolostone at the source area and that there is a strong vertical gradient in the top 10 m of bedrock which is greater than the gradient in the bottom part of the overburden.

Figure 3.22 shows a comparison of the vertical hydraulic head profiles between the 15-port FLUTe multilevel system installed in UW16B and the 14-zone Westbay multilevel system installed in UW3. These two coreholes monitor approximately the same area of dolostone aquifer and have a similar number of monitoring ports, although UW3 monitors higher in the aquifer. There is a greater fluctuation in the hydraulic head profile for UW16B than in UW3. Since the FLUTe system has a continuous seal along the length of the corehole except where spacers are located at monitoring ports, cross connection of fractures is minimized and influences from other monitoring ports are low. This is in contrast to the Westbay system where seal lengths (2 m) are comparatively shorter and

packers are only installed above and below monitoring zones. This could increase the probability of cross connection between zones and could cause vertical head profiles to be blended, disguising zones of influence. It is difficult to determine if the differences between the hydraulic head profiles are related to the design of the multilevels; this can only be addressed by having the two systems installed in the same hole with the FLUTe system being installed and removed followed by a Westbay installation.

Figures 3.23 to 3.26 show hydrographs collected from the multilevel systems over a period of two weeks from December 1-14, 2005. Hydraulic head data were collected continuously from the time the multilevel system was installed and this two-week period was taken as representative along the transect. As can be seen by the plots, the hydraulic response is nearly identical for all ports throughout the entire depth of the aquifer. This would suggest a highly interconnected fracture network. All of the coreholes along the transect show a very similar temporal response to the pumping wells, with an increased head on a Friday and then decreasing again by Monday. This suggests that the fracture network is highly interconnected vertically as well as horizontally, which is consistent with Parker et al. (2006b) and Lotowater Ltd. (1997). The hydrographs from UW4 (Figure 3.24), UW6 (Figure 3.25), and UW3 (Figure 3.26), show the uppermost monitoring ports have a dampened response to municipal pumping relative to deeper ports, this is also seen by Parker et al. (2006b) at the metolachlor source area, and they conclude that this is related to zones of lower vertical hydraulic conductivity within the upper 12 m of rock. This is consistent with the largest head differentials occurring between the shallowest port and the next deepest ports in the dolostone aquifer. The ports installed in the underly-

ing Rochester Formation shale also show a dampened response to aquifer pumping which shows the shale acts as an aquitard.

The vertical hydraulic head profiles and the hydrographs taken from the coreholes along the transect suggest the presence of multiple flow zones within the aquifer, this is illustrated in Figures 3.27 and 3.28. These two figures show contours of hydraulic head along the transect taken from the multilevels and conventional wells OW24, OW42, and OW13. Each figure shows a strong downward gradient in the upper 10-15 m of bedrock below which appears to be a gradient shift from east to west along the transect. Minor fluctuations in the hydraulic head magnitude occur between Figures 3.27 and 3.28, however the general gradient trends are similar.

Plots of the potentiometric surfaces at 270 *masl* (Figures 3.29 and 3.30) show a flow direction towards the transect in a southern direction. Figures 3.29 and 3.30 are similar to figures presented in Burns (2005), however the current figures were contoured using computer software instead of by hand. Deeper potentiometric surfaces at 255 *masl* and 235 *masl* are plotted in Figures 3.31 and 3.32. These figures show a change of flow direction of almost 90 degrees towards the west. More data points are required to verify this direction change, however this direction concurs with the regional flow direction towards the Grand River to the west (Figures 3.33 and 3.34). However, Figures 3.33 and 3.34 were plotted by Lotowater Ltd. in 1997 and regional pumping rates may have changed and flow directions could have been altered since that time.

3.4 Rock Core Concentrations

3.4.1 Metolachlor

The results of the rock core samples analysed for metolachlor were reported from the laboratory as total mass of metolachlor per mass of wet rock (Figure 3.35); these data include the metolachlor mass sorbed onto the rock matrix as well as the mass in the porewater. No clear trends are observed from the data as each corehole is highly variable with depth (Figure 3.35).

When the analytical results are converted to equivalent porewater concentrations as described in section 2.4, the trends are the same as the total rock core data and the decrease in detection limits in the shale are attributed to higher sorption (Figure 3.36). In the UW5 profile (Figure 3.36), the samples with detectable metolachlor concentrations occur between approximately 260 and 225 $masl$, with the peak concentration of 318 $\mu g/L$ occurring at 232 $masl$. Results from UW4 are sporadic and of the 10 samples with detectable levels of metolachlor, only 5 were quantifiable. The peak concentration of 301 $\mu g/L$ occurred at approximately 187 $masl$. Although UW13 has detectable metolachlor concentrations throughout the entire aquifer and into the underlying shale, it has the lowest porewater concentrations of the transect holes. The highest concentrations occur in the upper part of the aquifer between 283 to 247 $masl$ and the maximum concentration of 51 $\mu g/L$ occurs at approximately 263 $masl$. All detectable metolachlor results from UW6 occur between 240 and 200 $masl$. The maximum concentration in UW6 is 241 $\mu g/L$ found at approximately 201 $masl$. No metolachlor analyses were done on rock core

from UW3 due to an adverse reaction between the bottle septa and the pentane used for preservation and extraction. This caused the septa to leak, which compromised the samples.

Figure 3.37 shows the rock core data converted to equivalent porewater concentrations contoured along the transect; the data are displayed using log concentrations. This figure shows much less metolachlor at UW13 with highest concentrations to the east and west. These results were contoured with the linear kriging option and used an anisotropy ratio of 8:1, which reflects the strong horizontal fracture and bedding planes throughout the site, which shows the lateral spreading of the plume do to transverse dispersion and matrix diffusion.

3.4.2 TCE

The rock core TCE results are reported from the laboratory as total mass of TCE per mass of wet rock. These data, presented in Figure 3.38, include the mass sorbed onto the rock matrix as well as the mass in the porewater. Each corehole shows variable but low concentrations throughout the aquifer and the majority of the samples are non-quantifiable. Although Figure 3.38 exhibits no obvious trends, there are more detectable values at 250-230 $masl$, peak concentrations appear between these elevations, except in UW13. UW13 has the highest concentration of TCE in the rock core of any corehole along the transect (1354 $\mu g/L$).

Figure 3.39 presents the rock core data converted to an equivalent porewater concentration for coreholes along the transect. The trends between TCE distributions shown

on Figure 3.38 and 3.39 are similar. The detection limits decrease at or near the shale-dolostone interface due to sorption. With higher sorption in the rock matrix of the shale, contaminants are less likely to go into solution and therefore contaminants have a much lower concentrations in the shale. Although TCE was found throughout the entire length of the dolostone aquifer and into the underlying shale at UW5 (Figure 3.39), the quantifiable detections were concentrated in an area between 253 and 235 $masl$. The maximum concentration of 120 $\mu g/L$ occurred at 237 $masl$. UW4 also had detectable concentrations of TCE throughout the aquifer, however there were only two quantifiable detections located at approximately 244 $masl$. Stated earlier, UW13 has the highest concentration of TCE in the rock core and it has quantifiable detections throughout the entire aquifer. There appears to be three zones where quantifiable detections occur; 280-255 $masl$, 245-220 $masl$, and 180-170 $masl$. The maximum concentration of TCE occurs at 262 $masl$ (1354 $\mu g/L$). UW6 has the least amount of TCE detections, and only three of them are quantifiable. The peak concentration of 142 $\mu g/L$ occurs at 262 $masl$. UW3 had the least amount of non-detects of all the coreholes and retained a relatively consistent concentration profile with depth. The maximum concentration occurred at 242 $masl$ (353 $\mu g/L$).

Figure 3.40 shows the contoured rock core log concentrations converted to equivalent porewater concentrations. This contoured TCE distribution shows the low concentrations found in UW6 and the high concentrations found in UW4 and UW13. Figure 3.40 also shows the "hot spots" in the various coreholes, represented by darker shades of red. These data were contoured using the linear kriging option in Surfer 8^{TM} and an anisotropy ratio

of 8:1, which reflects the strong horizontal fracture and bedding planes across the site. This anisotropy in the flow direction will be discussed further in a later section.

3.4.3 Other VOCs

In this section, other VOCs refers to PCE, c-DCE, and t-DCE, all of which were analysed along with TCE in the rock core. Figure 3.41 shows the total PCE concentrations in the rock core. Detectable PCE concentrations are found throughout the entire depth of the aquifer in all of the coreholes along the transect, however very few of the detectable concentrations are quantifiable. Most of the quantifiable detections occur above 220 *masl*. UW3 is the only corehole along the transect not to have any quantifiable PCE detections. Turner (2001) states that PCE is a common impurity in commercially available TCE, however due to the large number of PCE detections, PCE may be a part of a multi-component DNAPL source.

Figure 3.42 shows the total c-DCE rock core concentrations for the coreholes along the transect. Rock core data from UW4 was not analysed for c-DCE. As was the case for PCE in Figure 3.41, c-DCE is detected throughout the entire depth of the aquifer in all of the corehole that analysed for c-DCE along the transect. Both UW5 and UW6 have no quantifiable detections of c-DCE. UW13 has the highest concentrations of c-DCE in the rock core and all of the detectable concentrations are found above 220 *masl*. UW3 has detectable concentrations of c-DCE throughout the entire depth of the corehole.

Figure 3.43 shows total t-DCE rock core concentrations for the coreholes along the transect, both UW4 and UW3 were not analysed for t-DCE. Of the wells that were analysed

for t-DCE, very few detections were found. UW5 has one detectable t-DCE concentration, although not quantifiable, at approximately 258 *masl*. The rock core data analysed from UW13 has the highest concentrations and the highest number of detections for t-DCE. The maximum concentration occurs at approximately 278 *masl* and it is also the highest total rock concentration of any analyte, including metolachlor at 2.1 $\mu g/g$. UW6 has a cluster of non-quantifiable detections between 245 and 225 *masl*, and two quantifiable detections at approximately 187 *masl*.

3.5 Multilevel Groundwater Monitoring

3.5.1 Metolachlor

Groundwater samples were collected on a monthly basis from all of the multilevel systems on site. Figure 3.44 shows representative concentration with depth profiles for UW16B in the source area (October, 2005), and the wells along the down-gradient transect. There are two distinct peaks in the concentration profile for UW16B, one at approximately 266 *masl* and the other at approximately 244 *masl*. The larger of the two peaks at 266 *masl*, has a concentration of 110 $\mu g/L$. The lower peak in UW16B coincides with the peaks in the down-gradient transect wells. Each down-gradient transect well shows a peak in concentration at approximately 240 *masl*, except for UW13, which has a much lower maximum value (4.5 $\mu g/L$) than other transect coreholes. The average down-gradient, maximum concentration is 11.3 $\mu g/L$ which is approximately one order of magnitude less than the maximum concentration from UW16B in the source area. However, if one looks

at the concentration of the lower source area peak, the concentration is 22 $\mu g/L$, which is only two times greater than the average, peak transect concentration of 11.3 $\mu g/L$.

Figures 3.45 to 3.50 show comparisons of metolachlor concentrations taken from multilevel systems over a three month period from October to December 2005, the respective vertical head profile for that sampling event, the calculated rock porewater concentration, horizontal hydraulic conductivity obtained from straddle packer testing, gamma log, and the corelog from the corehole.

Figure 3.45 is based on data collected from UW16B in the source area. Metolachlor concentrations obtained from the 15-port FLUTe multilevel system from October 2005 to December 2005 show that there is a large fluctuation in concentrations in the top 5 ports of the system. Port 3 had the largest concentration difference between October and November 2005 of 110 $\mu g/L$ and 49 $\mu g/L$, respectively. Concentrations did not fluctuate as much between November and December 2005 as they did between October and November 2005. The drop in concentration between port 5 and port 6 is coincident with the lack of vertical hydraulic gradient below port 5.

Figure 3.46 shows the data collected from UW5 along the down-gradient transect. Metolachlor concentration data collected from the 11-port FLUTe multilevel system for a period of three months shows very little change in concentration levels. Metolachlor concentration decreases between ports 6 and 7 and below port 7 the concentrations are largely not detected. This drop in concentration at port 7 is coincident with a large vertical hydraulic head differential between ports 6 and 7.

Metolachlor data collected over a three month period from the 12-port FLUTe multi-level system installed in UW4 is shown in Figure 3.47. Port 3 showed the most fluctuation in the metolachlor concentrations, increasing consistently over the three month period from 0.87 $\mu g/L$ in October 2005 to 5.3 $\mu g/L$ in December 2005, other ports only change by $\pm 1 \mu g/L$.

Figure 3.48 shows the metolachlor concentration data collected over a three month period from October to December 2005 in the 10-port FLUTe multilevel system installed in UW13. The data show ports 5 and 6 having the only detectable metolachlor and the concentrations are very stable over the three month period.

Metolachlor data collected from the 12-port FLUTe multilevel system installed in UW6 over a three month period can be seen in Figure 3.49. The sample from port 7 for the sampling round in October 2005 was broken and was not analysed, however all the data suggest the concentrations are stable over the three month period. No ports below port 7 have any detectable metolachlor.

Figure 3.50 shows metolachlor data collected from the 14-zone Westbay multilevel system installed in UW3. Zones 8, 9 and 10 have multiple monitoring ports in order to assess any chemical stratification within the zone. Zone 9 which is approximately 10 m long, has three monitoring ports, one in the middle of the zone and one in the top and bottom of the zone. In October 2005 all three monitoring ports were sampled and the port in the middle of zone 9 showed the highest metolachlor concentration, and the bottom port showed the next highest concentration. Port 10 had two monitoring ports installed and the bottom of the two ports had the highest concentration of metolachlor.

In November and December 2005, only the monitoring ports from zones 9 and 10 with the highest concentrations were sampled which was representative of the entire zone. These data show that only zones 9 and 10 have detectable concentrations of metolachlor; zone 9 is very stable and zone 10 shows a slight increase over the three month period.

Figures 3.51 to 3.55 show the concentration with time profiles for the transect multilevel systems. It can be seen in these figures that the concentrations in the multilevel systems are stable over time and the first sampling round immediately following the multilevel installation is very near the value acquired months afterwards. Figure 3.53 exhibits anomalous metolachlor data from March, 2005 for ports 5 and 6, which were below the detection limit.

Metolachlor concentrations from the multilevel systems installed along the transect were contoured and are shown in Figure 3.56. Using data collected in December 2005, the data was contoured using the linear kriging option with an anisotropy ratio of 8:1. This most likely represents the dominance of horizontal flow in the dolostone aquifer. These data show that the plume extends the entire width of the transect and is not bounded on either end. The highest concentrations occur in the middle part of the dolostone aquifer between 240 and 235 *masl* and UW13 has much lower concentrations than other coreholes along the transect.

3.5.2 TCE

Figure 3.57 shows aqueous TCE concentrations collected from multilevel systems in October 2005. UW16B in the source area was plotted with the transect multilevels for compari-

son. The concentration versus depth profile for UW16B shows the largest concentration of 28.1 $\mu g/L$ occurring in the shallowest port, and then decreasing towards the bottom port in the dolostone aquifer. A second peak in TCE concentration occurs at approximately 243 $masl$, which is coincident with the concentration peak observed for metolachlor in Figure 3.44. This lower concentration peak of 8.2 $\mu g/L$ occurs at the same elevation as the peak concentrations in the down-gradient transect multilevels. The average peak concentration of the down-gradient multilevels is 1.4 $\mu g/L$ which is approximately twenty times lower than the peak concentration from UW16B. However, upon comparison between the lower source area peak at 243 $masl$ and the down-gradient peaks occurring at approximately the same elevations, the difference is only six times. The concentrations from UW13 are the lowest of all the transect multilevels and values are barely above the detection limit of 0.1 $\mu g/L$. TCE concentrations in UW5 and UW3 which are on the extreme ends of the transect have approximately the same concentrations.

Figures 3.58 to 3.63 show comparisons of TCE concentrations taken from multilevel systems over a three month period from October to December 2005, the respective vertical head profile for that sampling event, the calculated rock porewater concentration, horizontal hydraulic conductivity data obtained from straddle packer testing, gamma log, and the corelog from the corehole.

Figure 3.58 shows TCE data obtained from the 15-port FLUTe multilevel system installed in UW16B in the source area. TCE data above port 6 fluctuates more than in port 6 and below. Port 2 changed by almost 7 $\mu g/L$ between November and December 2005, and port 4 increased in concentration from 9.1 $\mu g/L$ in October 2005 to 19.1 $\mu g/L$

in December 2005. Port 8 increased from 8.3 $\mu g/L$ in November 2005 to 11.5 $\mu g/L$ in December 2005. Port 9 decreased in concentration from 5.5 $\mu g/L$ in November 2005 to 1.8 $\mu g/L$ in December 2005.

Figure 3.59 shows TCE concentration data collected from the 11-port FLUTe multilevel system installed in the down-gradient transect corehole UW5. Due to the low concentrations of TCE obtained from UW5, very small changes in concentrations are enhanced with the small scale. The largest concentration difference occurred in port 7 where it increased from 0.7 $\mu g/L$ in October 2005 to 2.3 $\mu g/L$ in November 2005. There is a decrease in TCE concentration of approximately four times from port 6 to port 7 which is coincident with a large vertical hydraulic head drop.

Figure 3.60 shows TCE data collected from the 12-port FLUTe multilevel system installed in UW4. TCE concentrations between November and December 2005 are very similar, however large differences occur in ports 3 and 7 between October and November 2005. Port 3 decreased in concentration from 2.2 $\mu g/L$ to 0.5 $\mu g/L$ and Port 7 increased in concentration from 0.8 $\mu g/L$ to 2.4 $\mu g/L$. Port 12 initially showed a relatively high TCE concentration (1.1 $\mu g/L$), however it was not subsequently sampled in order to preserve the hydraulic head profile in the shale. This high concentration was likely due to cross connection during the FLUTe installation and would likely decrease over time.

TCE concentration data collected from the 10-port FLUTe multilevel system installed in UW13 shows the lowest peak concentrations of all the coreholes along the down-gradient transect (Figure 3.61). Port 6 has the highest concentration of TCE and port 5 is the only other port to have detectable TCE; the concentrations are stable over the three month

period.

Figure 3.62 shows data collected from the 12-port FLUTe multilevel system installed in UW6. The peak concentration occurs in port 6, however in October 2005 the peak occurred in port 5. Port 11 showed a relatively high concentration (1.5 $\mu g/L$) in October 2005 and gradually decreased to below the detection limit by December 2005. This was most likely due to cross contamination during the installation of the FLUTe multilevel system and over time due to low flow in the shale aquitard, the TCE concentration was decreased to actual formation concentrations.

Figure 3.63 show the TCE data collected from the 14-zone Westbay multilevel system installed in UW3. These data show samples collected over a three month period and the concentrations are very similar over this time period. The maximum TCE concentration occurs in zone 9 and port 10 is the only other zone of the 14 zones to have detectable TCE. Minimal disturbance and cross contamination is achieved during the Westbay installation and therefore concentrations stabilize much more quickly than the FLUTe installations.

Figures 3.54, 3.55, 3.64, and 3.65 show the TCE concentration versus time profiles for each port in the various multilevel systems. TCE data for UW13 were not plotted because as of March 2004, concentrations were not detectable and in October 2005 when the analytical laboratory was changed and the detection limit decreased from 1.0 $\mu g/L$ to 0.1 $\mu g/L$, the values were discovered to be slightly above the new detection limit. Concentrations for TCE fluctuate more than concentrations for metolachlor. It appears that coreholes with FLUTe multilevel systems take 3-4 sampling rounds before the TCE concentrations stabilize; data from the Westbay multilevel system installed in UW3 do

not show this fluctuation with time, however it does have the least sampling events. Figures 3.54, 3.55, 3.64, and 3.65 show the effect of the mixing of groundwater during the installation of the FLUTe multilevel system, and since there is less disturbance from the Westbay system during installation, the mixing is not encountered in UW3 and the TCE concentrations are relatively stable over time.

TCE concentrations were contoured in Figure 3.66 using the linear kriging option and an anisotropy ratio of 8:1. The shape of the contoured zone reflects the dominance of horizontal flow in the dolostone aquifer. The shape and extent of the plume is very similar to the metolachlor plume (Figure 3.56), except it is much narrower vertically. The highest concentrations occur in the middle part of the dolostone aquifer between approximately 240 and 235 *masl*.

Figure 3.67 shows the concentrations of both metolachlor and TCE in the various ports in the respective multilevel systems along the transect. The peak concentrations of both metolachlor and TCE occur in the same ports and at approximately the same elevations along the transect. The metolachlor and TCE originated from different sources, however they both are following the same migration pathways and the plumes are focussed vertically along the transect from the respective source areas.

3.5.3 Hydrochemistry

Inorganic hydrochemistry data were collected from UW16B in the source area and from UW13 on the down-gradient transect in February 2005 prior to the installation of the other multilevels systems along the transect. Figure 3.68 shows the results for UW16B

indicating similar trends for both metolachlor and TCE; the shallowest ports have the highest concentrations for the inorganic parameters, and there is a concentration peak at approximately 240 *masl*. Figure 3.69 shows a comparison between hydrochemistry results collected from UW16B on May 2001, by Turner (2001), and results of sampling during this study in February 2005. The profiles for each constituent are similar, however at approximately 230 *masl* the calcium, chloride, sodium and total dissolved solid profiles show lower concentrations in 2001.

Figure 3.70 shows the hydrochemistry results for sampling UW13 in February 2005. The vertical trends for magnesium, calcium, chloride, sodium, sulphate, and total dissolved solids are similar. Groundwater in the Rochester Formation shale is saline and brackish, due to very high total dissolved solids, chloride and sodium concentrations. These high concentrations in the shale could be due to the presence of modified ancient sea water that was deposited in this unit (Lotowater Ltd., 1997). Both alkalinity and total nitrogen concentrations decrease with depth and do not increase in the shale. The decrease in nitrogen is coincident with the increase in sulphate concentrations which would suggest reducing conditions deep in the aquifer and into the underlying Rochester Formation shale. The alkalinity profile has a relatively large decrease in concentration at approximately 220 *masl*, in port 6 where the maximum concentration of metolachlor was detected.

The similarity in results from inorganic hydrochemistry sampling between 2001 and 2005 indicates the substantial stability of the plume chemistry even though the flow system has strong instability.

3.5.4 Isotopes

Figure 3.71 is a comparison of ^{3}H and ^{18}O data collected from UW16B in May 2001 (Turner, 2001), and that from the current study collected in February 2005. The tritium data are very similar, however values at approximately 245 and 230 *masl* are depleted in 2005, which could be related to flushing in that zone of older water or the lack of vertical groundwater movement down through those zones. ^{18}O data collected in May 2001 shows an enrichment in concentration compared to data from February 2005. However, because the tritium and 18-oxygen data from 2001 and 2005 are similar, this provides further evidence of the stability in the chemical composition of the groundwater in the dolostone aquifer.

Figure 3.72 shows isotopic data collected at UW16B and UW13 in February 2005. The tritium values for both UW16B and UW13 are approximately 20 TU in the upper 20-30 m of bedrock which is typical for tritium deriving from precipitation between 1970 and 1995 (Lotowater Ltd., 1997). Tritium was detected deep in the aquifer for both UW16B and UW13, with detectable tritium found in the underlying shale of UW13. This was observed by Lotowater Ltd. (1997) and they concluded that this was related to a combination of natural movement of recent groundwater vertically through the aquifer, artifacts of the mixing of groundwater in the open borehole, and also the presence of known and unknown open test holes or wells in the vicinity that provide conduits from upper parts of the dolostone aquifer to deeper parts.

The ^{18}O and ^{2}H data from UW13 both show enriched values at depth in the aquifer and data collected from the bottom port (Figure 3.72, which is in the shale, has values similar

to values from the middle and upper parts of the dolostone aquifer. Similar to the tritium profile, ^{18}O and ^{2}H being found in the shale is most likely due to mixing of groundwater during the installation of the FLUTe multilevel system and since groundwater flow rates are likely small in the underlying shale, water mixed from the surface has a long residence time.

$\delta^{18}O$ and $\delta^{2}H$ are plotted against the Canadian Meteoric Water Line (CMWL) in Figure 3.73. The CMWL was determined based on the formula provided by Clark and Fritz (1997):

$$\delta^{2}H = 7.75 \cdot (\delta^{18}O) + 9.83 \tag{3.1}$$

These data show that most of the points for UW13 fall closer to the CMWL than do the points from UW16B. This could be due to the fact that there is greater hydraulic connection between the overburden and the dolostone aquifer at UW16B than at UW13. This greater connection decreases the groundwater residence time in the overburden and allows for more variation in the data. Data falling along the CMWL is due to recharge from precipitation, data below the CMWL have been affected by evaporation and the data above may be related to melting snow water (Clark and Fritz, 1997). UW16B has more data points falling below the CMWL and therefore the water is more likely effected by evaporation in the overburden before reaching the bedrock which may indicate a greater vertical hydraulic connection between the overburden and the dolostone aquifer at UW16B than at UW13.

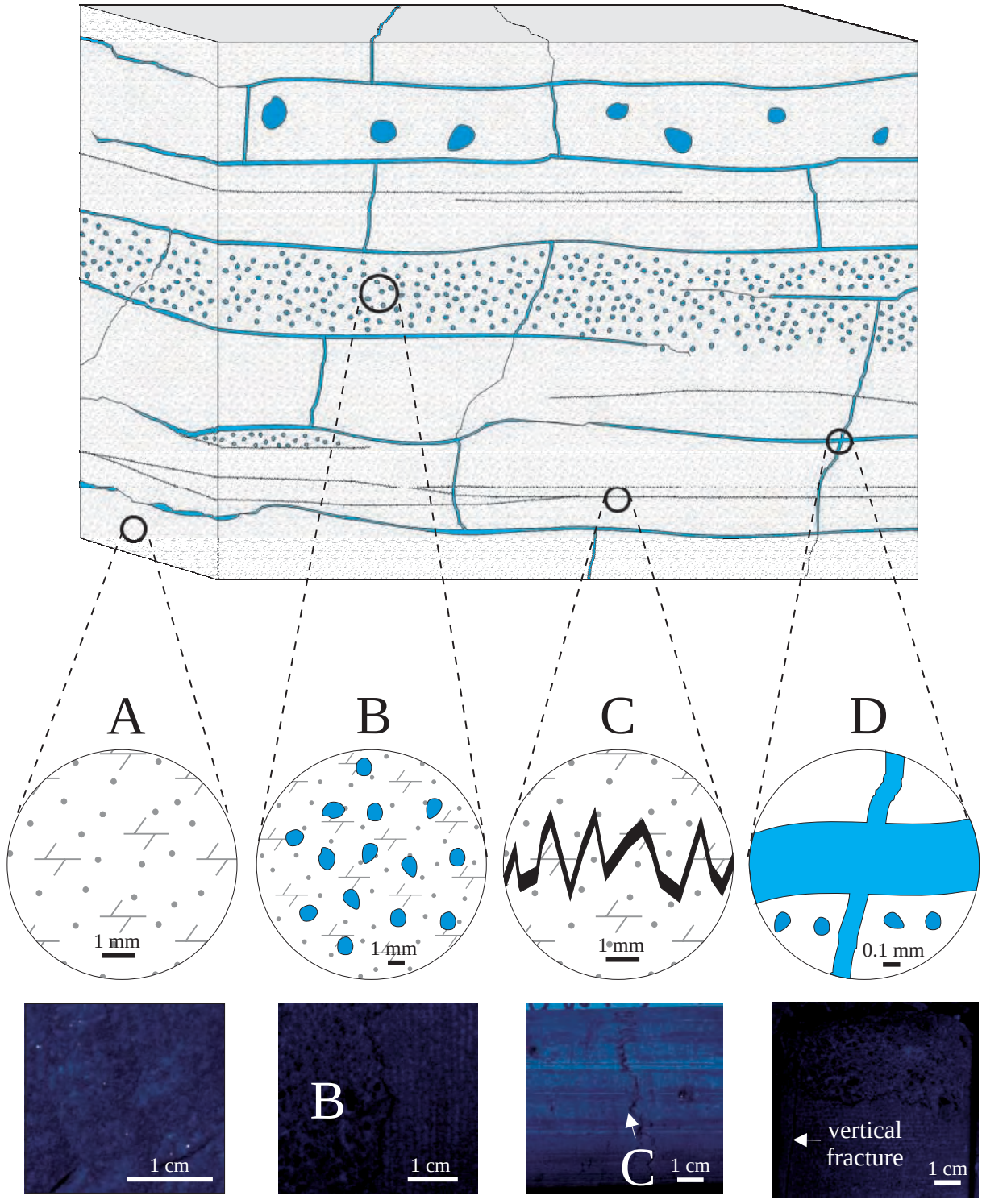


Figure 3.1: Porosity observed in the Guelph and Lockport Formation dolostone in Cambridge, Ontario. The dolostone matrix is generally massive with <10% intercrystalline porosity [A] and may contain pinpoint porosity (pores $\leq 3mm$) and vuggy porosity (pores >3mm)[B], in addition to stylolite partings [C] and horizontal and vertical fractures [D]. Adapted from Turner (2001).

Corelog Unit ID	Unit Description	Unit Symbol	Lithologic Unit ID & Descritption
A	DOLOSTONE, very weathered, broken-up & fractured, pinpoint porosity with vugs, no stylolites, Fe staining		a — Pinpoint porosity (5-10%) with vugs, stylolites, no fossils
B	DOLOSTONE, pinpoint and vuggy porosity, few to no fractures, no stylolites		
D	DOLOSTONE, pinpoint porosity (5-12%), abundant fractures (broken-up in zones), few to abundant stylolites, few to no fossils		
H	DOLOSTONE, pinpoint and vuggy porosity, abundant fractures (broken-up & Fe staining), abundant stylolites, no fossils		
I	DOLOSTONE, pinpoint and vuggy porosity, abundant fractures (broken-up & Fe staining), few stylolites, few fossils		
C	DOLOSTONE, pinpoint porosity (2-5%), abundant stylolites, few fractures (some Fe staining), few fossils (crinoids, stromatoporoids)		b — Densely stylolitic zones, pinpoint porosity (3-9%) with vugs, crinoids
E	DOLOSTONE, pinpoint porosity (3-10%) with few vugs, few stylolites, few to no fractures, few fossils		
E/F	DOLOSTONE, pinpoint porosity (3-5%) with few vugs, few stylolites, no fractures, no fossils		
J	DOLOSTONE, pinpoint porosity (5-10%), abundant stylolites, few fractures, few to no fossils		
K	DOLOSTONE, pinpoint porosity (7-10%), abundant stylolites, no fractures, fossiliferous (crinoids)		
T	DOLOSTONE, pinpoint porosity (1-7%), abundant stylolites, no fractures, fossils (crinoids)		
U	DOLOSTONE, pinpoint porosity (3-7%), abundant stylolites, few fractures, fossiliferous (crinoids), some shale seams		
Q	DOLOSTONE, pinpoint porosity (7-10%), few to no stylolites, few to no fractures, few fossils (crinoids)		c — High pinpoint porosity (10%), few to no stylolites
F/G	DOLOSTONE, vuggy porosity, fossiliferous (crinoids, corals, gastropods, few bryozoas), stylolites, fractures		d — Highly fossiliferous, many interconnected voids, stylolites
G	DOLOSTONE, pinpoint and vuggy porosity, fossiliferous (stromatoporoids, corals, few crinoids and gastropods), few to no stylolites, fractures		
F	DOLOSTONE, pinpoint and vuggy porosity, few to no fractures, few stylolites, few fossils		e — Pinpoint porosity (5%) with vugs, few stylolites
M	DOLOSTONE, pinpoint and vuggy porosity, no fractures, stylolites, fossiliferous (crinoids)		f — Pinpoint porosity (5%) with vugs, abundant crinoids throughout, stylolites
P	DOLOSTONE, pinpoint and vuggy porosity, fractures, stylolites, fossiliferous (crinoids)		
S	DOLOSTONE, pinpoint porosity (5-10%), no fractures, stylolites, few fossils (crinoids)		
L	DOLOSTONE, vuggy porosity (spongy texture), fossiliferous (crinoids), stylolites, few to no fractures, few stylolites		g — Vuggy porosity with few zones of pinpoint porosity, spongy appearance, stylolites
O	DOLOSTONE, pinpoint and vuggy porosity, no fractures, stylolites, few fossils (crinoids)		
R	DOLOSTONE, pinpoint and vuggy porosity, abundant fractures (broken-up), few stylolites, no fossils		
V	DOLOSTONE, no visible porosity, no fractures, no stylolites, no fossils, abundant pyrite and glauconite		h — Pinpoint porosity (1% - not visible), pyrite and glauconite, no stylolites, no fossils
W	SHALE, interbedded with dolostone, few fossils in dolostone interbeds, no fractures, no stylolites		i — Dolomitic Shale

Figure 3.2: Corelog Units were determined from core logs of the dolostone aquifer, based on fracture frequency, stylolite abundance, porosity, and fossil content. The 24 Corelog Units were further subdivided into 9 lithologic units based on matrix properties

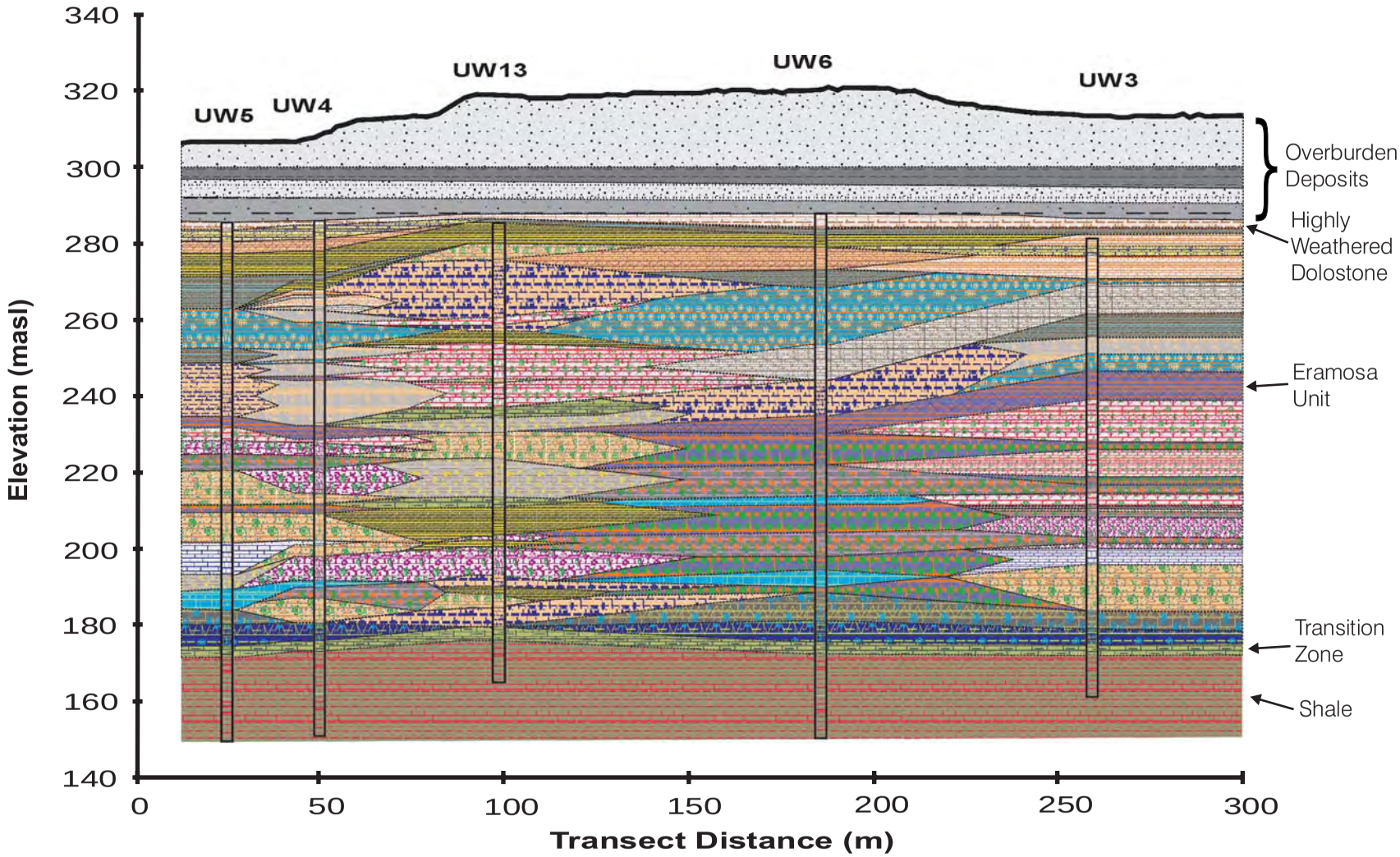


Figure 3.3: Corelog Units defined by fracture and matrix characteristics combined, were correlated across the transect based on the corelogs and units with similar descriptions. Very few units are continuous along the transect, however Corelog Units A, J, V, and W were described in all corelogs

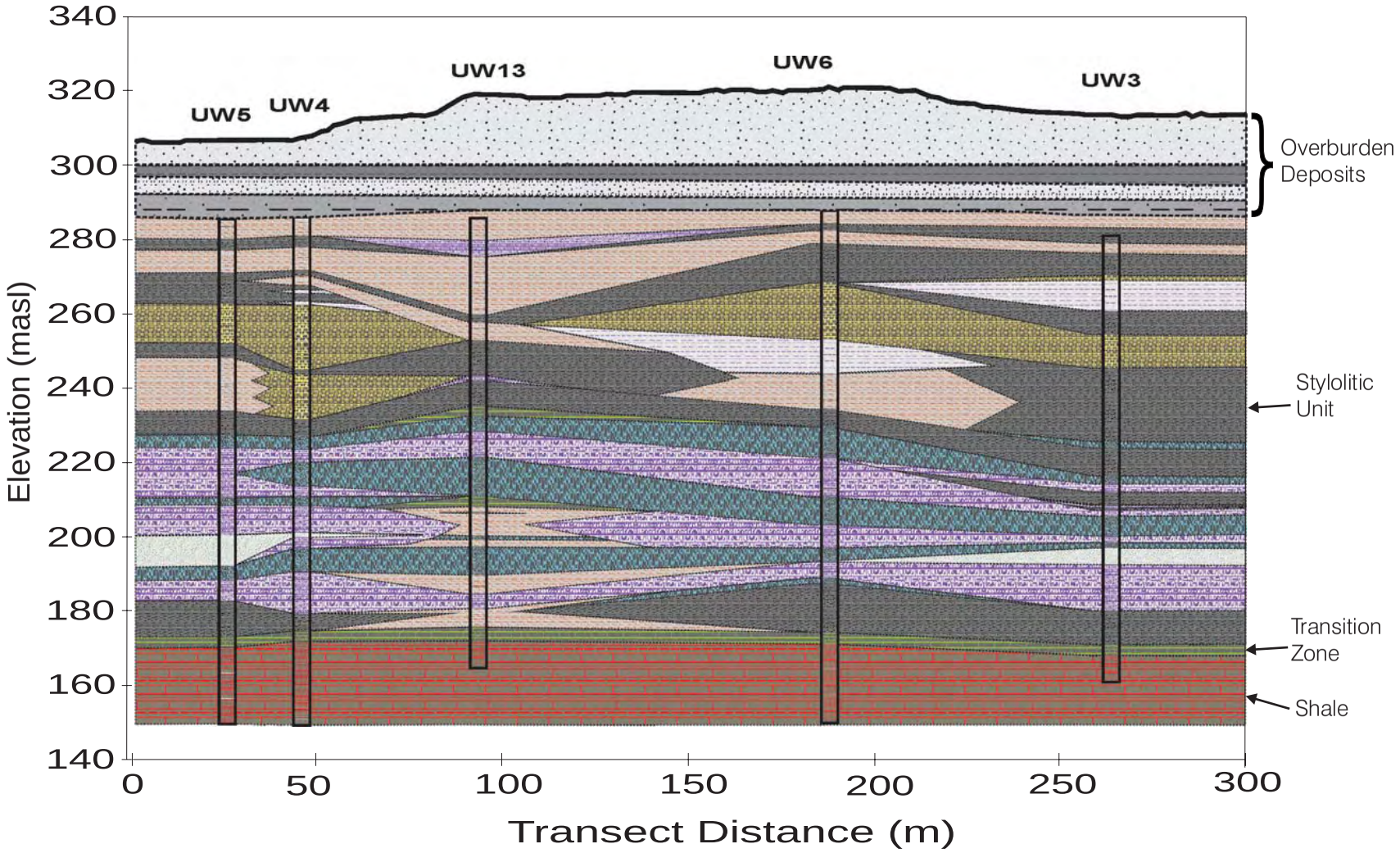


Figure 3.4: Lithologic units were correlated across the transect based on the matrix properties of the dolostone described from corelogs. The matrix properties exclude fractures as focussed primarily on matrix porosity, which includes vuggy and pinpoint porosities as well as stylolites and fossils. Many units are continuous along the transect which indicates the high degree of matrix uniformity at the study site

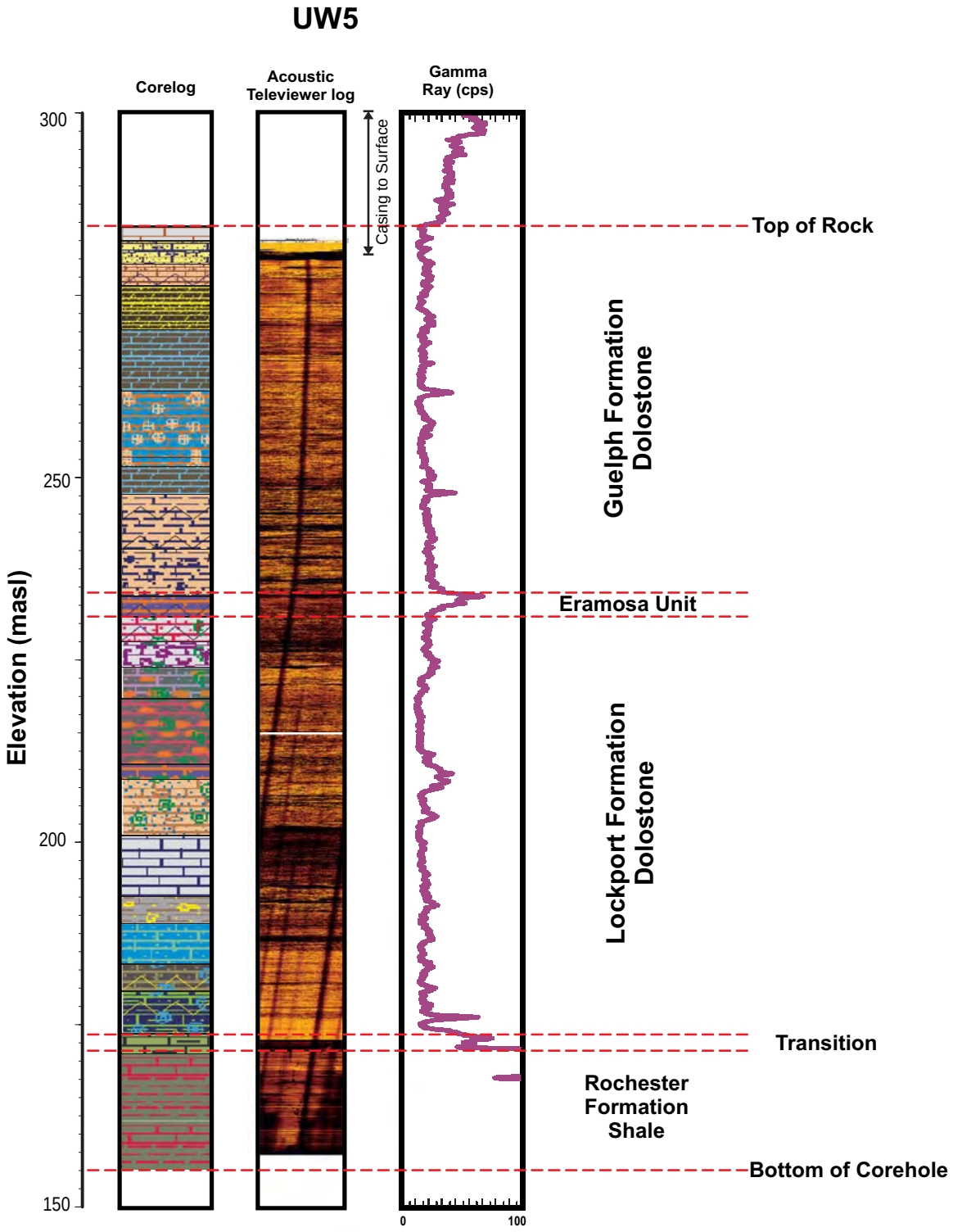


Figure 3.5: Various logs collected from UW5 showing the corelog; acoustic televiewer image; and gamma log which is representative of units with high clay/shale content. The Eramosa unit is indicated by Corelog Unit J and the thin gamma peak at approximately 232 masl. The gamma log also clearly identifies the dolostone-shale interface and the transition unit overlying it. Colour changes in the acoustic televiewer log represent changes in stratigraphy/lithology and the black horizontal lines represent either bedding planes or fractures.

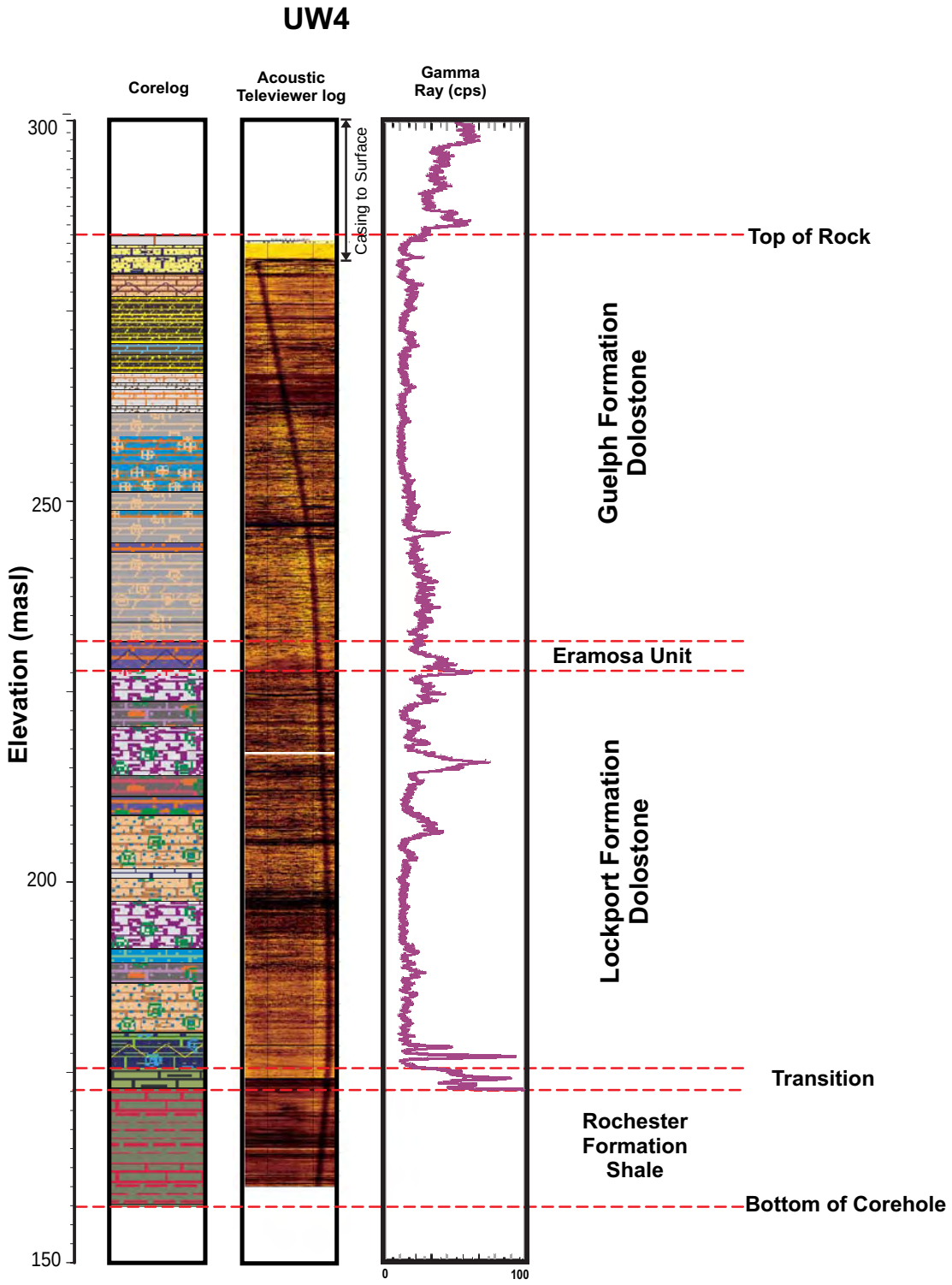


Figure 3.6: Various logs collected from UW4 showing the corelog; acoustic televiewer image; and gamma log which is representative of units with high clay/shale content. The Eramosa unit is indicated by Corelog Unit J and the thin gamma peak at approximately 230 masl. The gamma log also clearly identifies the dolostone-shale interface and the transition unit overlying it. Colour changes in the acoustic televiewer log represent changes in stratigraphy/lithology and the black horizontal lines represent either bedding planes or fractures.

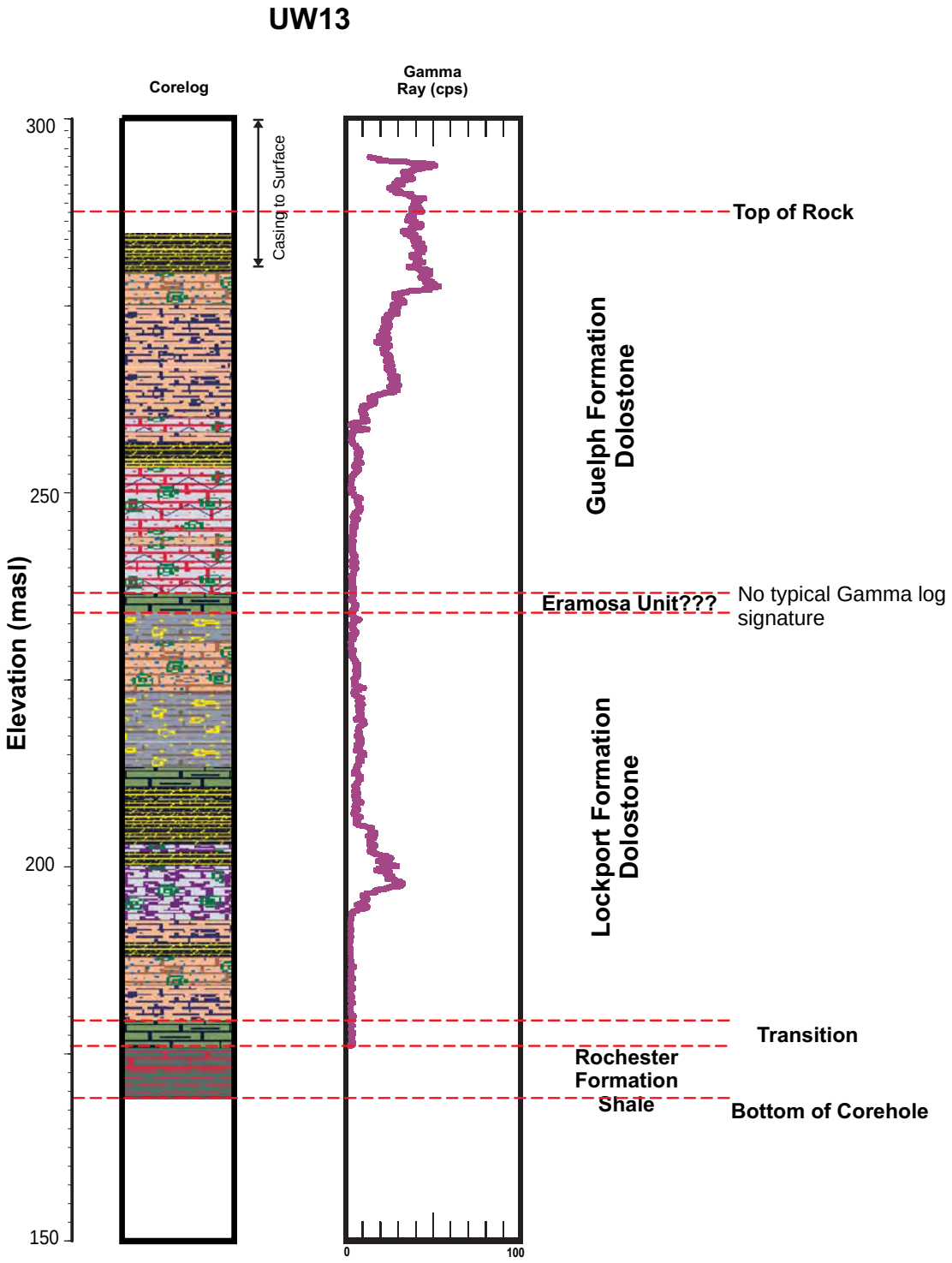


Figure 3.7: Corelog and gamma log from UW13 which reveals units with high clay/shale content. The Eramosa unit is indicated by Corelog Unit J and the thin gamma peak, however at this location it is not observed.

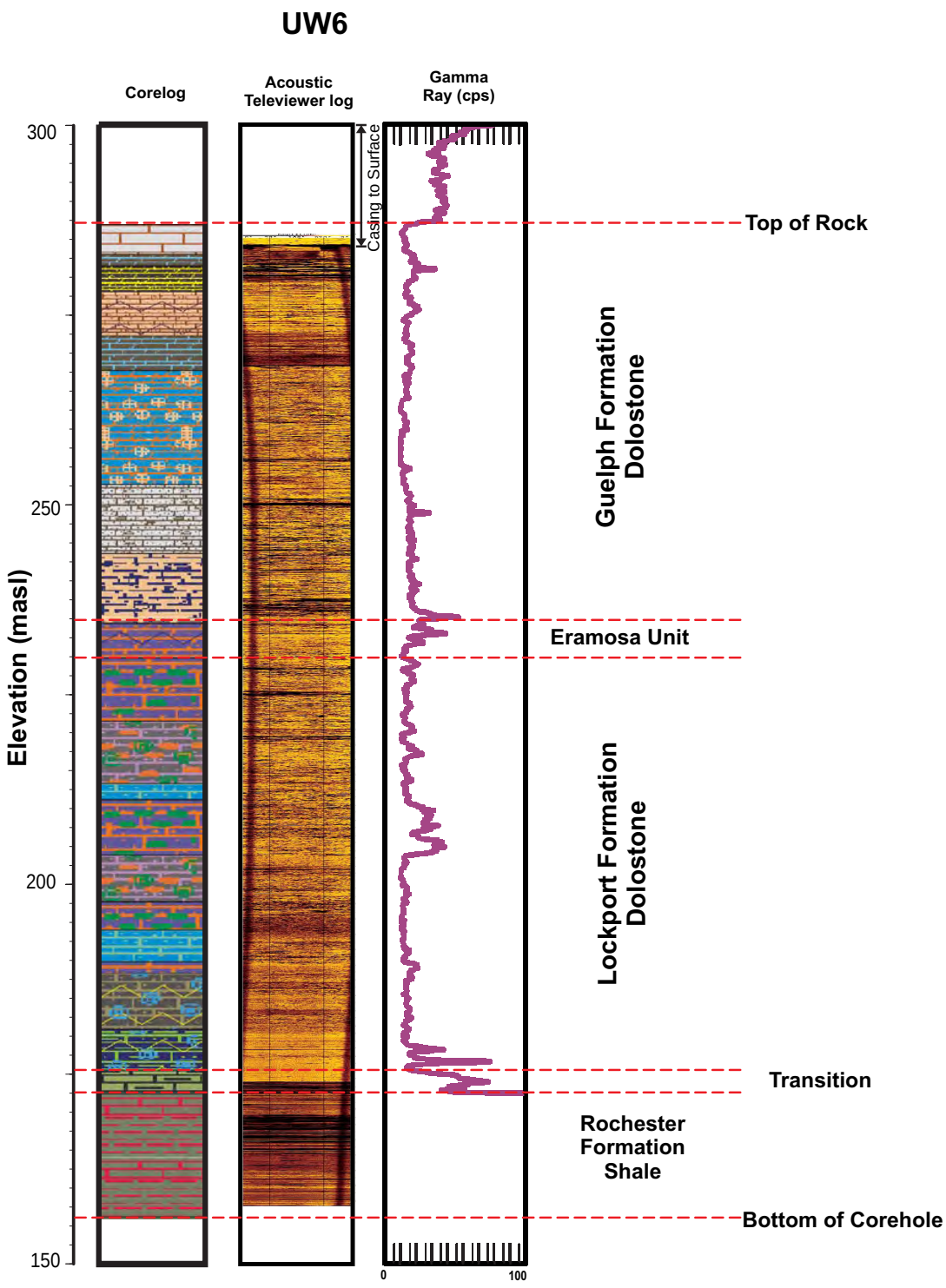


Figure 3.8: Various logs collected from UW6 including a corelog, acoustic televiewer image, and gamma log which defines units with high clay/shale content. The Eramosa unit is defined based on corelogs and the gamma peak at approximately 232 masl if evident. Colour changes in the acoustic televiewer log represent changes in stratigraphy/lithology and the black horizontal lines represent either bedding planes or fractures.

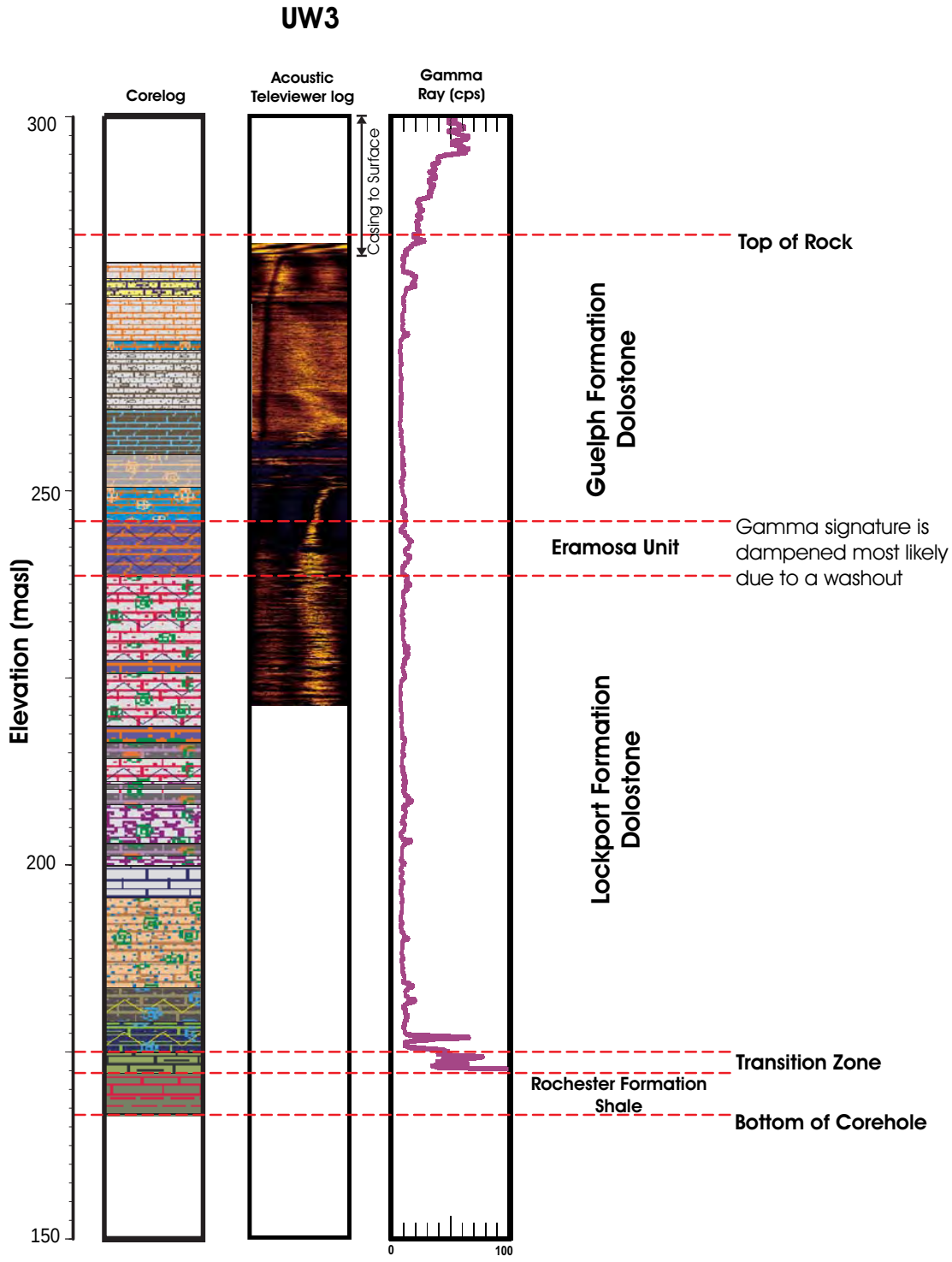


Figure 3.9: Various logs collected from UW3 including a corelog, acoustic televiewer image, and gamma log which defines units with high clay/shale content. The Eramosa unit was not clearly defined in this hole because of a large washout that occurred during drilling. Colour changes in the acoustic televiewer log represent changes in stratigraphy/lithology and the black horizontal lines represent either bedding planes or fractures.

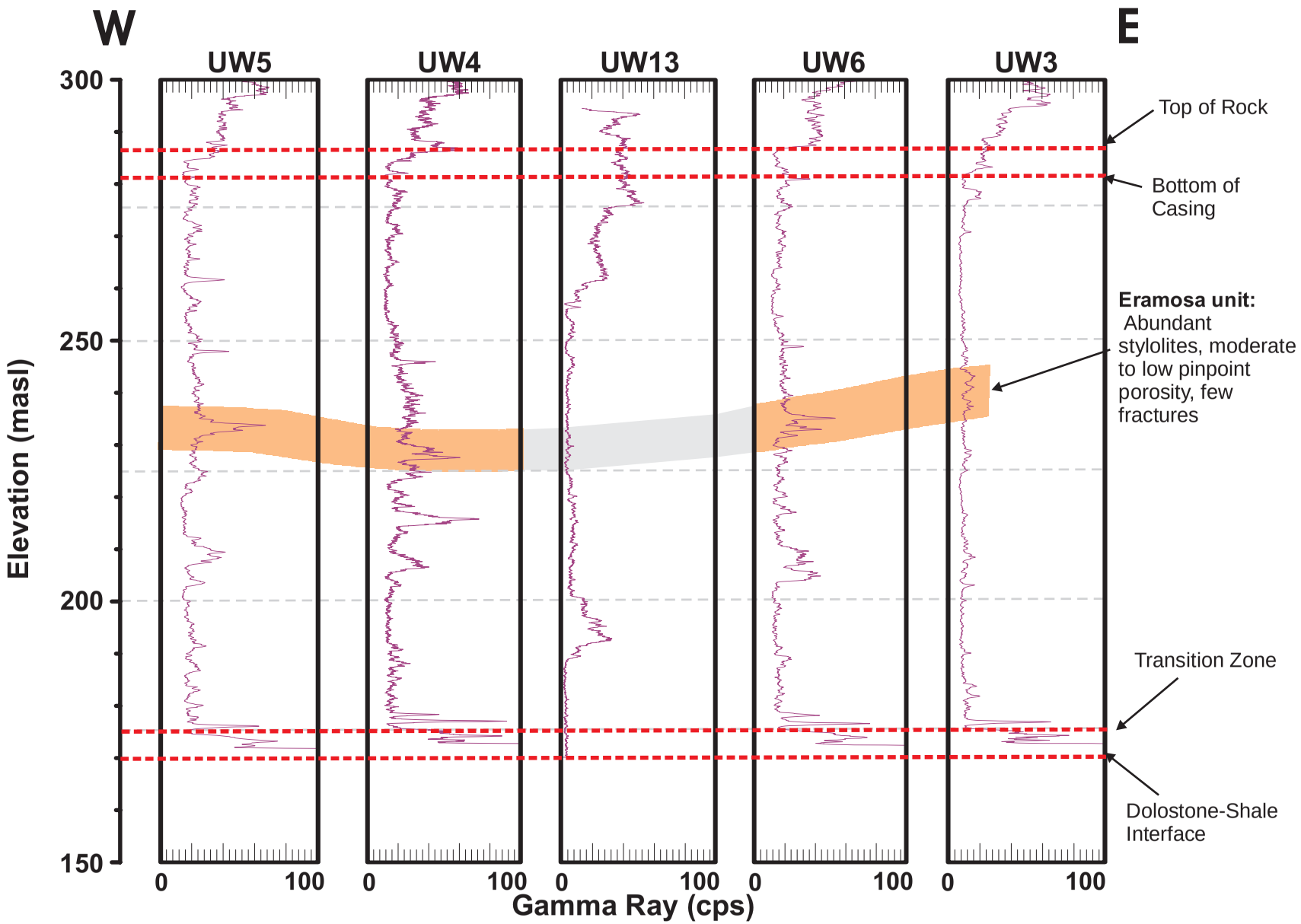


Figure 3.10: Natural gamma logs collected along the transect define a peak at approximately 230 masl which is coincident with Corelog Unit J described in corelogs and is determined to be the Eramosa unit. UW13 did not show the typical gamma peak associated with the Eramosa unit and it was not described in corelogs.

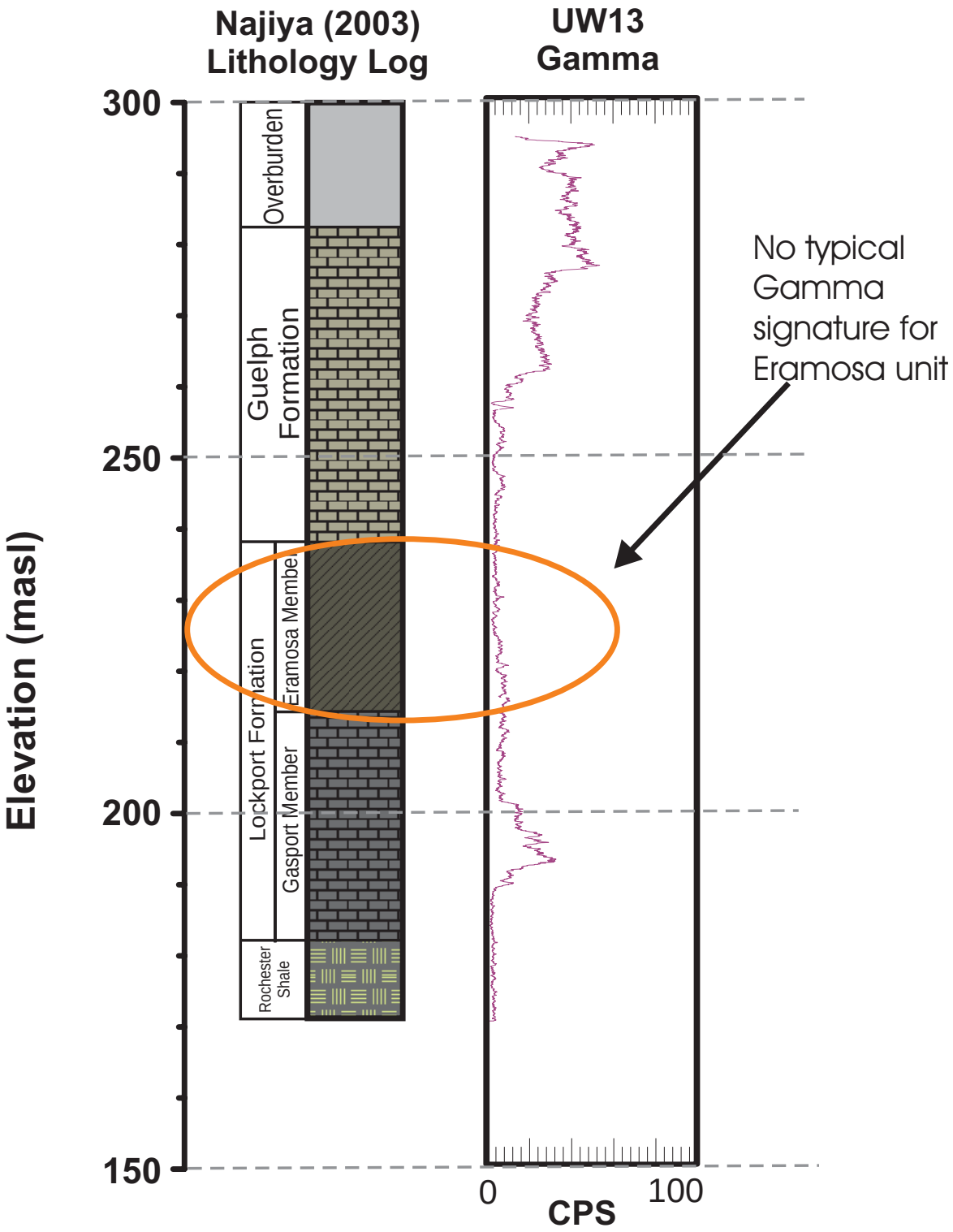


Figure 3.11: Lithology log of UW13 from Najiya (2003) which shows the presence of the Eramosa unit, however corelogs from Turner (2001) and gamma logs do not indicate the presence of the Eramosa unit in UW13.

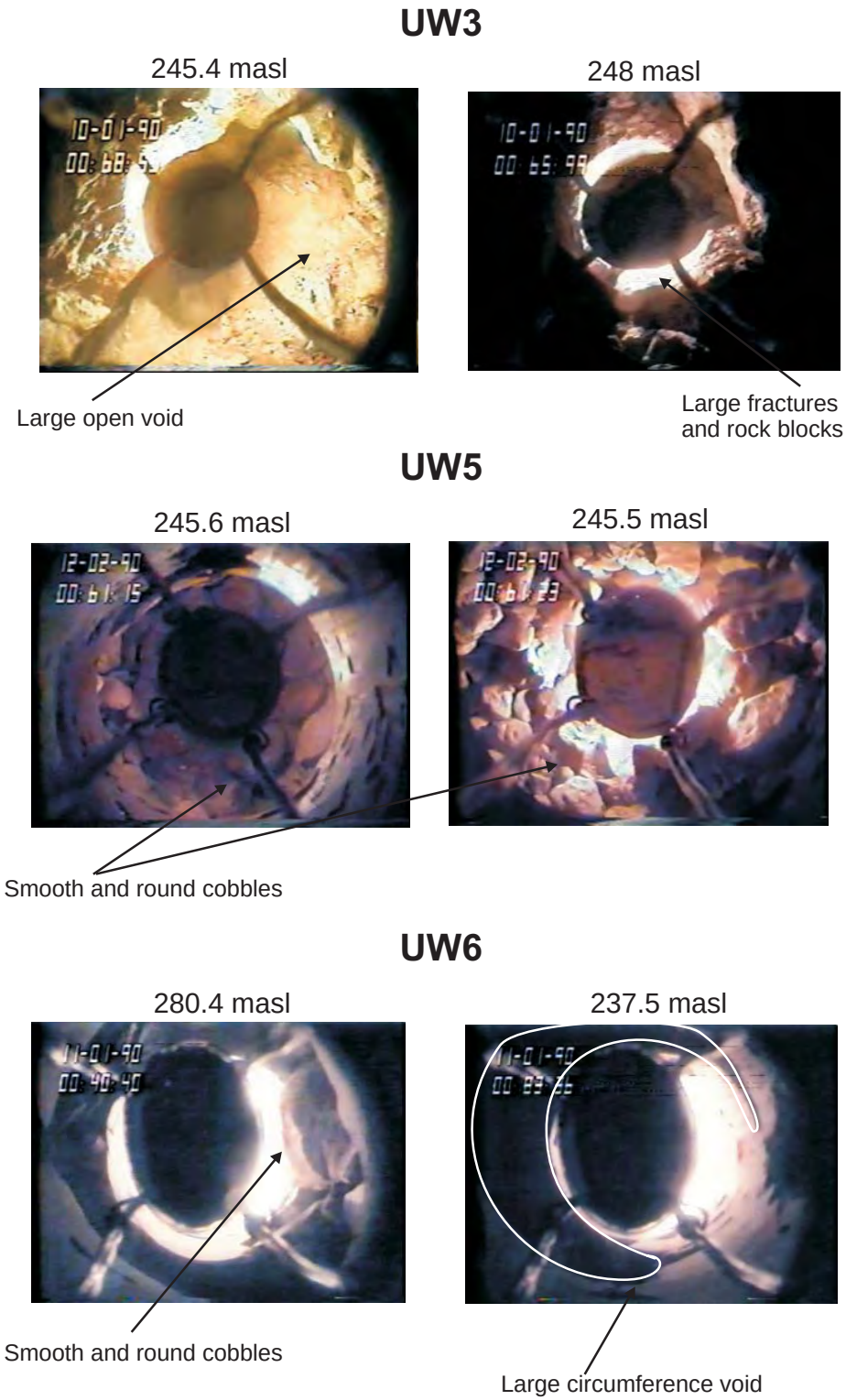


Figure 3.12: Borehole videos collected in UW3, UW5, and UW6 may provide evidence of karst features. These features may be zones of increased groundwater flow and contaminant transport. The light from the borehole video is pointing down the corehole.

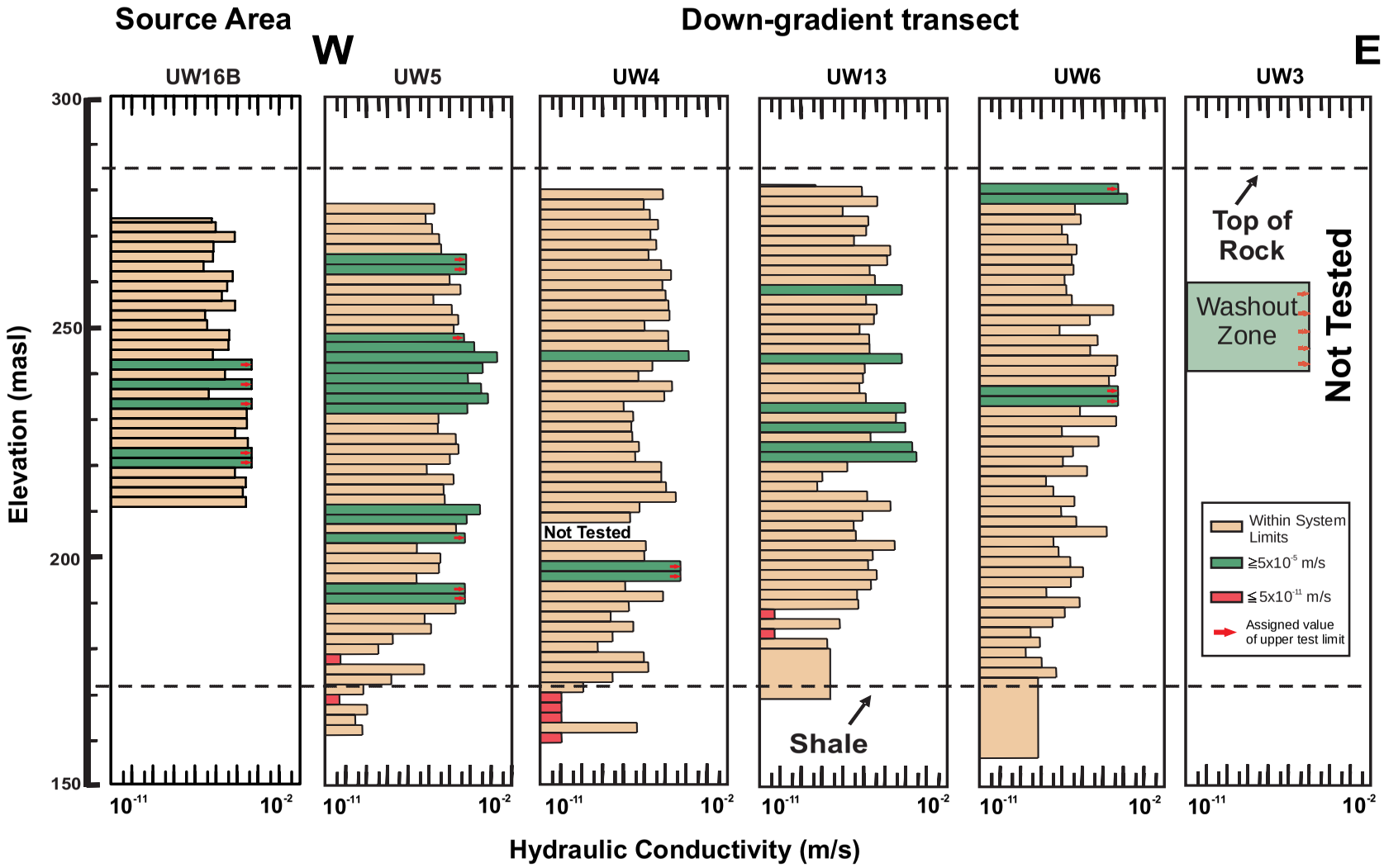


Figure 3.13: Hydraulic conductivity data from straddle packer testing. No data were collected from UW3 due to adverse hole conditions, however the zone indicated is where a large washout occurred which would have otherwise been a zone of high hydraulic conductivity. A zone of high hydraulic conductivity occurs between approximately 230 and 250 masl along the transect. Although there are values above the upper limit of the test apparatus, these values should only be considered as the upper limit due to data collection biases. The hydraulic conductivity profile for UW16B was completed to the bottom of the original corehole to a depth of 100 *mbgs*. Data for the profile was adapted from Plett (2002).

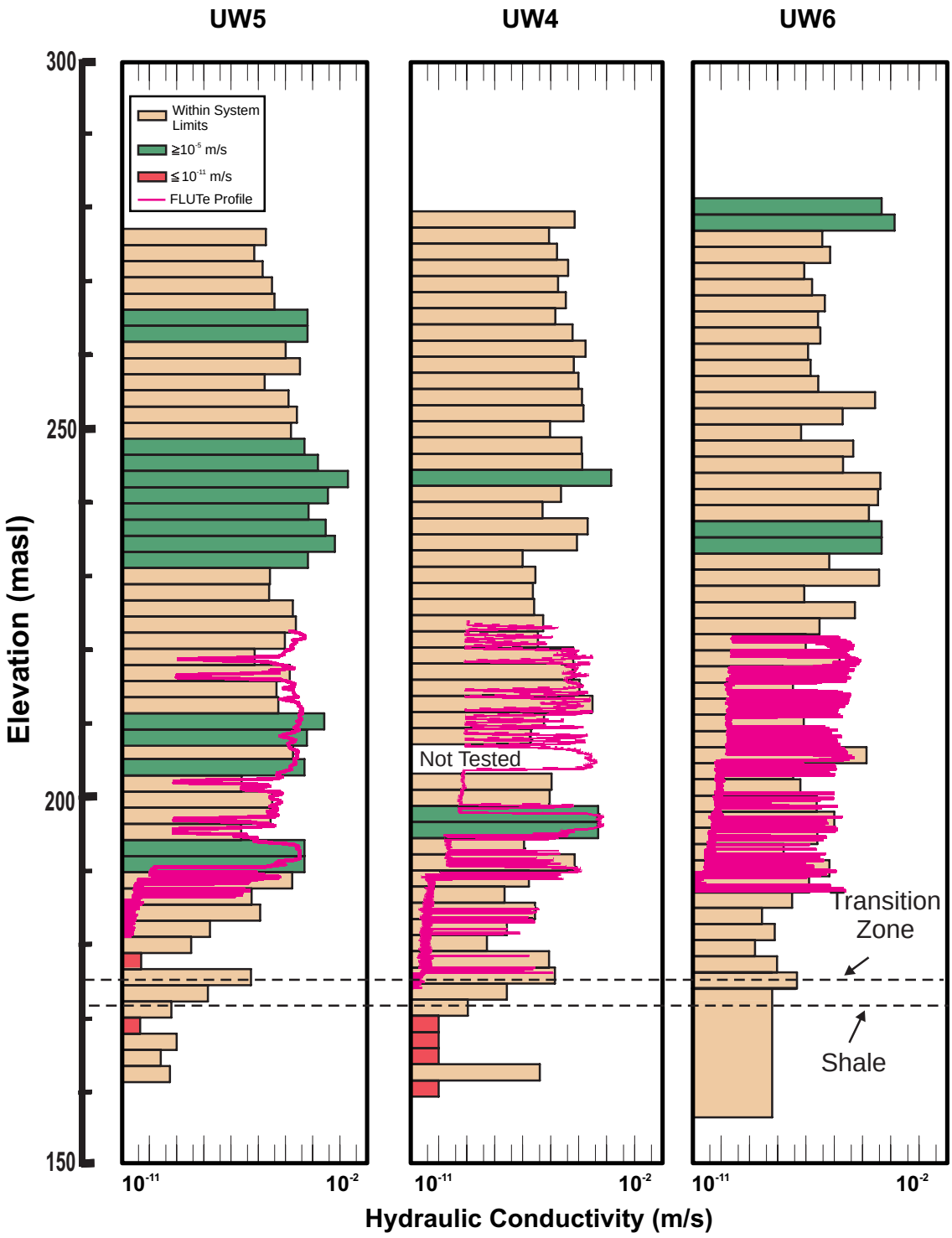


Figure 3.14: A comparison of bulk horizontal hydraulic conductivity obtained from straddle packer testing at 2.2 m intervals and FLUTe profiling. Data from FLUTe profiling were discarded above 225 masl due to problematic data.

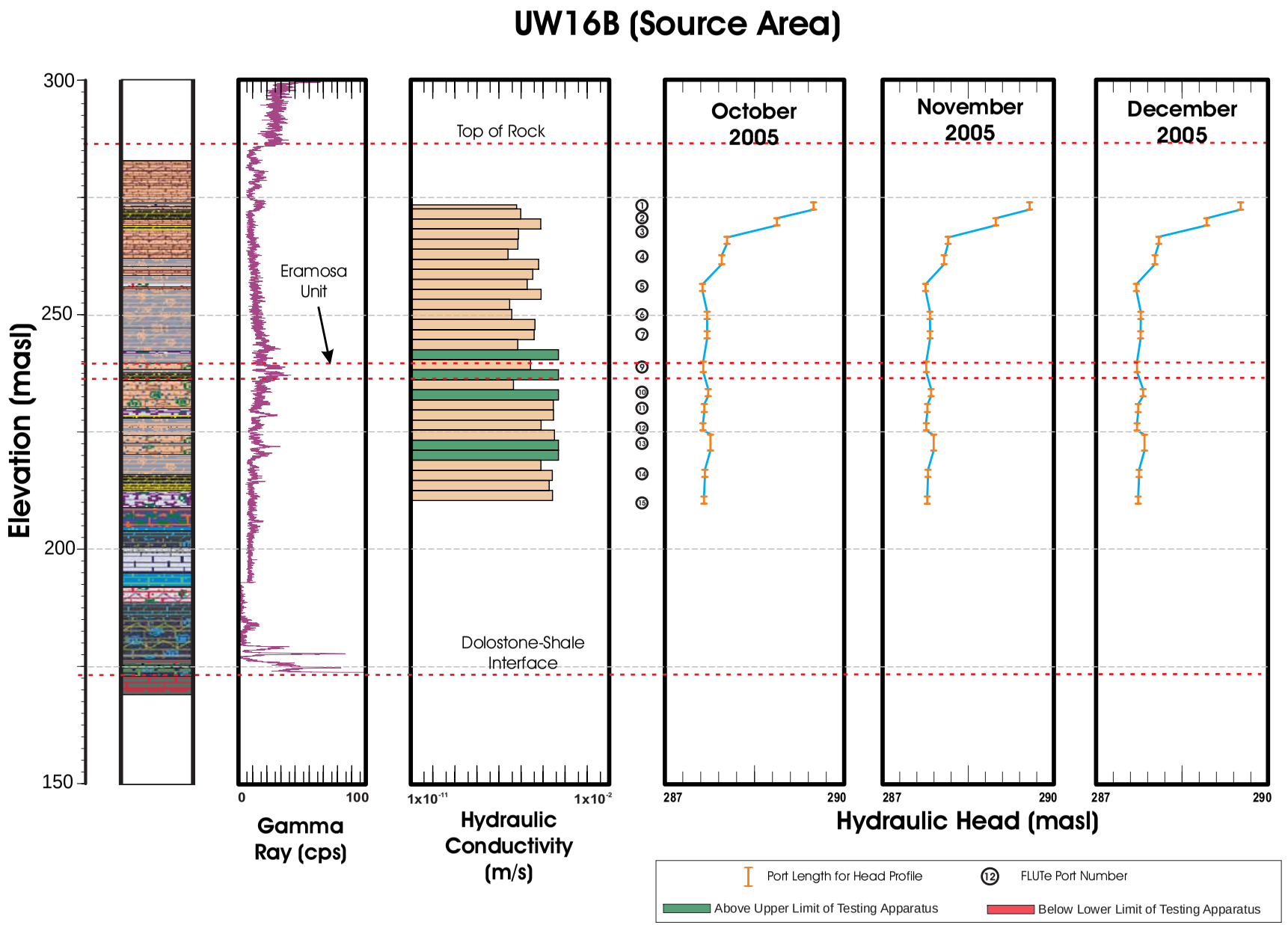


Figure 3.15: UW16B hydraulic head profiles for three representative time periods from the 15-port FLUTe multilevel system. The corelog along with gamma log and hydraulic conductivity data are shown for correlation. The vertical head profiles show a strong vertical gradient in the top five ports, below which no significant vertical gradient exists. Hydraulic conductivity profile for UW16B adapted from Plett (2002).

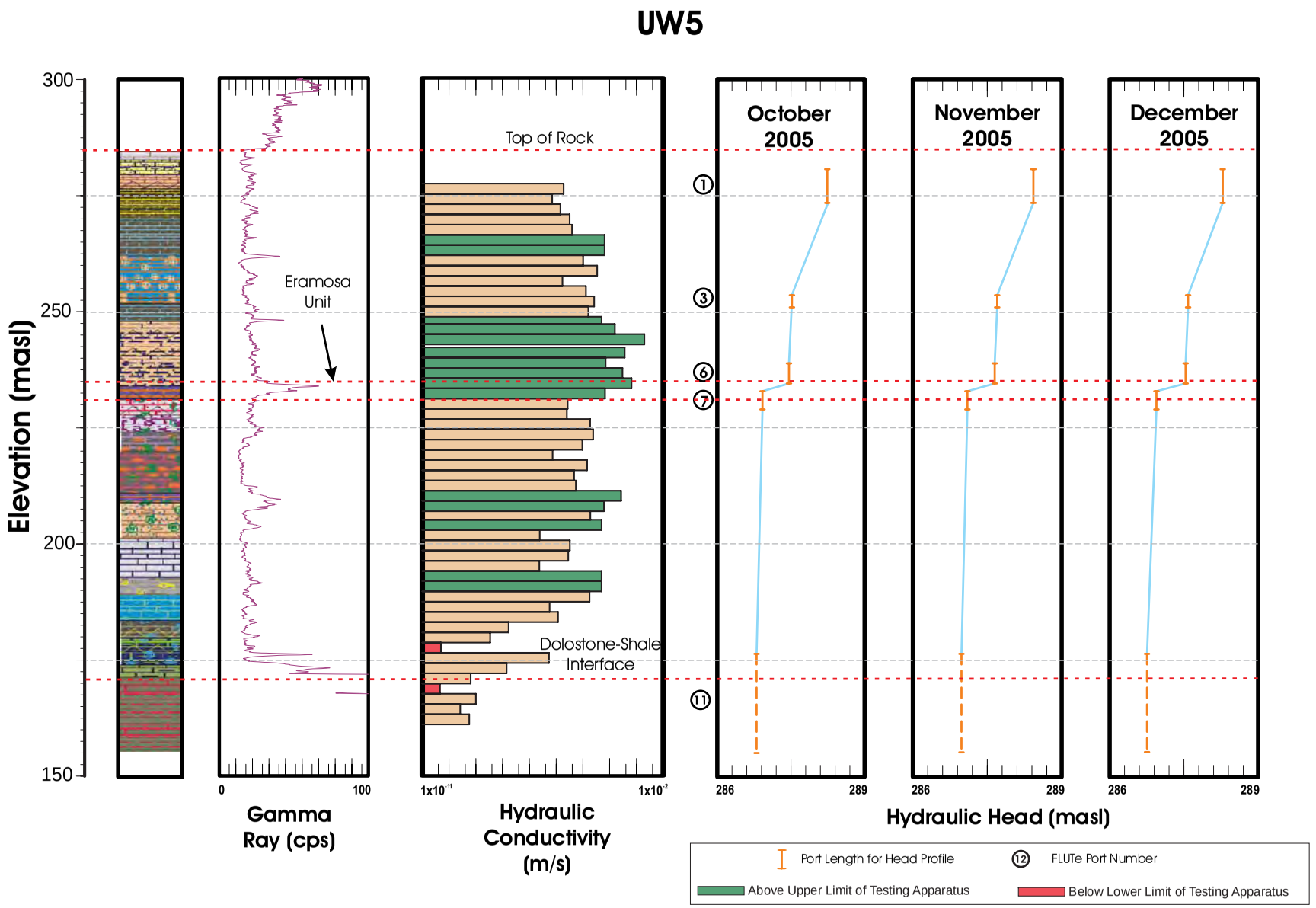


Figure 3.16: UW5 hydraulic head profiles for three representative time periods collected from the 11-port FLUTe multilevel system. The corelog along with gamma log and hydraulic conductivity data are shown for correlation. The vertical head profiles show a strong vertical gradient between port 6 and 7, which are located across the Eramosa unit identified by the gamma peak and Corelog Unit J at 232 masl.

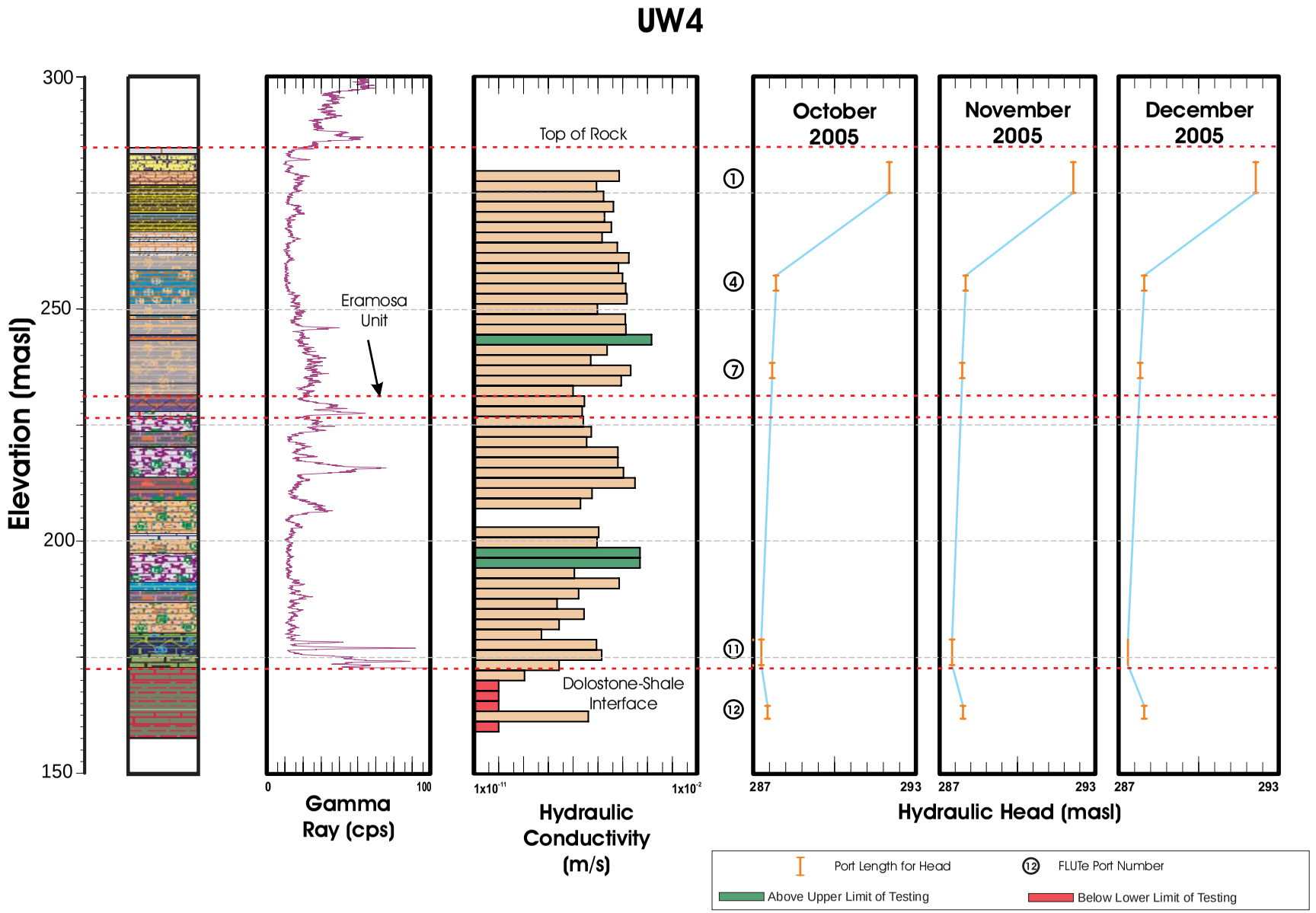


Figure 3.17: UW4 hydraulic head profiles for three representative time periods collected from the 9-port FLUTe multilevel system. The corelog along with gamma log and hydraulic conductivity data are shown for correlation. The vertical head profiles show a strong vertical gradient from port 1 in the top of bedrock and port 4. A slight vertical gradient is present from the shale into the overlying dolostone.

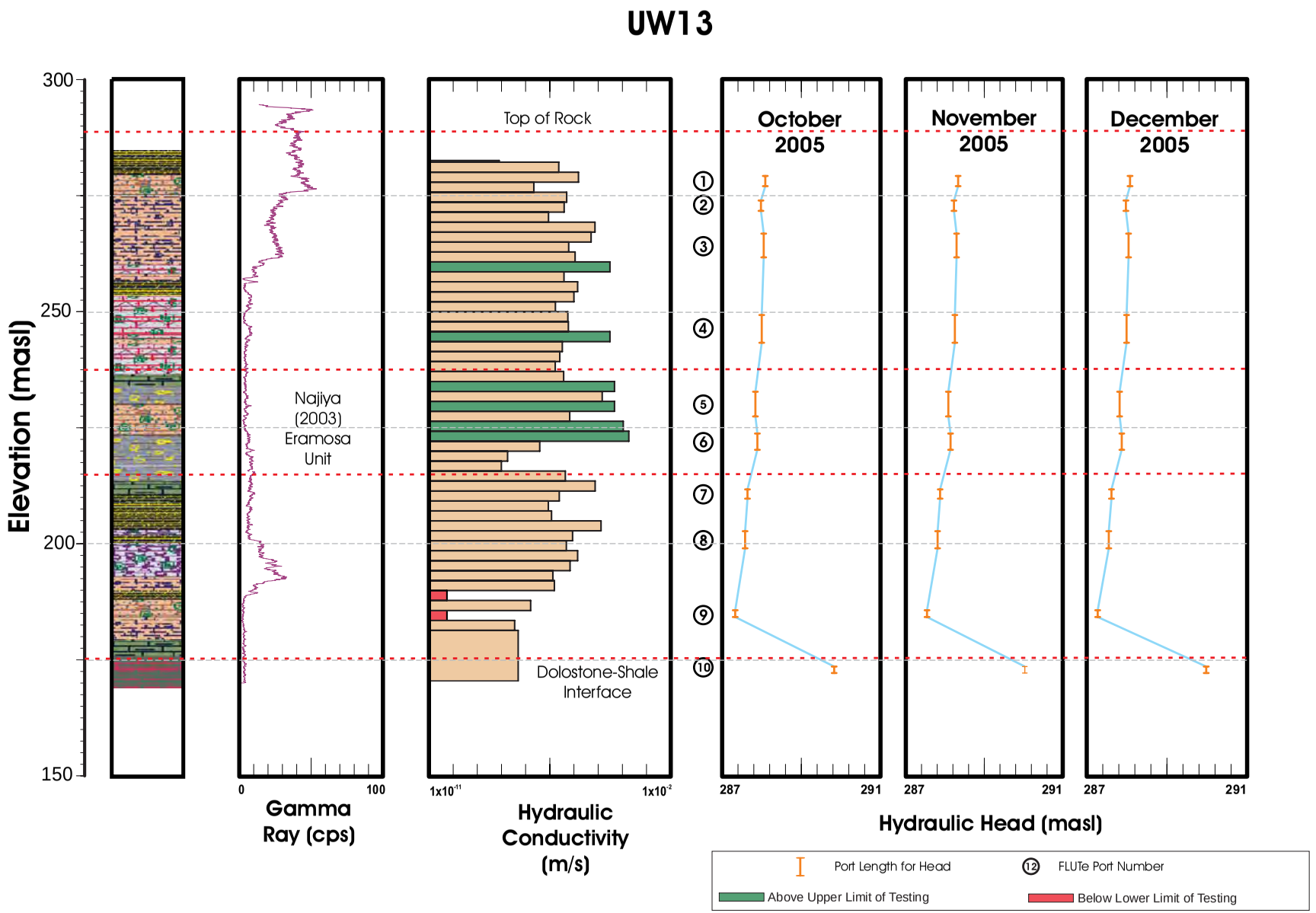


Figure 3.18: UW13 hydraulic head profiles for three representative time periods collected from the 10-port FLUTe multilevel system. The corelog along with gamma log and hydraulic conductivity data are shown for correlation. The vertical head profiles show a strong upward gradient from the shale into the overlying dolostone.

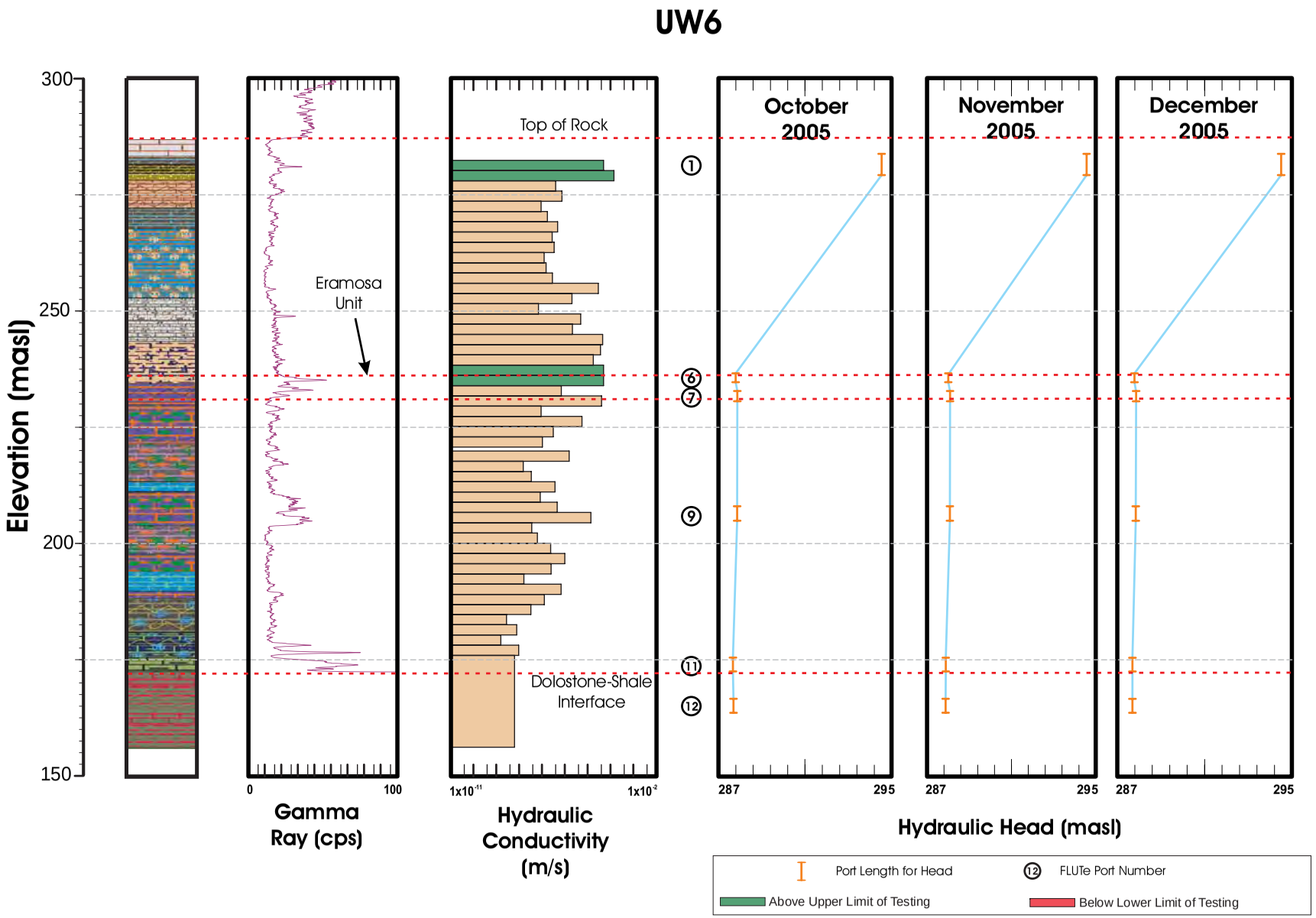


Figure 3.19: UW6 hydraulic head profiles for three representative time periods collected from the 12-port FLUTe multilevel system. The corelog column along with gamma log and hydraulic conductivity data are shown for correlation. The vertical head profiles show a strong gradient in the upper bedrock towards port 6 in the middle of the dolostone aquifer.

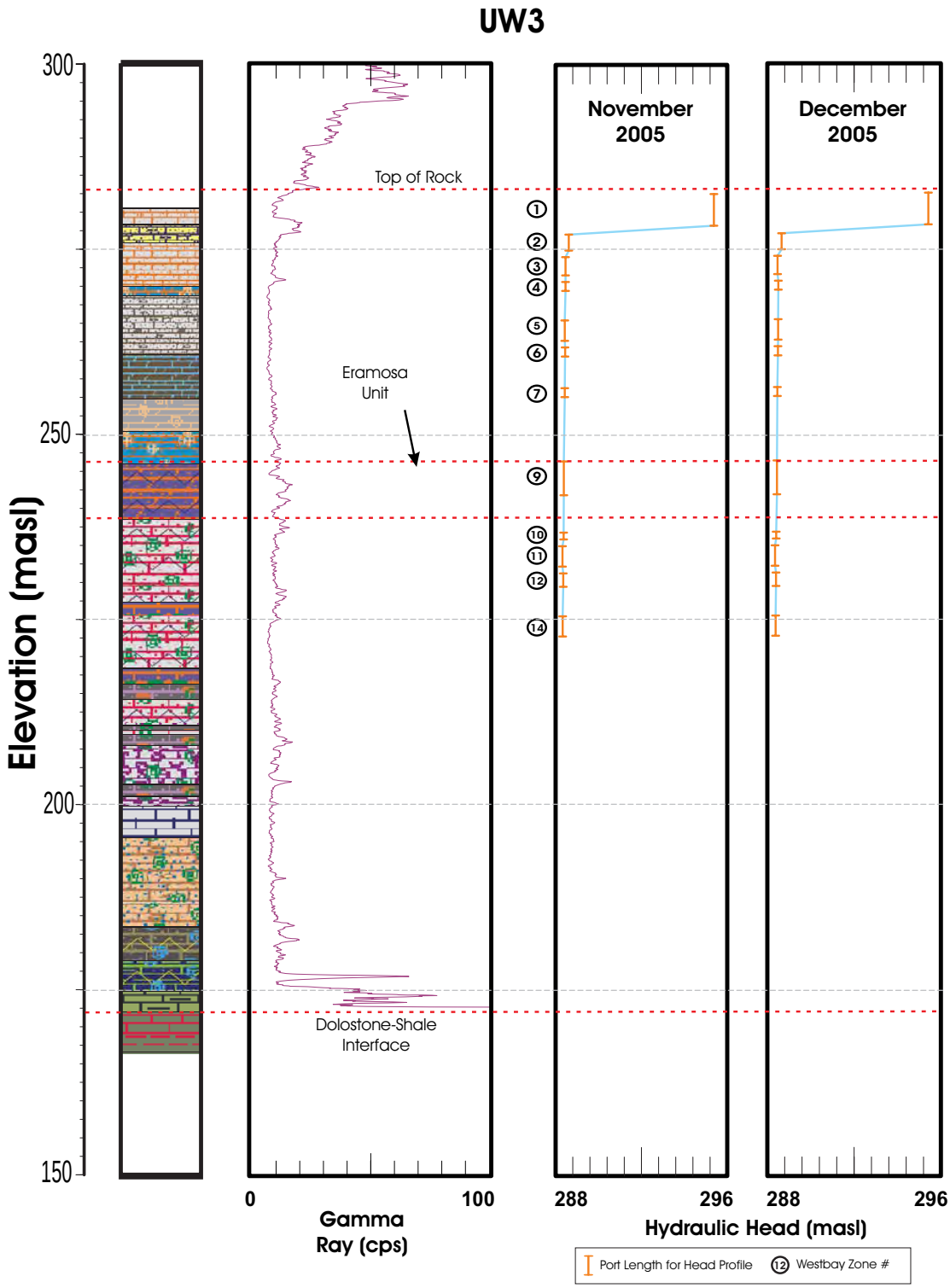


Figure 3.20: UW3 hydraulic head profiles for two representative time periods collected from the 14-zone Westbay multilevel system. The corelog column and gamma log are shown for correlation. The vertical head profiles show a strong vertical gradient in the upper two monitoring ports near the top of bedrock and essentially no strong vertical gradient throughout the rest of the hole.

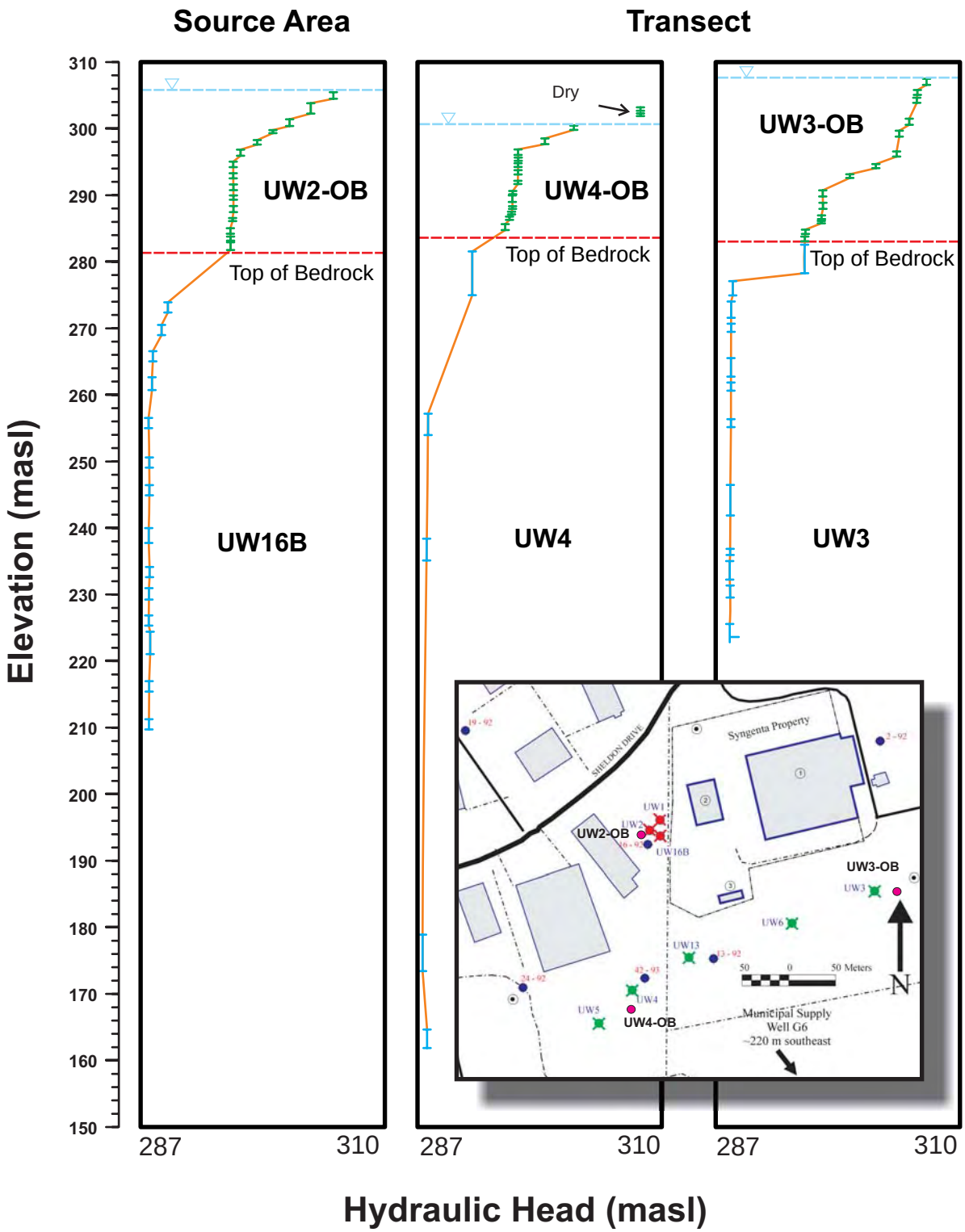


Figure 3.21: Composite vertical hydraulic head profiles from three overburden multilevel systems installed near existing multilevel systems installed in the dolostone aquifer. The overburden multilevel system installed near the metolachlor source area (UW16B) shows no vertical head loss through the overburden indicating strong hydraulic connection with the bedrock which is likely the location that DNAPL metolachlor entered the bedrock aquifer system.

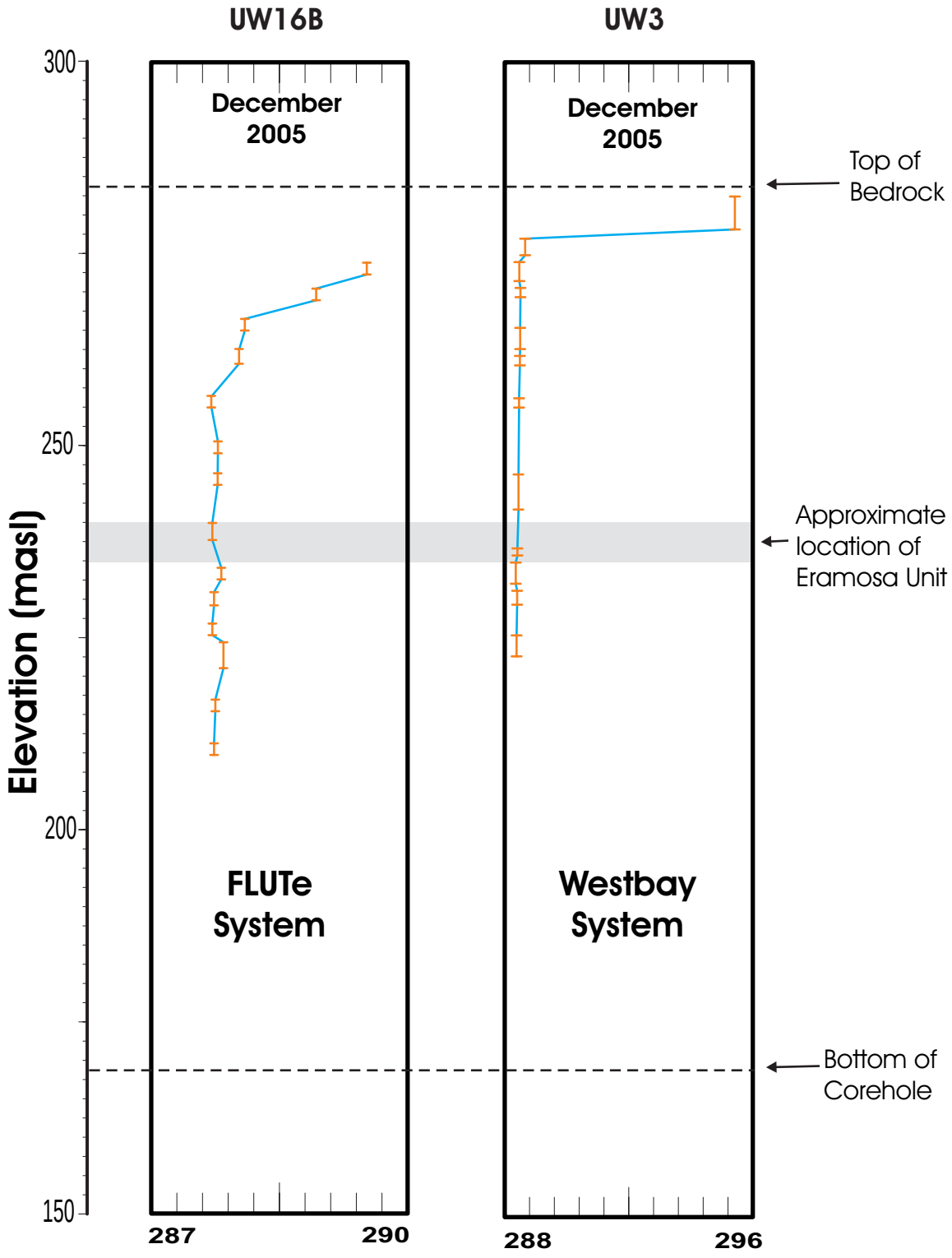


Figure 3.22: Comparison between the 15-port FLUTe multilevel system in UW16B and the 14-zone Westbay multilevel system in UW3. These two systems monitor generally the same depth of the aquifer, however it appears that the FLUTe multilevel is more variable with depth. However it is unknown whether this is related to hydrogeologic conditions or equipment biases.

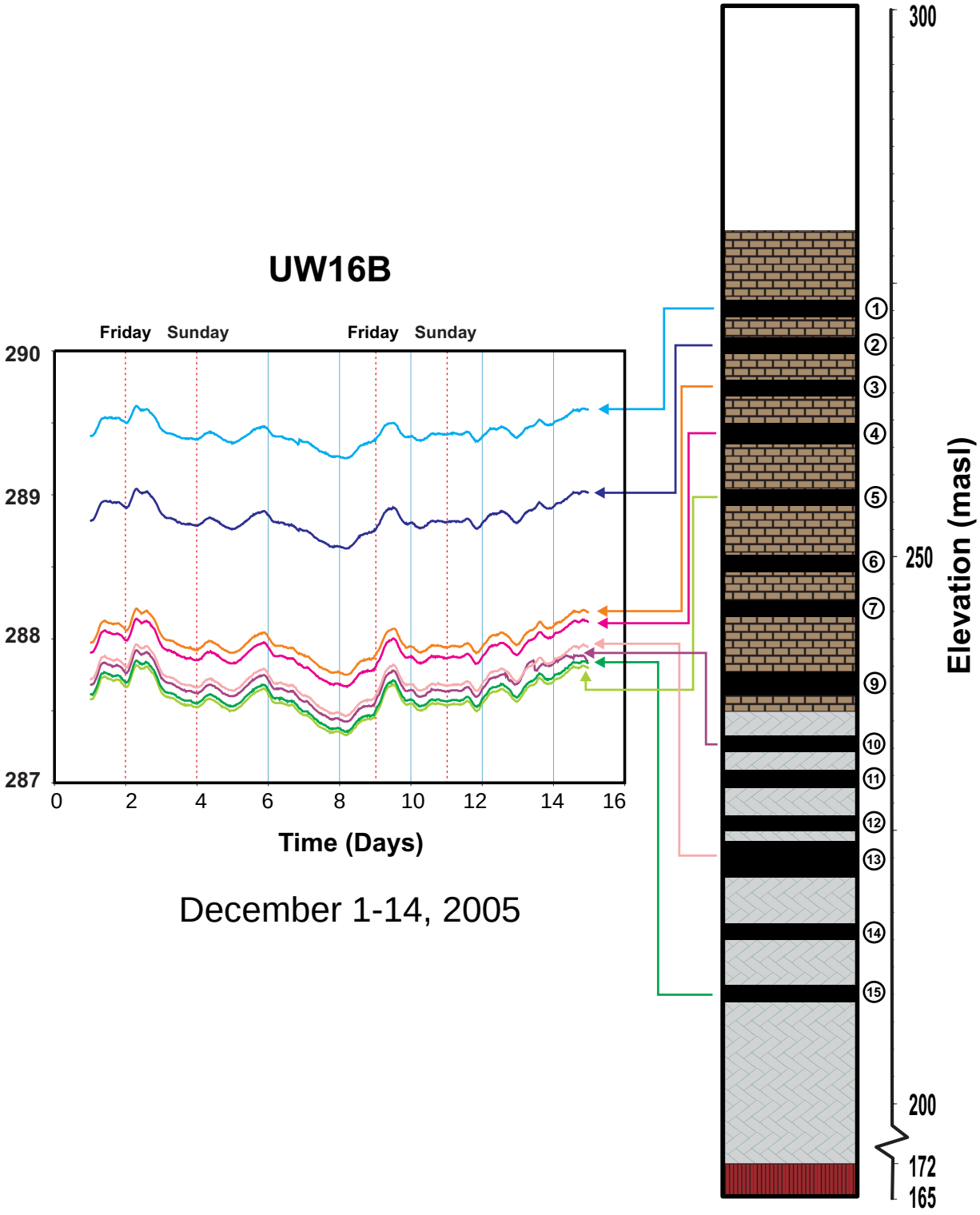


Figure 3.23: Hydraulic head data collected over a two week period as representative of UW16B.

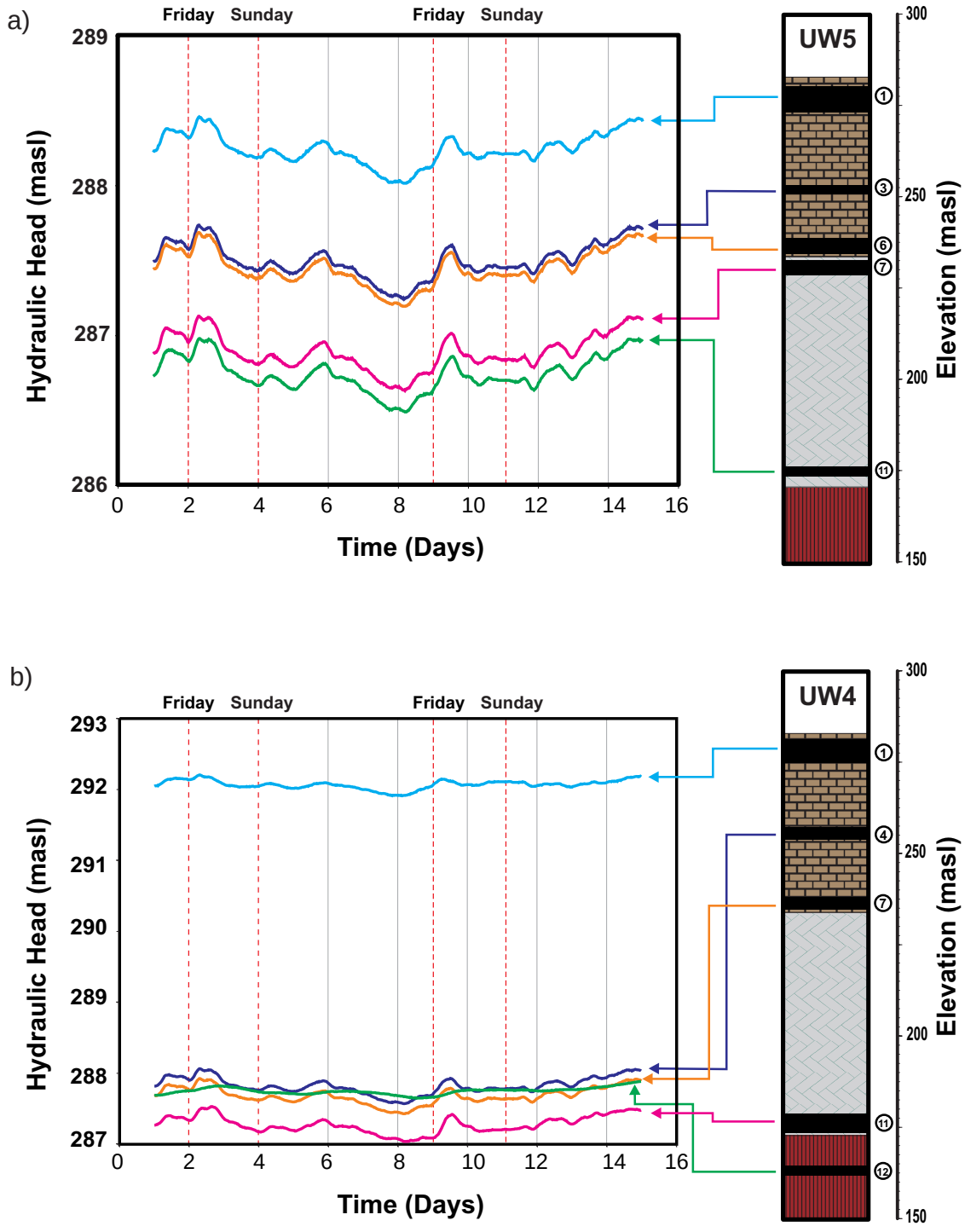


Figure 3.24: Hydraulic head data collected over a two week period as representative for UW5 (a) and UW4 (b).

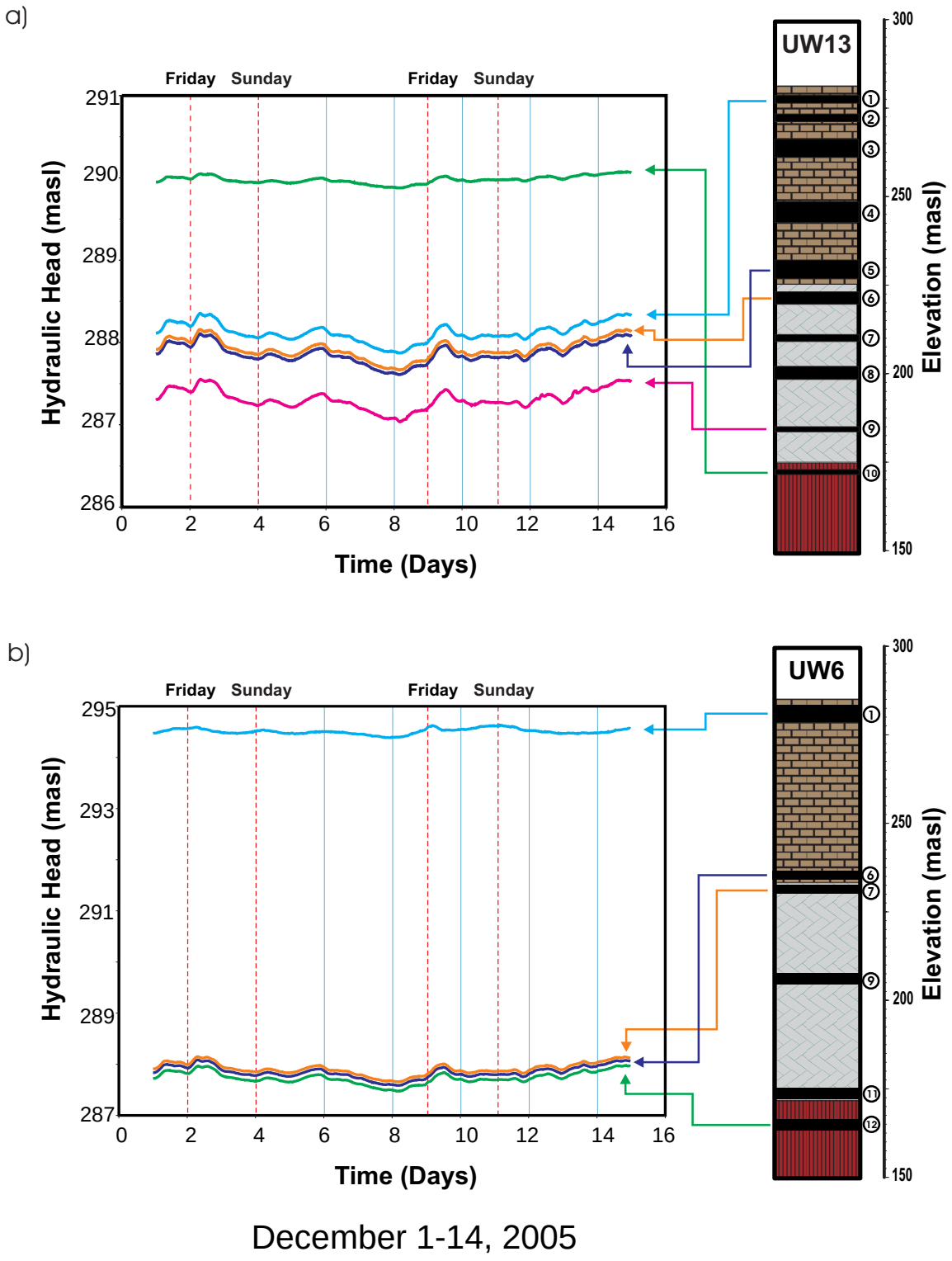


Figure 3.25: Hydraulic head data collected over a two week period as representative for UW13 (a) and UW6 (b).

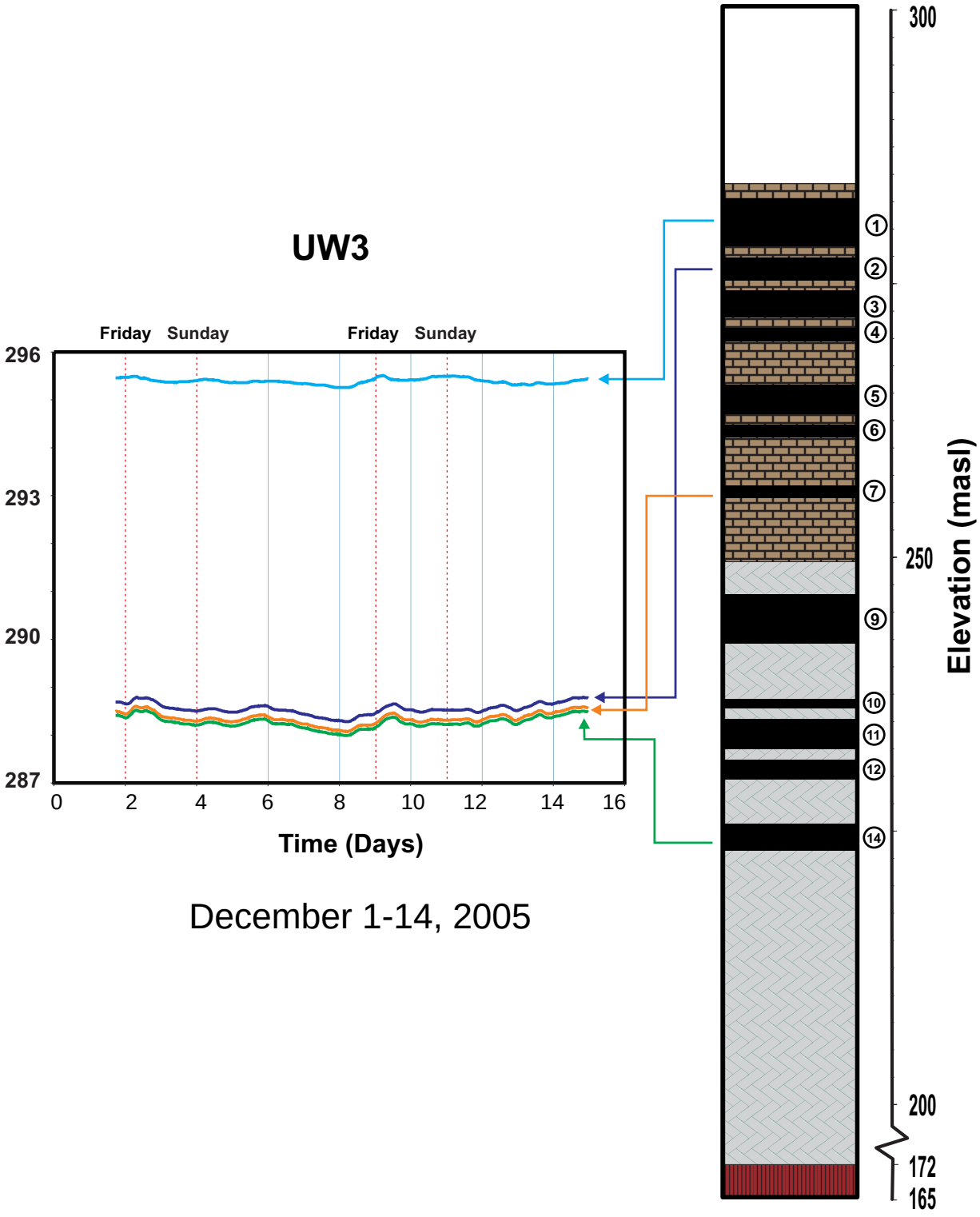


Figure 3.26: Hydraulic head data collected over a two week period as representative for UW3. A large vertical gradient occurs between the top two zones.

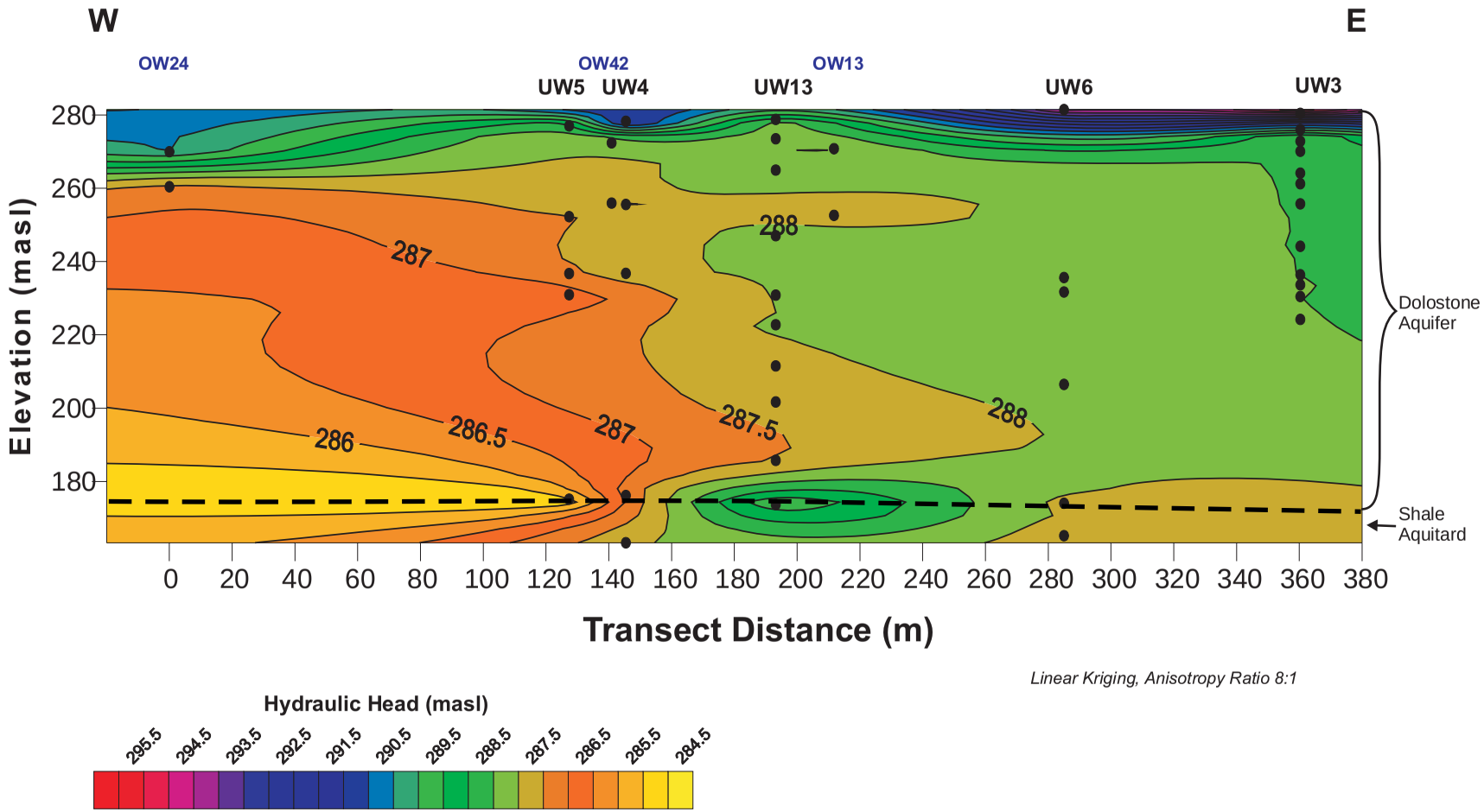


Figure 3.27: Hydraulic head contoured along the transect from conventional wells and multilevel systems in November 2005. These data are contoured using linear kriging and an anisotropy ratio of 8:1 to represent the preferential horizontal fractures and bedding planes.

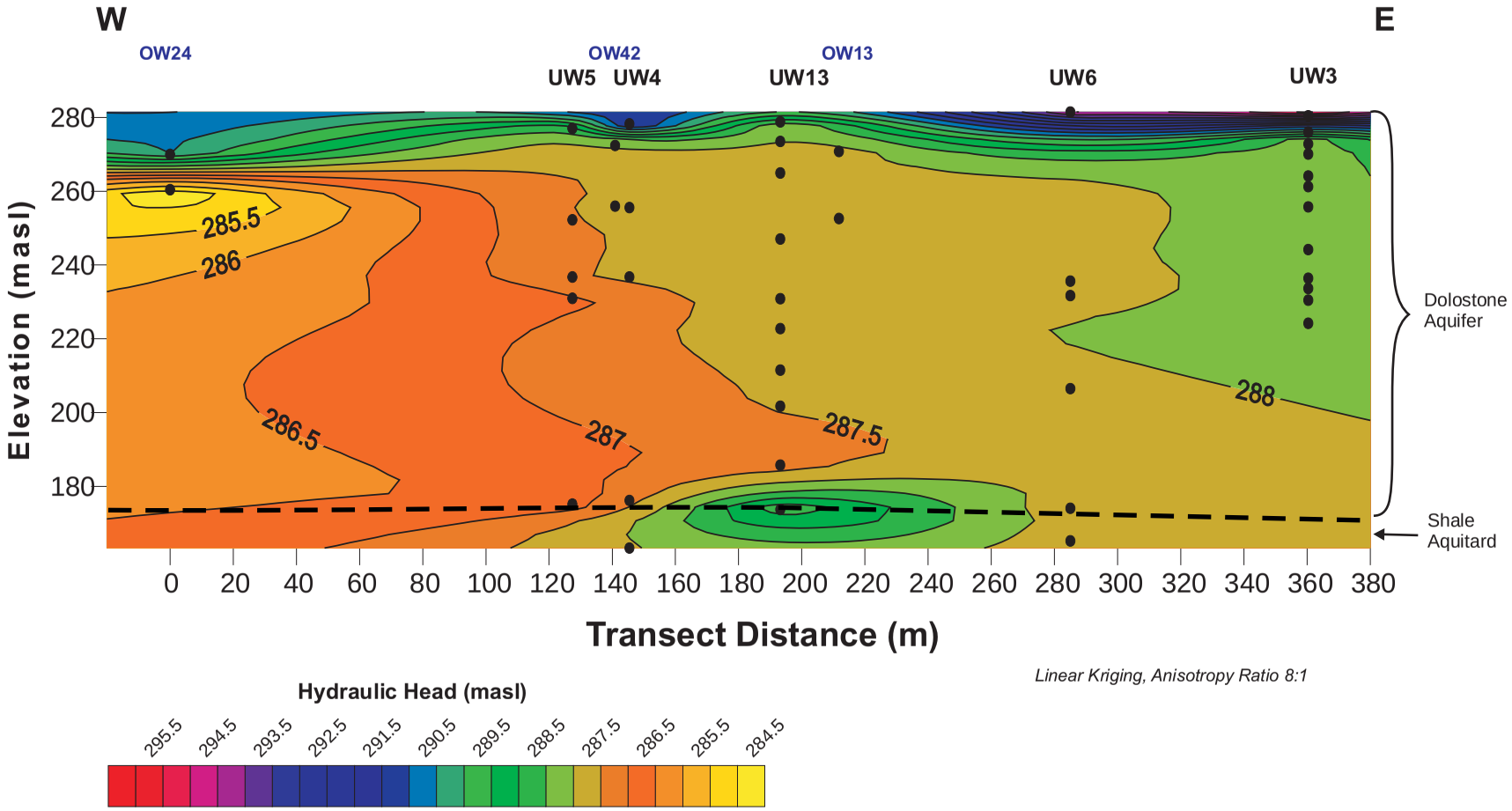


Figure 3.28: Hydraulic head contoured along the transect from conventional wells and multilevel systems in November 2005. These data are contoured using linear kriging and an anisotropy ratio of 8:1 to represent the preferential horizontal fractures and bedding planes.

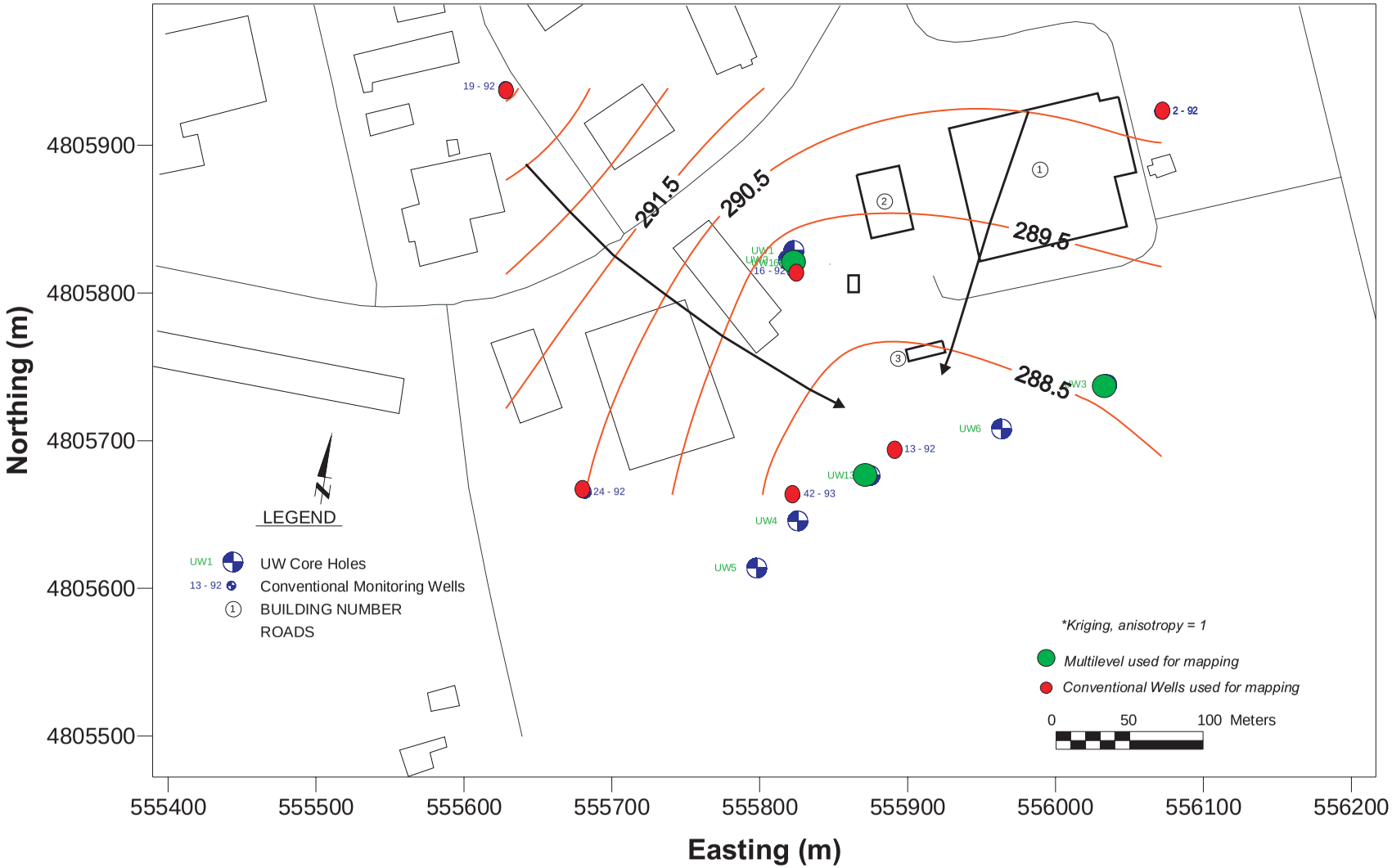


Figure 3.29: The potentiometric surface at 270 masl plotted for November, 2005 show a southward groundwater flow direction towards the transect. Conventional wells and multilevel systems screened near 270 masl were used for this surface.

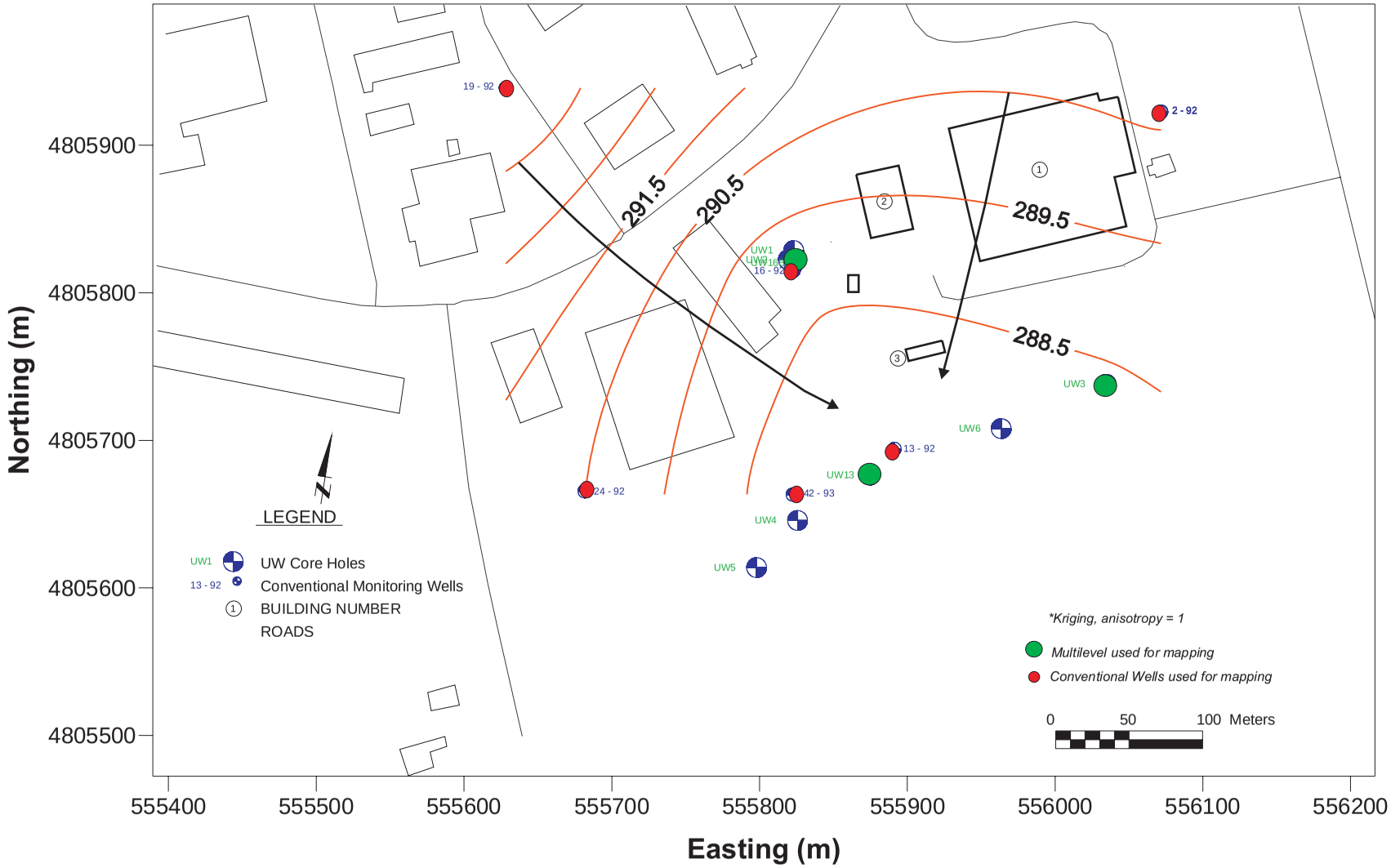


Figure 3.30: The potentiometric surface at 270 masl plotted for December, 2005 show a southward groundwater flow direction towards the transect. Conventional wells and multilevel systems screened near 270 masl were used for this surface.

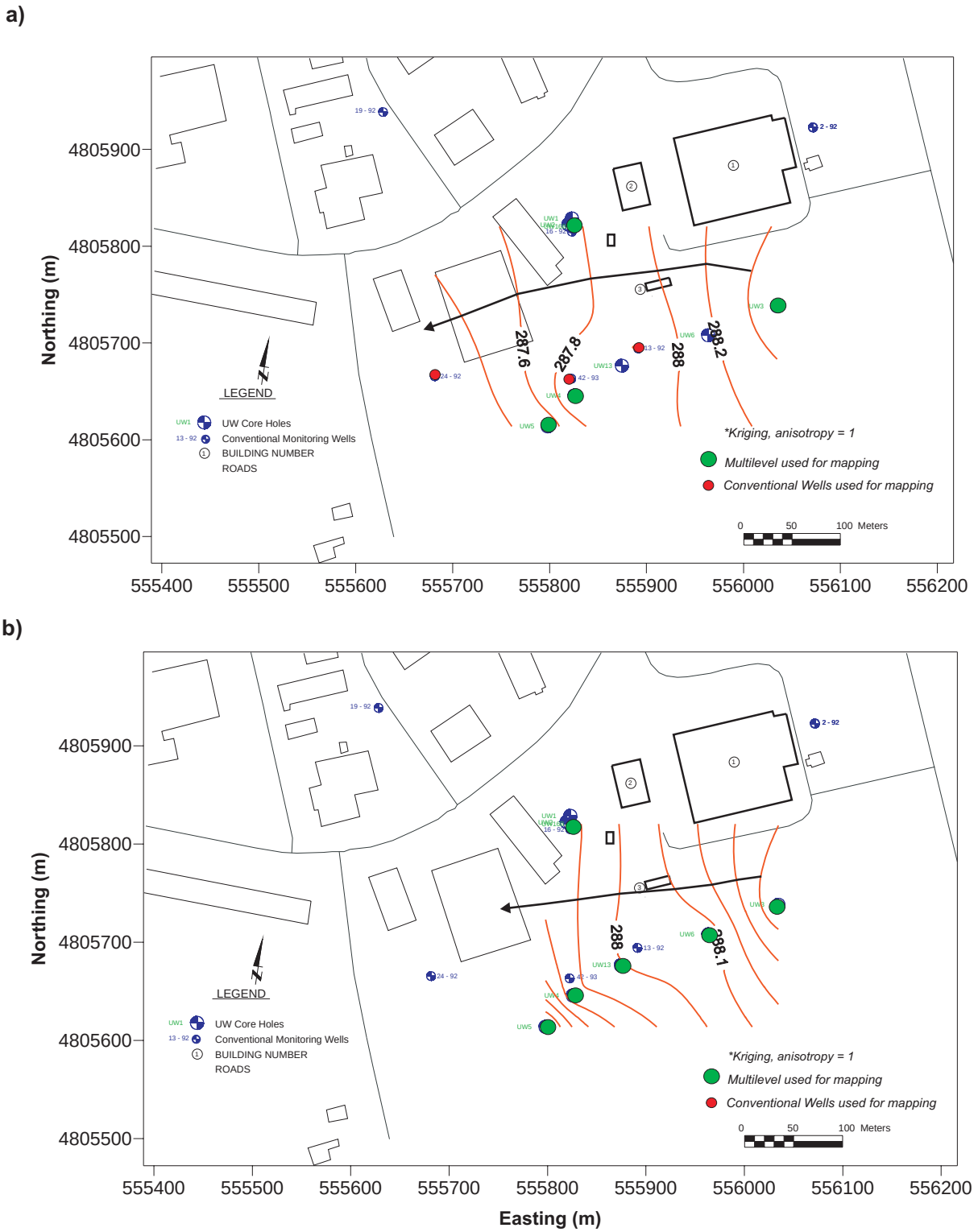


Figure 3.31: Potentiometric surfaces for a) 250 masl on November, 2005, which includes conventional wells and multilevels, and b) 235 masl on November, 2005, which only includes multilevel data points. Hydraulic gradients from these elevations show a flow direction to the west.

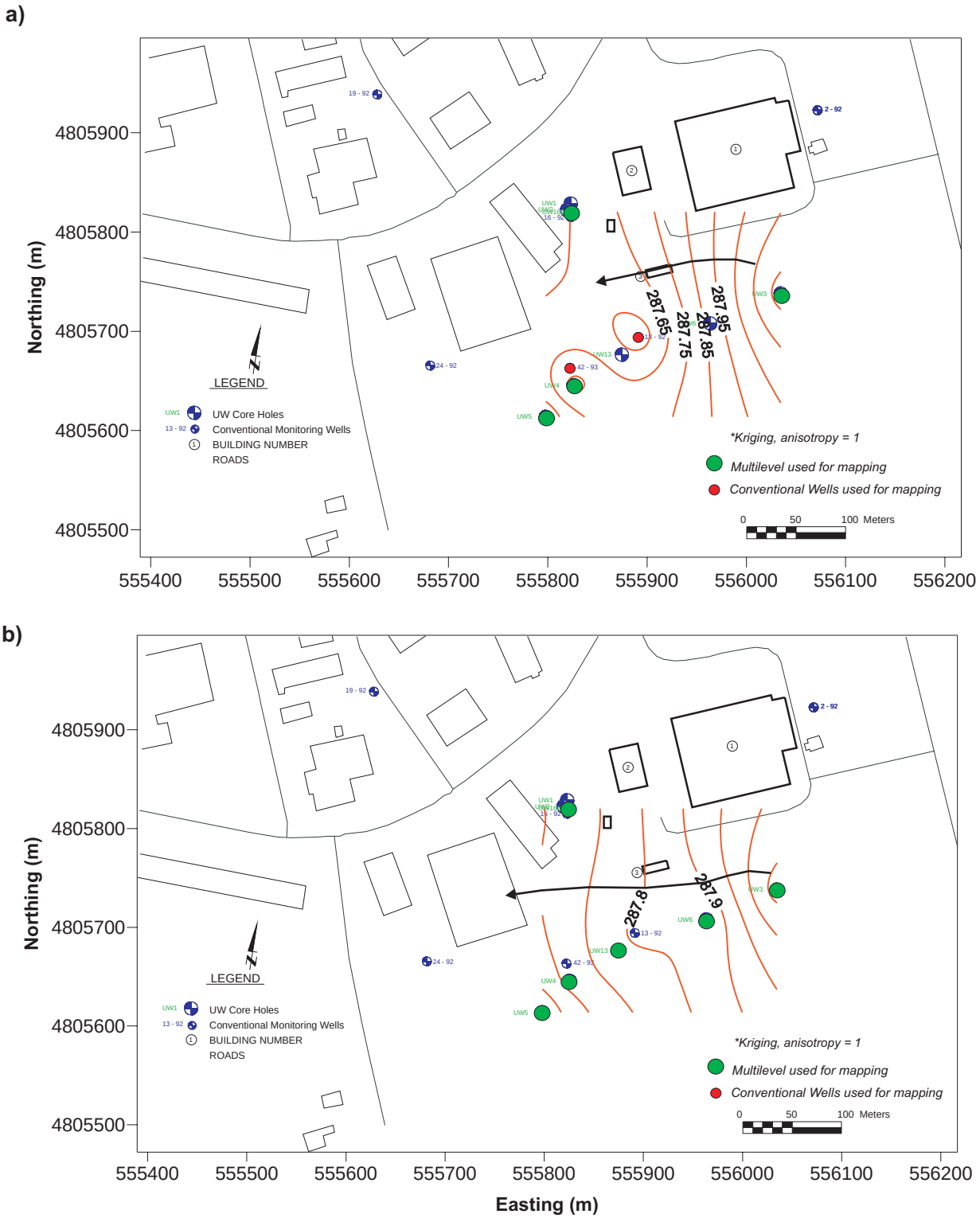


Figure 3.32: Potentiometric surfaces for a) 250 masl on December, 2005, which includes conventional wells and multilevels, and b) 235 masl on December, 2005, which only includes multilevel data points. Hydraulic gradients from these elevations show a flow direction to the west.

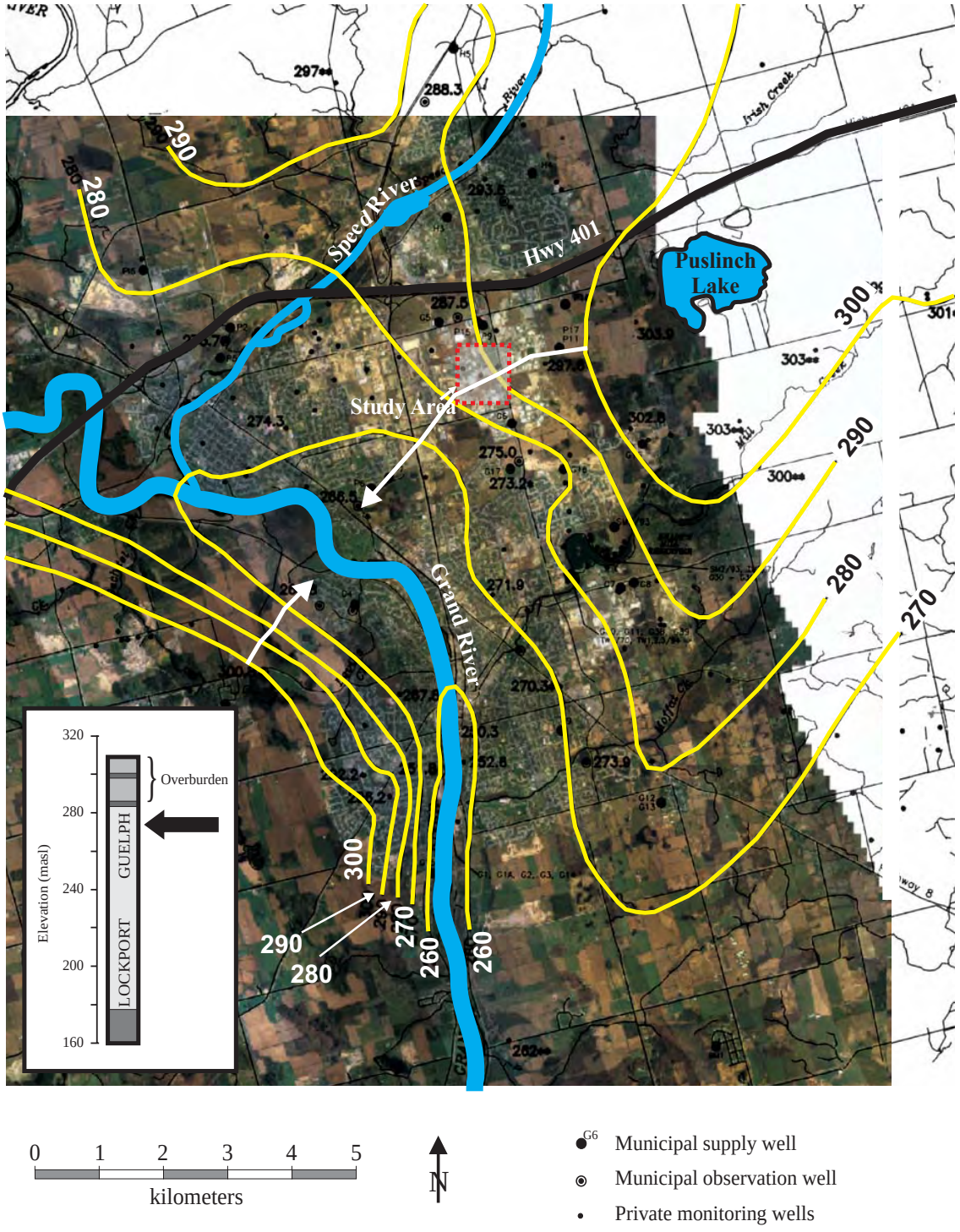


Figure 3.33: Regional potentiometric surface for the upper Guelph Formation dolostone based on data from Lotowater Ltd. (1997). Groundwater flow in the study area is to the south-west, towards the Grand River (Adapted from Burns (2005).

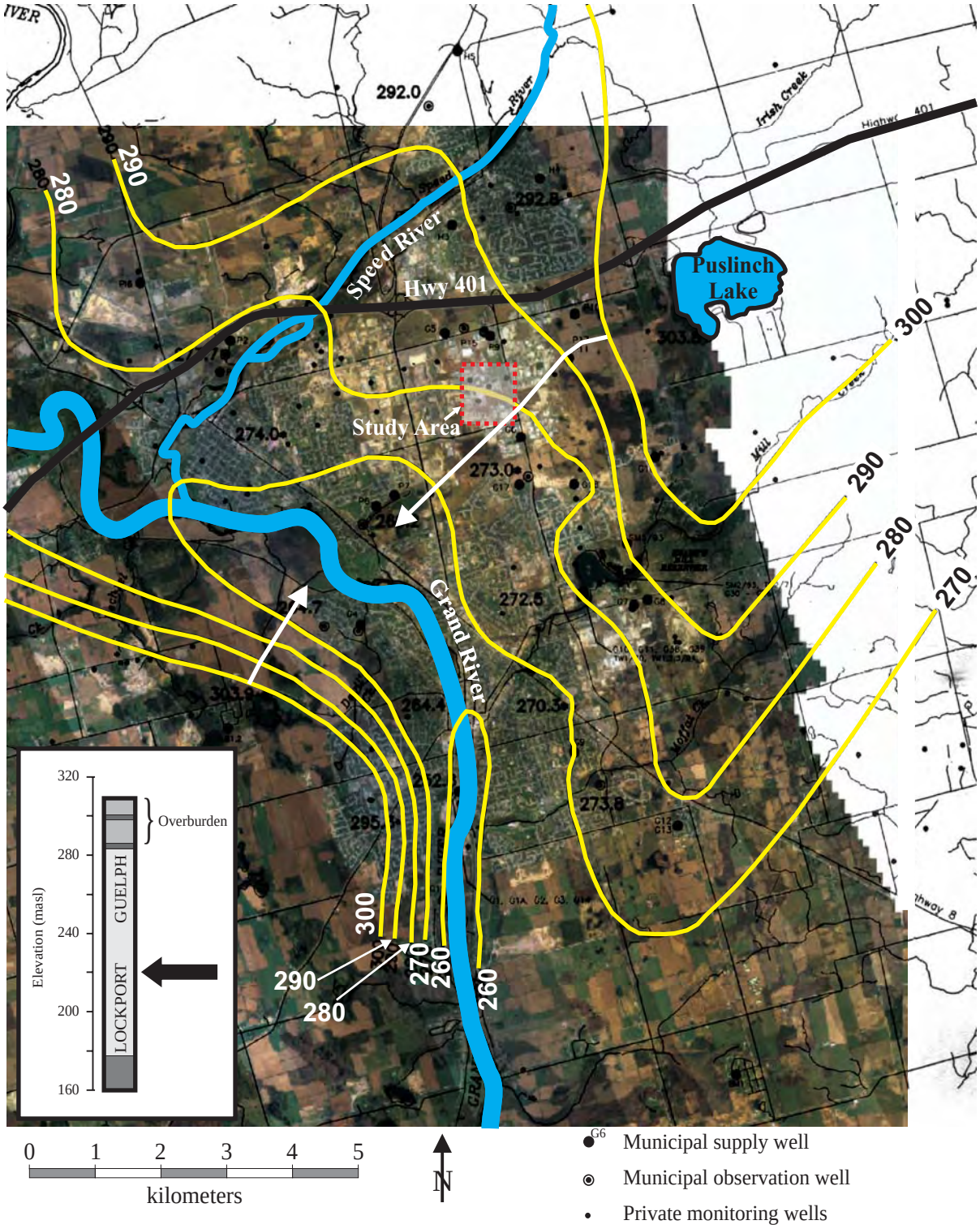


Figure 3.34: Regional potentiometric surface for the Lockport Formation dolostone based on data from Lotowater Ltd. (1997). Groundwater flow in the study area is to the southwest, towards the Grand River (Adapted from Burns (2005).

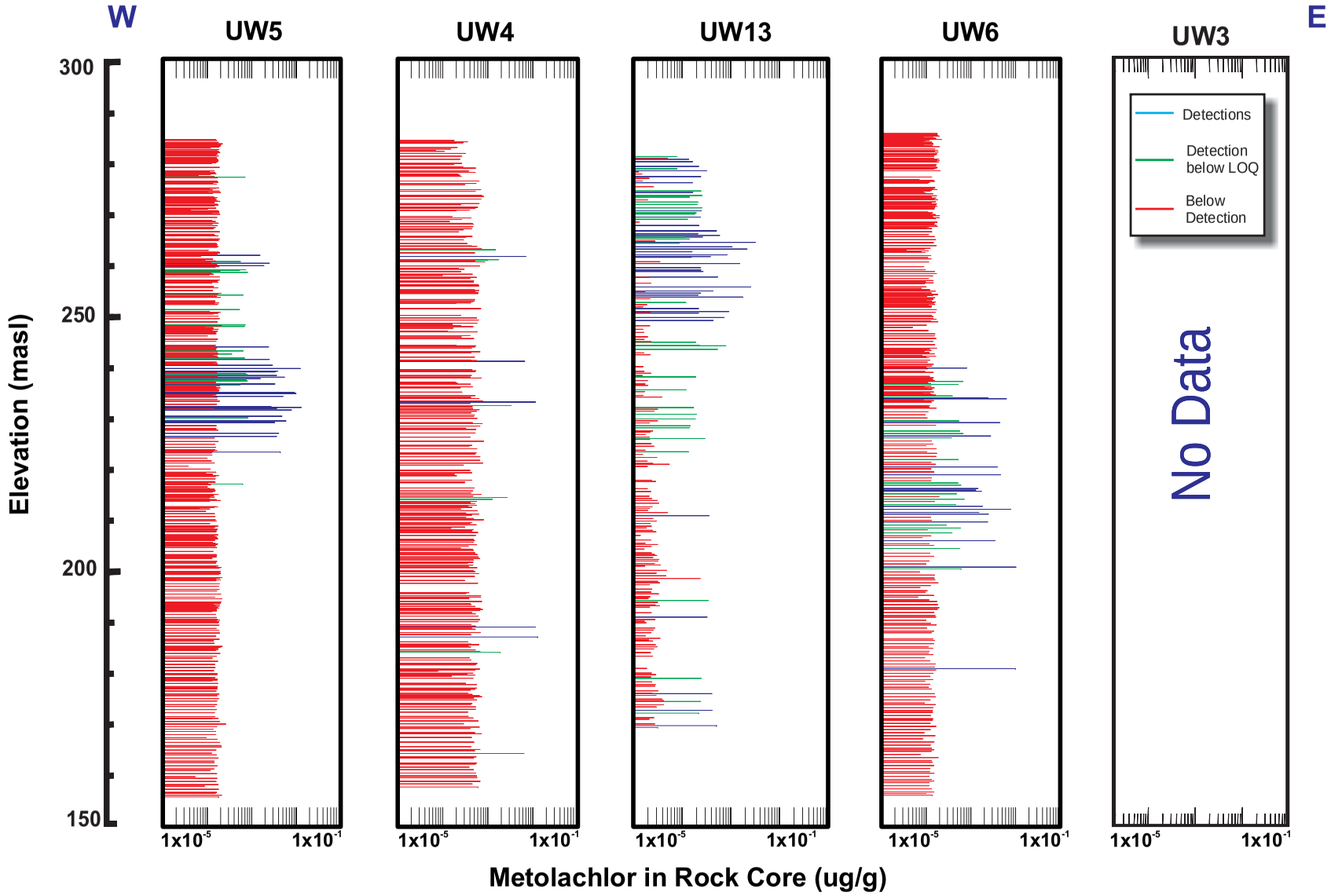


Figure 3.35: Total metolachlor rock concentrations from coreholes along the transect. Metolachlor samples were not analysed from UW3 due to a storage problem.

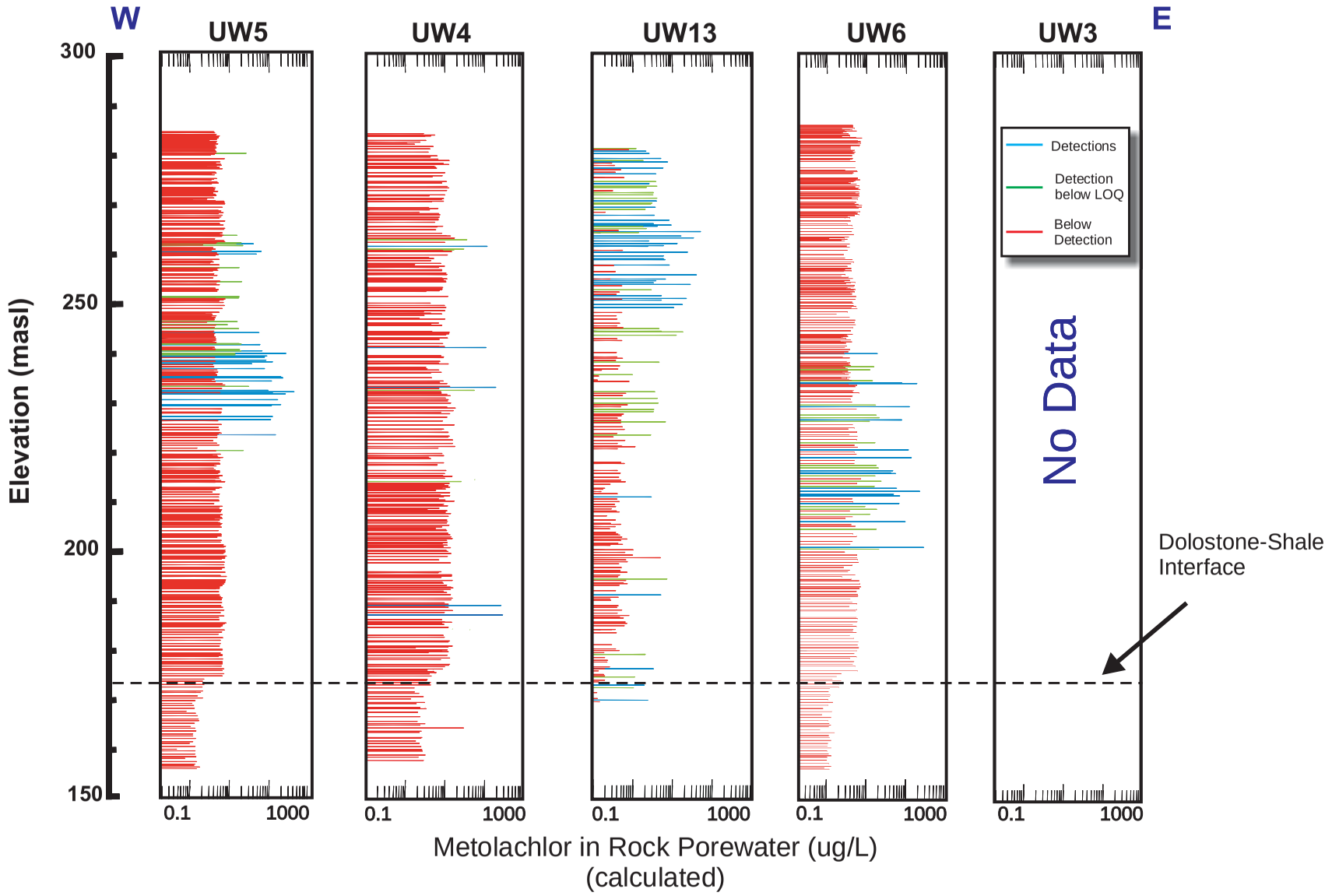


Figure 3.36: Metolachlor rock core concentrations converted to equivalent porewater concentrations along the transect.

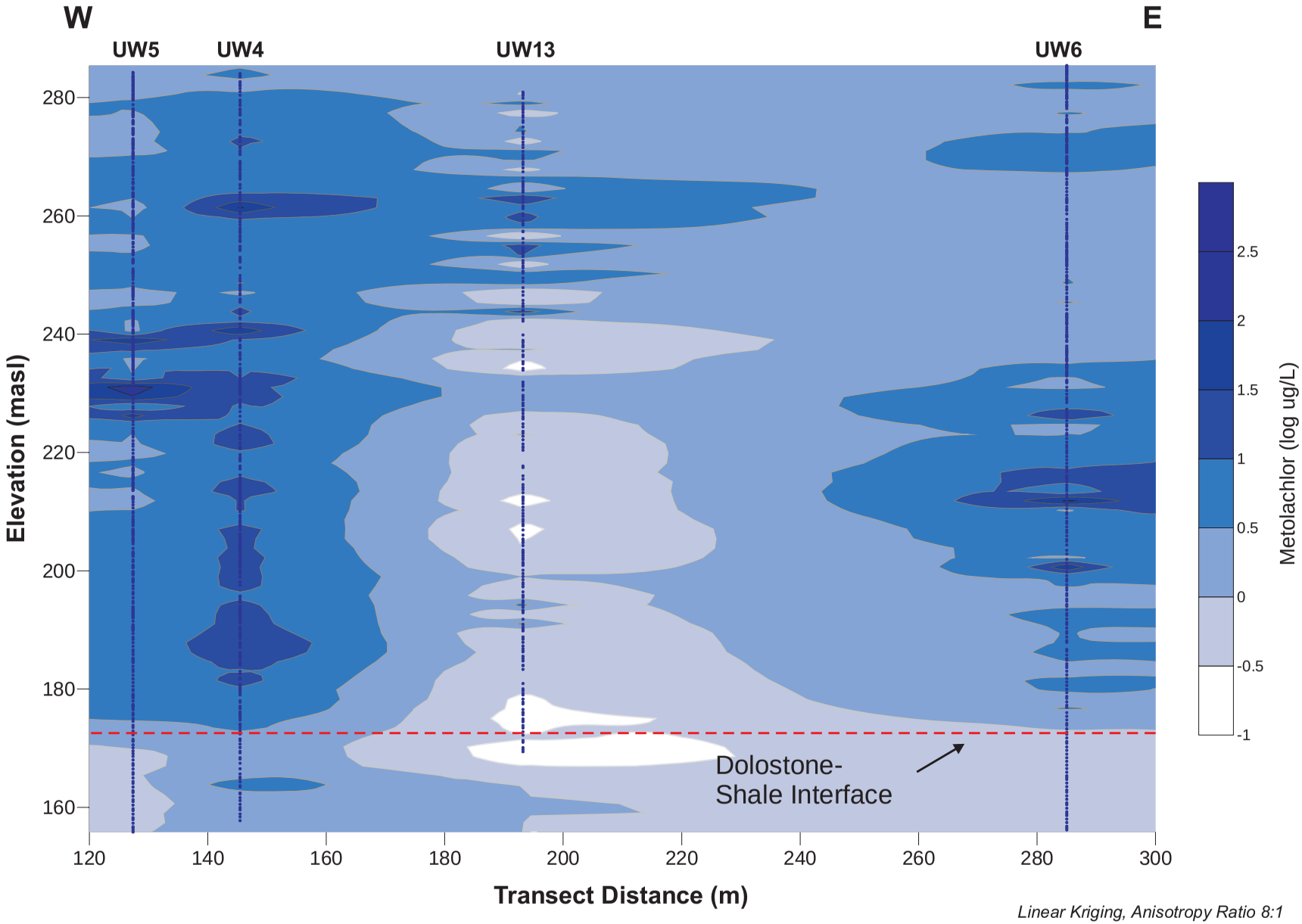


Figure 3.37: Metolachlor rock core concentrations converted to equivalent porewater concentrations along the transect are contoured to show where local maximum concentrations occur and to determine if any laterally extensive contamination zones are present.

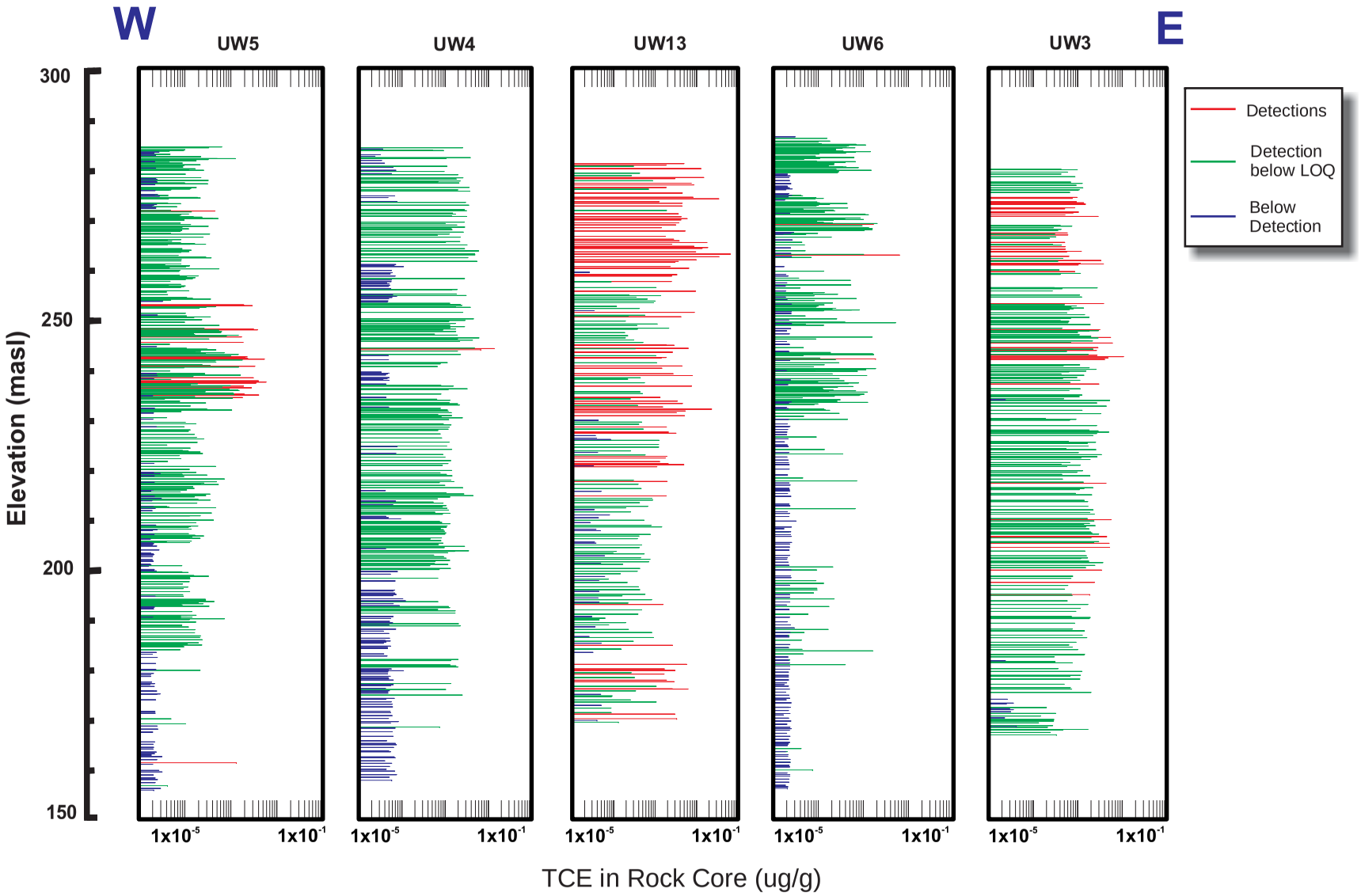


Figure 3.38: Total TCE rock concentrations from coreholes along the transect. UW13 has the highest TCE concentrations in the rock core.

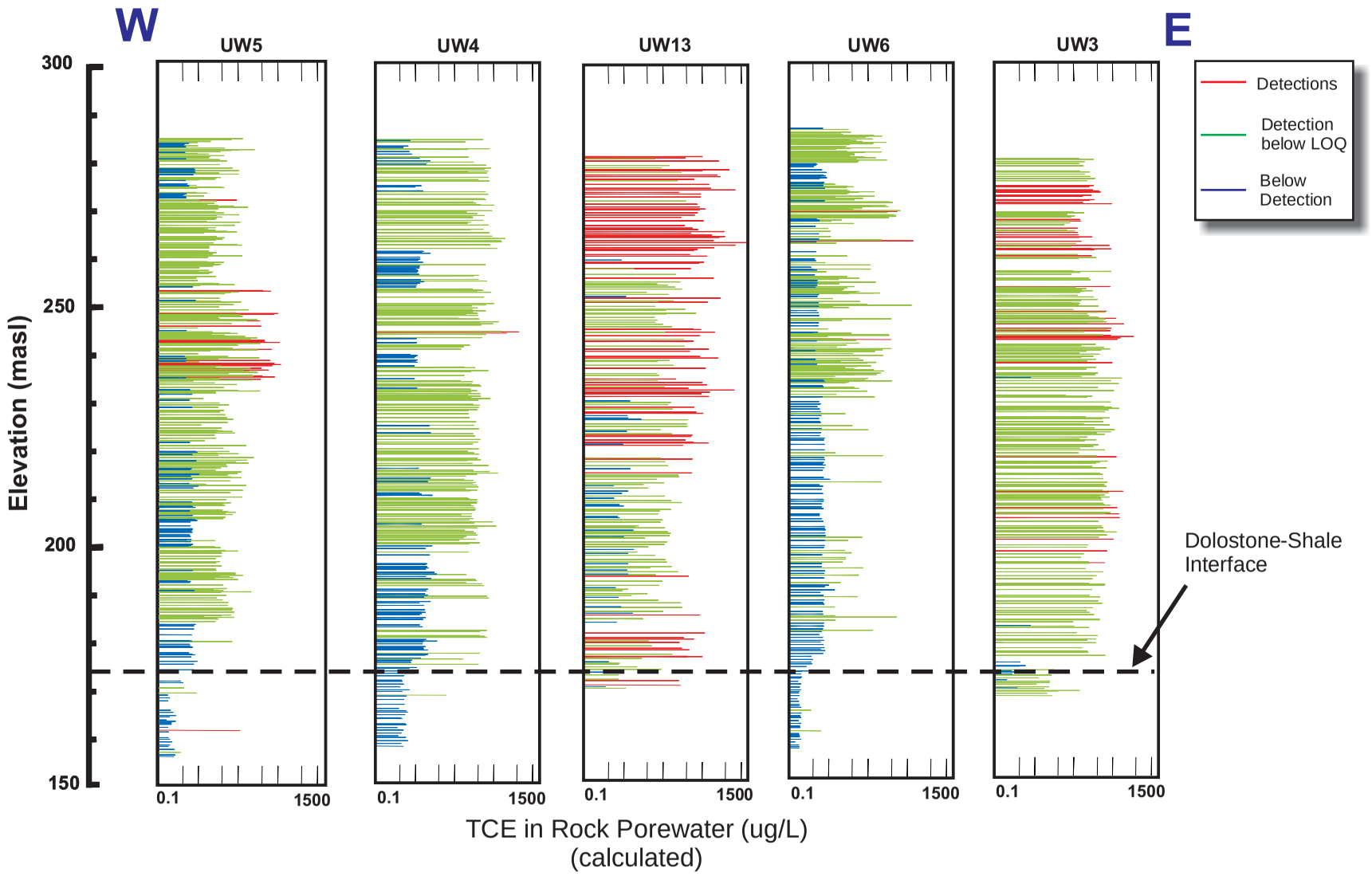


Figure 3.39: TCE rock core concentrations converted to equivalent porewater concentrations along the transect.

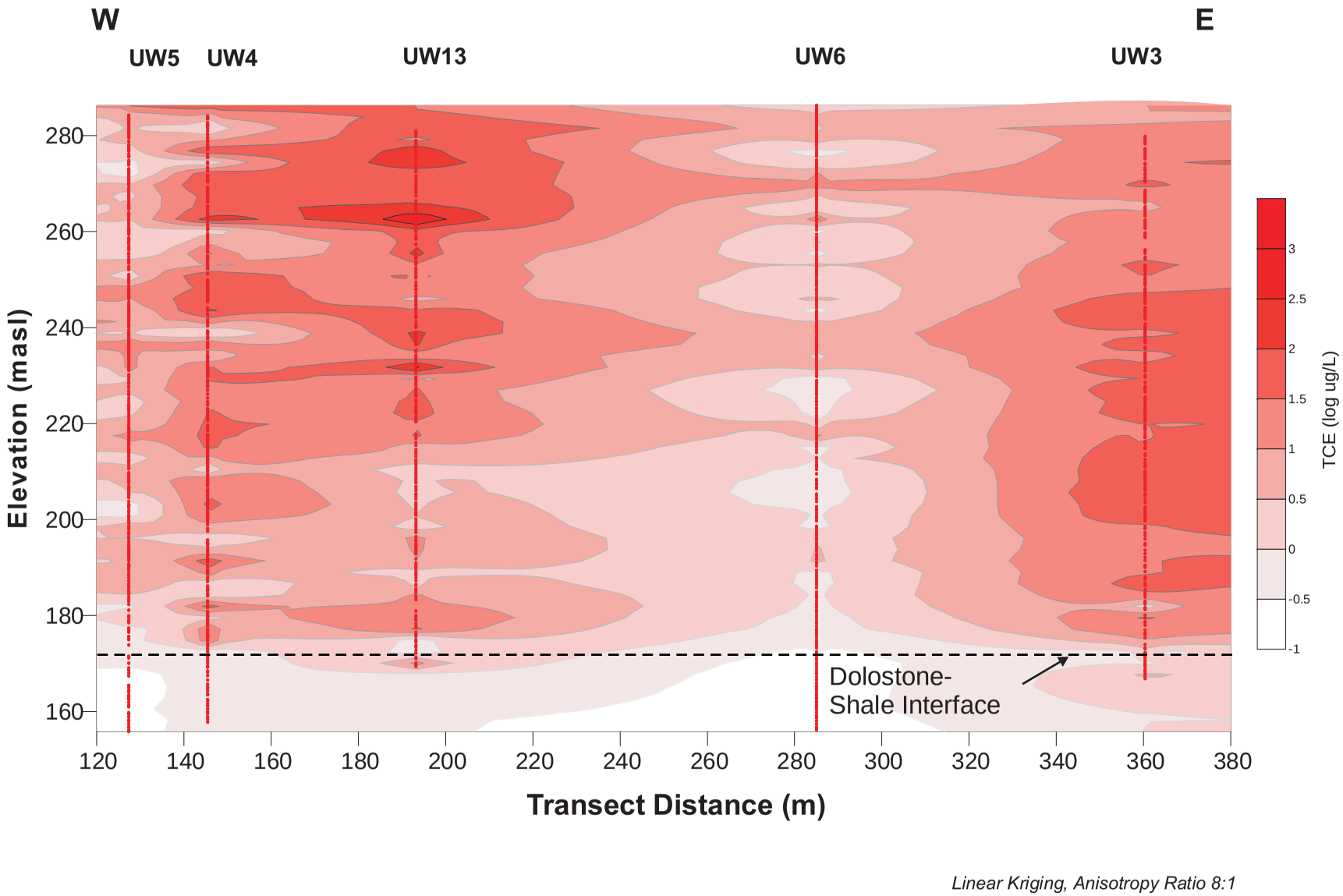


Figure 3.40: TCE rock core log concentrations converted to equivalent porewater concentration. The contoured data show occurrence of high concentrations zones which may be related to hydraulically active fractures. These data were contoured using linear kriging and an anisotropy ratio of 8:1.

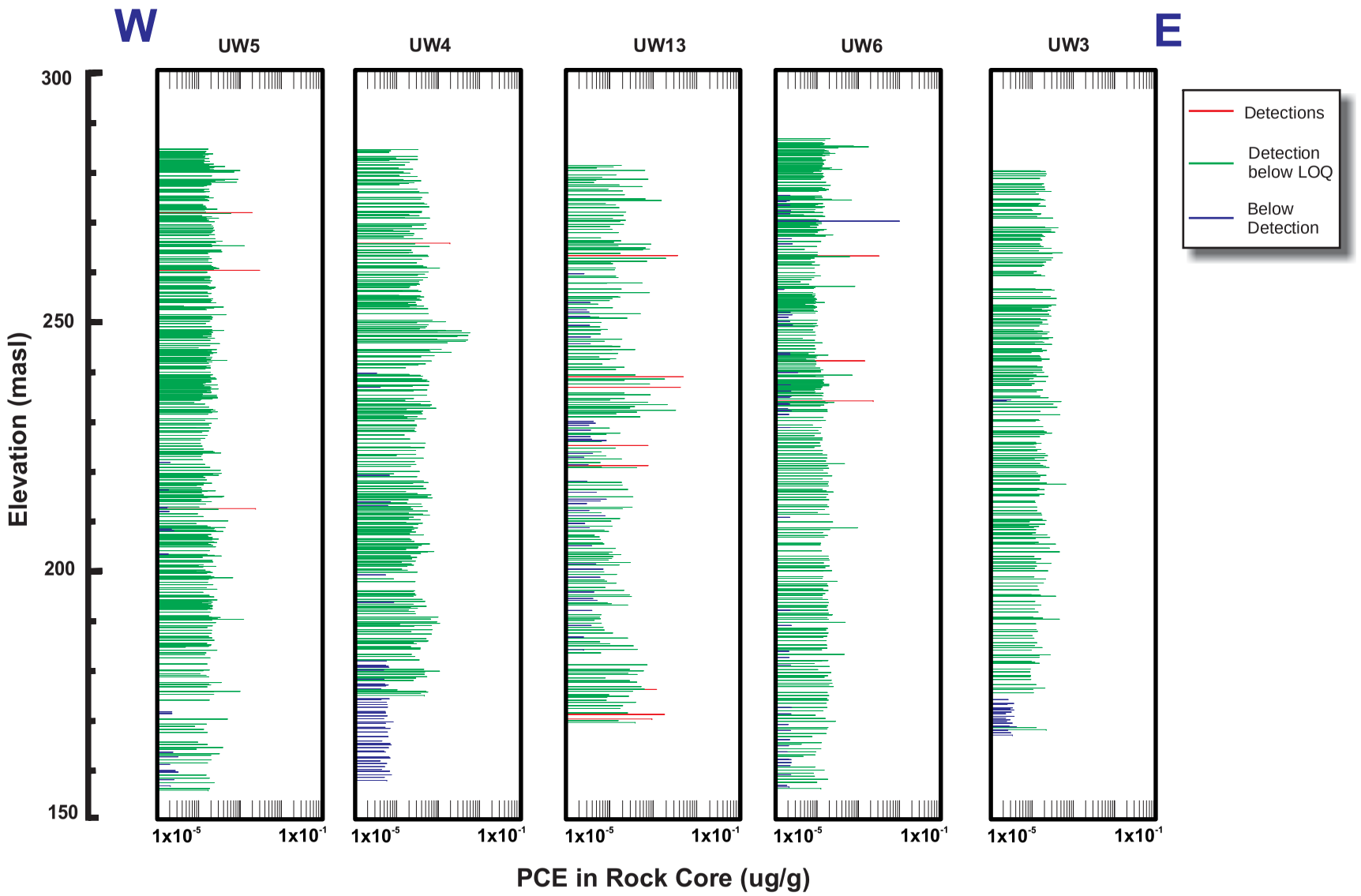


Figure 3.41: Total PCE concentrations in rock core collected along the transect during drilling at the Cambridge site.

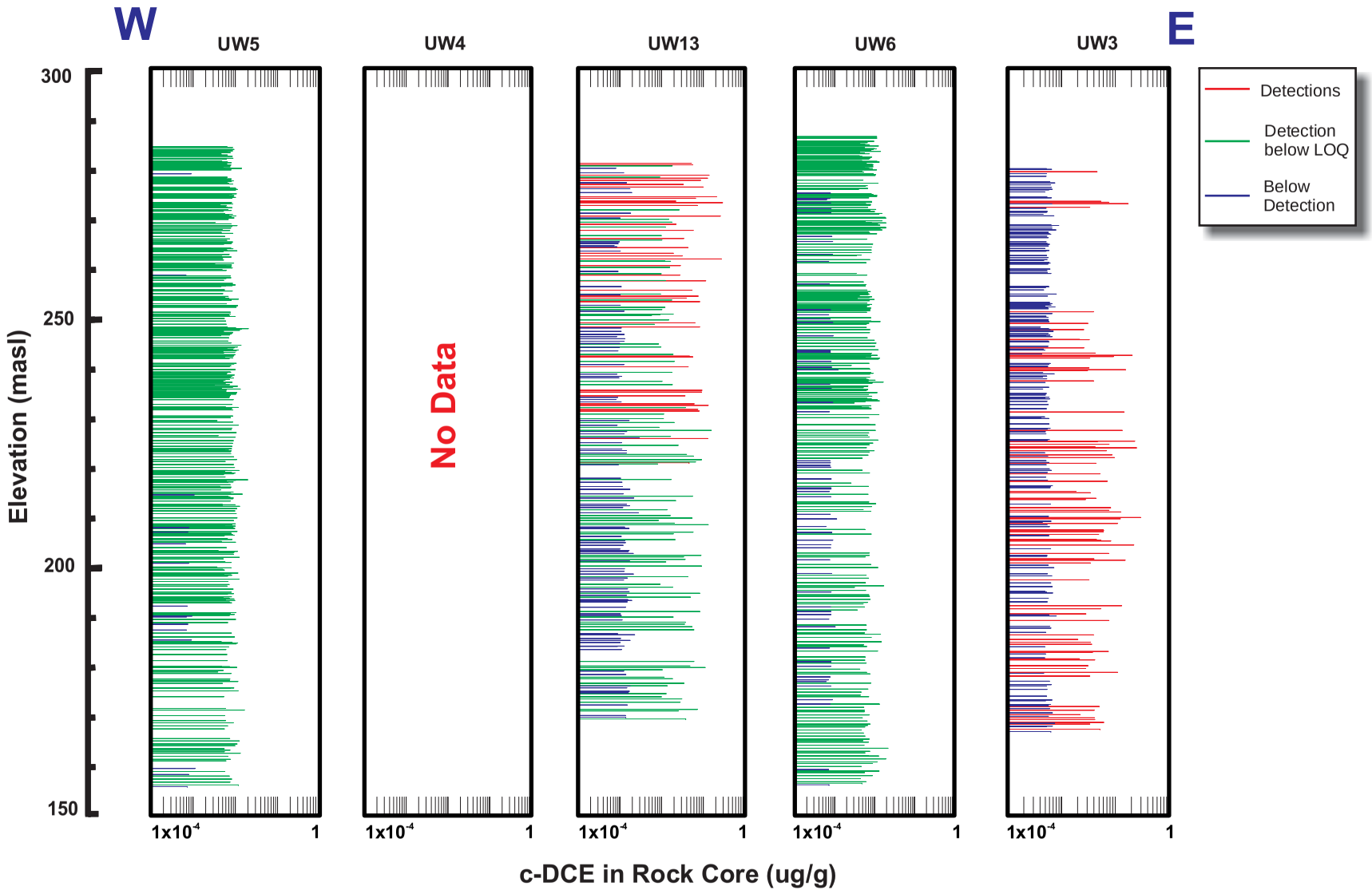


Figure 3.42: Total cDCE concentrations in rock core collected along the transect during drilling at the Cambridge site. cDCe was not analysed for in UW4.

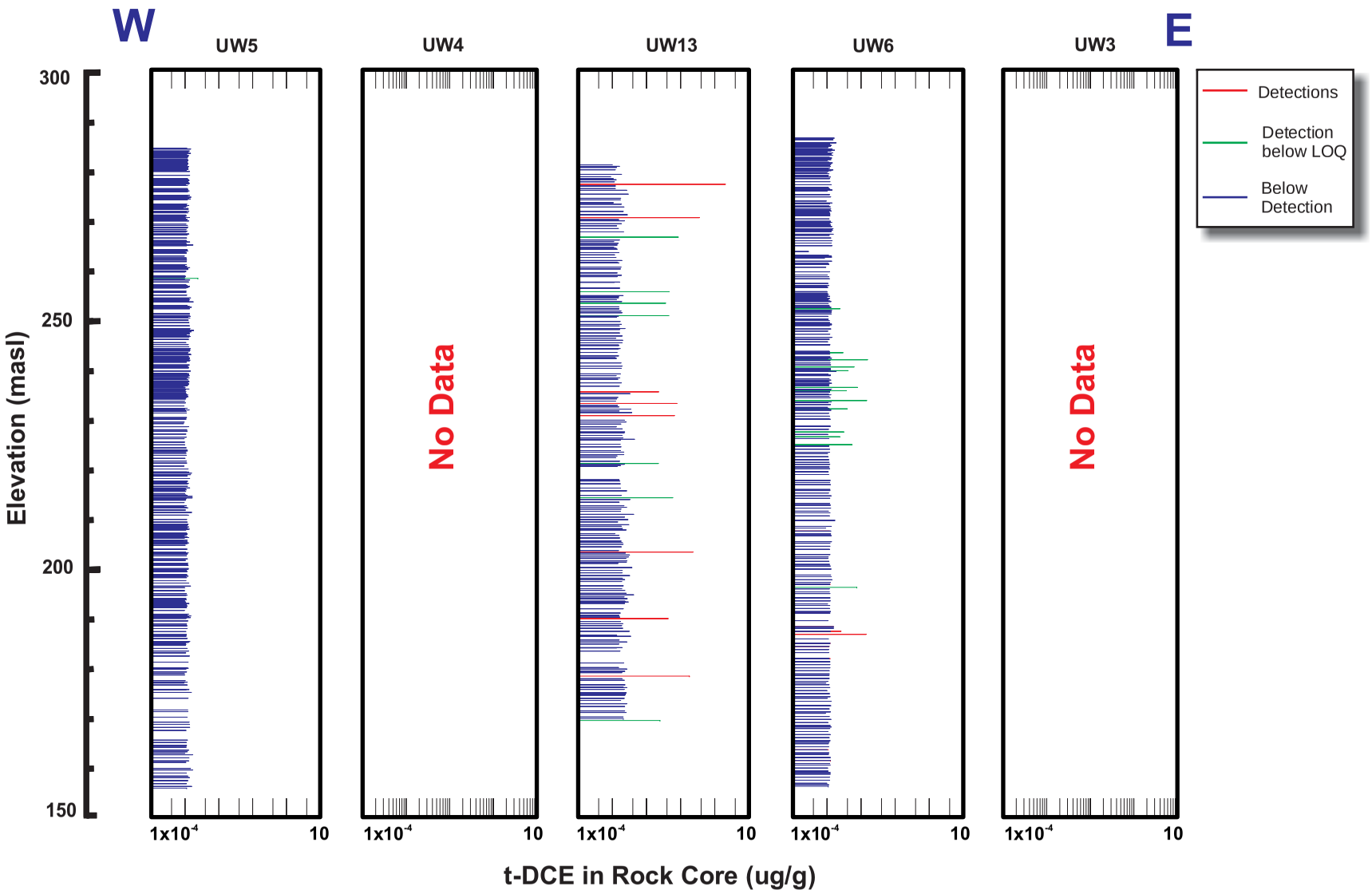


Figure 3.43: Total tDCE concentrations in rock core collected along the transect during drilling at the Cambridge site. tDCe was not analysed for in UW4 or UW3. UW13 has extremely high values of tDCE in rock core, although the number of detections is low, the concentrations are much higher than TCE.

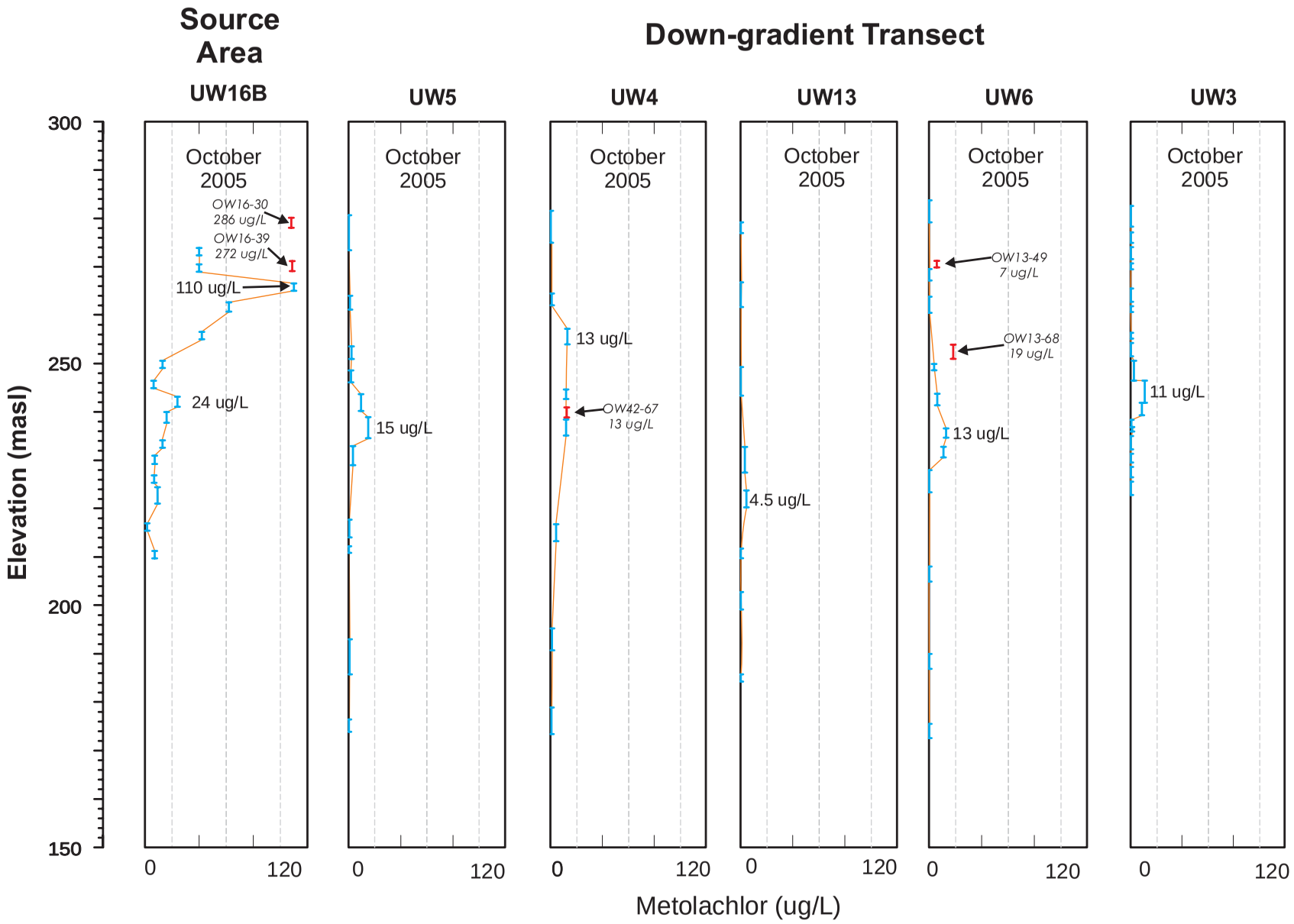


Figure 3.44: Metolachlor concentration profiles from multilevel systems in UW16B and on the transect. These data show a large concentration peak in the upper bedrock and a lower peak in the middle part of the dolostone which coincides with the transect peak concentrations.

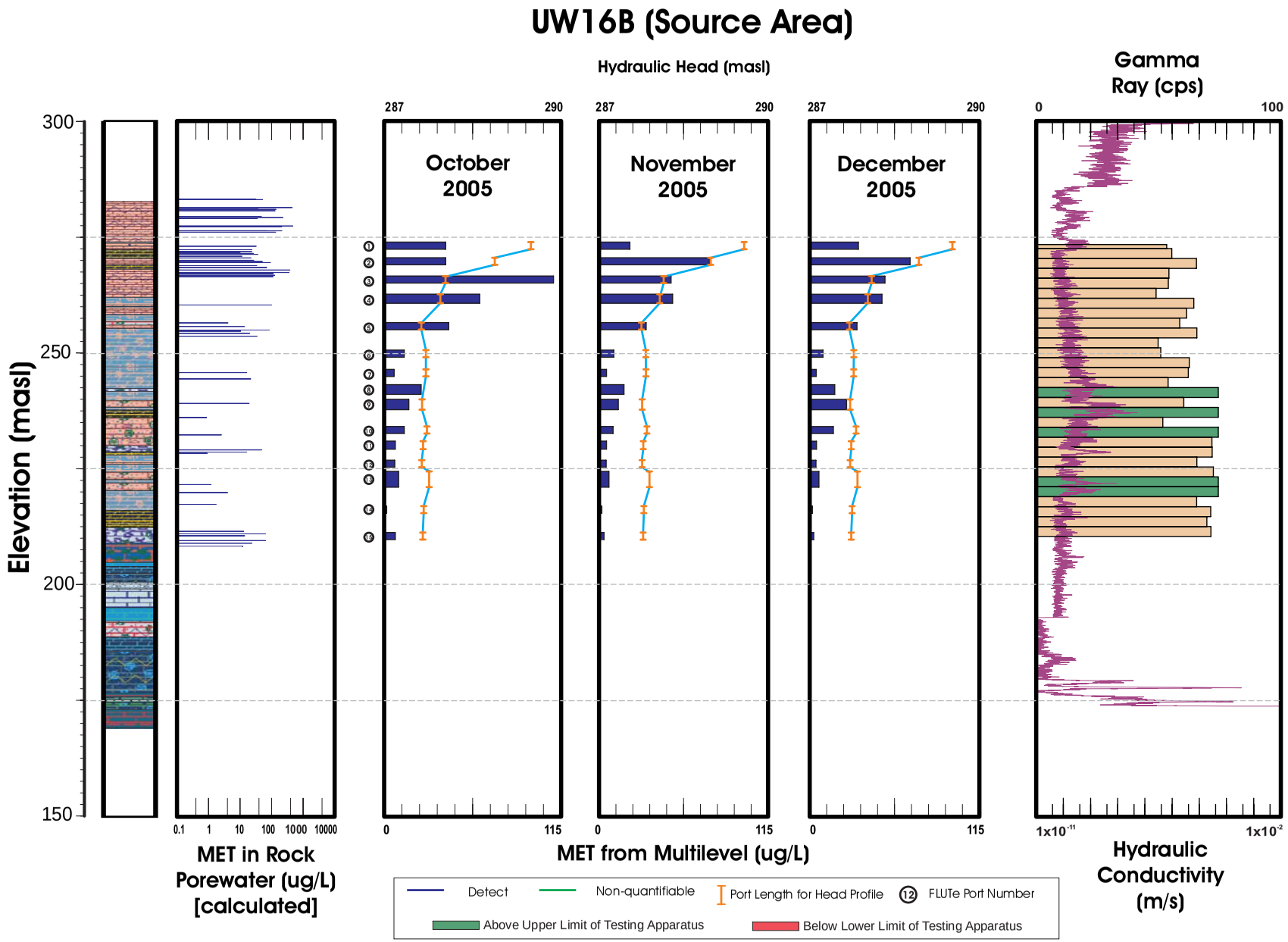


Figure 3.45: Metolachlor concentration results from UW16B taken over a three month period. Rockcore porewater, hydraulic head, corelog, gamma and hydraulic conductivity are presented for comparison. The upper zones show the highest metolachlor concentrations where the strongest vertical gradients exist. Hydraulic conductivity profile for UW16B adapted from Plett (2002).

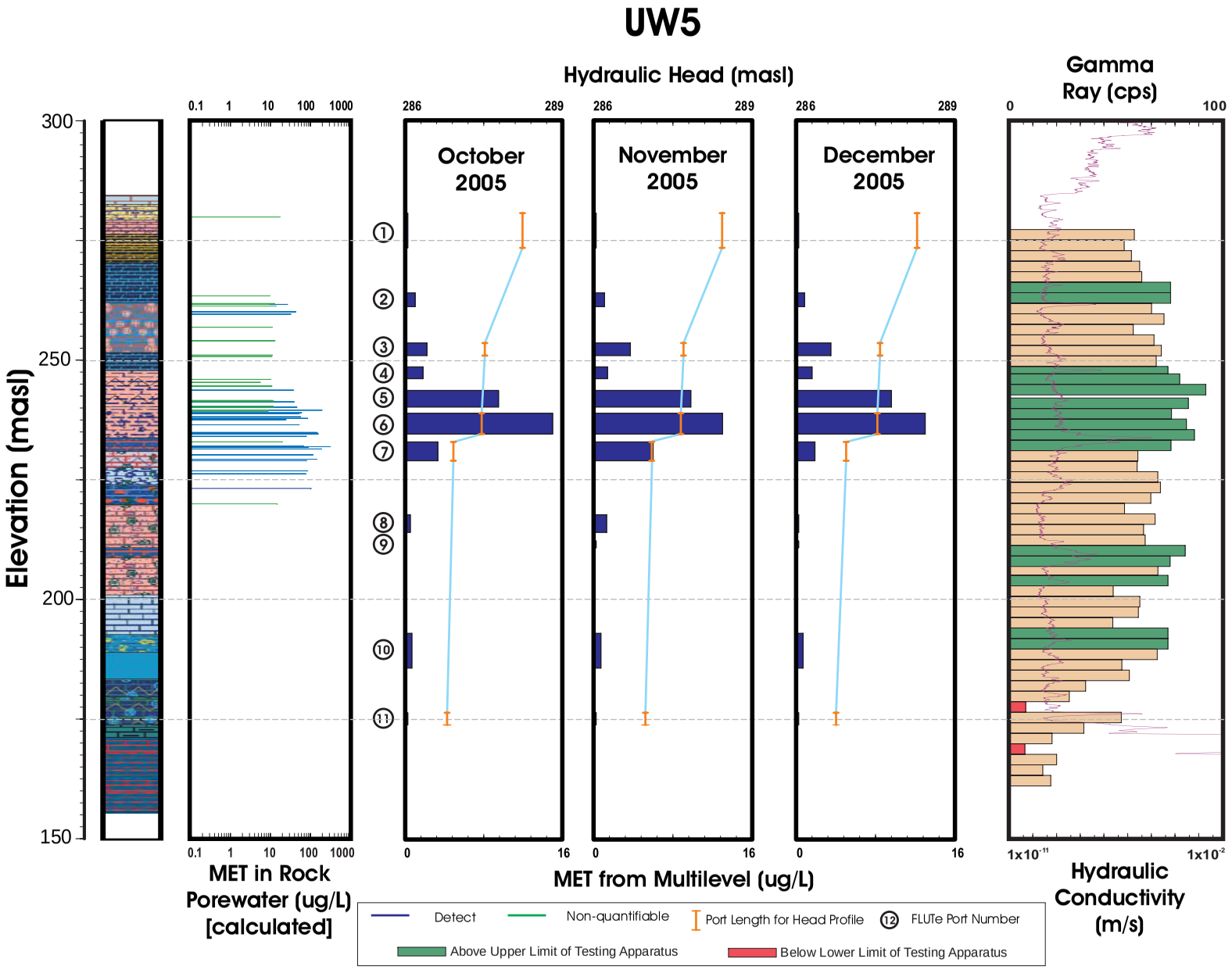


Figure 3.46: Metolachlor concentration results from UW5 taken over a three month period. Rockcore porewater, hydraulic head, corelog, gamma and hydraulic conductivity are presented for comparison. The peak in metolachlor concentration occurs just above the gamma peak and a large concentration decline occurs coincidentally with a vertical hydraulic head differential.

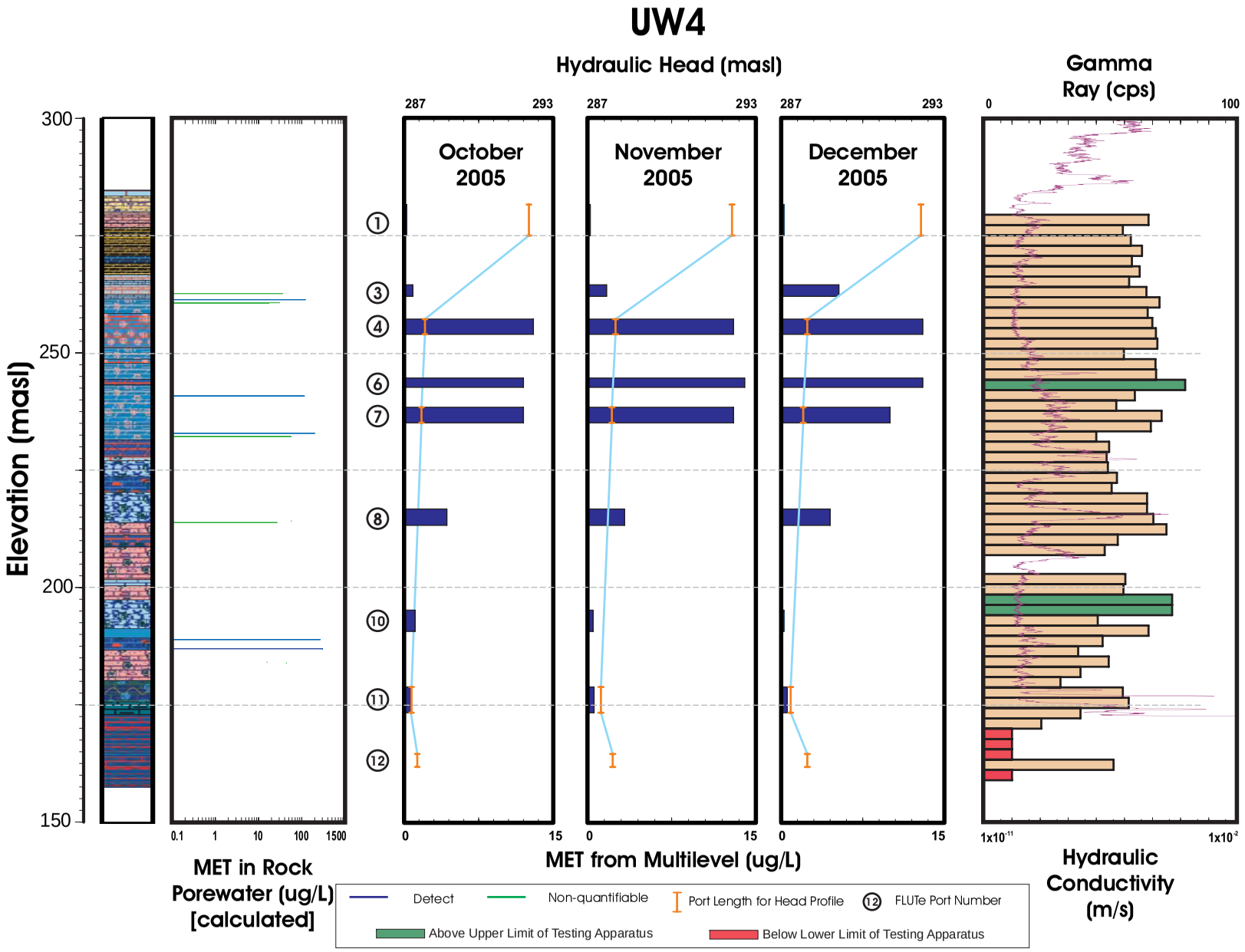


Figure 3.47: Metolachlor concentration results from UW4 taken over a three month period. Rockcore porewater, hydraulic head, corelog, gamma and hydraulic conductivity are presented for comparison. The majority of the metolachlor occurs above the gamma peak at approximately 230 masl which is considered the Eramosa unit.

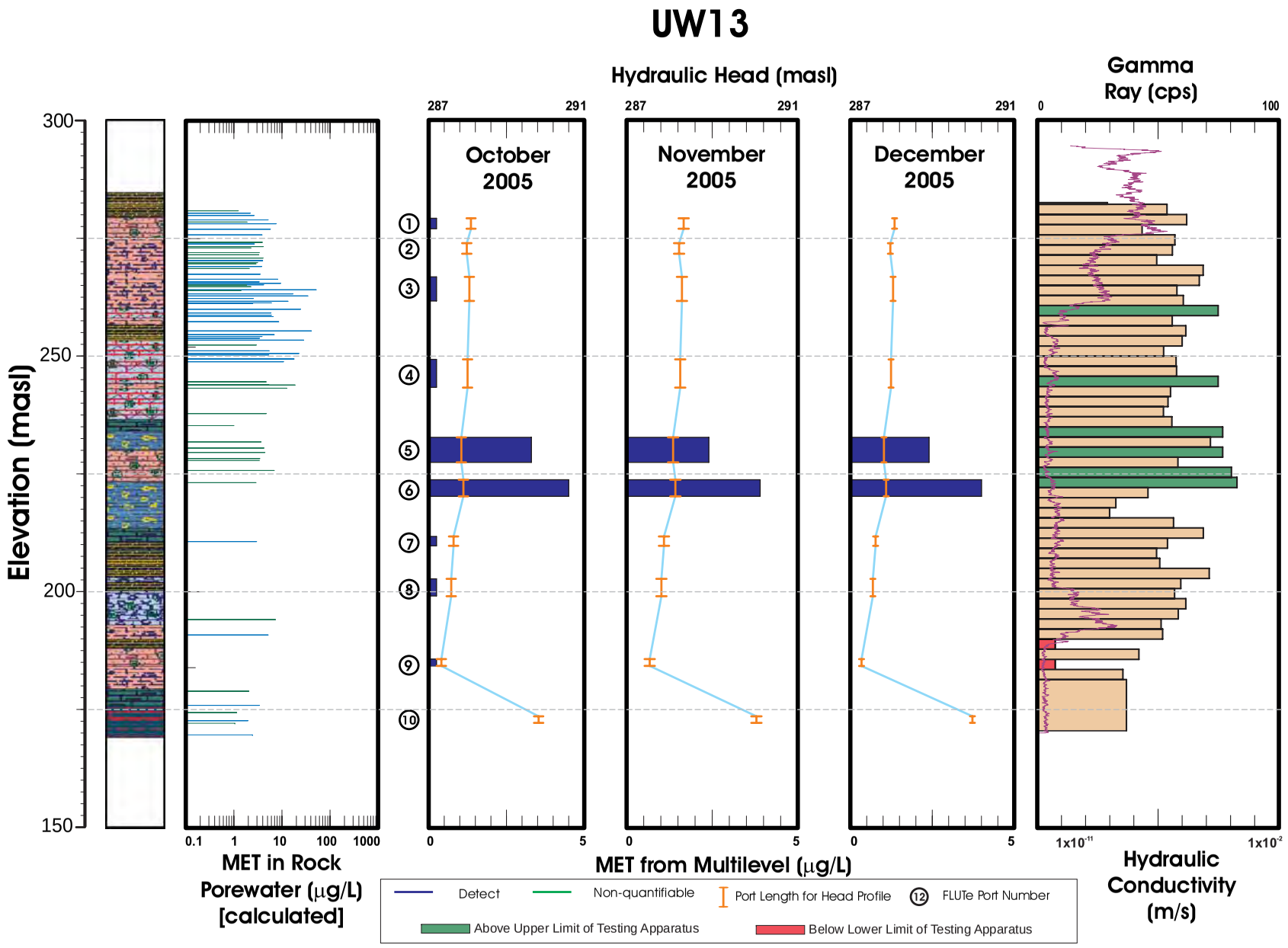


Figure 3.48: Metolachlor concentration results from UW13 taken over a three month period. Rockcore porewater, hydraulic head, corelog, gamma and hydraulic conductivity are presented for comparison. Metolachlor concentration results are the lowest of all peak concentrations along the transect and the peak in port 6 occurs deeper than other concentration peaks along the transect.

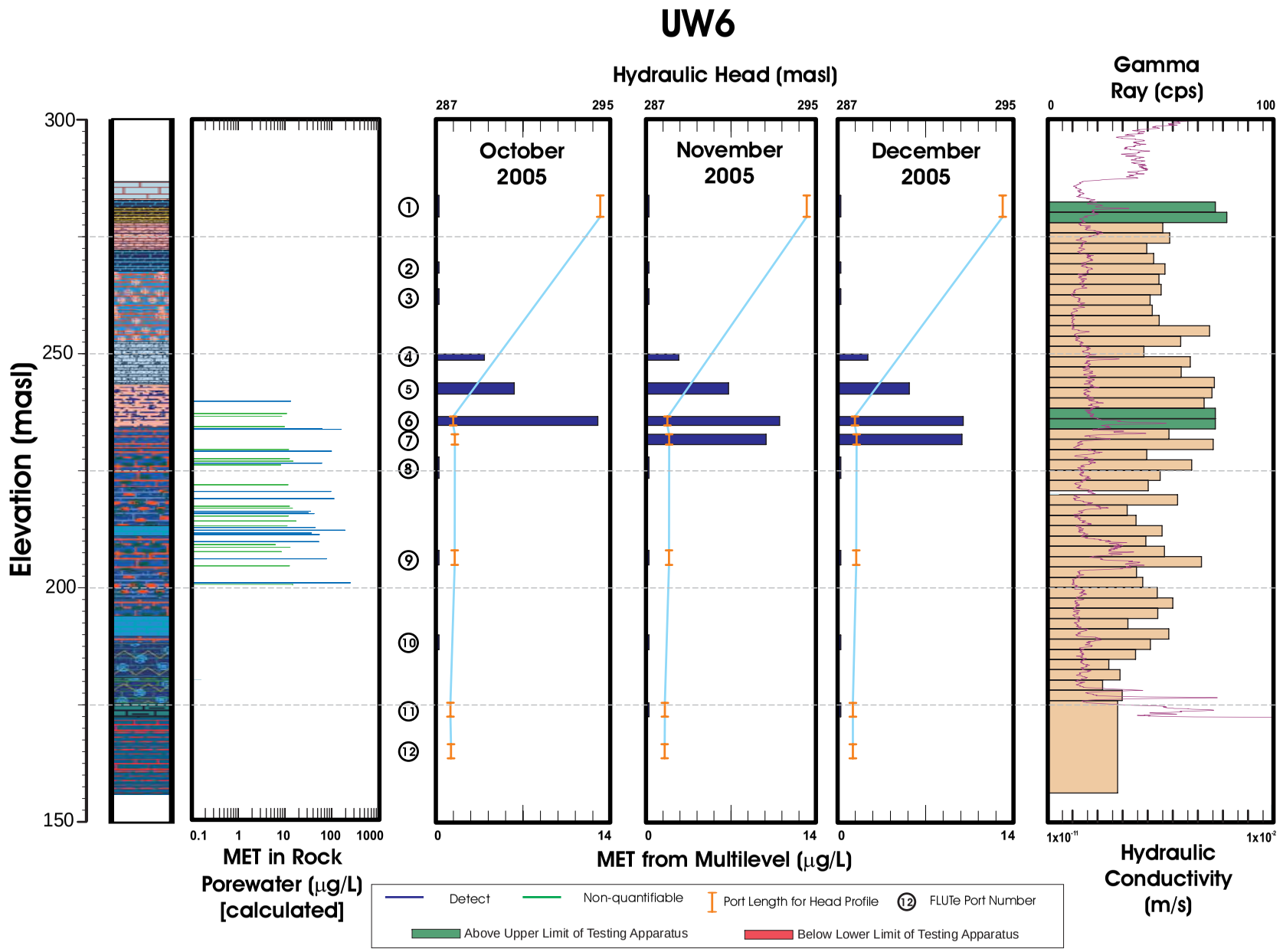


Figure 3.49: Metolachlor concentration results from UW6 taken over a three month period. Rockcore porewater, hydraulic head, corelog, gamma and hydraulic conductivity are presented for comparison. The highest concentrations are coincident with the Eramosa unit at approximately 235 masl.

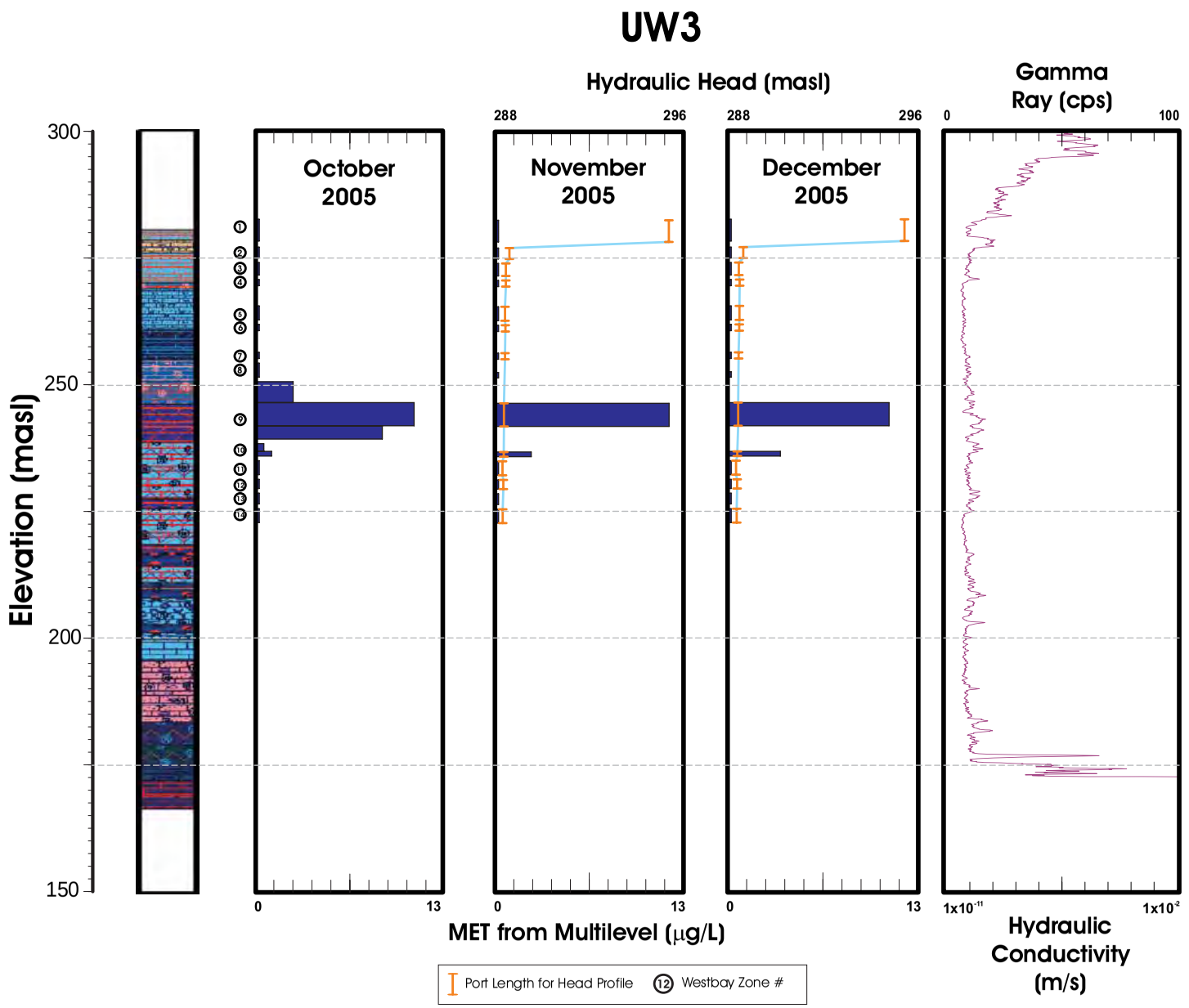


Figure 3.50: Metolachlor concentration results from UW3 taken over a three month period. Hydraulic head, corelog, and gamma are presented for comparison. The highest concentration zone coincides with the large washout observed in borehole video.

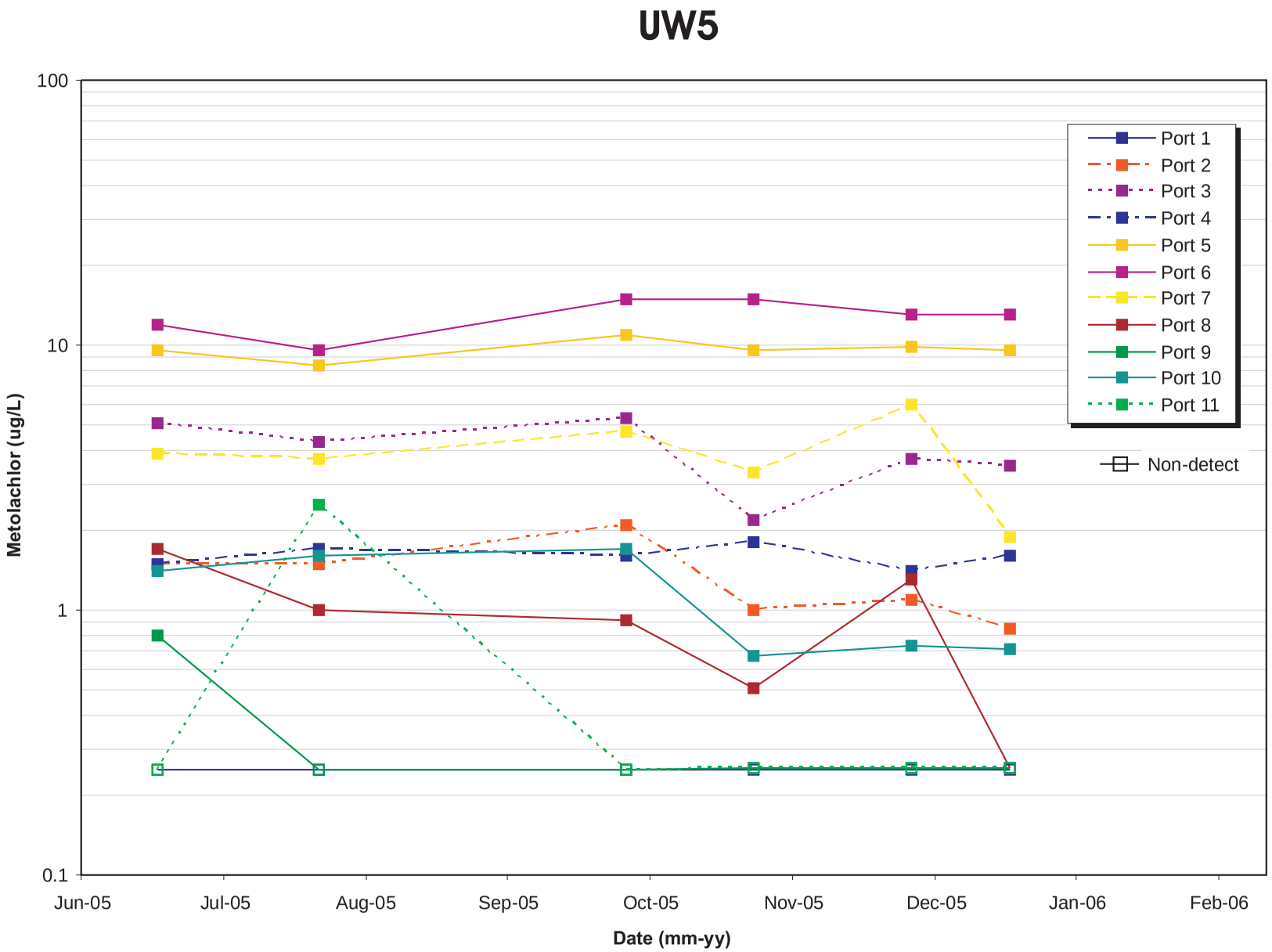


Figure 3.51: Metolachlor concentration versus time in UW5 multilevel ports. Since June 2005, these data have been consistent.

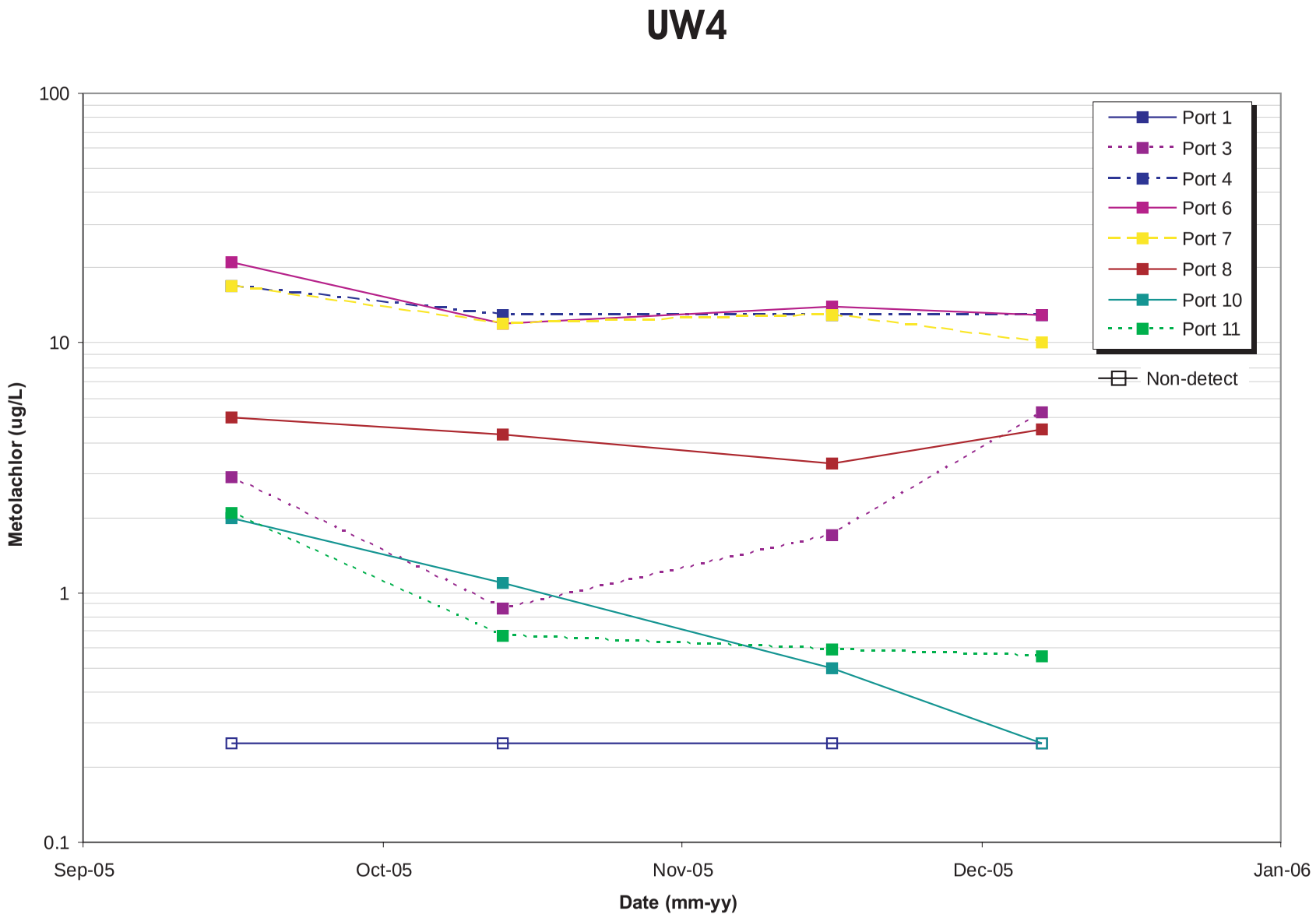


Figure 3.52: Metolachlor concentration versus time in UW4 multilevel ports. Since September 2005, these data have been consistent.

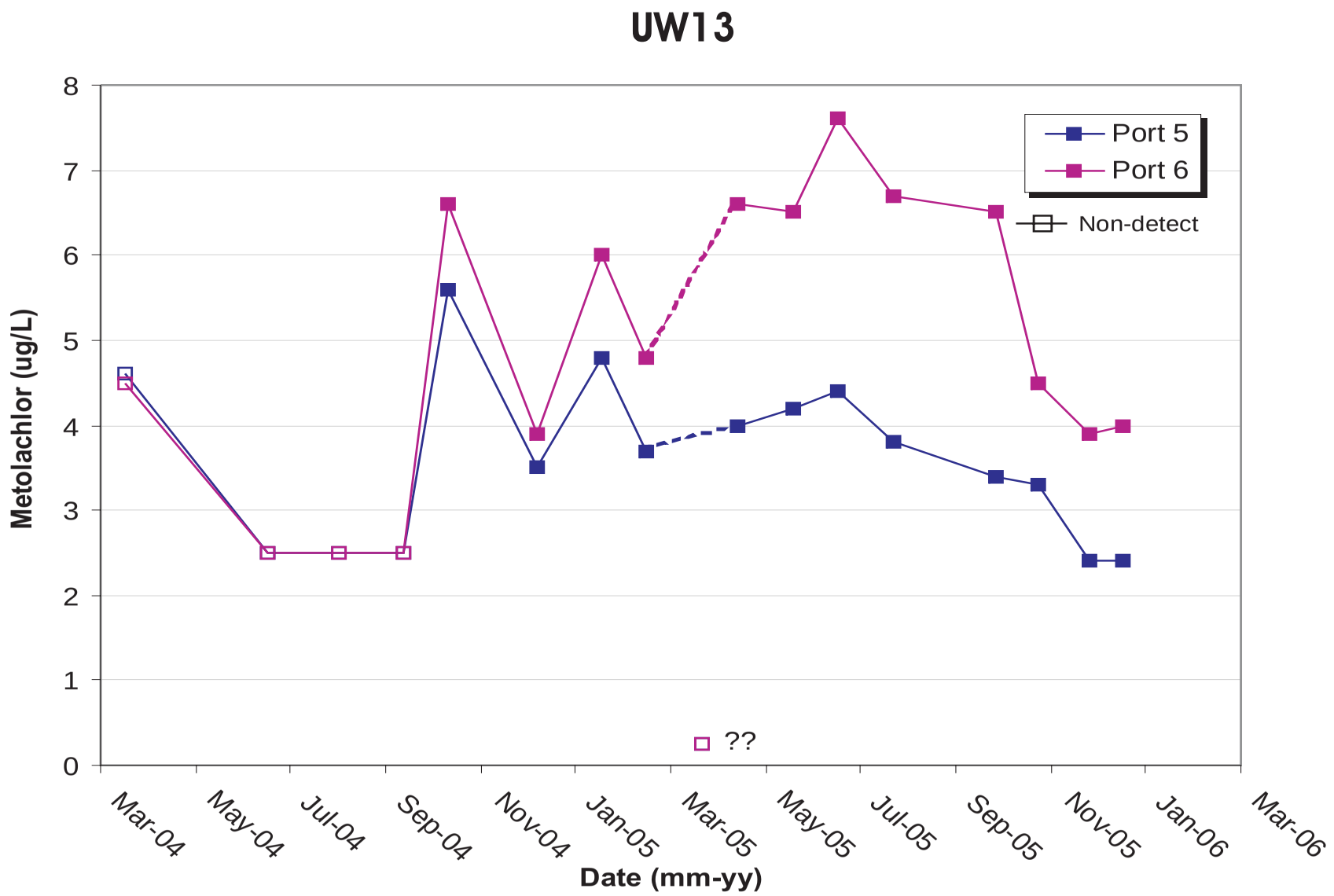


Figure 3.53: Metolachlor concentration versus time in UW13 multilevel ports. Sampling has occurred in this multilevel since March, 2004. One anomalous reading for both ports 5 and 6 occurred in March, 2005

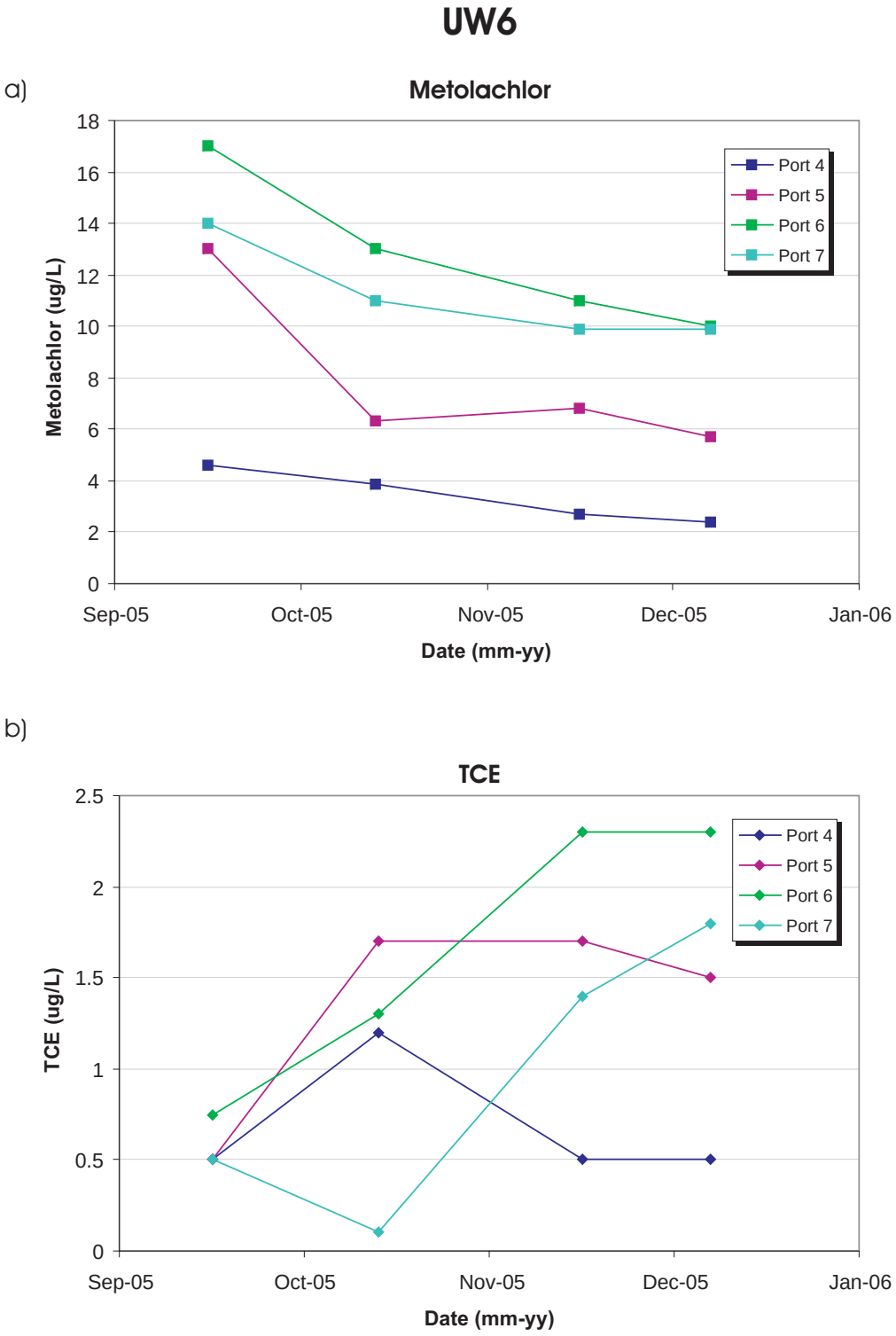


Figure 3.54: Concentrations versus time for the 12-port FLUTe multilevel system in UW6. a) Metolachlor concentrations have dropped slowly and steadily in ports 4, 5, 6, and 7. No other ports have detectable concentrations of metolachlor or b) TCE is detected with much lower concentrations however the concentrations are not consistent with time

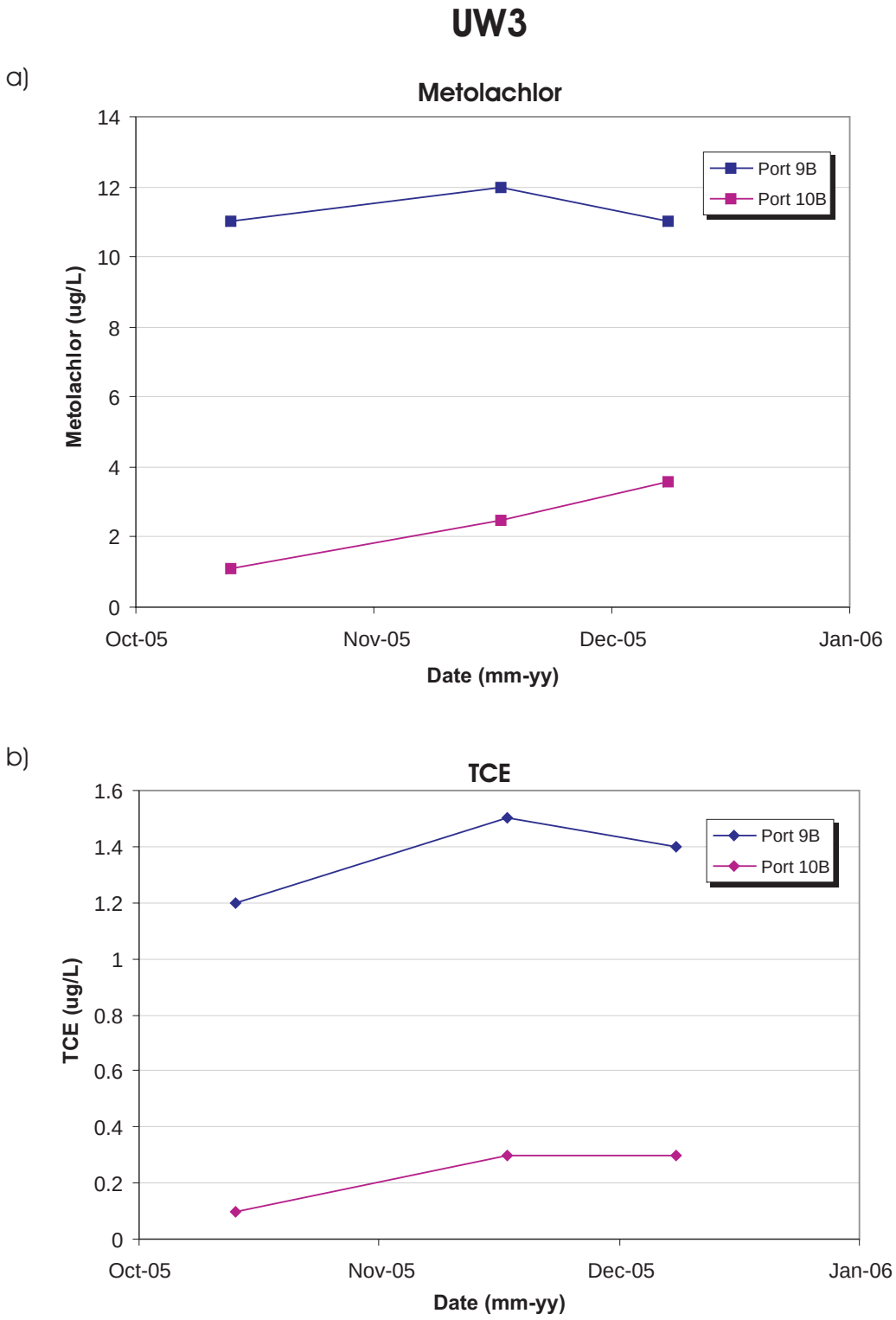


Figure 3.55: Concentrations versus time for the 14-zone Westbay multilevel system in UW3. Neither a) metolachlor of b) TCE have changed substantially, however only three sampling rounds have been done in this multilevel system

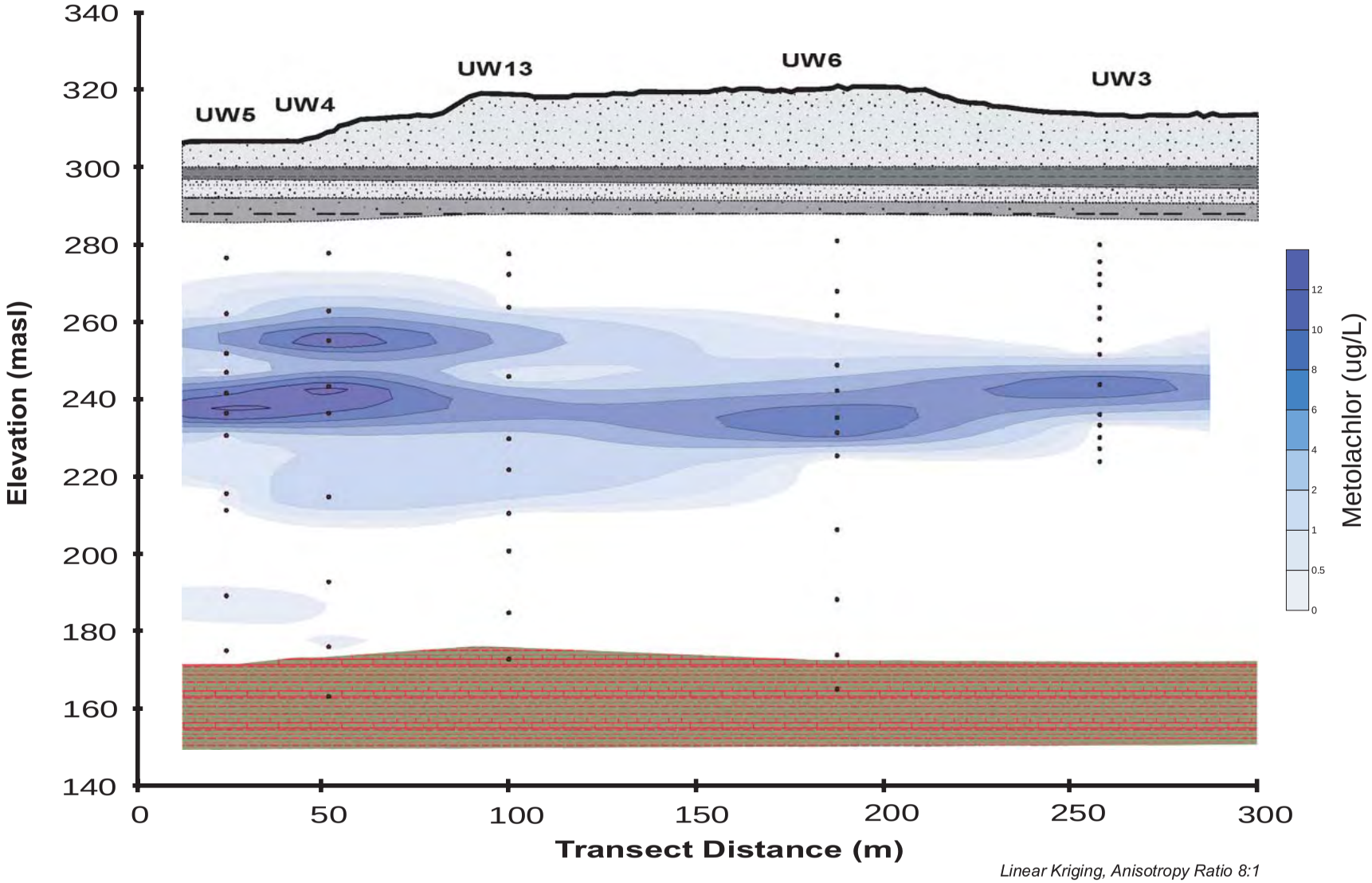


Figure 3.56: The metolachlor plume (contoured using December 2005 data) across the transect is vertically narrow and laterally extensive. The plume is not bounded on the ends and therefore the full width of the plume is unknown

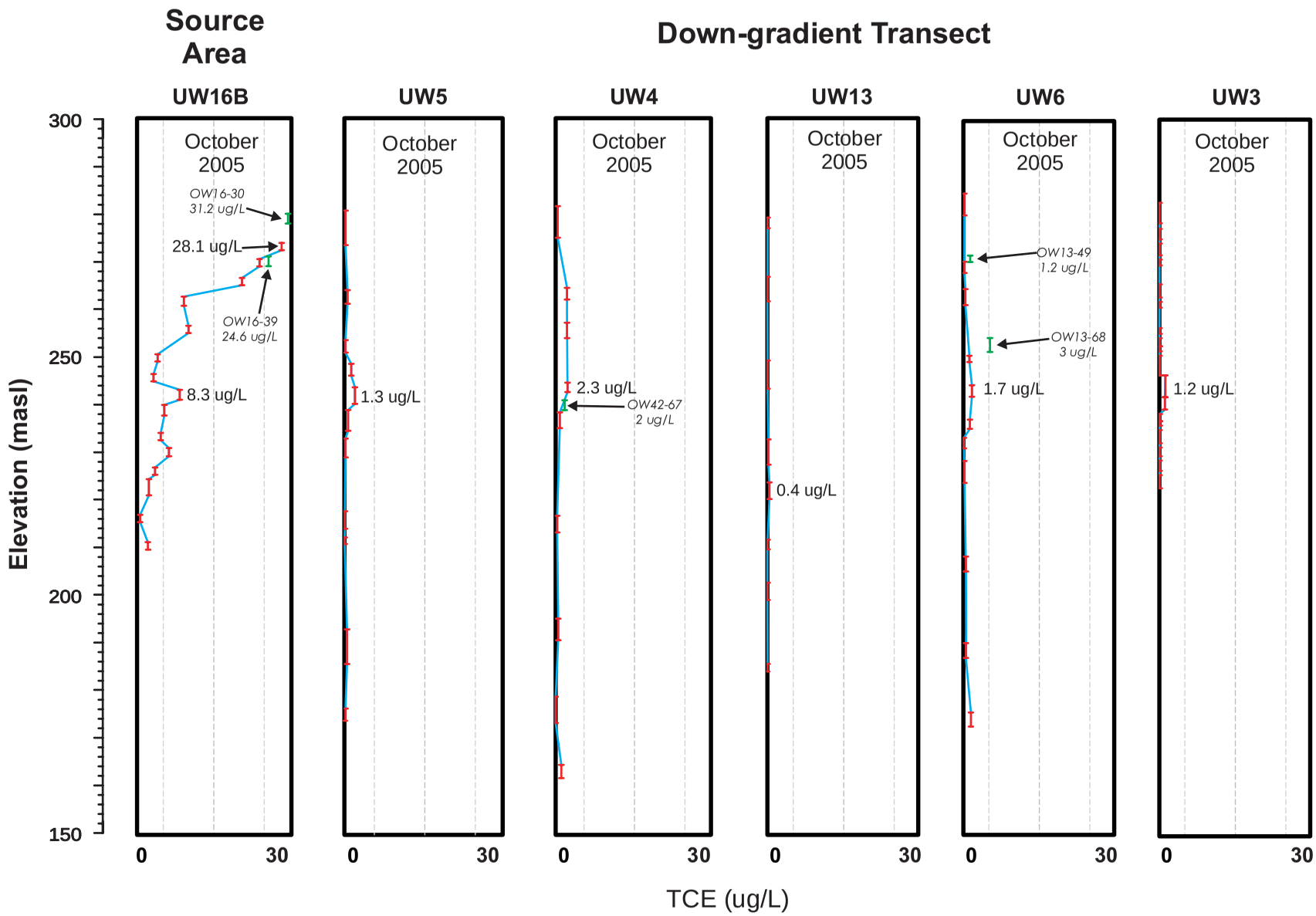


Figure 3.57: TCE concentration profiles from multilevel systems in UW16B and on the transect. These data show a large concentration peak in the upper bedrock and a lower peak in the middle part of the dolostone which coincides with the transect peak concentrations. UW13 has the lowest TCE concentrations of the other transect holes.

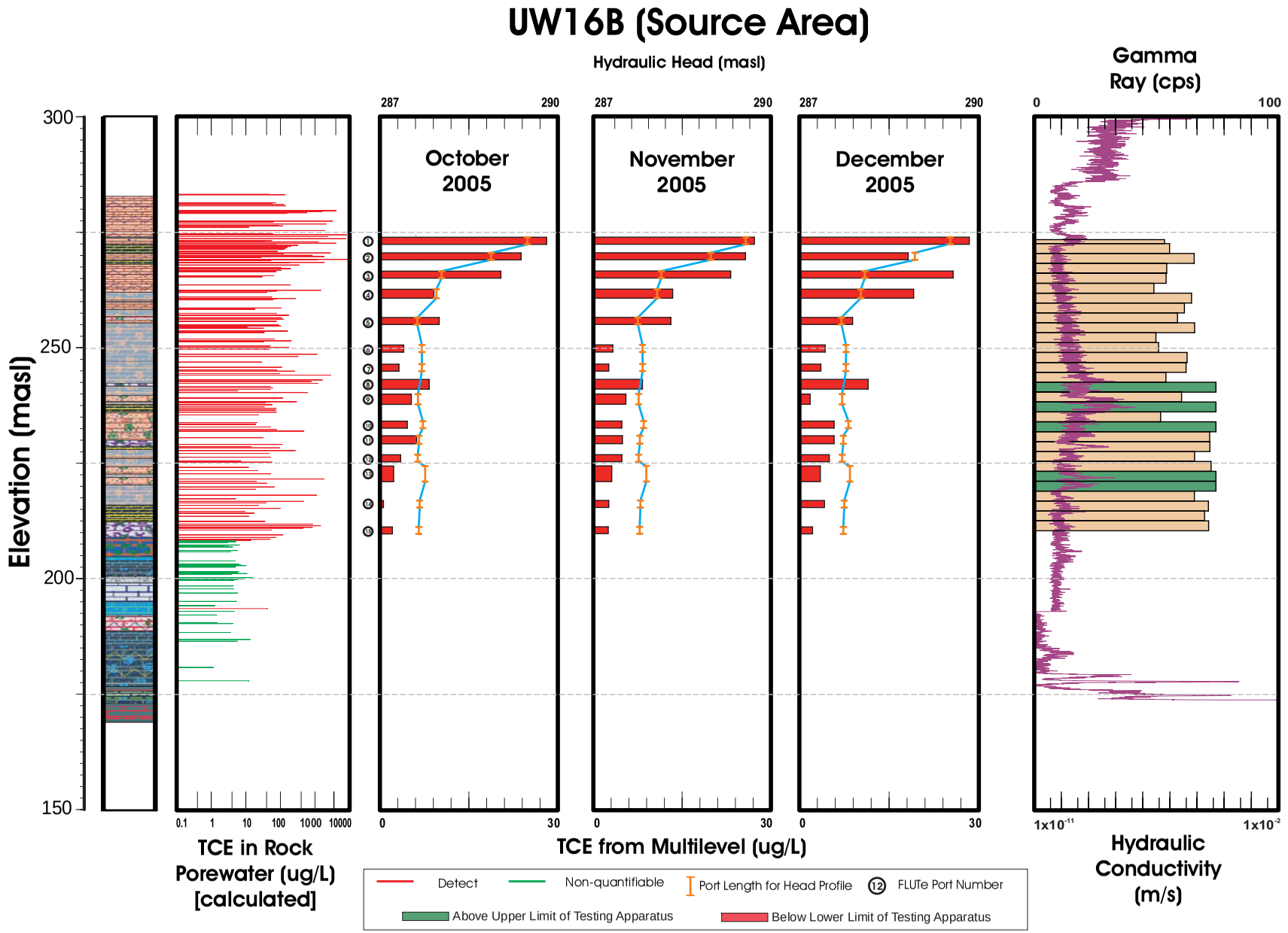


Figure 3.58: TCE concentration results from UW16B in the source area taken over a three month period. Hydraulic head, corelog, and gamma are presented for comparison. Hydraulic conductivity profile for UW16B adapted from Plett (2002).

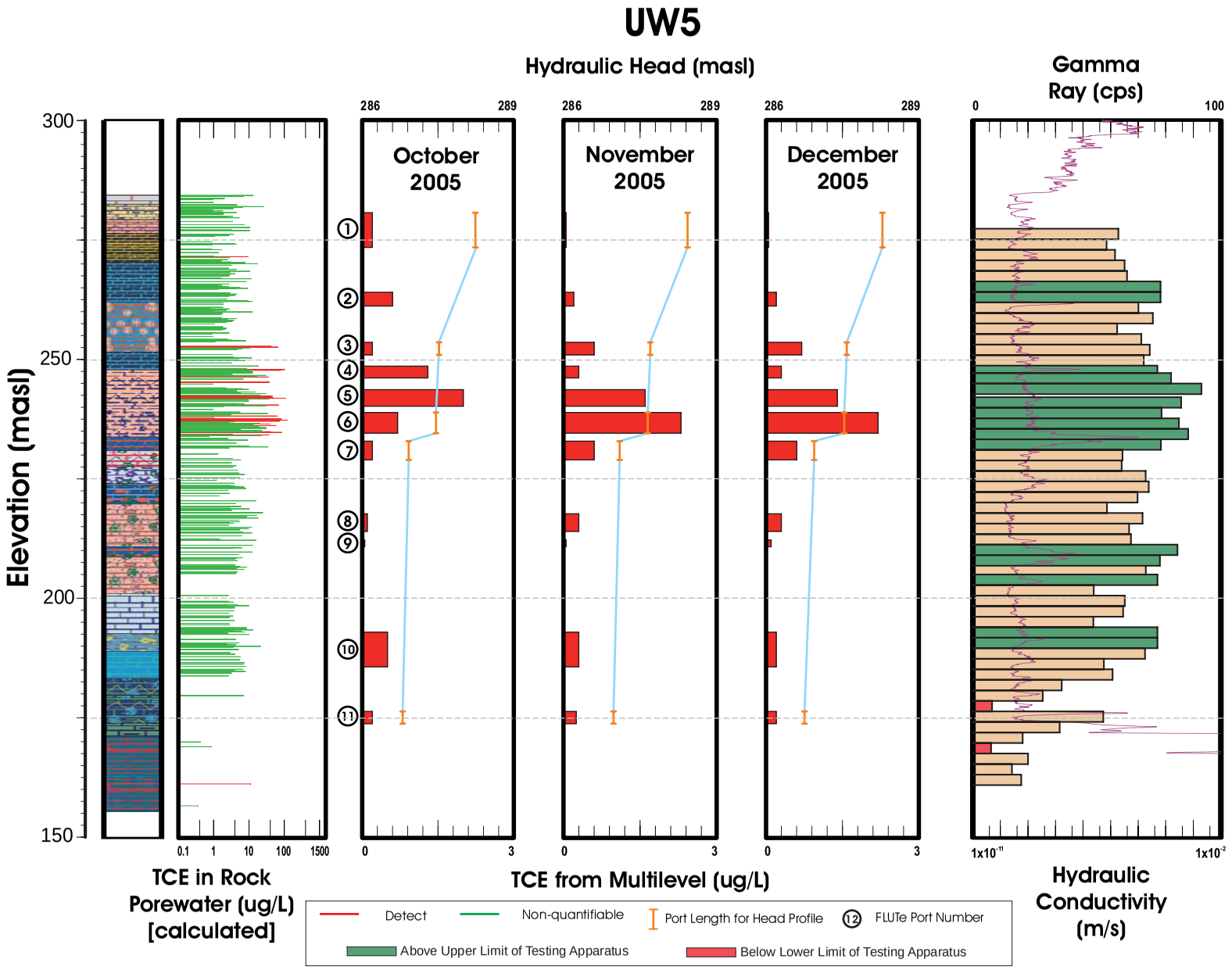


Figure 3.59: TCE concentration results from UW5 in the source area taken over a three month period. Hydraulic head, corelog, and gamma are presented for comparison. The peak TCE concentrations are coincident with the peak concentrations from porewater data. A large concentration decline occurs across the Eramosa unit where an increase in vertical gradient occurs.

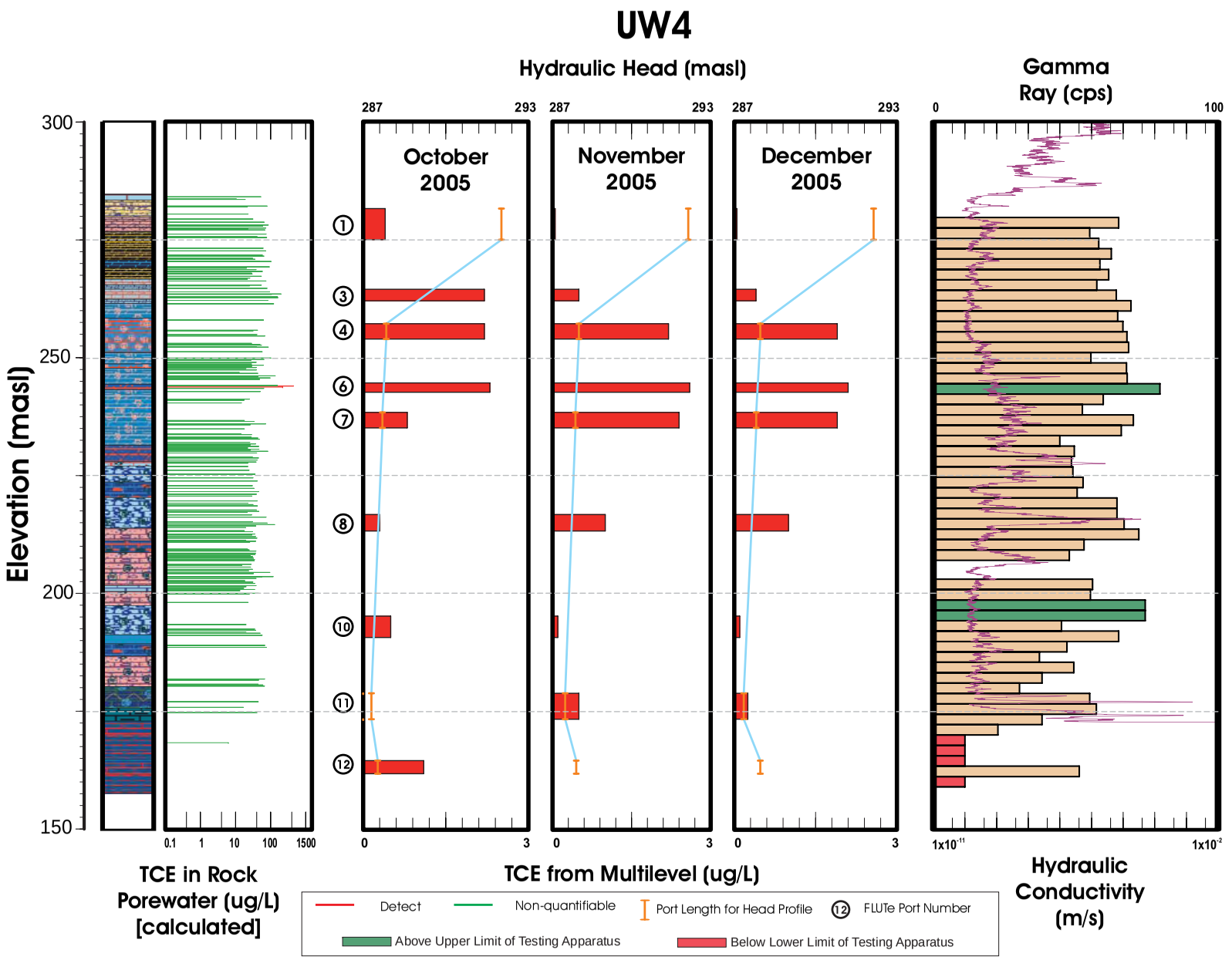


Figure 3.60: TCE concentration results from UW4 in the source area taken over a three month period. Hydraulic head, corelog, and gamma are presented for comparison. Most of the TCE concentration occurs above the Eramosa unit at approximately 230 masl.

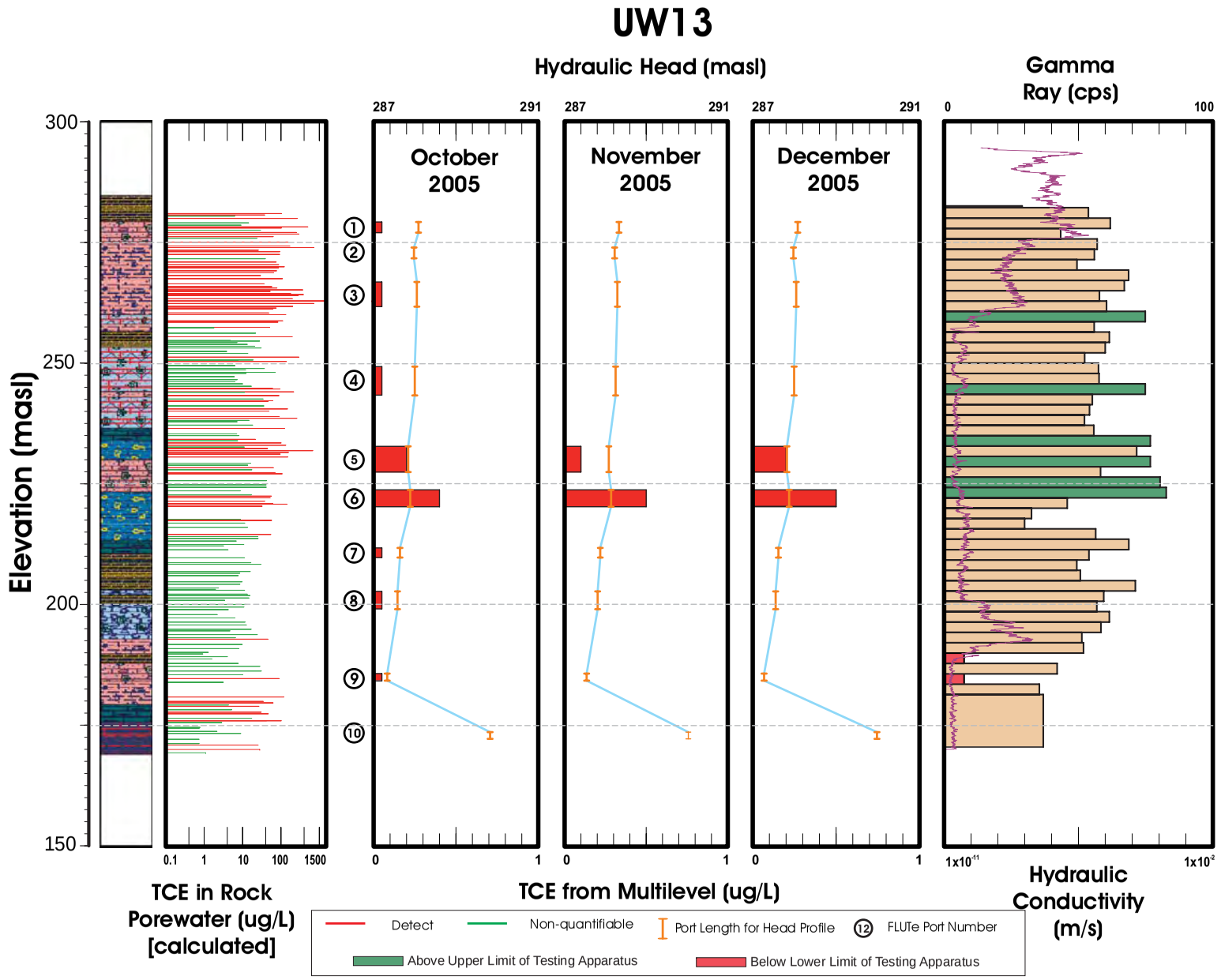


Figure 3.61: TCE concentration results from UW13 in the source area taken over a three month period. Hydraulic head, corelog, and gamma are presented for comparison. Only ports 5 and 6 have detectable levels of TCE, however they are very low. These data are at the same elevation as a zone of increased hydraulic conductivity shown by straddle packer tests.

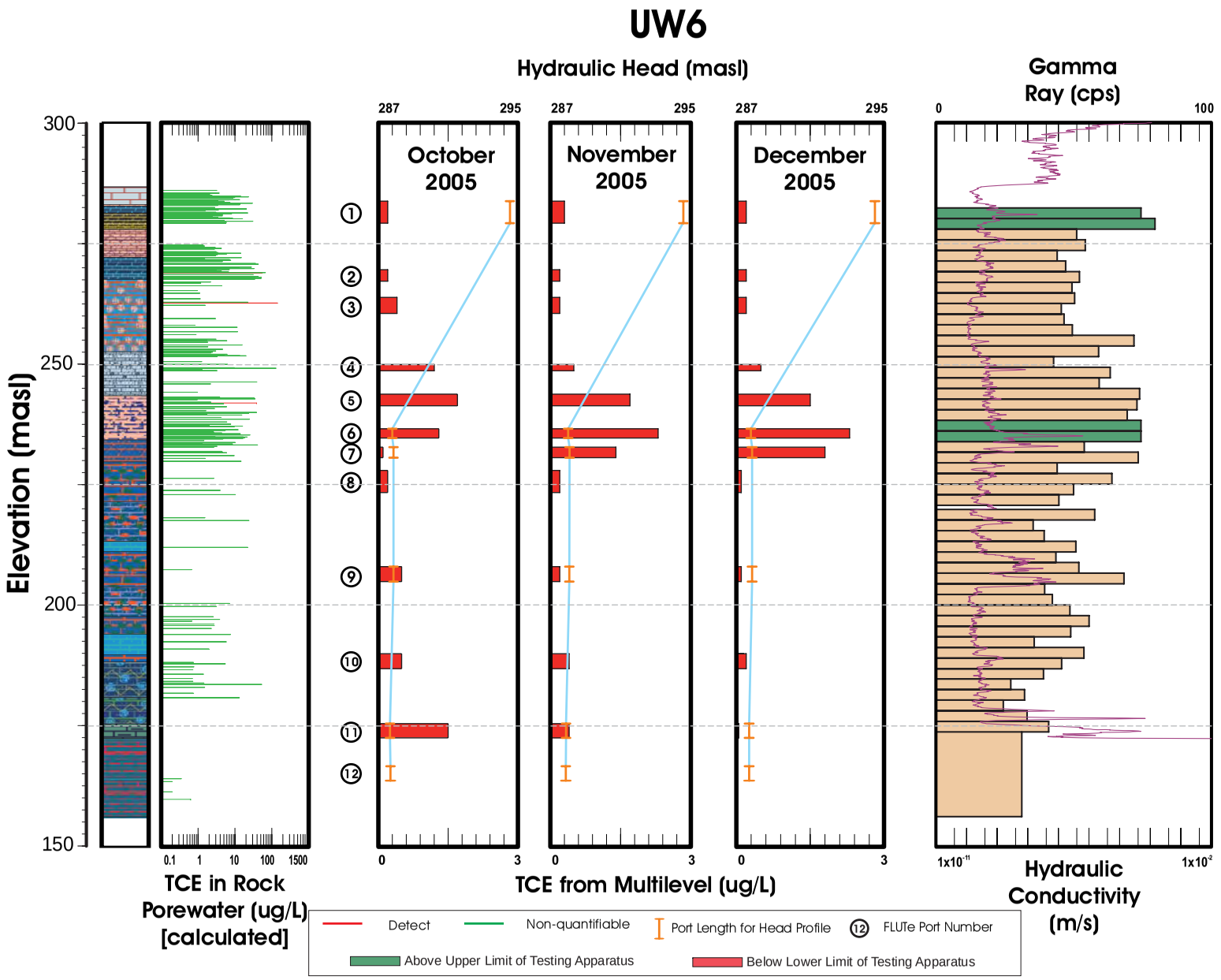


Figure 3.62: TCE concentration results from UW6 in the source area taken over a three month period. Hydraulic head, corelog, and gamma are presented for comparison. Detectable concentrations of TCE occur at or above the Eramosa unit defined by the gamma and corelogs at approximately 232 masl

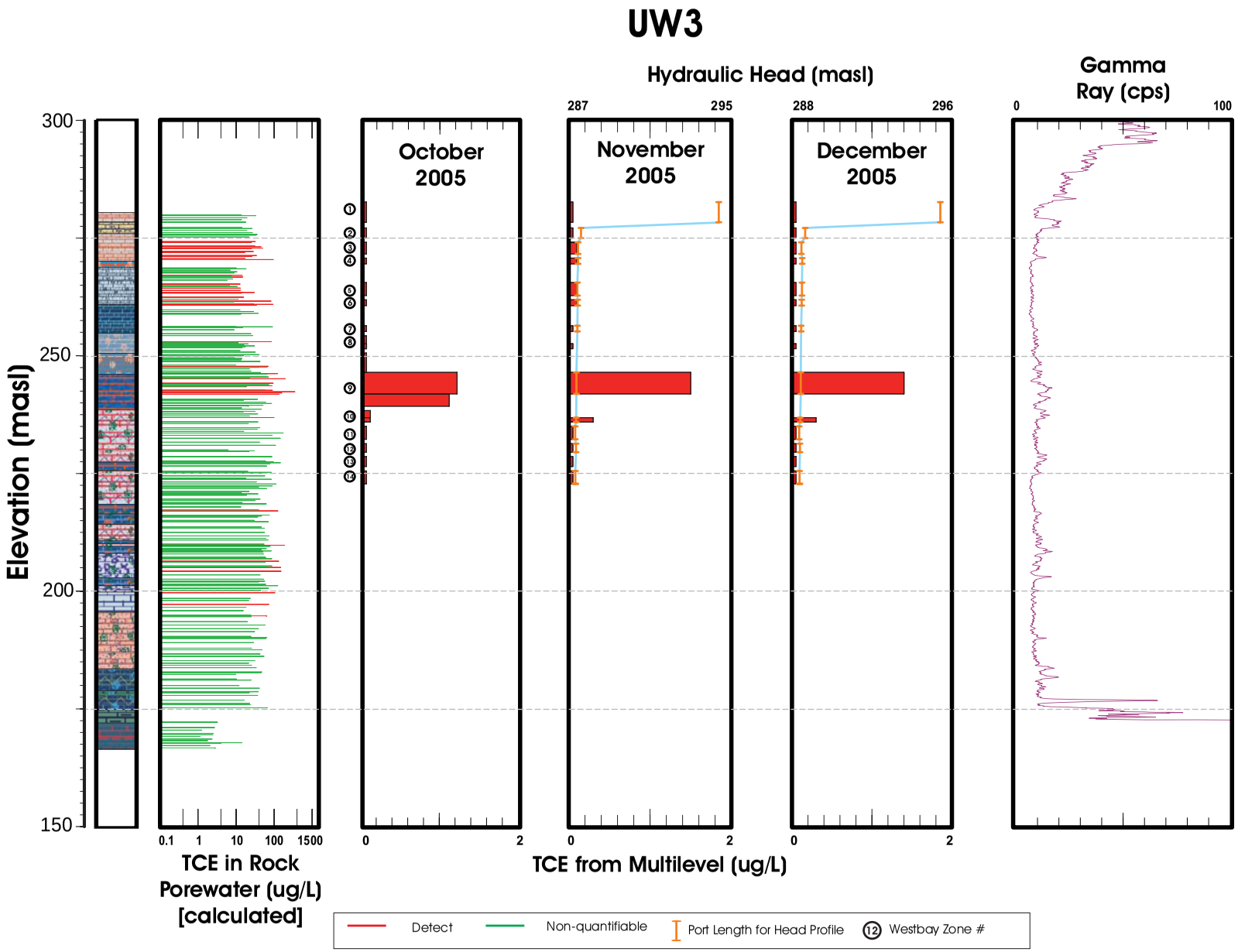


Figure 3.63: TCE concentration results from UW3 in the source area taken over a three month period. Hydraulic head, corelog, and gamma are presented for comparison. Detectable concentrations of TCE occur only in zones 9 and 10 which is in the same zone as a large washout in the dolostone.

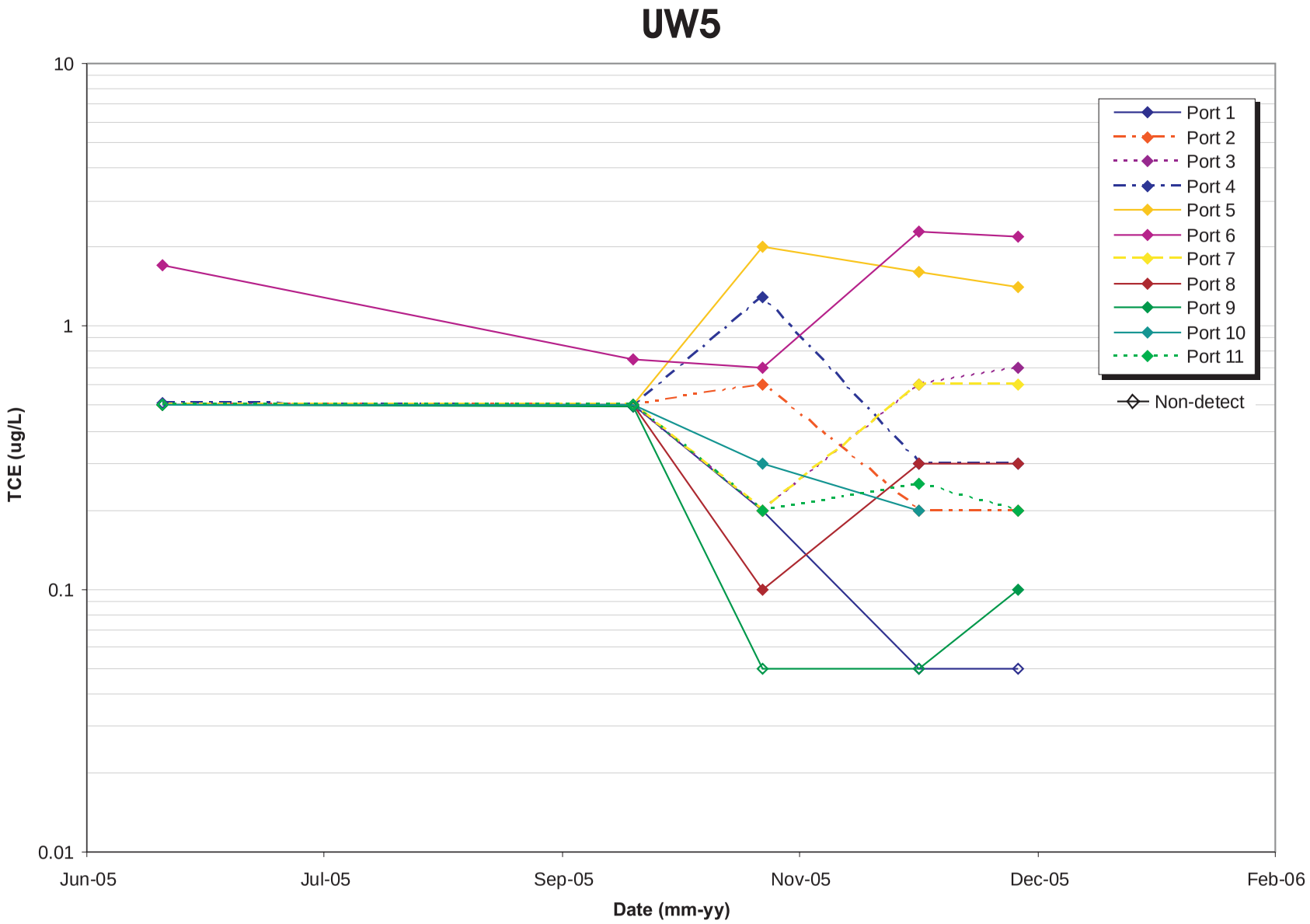


Figure 3.64: TCE concentration versus time data collected from the 11 ports in Multilevel UW5. Data are unstable at first and begin to level out after four sampling rounds

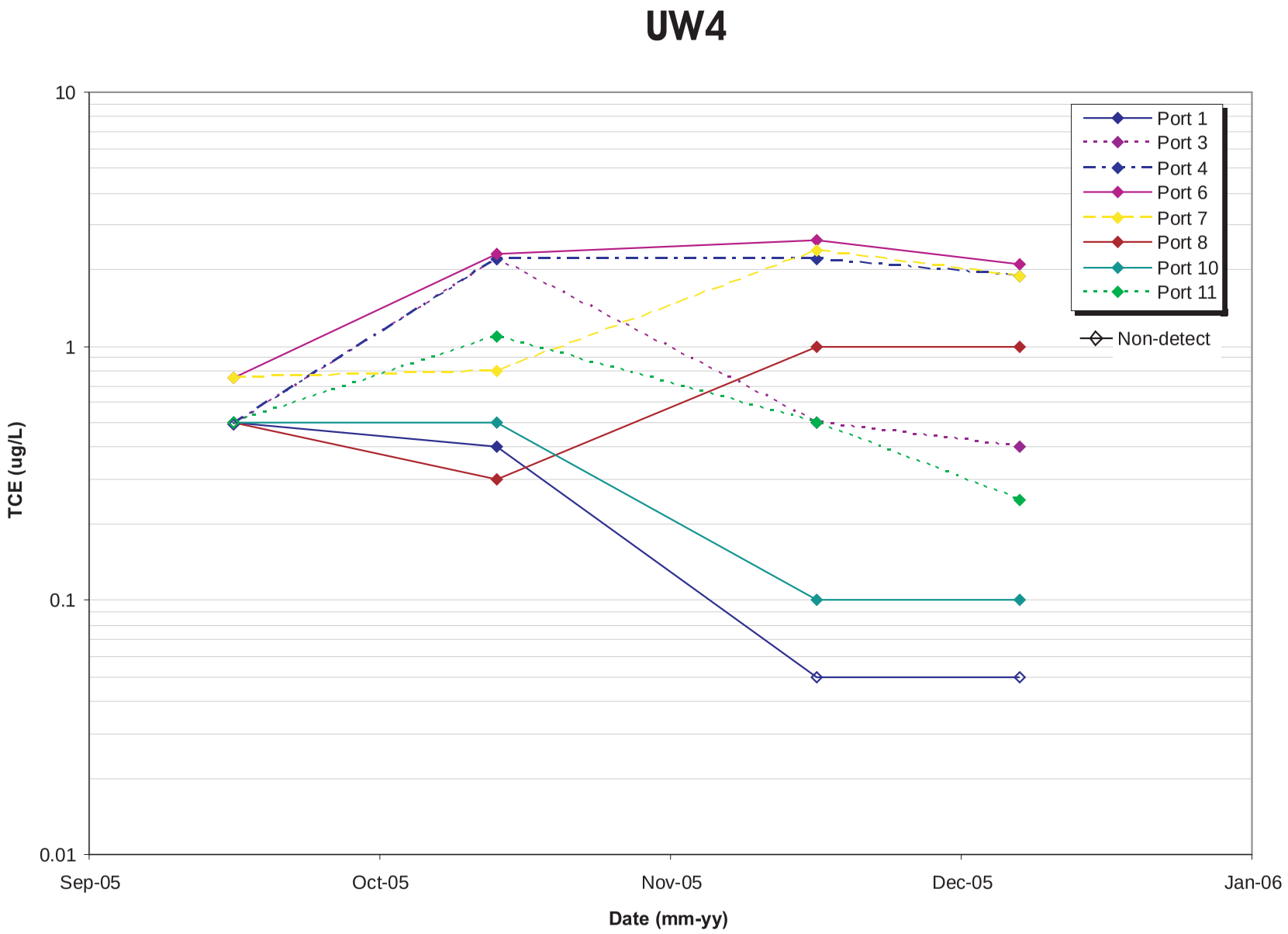


Figure 3.65: TCE concentration versus time data collected from the 9 ports in Multilevel UW4. Data are unstable at first and begin to level out after the third sampling round

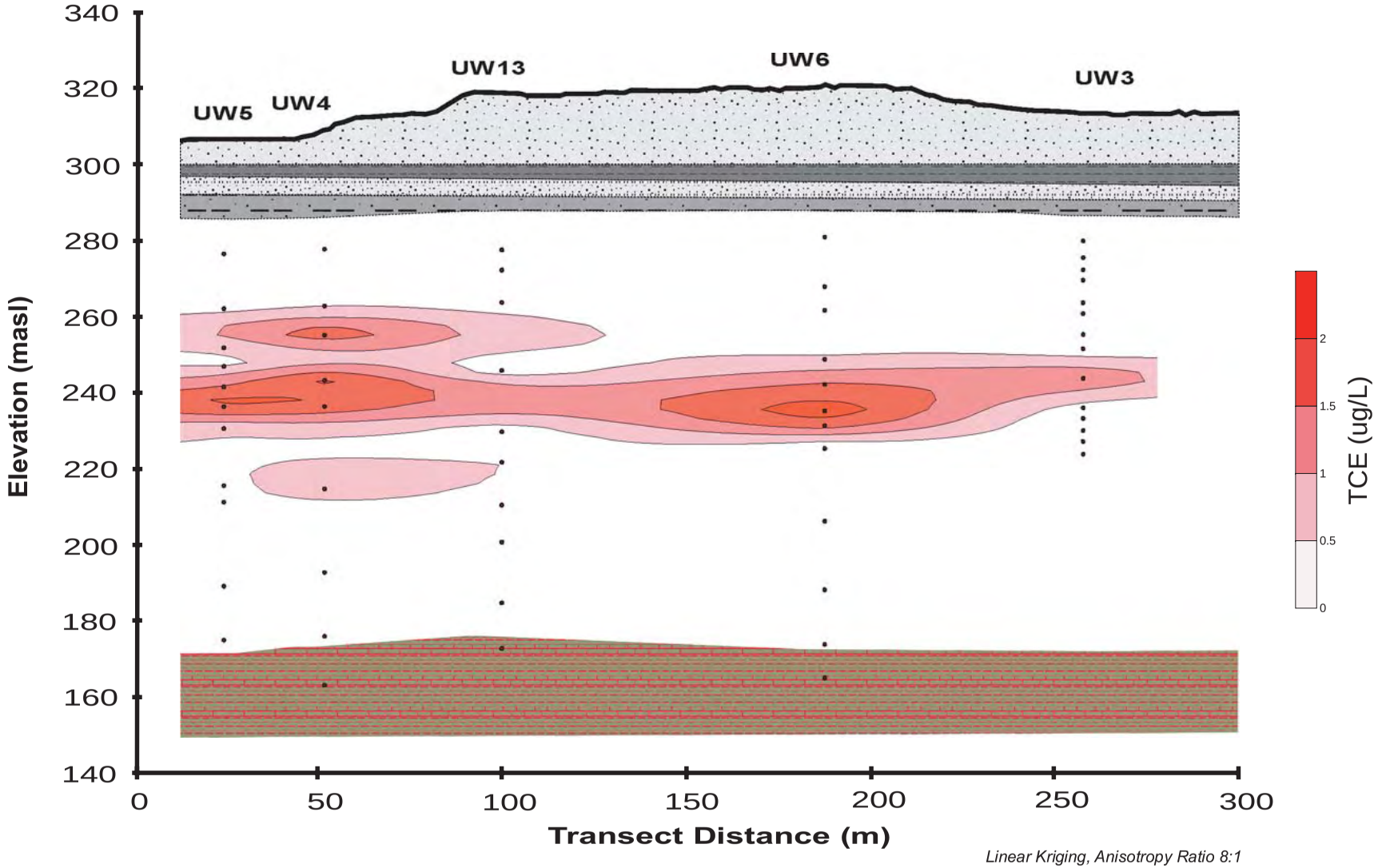


Figure 3.66: TCE concentration data contoured from multilevels along the transect. The highest levels of TCE occur in the middle part of the aquifer at approximately 240 masl. Although the TCE concentrations are low ($< 3\mu g/L$) along the transect, the full width of the plume has not been determined. The TCE data, from December, 2005 was contoured using linear kriging and an anisotropy ratio of 8:1.

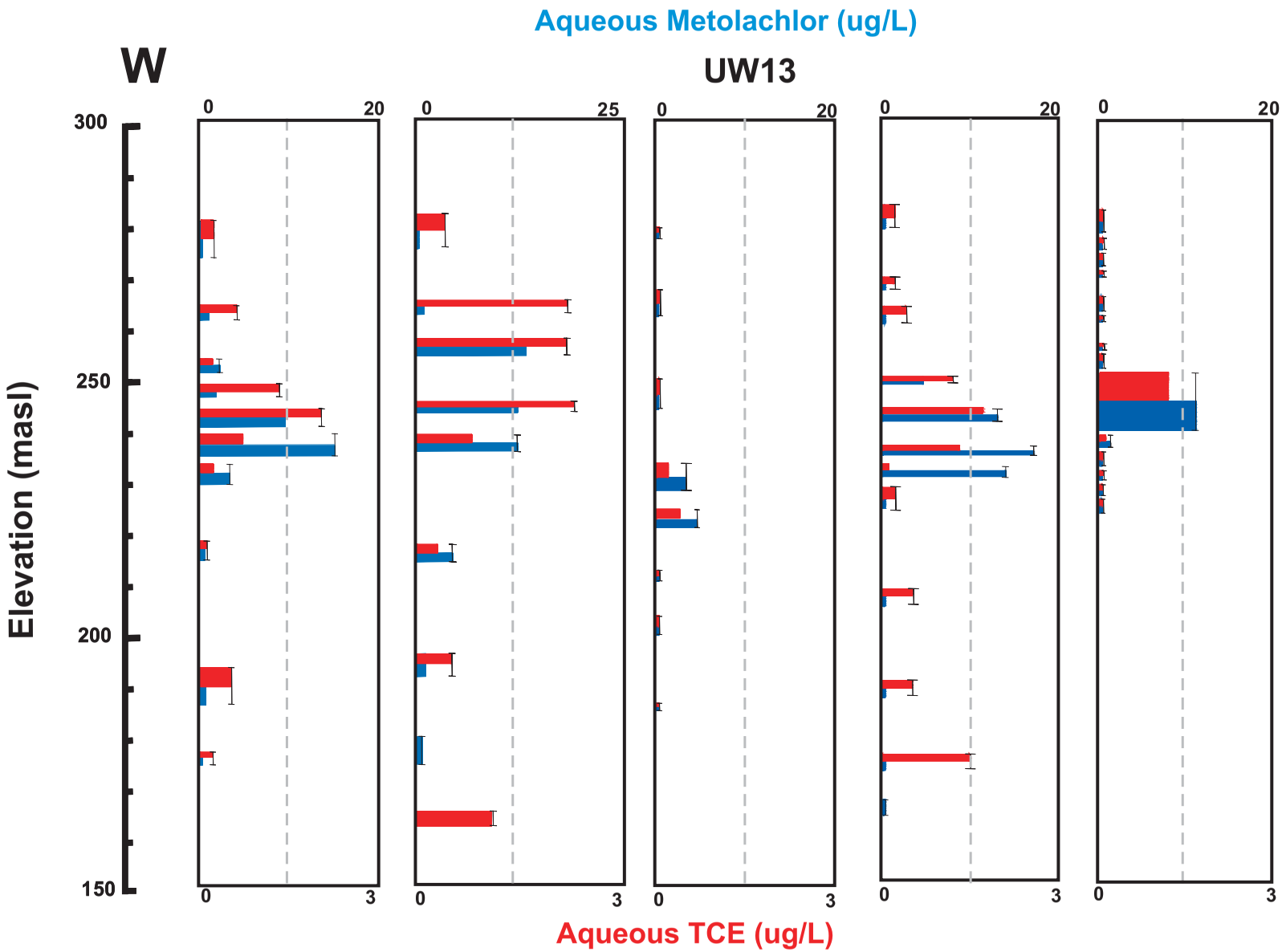


Figure 3.67: Metolachlor and TCE results from multilevel sampling on October, 2005 show the two plumes, which originate from separate sources are localized in the dolostone aquifer at the same depths. This suggests that the two plumes are migrating in a shared pathway from the respective source areas to the transect.

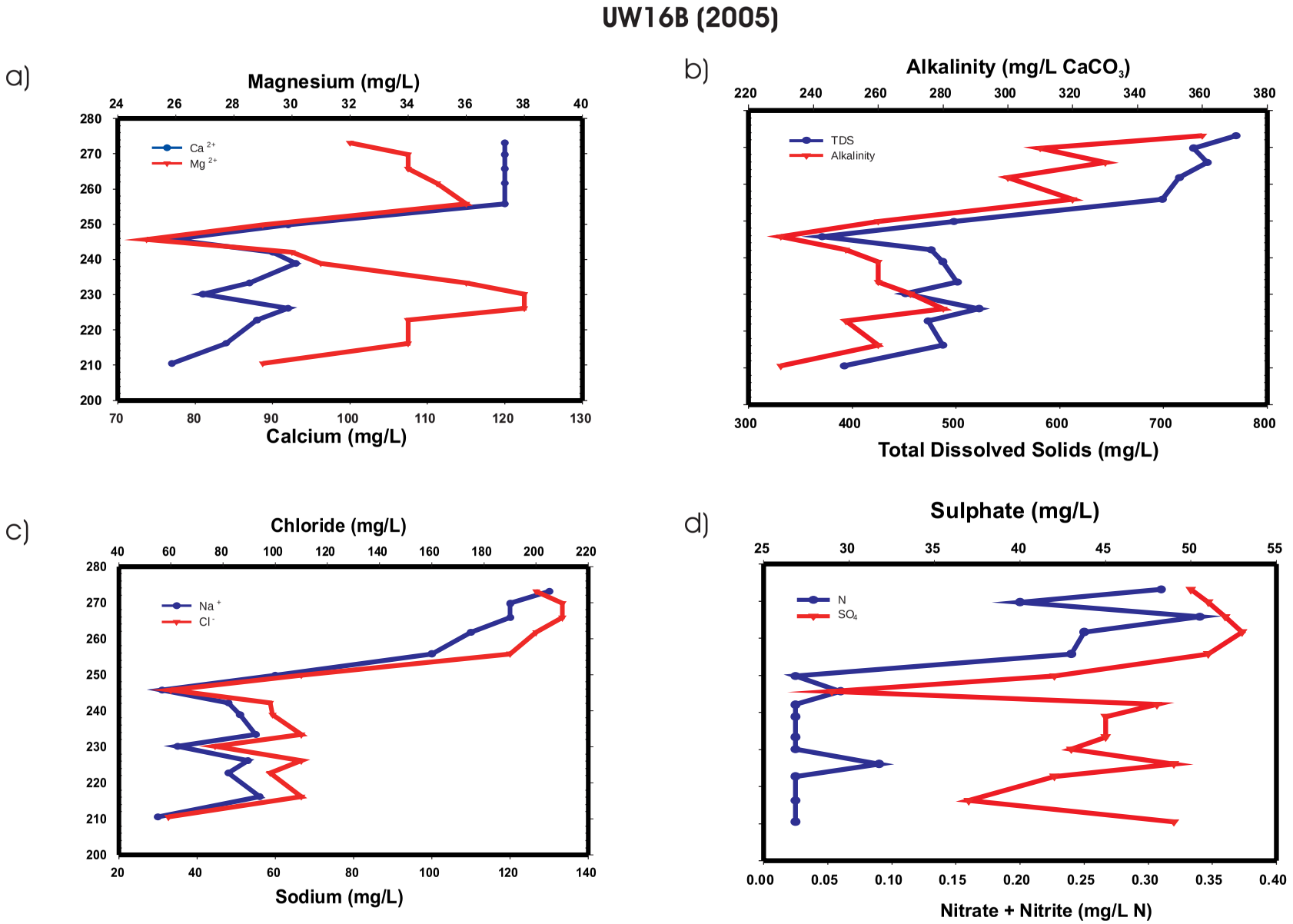


Figure 3.68: Inorganic hydrochemistry results collected from UW16B (source area) in February, 2005. Results for calcium and magnesium (a) show high concentrations in the upper bedrock. Concentrations are depleted at approximately 240 masl and then another peak in concentrations occurs at approximately 225 masl. This trend is similar for (b) TDS and alkalinity, (c) sodium and chloride, and (d) sulphate results.

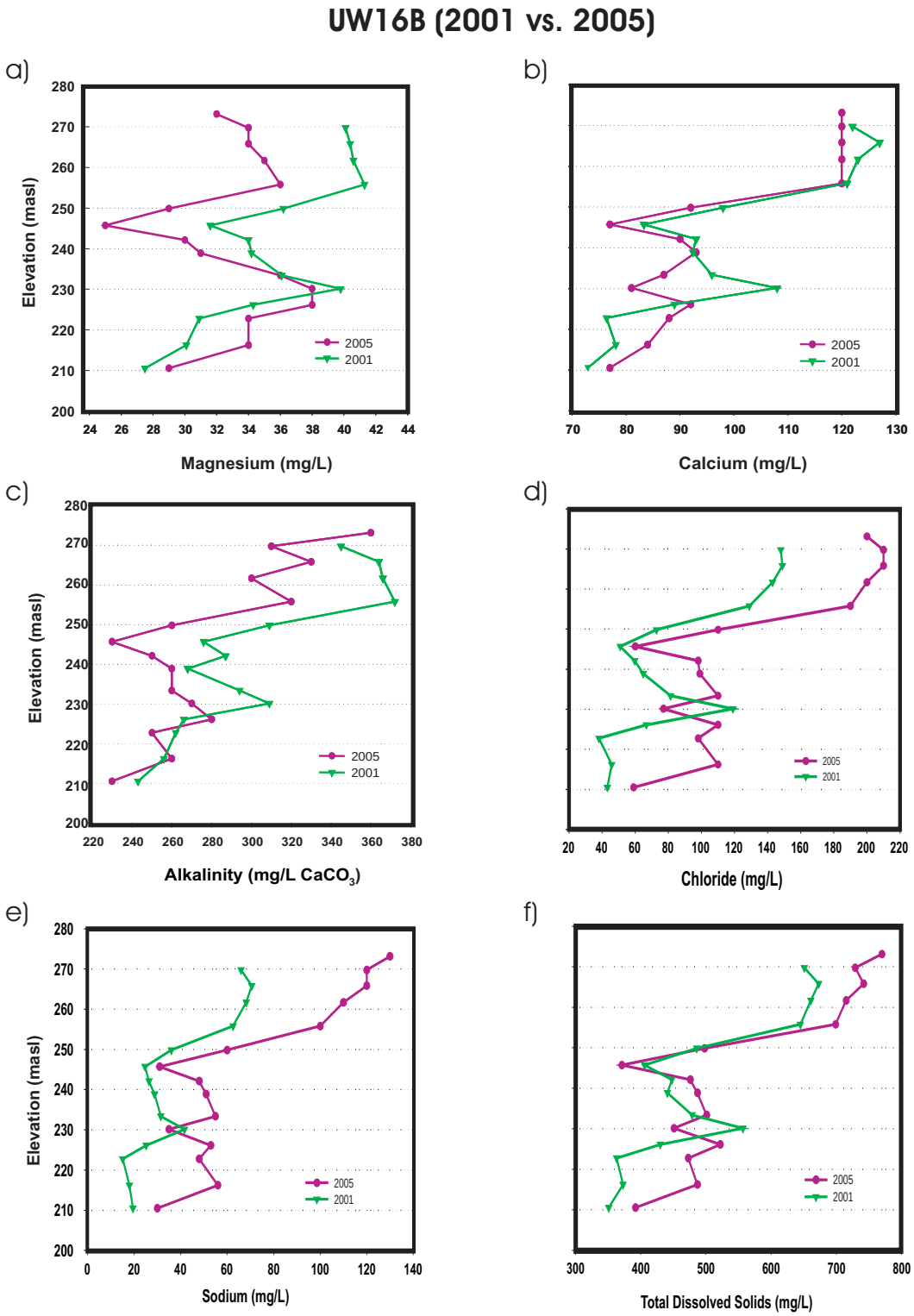


Figure 3.69: The inorganic hydrochemistry results from 2001 and 2005 in UW16B are very similar suggesting the hydrochemistry of the dolostone is very stable. a) magnesium, b) calcium, c)alkalinity, d) chloride, e) sodium, and f)TDS all show depleted concentrations from 2005 at approximately 245 masl, which is similar to results from 2001. Inorganic hydrochemistry results from 2005 show an additional zone of concentration depletion at 230 masl, which is an increase in concentration in 2001 (b,d,e,f). 2001 data from Turner (2001).

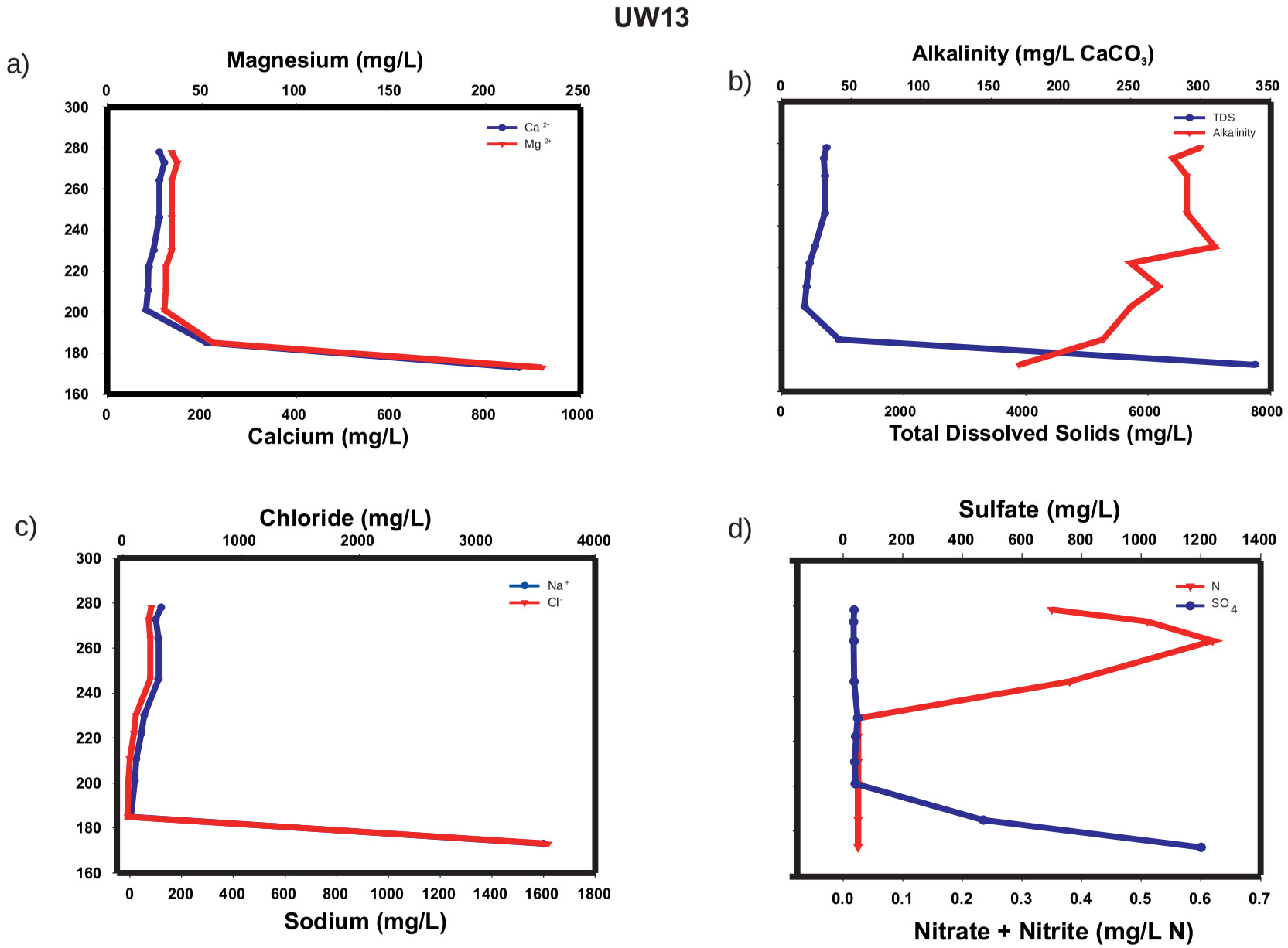


Figure 3.70: Inorganic hydrochemistry results collected from UW13 (transect) in February, 2005. Results for calcium and magnesium (a) show a large concentration increase in the shale (Port 10). This trend is similar for (b) TDS and alkalinity, (c) sodium and chloride, and (d) sulphate results.

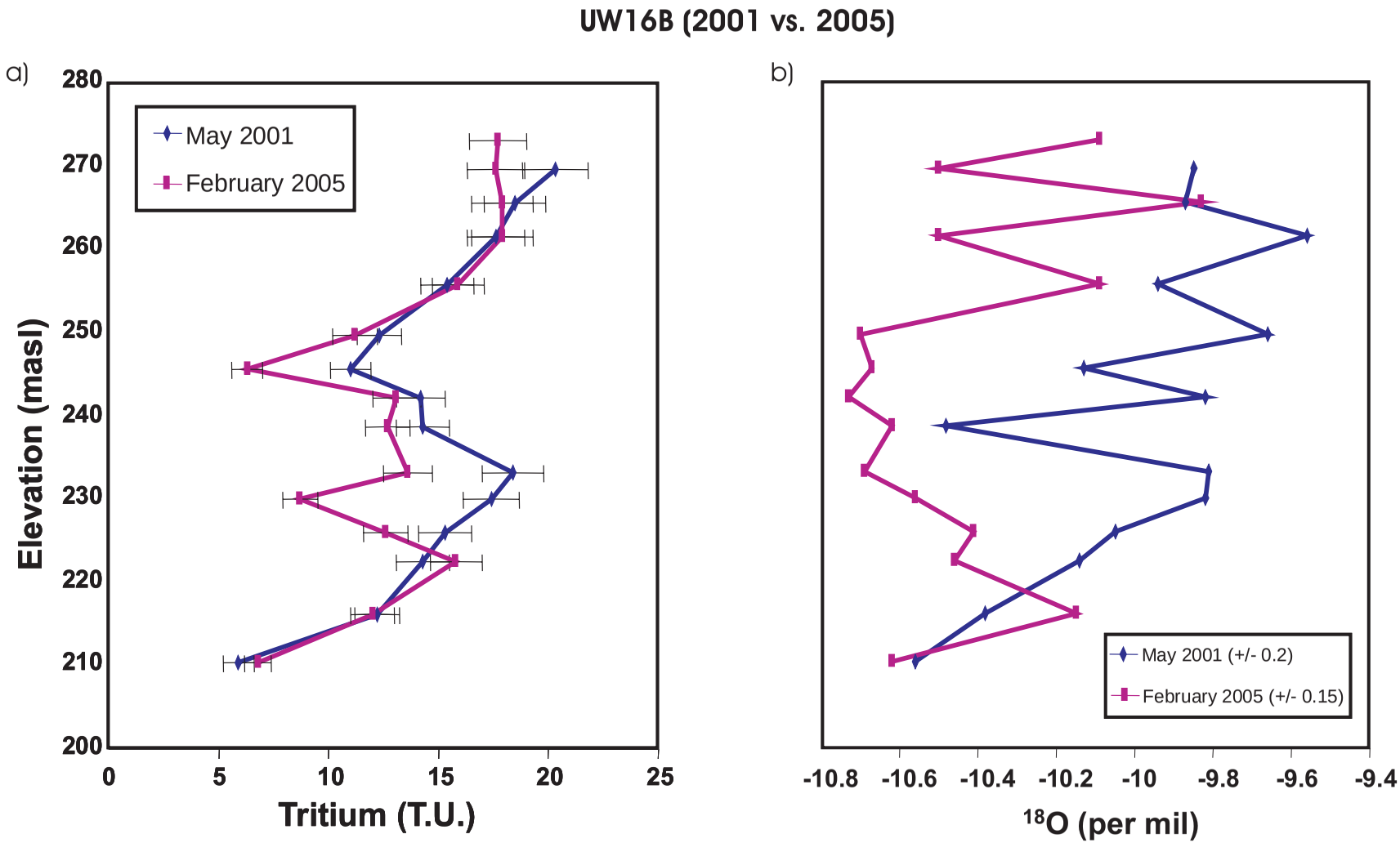


Figure 3.71: Tritium (a) and ^{18}O (b) results in UW16B from 2001 and 2005 are compared. Tritium data are similar, however results from 2005 are more depleted in concentration in two zones. ^{18}O data are also similar, however concentrations are depleted in 2005. 2001 data from Turner (2001).

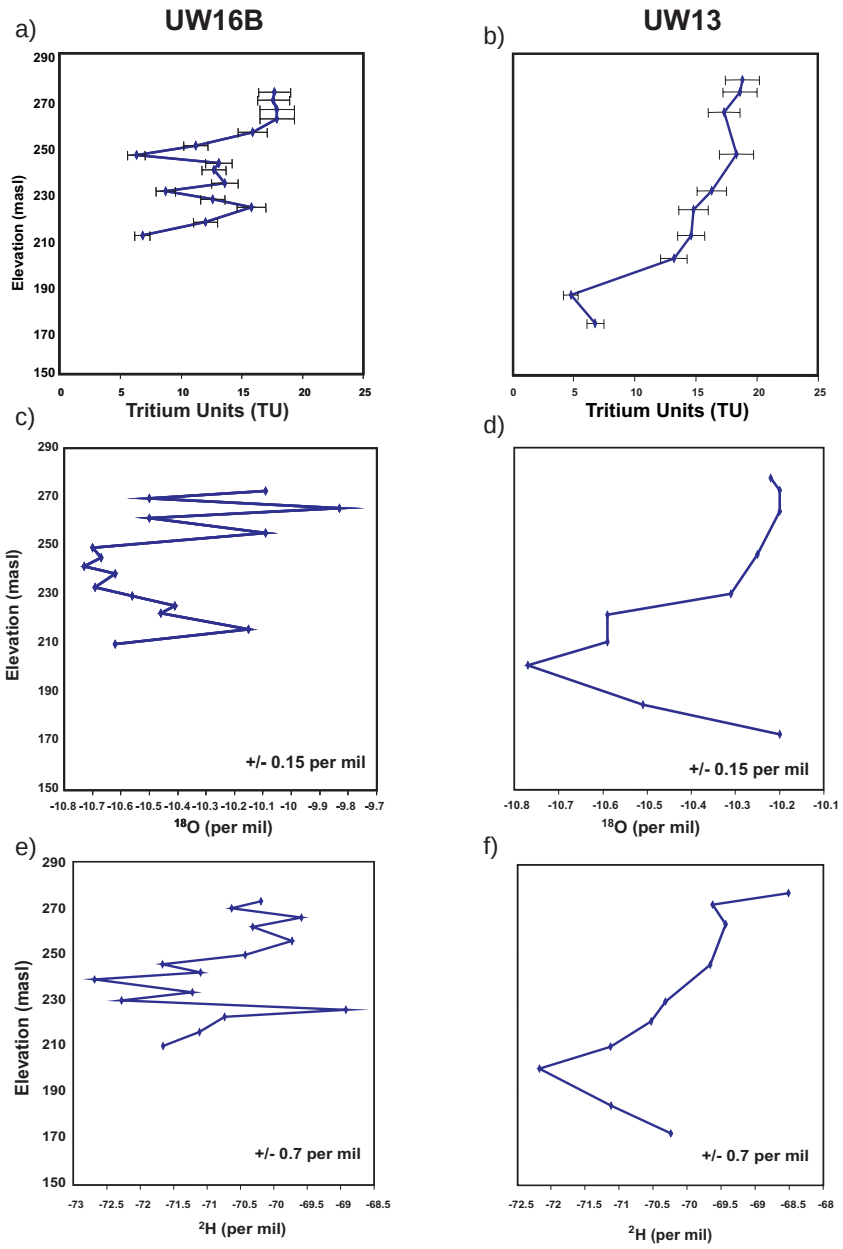


Figure 3.72: Isotope results collected from UW16B and UW13 in February 2005. Tritium data for UW16B (a) is more variable with depth than UW13 (b). The increased tritium concentration in the bottom port of UW13 may be related to open-hole groundwater mixing. ^{18}O from UW16B (c) and UW13 (d) shows that UW16B has more concentration variability with depth than UW13. Deuterium data from UW16B (e) and UW13 (f) also shows more variability with depth than UW13. This variability in the isotope concentrations in UW16B may be related to the increased hydraulic connection to the overburden.

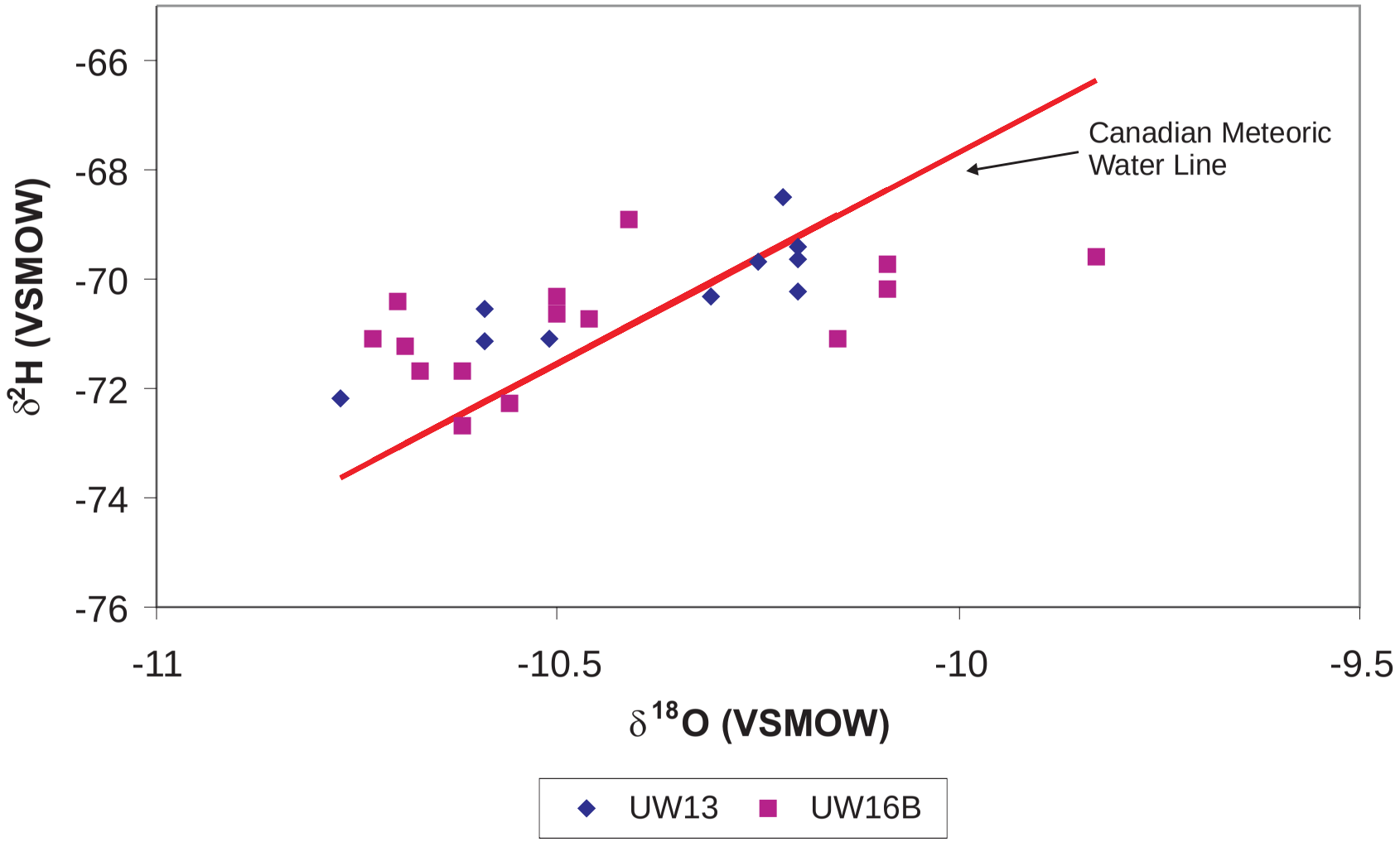


Figure 3.73: Isotopic comparison between $\delta^{18}O$ (‰ $VSMOW$) and $\delta^{2}H$ (‰ $VSMOW$) along with the Canadian Meteoric Water Line (CMWL) as a reference. UW16B data show a greater variability in relation to the CMWL than does UW13 which may suggest that the groundwater from UW16B shows evaporation effects, which in turn suggest that the hydraulic connection between the overburden and the bedrock is greater near UW16B than at UW13.

Chapter 4

Discussion

4.1 Evidence for Strong Natural Attenuation of Metolachlor and TCE

Metolachlor concentrations in groundwater decrease strongly over a relatively short distance from the source area to the down-gradient transect as shown on Figures 4.1 and 4.2, representing the concentrations along the north-south line between the source area and the municipal supply well G6. Figure 4.2 part a, adapted from Burns (2005), shows the metolachlor concentrations versus time from conventional wells OW16 in the source area and from OW13 and OW42 along the transect. A one order of magnitude decline in metolachlor concentration occurs over approximately 150 m between the source area and the transect, and then over the next 850 m to G6, the concentration decreases by another order of magnitude. Figure 4.3 shows the metolachlor concentration versus time for the time period since metolachlor was first detected in G6 (2001-present), along with the

average concentrations for OW16 (297.8 $\mu g/L$), OW13 and OW42 (15.3 $\mu g/L$), and G6 (1.1 $\mu g/L$). This figure indicates that the metolachlor concentrations in the conventional monitoring wells decrease by approximately a factor of 300 overall between the source area and G6. Figure 4.1 shows that these conventional wells are positioned in the upper half of the dolostone. There are only four of these wells located on the transect. Therefore, on their own, they cannot be viewed as indicative of maximum concentrations on the transect because higher concentrations could occur elsewhere on the transect. However, the transect monitoring using the multilevel systems represents detailed coverage of the transect and shows similar metolachlor concentrations during the same general time period (Figure 3.44). The vertical sampling intervals for the conventional wells on the transect range in length from 1.2 to 3.1 m and the intervals for the multilevels on the transect range from 1.2 to 11.3 m. Therefore the concentrations are reasonably comparable. Also, the multilevel system in the source area (UW16B) has a similar maximum concentration with the two conventional wells at this location. Thus, all of the monitoring results from the transect confirm that the maximum metolachlor values are an order of magnitude (one tenth) below the source area values (i.e. OW16/UW16).

Turner (2001) concluded that TCE monitoring also shows a strong concentration decline from the TCE source area to the downgradient monitoring locations. Figure 4.5 shows two conventional monitoring wells near the TCE source area, which is situated 210 m north of the metolachlor source area. These two wells are positioned in the overburden at depths of 12.1 and 19.6 $mbgs$, near the industrial property where TCE DNAPL likely went into the subsurface (Dames and Moore, 1998). Turner (2001) concluded that

the persistent TCE plume in the dolostone originated due to TCE DNAPL that entered the dolostone decades ago. There is one well in the dolostone near the TCE source area (OW19-35) and it shows no TCE, indicating that the TCE descended into the bedrock at a location downgradient or offgradient from this location. Figure 4.5 shows the TCE concentration decline from approximately 300 $\mu g/L$ in the TCE overburden source area, to a mean concentration of 28 $\mu g/L$ at the metolachlor source area (OW16/UW16B) located 210 m downgradient, to a mean of 2.5 $\mu g/L$ on the transect, 150 m further downgradient, to below the 0.1 $\mu g/L$ TCE detection limit at G6. An explanation for why TCE is below detection in G6 is provided later in this section. Like metolachlor, the TCE concentrations found in the multilevel systems on the transect are similar to those found in the four conventional wells on the transect (Figure 3.57). Therefore, the transect provides confirmation of the strong natural attenuation of TCE migrating from the source zone through the transect towards G6.

The strong natural decline of metolachlor and TCE from the source areas to the transect and then to municipal supply well G6 may be caused by various attenuation processes, including dispersion, matrix diffusion, degradation, and in G6, by mixing water from different depths (open interval depth is approximately 53 m). The potential for metolachlor degradation is considered here first.

Turner (2001) concluded based on a personal communication with John Purdy, the chemist employed by the metolachlor site owner, that metolachlor metabolites (degradation products) were detected in groundwater samples in OW16 and that they decrease proportionately with metolachlor between conventional well OW16 and the down-gradient

conventional wells along the transect. According to Turner (2001), this suggests that metolachlor degradation is occurring slowly, if at all. The metabolite concentration data came from non-calibrated open-scan analysis, which is semi-quantitative. A laboratory microcosm study by McMaster (1996) determined that biotransformation of metolachlor from the site was extremely slow at best and Burns (2005) indicated that even less biotransformation will likely occur deep in the dolostone aquifer because more reducing and anaerobic conditions exist. Therefore the decrease in metolachlor concentration between the source area and the transect and between the transect and G6 is most reasonably attributed to physical processes with negligible degradation.

Burns (2005) projected the attenuation (concentration decline) of metolachlor from the source area (OW16/UW16B) through the transect (OW13/OW42) southward to well G6, as shown on Figure 4.2 part b. This projection uses a straight-line on double log scale between the metolachlor source area, the transect and G6. The inset projection on Figure 4.2 part b represents the semilog case and it uses the same projection as the log-log case. The metolachlor concentration projected to well G6 is 6 $\mu g/L$ which is greater than the actual maximum value detected of 1.9 $\mu g/L$. Burns (2005) concluded that the difference between the projected metolachlor value at G6 and the maximum value at this well is caused by well-bore mixing in G6. The double-log, linear projection used by Burns (2005) results in a minimal concentration decline over the 900 m between the transect and G6. The data show the strongest decline occurs nearest the source and the decline is smaller further from the source. This suggests that dispersion and other attenuating processes are most effective nearest the source.

The monitoring along the transect has established the minimal width and vertical position of the metolachlor and TCE plumes as shown on Figures 4.4 and 4.6. The down-gradient plume has widened to over 250 m laterally due to transverse dispersion, although the full width of the plume is unknown. Additional coreholes would need to be drilled to determine the full width of the plume; one to the east of UW3 and one to the west of UW5. All of the contamination occurs in the middle part of the dolostone aquifer along the transect (Figures 4.4 and 4.6), whereas the multilevel in the metolachlor source area (UW16B) shows contamination to the bottom monitoring port at approximately 100 $mbgs$. For metolachlor, the plume on the transect has a vertical thickness of approximately 16 m and the length of the open interval of G6 is 53 m. Projecting the elevation of the general plume thickness (248-228 $masl$) onto the open interval of G6, it is possible to account for metolachlor concentration decline between the projected value of 6 $\mu g/L$ and the maximum detected value of 1.9$\mu g/L$ based on well-bore mixing. The plume thickness is approximately 30% of the thickness of the entire open interval of G6, therefore with a dilution factor of 0.3, 6 $\mu g/L$ could easily be reduced to 1.9 $\mu g/L$ based on dilution within the well screen. This well-bore mixing calculation is based on the assumption that well-bore mixing can be represented simply by the proportioning of plume water and clean water extracted by G6 according to the plume thickness and well bore length. Other factors may be influencing the proportions of these waters drawn into this well.

The linear, double log plot used by Burns (2005) in Figure 4.2 was used for this thesis also to make a projection of TCE to G6, shown on Figure 4.5 part b. In the metolachlor projection by Burns (2005) there are two data locations (the metolachlor

source area and the transect), however, in the TCE projection there are three locations on the projection line upgradient of G6: the TCE source area, the OW16/UW16B area, and the transect. The TCE source area values are from the overburden. TCE is projected to have a concentration in G6 of 4 $\mu g/L$ using a best fit straight line through three points on the log-log graph in Figure 4.5. A projected TCE concentration of 0.025 $\mu g/L$ is obtained based on a two data point line (the OW16/UW16B area and the transect). The conventional wells with the highest mean concentration were used to plot the straight line. Because the projected concentrations for both metolachlor and TCE are similar and TCE has not been detected in G6, it appears that TCE is attenuated more than metolachlor. This attenuation is likely due to biodegradation, which is discussed below.

4.2 Evidence for TCE Degradation

Typical products of TCE degradation (cis-DCE and trans-DCE) occur in the conventional wells, the multilevel systems and rock core analyses. Many studies show that the presence of cis-DCE and trans-DCE in TCE contaminated groundwater are the result of microbial degradation under reducing redox conditions (Vogel et al., 1987; Chapelle, 2001; Wiedemeier et al., 1999). Based on a literature review, Pierce (2005), and Pierce et al. (2006) indicate that very few field studies of TCE degradation in bedrock are reported and no studies indicate the influence on degradation of processes occurring in the rock matrix. Pierce (2005) and Pierce et al. (2006) provide evidence of TCE degradation, both biotic and abiotic in fractured sandstone in California. Figure 4.9 shows the occurrence of c-DCE and t-DCE in both the rock core and the multilevel system in the metolachlor source

area (OW16/UW16B area). These apparent TCE degradation products also occur in the conventional monitoring wells at this location (Figure 4.9).

Figure 4.9 indicates that in some of the multilevel monitoring zones, the c-DCE values actually exceed the TCE concentration, particularly in the deeper ports. In many of the rock core samples in the same general depth interval, t-DCE is dominant, however in the multilevel system, t-DCE is present but at very low concentrations. The average concentration of TCE in OW16 is 28 $\mu g/L$, c-DCE occurs in OW16 with an average concentration of 19.7 $\mu g/L$ and t-DCE occurs at an average concentration of 3.3 $\mu g/L$.

Figures 4.10 to 4.14 show the PCE, TCE, c-DCE, and t-DCE data collected along the transect from the rock core converted to an equivalent porewater concentration, along with the respective data collected from the multilevel systems. Figure 4.10 shows the TCE degradation products for UW5. The only detectable degradation product from multilevel samples is c-DCE. Concentrations of c-DCE are very similar to concentrations of TCE, port 4 contained higher concentrations of c-DCE than TCE. Figure 4.11 shows degradation products collected from UW4. The only detectable degradation product in groundwater samples from the multilevel system is c-DCE. These data are generally lower in concentration than TCE, however the concentrations are similar. The peak concentration of 1 $\mu g/L$ was obtained from ports 7 and 8, which are the locations of the peak TCE concentrations. UW13 has very high concentrations of t-DCE in the rock core, however based on Figure 4.12, the only degradation product detected in the groundwater from the multilevel system in this hole is c-DCE. The concentrations of c-DCE in UW13 are very similar to TCE, and port 5 has a higher concentration of c-DCE (0.7 $\mu g/L$) than TCE (0.2$\mu g/L$). Figure 4.13

shows the degradation products obtained from the multilevel system installed in UW6. The only degradation product detected is c-DCE and the concentrations are generally lower than TCE, however not substantially. The maximum concentration of c-DCE (1 $\mu g/L$) occurs in port 6, where the maximum concentration of TCE occurs.

Figure 4.14 shows the degradation products detected in the groundwater samples from the multilevel system in UW3. The rock core data from UW3 shows that c-DCE concentrations are much higher than TCE, however samples collected from the multilevel system show the maximum concentration of c-DCE (0.8 $\mu g/L$) to be slightly less than TCE (1.4 $\mu g/L$). Port 10 shows identical concentrations for both TCE and c-DCE. This suggests that greater degradation may be occurring at this depth.

In order to assess the role of microbial degradation, it is important to identify the redox potential of the aquifer (Wiedemeier et al., 1999; Chapelle, 2001). Inorganic hydrochemistry data was collected from multilevels in UW16B and UW13 in February 2005 (Figures 3.68 to 3.70). These data collected from the multilevel systems agree with Pierce et al. (2006), and suggest that redox conditions within the dolostone aquifer could support microbial processes and are therefore conducive to TCE degradation.

PCE was detected in rock core samples with a maximum concentration of 1658 $\mu g/L$ in UW16B and 87 $\mu g/L$ on the transect, however it was not detected in any groundwater samples collected from the conventional wells or multilevel system installed in the metolachlor source area or on the transect. The source of this PCE is unknown. It is unknown how much of the degradation products are related to PCE degradation, and a study of carbon isotopes similar to Pierce (2005), would need to be initiated to determine the origin

of the plume and the extent of PCE degradation.

In conclusion, metolachlor has been detected since 2001 and continues to persist in municipal supply well G6. The detection limit for TCE is much lower that for metolachlor and nevertheless no TCE or TCE degradation products have been detected in this well. It is unlikely that TCE plume retardation is responsible for the non-detection because metolachlor has stronger sorption and would therefore move more slowly than TCE in respect to the groundwater flow velocity. Therefore it is concluded that degradation by microbial reductive dechlorination has enhanced the attenuation of TCE.

4.3 Hydrogeologic Influences on Plume Position on the Transect

Turner (2001) and Burns (2005) present groundwater data from the source area (UW16B/OW16 area) showing that the highest metolachlor and TCE concentrations occur in the upper 20 m of the dolostone with a smaller local maximum concentration zone in the middle of the dolostone aquifer (Figure 4.15). However, monitoring on the transect shows a single peak concentration zone for both metolachlor and TCE only in the middle of the aquifer (Figures 4.16 to 4.20).

Hypotheses to address the downward plume migration will be addressed further below and include: i) strong downward gradients in the upper bedrock, ii) a zone of abundant stylolites in the middle of the aquifer, iii) a high hydraulic conductivity zone near the middle of the aquifer, and iv) karst features which may be coincident with high hydraulic

conductivity zones.

A strong downward gradient exists in the shallowest five multilevel ports located in the upper 20 m of bedrock in UW16B. This downward gradient of 0.1 through the upper 20 m of dolostone is coincident with the highest concentrations observed in UW16B for both metolachlor and TCE (Figure 4.15). The gradient may be responsible for the lower peak in concentration for both metolachlor and TCE at approximately 240 $masl$, and due to back diffusion from the rock matrix, which provides a constant source of contamination for the lower concentration peak (Parker et al., 2006b).

The lower peak in metolachlor and TCE concentration occurs just above or slightly within the Eramosa unit defined for UW16B by the gamma peak at approximately 240 $masl$ (Figure 4.15). The Eramosa unit was defined for this thesis as having abundant stylolites and Langer (1999) and Langer et al. (1999) concluded that stylolites may be a substantial source of organic carbon and could cause organic contaminants such as TCE to preferentially sorb onto the surfaces of such structures. The sorption of contaminants onto this unit could act as a sink, and prevent vertical contaminant migration through the dolostone.

Intervals of high hydraulic conductivity determined from straddle packer tests (Figure 4.15) are coincident with the Eramosa unit at UW16B. These intervals may represent potentially active groundwater flow zones in the fracture network. If these zones are active groundwater flow zones, they may be impacted by dissolution and karst features may be present. No evidence for karst features is observed in UW16B, however, UW16A (discussed in section 3.1), did collapse and the corehole was abandoned at approximately 42

mbgs, which may have been related to karst features. If karst features are coincident with the zones of high hydraulic conductivity, then conduits may be available for contaminant transport which would allow the contaminant plume to travel in a direction that opposes the general groundwater flow direction. This discussion will be addressed further in section 4.4.

Therefore, the higher concentrations in the upper 20 m of dolostone most likely migrated downward to the middle of the dolostone aquifer due to the vertical gradients present in the shallow bedrock in UW16B. The Eramosa unit, which contains abundant stylolites may be acting as a carbon source allowing contaminants to sorb and preventing the downward migration of both metolachlor and TCE. The high hydraulic conductivity zones near the Eramosa unit, which may contain karst features most likely provide a conduit for contaminant flow downgradient towards the transect in the middle of the aquifer at approximately 240 *masl*.

The metolachlor and TCE plumes are vertically narrow and laterally extensive along the transect (Figures 4.7 and 4.8). Figures 4.7 and 4.8 show the metolachlor and TCE plumes respectively, overlain on the corelogs along the transect. The highest concentration contours ($\geq 6\mu g/L$ for metolachlor and $\geq 1.5\mu g/L$ for TCE) occur at approximately 240 *masl*, which corresponds to the location of the Eramosa unit identified from the gamma logs and Corelog Unit J based on core logs (Figures 4.16 to 4.20). The Eramosa unit was described in corelogs as having abundant stylolites, very few fractures and moderate pinpoint porosity. The Eramosa unit may be an area of high contaminant sorption and could therefore prevent contaminants from traveling downward through the dolostone

aquifer. UW13 is the exception along the transect in that there was no evidence for the Eramosa unit based on gamma logs and Corelog Unit J was not described in the core logs from Turner (2001). Decreased concentrations of metolachlor and TCE were both observed from the multilevel system in UW13 in comparison to other transect multilevels. The deficiency of the Eramosa unit at UW13 may not provide a source for back diffusion (contaminant sink) and may be responsible for the lower concentrations of metolachlor and TCE obtained from the multilevel system (Figure 4.18).

Figure 3.14 shows the horizontal hydraulic conductivity profiles for the holes along the transect. There is a zone of higher hydraulic conductivity from approximately 232-250 *masl* along the transect (Figure 3.14). All of the holes along the transect show the highest hydraulic conductivity just above the Eramosa unit, this is evidence for a laterally extensive zone where the potential for flow is high. In UW4, UW5, and UW6, heat pulse flow meter results showed a decrease in open-hole vertical flow at the high hydraulic conductivity zones in the respective coreholes, suggesting horizontal flow may be dominant in those areas (Figures 4.16, 4.17, 4.19). UW16B, located in the source area, also shows increased hydraulic conductivity at approximately 240 *masl*, suggesting that this zone of increased flow along the transect may also extend to the source area and act as a conduit for contaminant flow. Figure 3.12 shows evidence of karst features from borehole video logs in UW3, UW5, and UW6, where all of the images occur in areas of high hydraulic conductivity. Perrin et al. (2006) discusses the potential for karst features in Cambridge and suggests that in the presence of karst conduits, the contaminant plume can be highly focussed in these zones and the plume could be narrowed significantly down-gradient of

the source area compared to an aquifer with no karst features. A combination of influences from karst features, and the sorptive properties of the Eramosa unit could be responsible for the vertically narrow and laterally extensive plume located in the middle part of the dolostone aquifer along the down-gradient transect.

Figures 4.16 to 4.20 show rock core data compared along side groundwater concentration data collected from multilevel systems. The cumulative equivalent mass of metolachlor and TCE are also determined and plotted adjacent to the rock core data. The cumulative mass data were integrated by calculating the mass values for each sample and assuming these values remained constant for the depth range between the midpoint to the sample above, and the midpoint to the sample below, and multiplying by the area to obtain a value on a horizontal per-metre-squared basis. Non-detect values were assigned a mass equivalent to half of the detection limit and values below the limit of quantitation were assumed to have a mass equal to the reported mass. These data show where contaminant mass has accumulated in the rock matrix over the full extent of each corehole, similar to studies completed by Sterling (1999) and Hurley (2003). The cumulative equivalent mass data shown in Figures 4.16 to 4.20, have a general trend of mass accumulation between Corelog Units that are fractured or have a vuggy porosity and Corelog Units that are not fractured or have pinpoint porosity. Using the cumulative equivalent mass and determining the cumulative mass percent determines that the centre of mass (50 % cumulative mass) of the rock core contamination for metolachlor and TCE occurs between 210 and 188 *masl*. This is approximately 25 m below the location of the Eramosa unit where most of the plume delineated from multilevel samples is found. In order to fully asses the discrepancy

between the rockcore plume position, which is located in the rock matrix where there is a large potential for contaminant storage, and the plume from multilevel sampling, which represents the fracture or fracture zone concentration, further study is required. Detailed concentration data acquired from the multilevel systems and the rockcore concentration data from the same multilevel zones is represented in Appendix A.

4.4 Inconsistencies between Plume and Potentiometric Surfaces

There is an inconsistency between the groundwater flow direction based on potentiometric surfaces for the middle zones in the dolostone aquifer, which show a westward hydraulic gradient and the metolachlor and TCE plumes that extend southward from the source area (UW16B/OW16 area) through the transect towards well G6. This inconsistency does not occur for the shallow part of the dolostone aquifer, for which the potentiometric surfaces show a southward gradient (Figures 3.29 and 3.30). Figures 3.31 and 3.32 represent the potentiometric surfaces in the middle part of the dolostone aquifer at 255 *masl* and 235 *masl*. The hydraulic gradient to the west is similar to the Regional hydraulic gradients determined by Lotowater Ltd. (1997), shown on Figures 3.33 and 3.34.

The consistency between the Lotowater Ltd. (1997) regional potentiometric surfaces and the local potentiometric surfaces presented in Figures 3.31 and 3.32, suggests that the westward hydraulic gradient indicated by those surfaces is real, rather than due to errors in the field data, although more data points need to be added to areas surrounding the study

site to confirm this gradient. Therefore, if the westward hydraulic gradient is accepted as real, the explanation of the discrepancy, most likely involves large scale anisotropy and/or karstic channels oriented southward. In this study, anisotropy refers to groundwater flow on a horizontal plane and describes the difference in the plume flow direction and the horizontal hydraulic gradients observed at the study site.

Lotowater Ltd. (1997) concludes that the hydraulic behavior of the dolostone at the study site is anisotropic and the distribution of hydraulic properties is highly irregular. Figure 4.21 shows fracture dip direction rose diagrams obtained from coreholes in the source area (UW16B, UW1, UW2) from Burns (2005), and coreholes along the transect from the current thesis (UW5, UW4, UW6). These data suggest a strong fracture orientation in an east-west direction in both the source area and on the transect, which is coincident with the regional and local flow directions in the middle part of the dolostone aquifer towards the west. Therefore, based on the presence of karstic features observed in borehole video and from acoustic televiewer logs, as well as the detection of metolachlor at persistent concentrations in municipal supply well G6, these data suggest the potential for anisotropy in the groundwater flow direction. The karst conduits may provide a preferential contaminant transport path towards G6 which opposes the general fracture orientation and hydraulic gradient to the west. Studying the potential for karst conduits may provide future insight into contaminant fate and transport at the study site in Cambridge, Ontario.

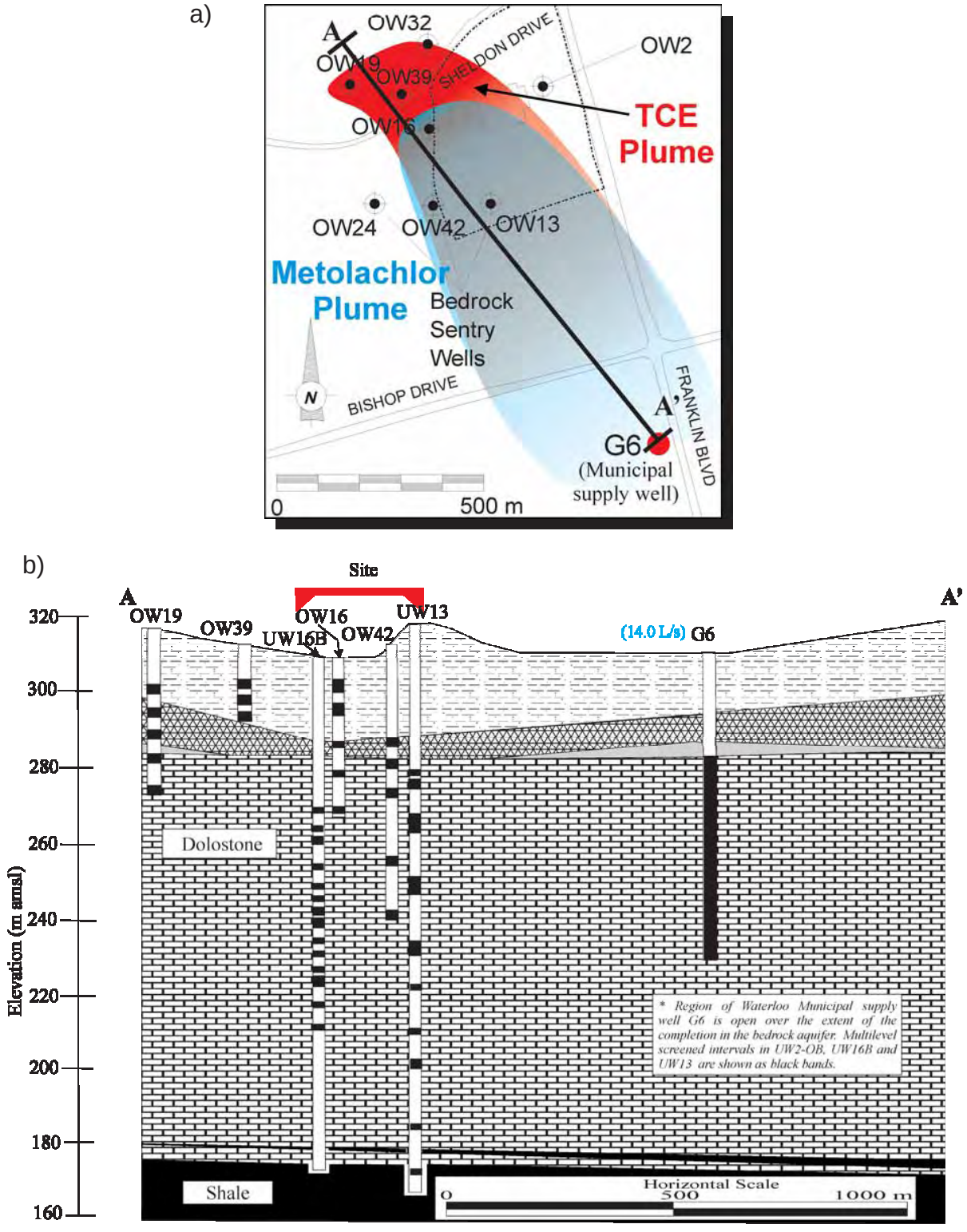


Figure 4.1: North-south line along conventional monitoring wells towards pumping well G6. a) Plan view of conventional monitoring wells and the approximate extent of the TCE and metolachlor plumes. b) Cross-section along the north-south line towards G6. Adapted from Burns (2005).

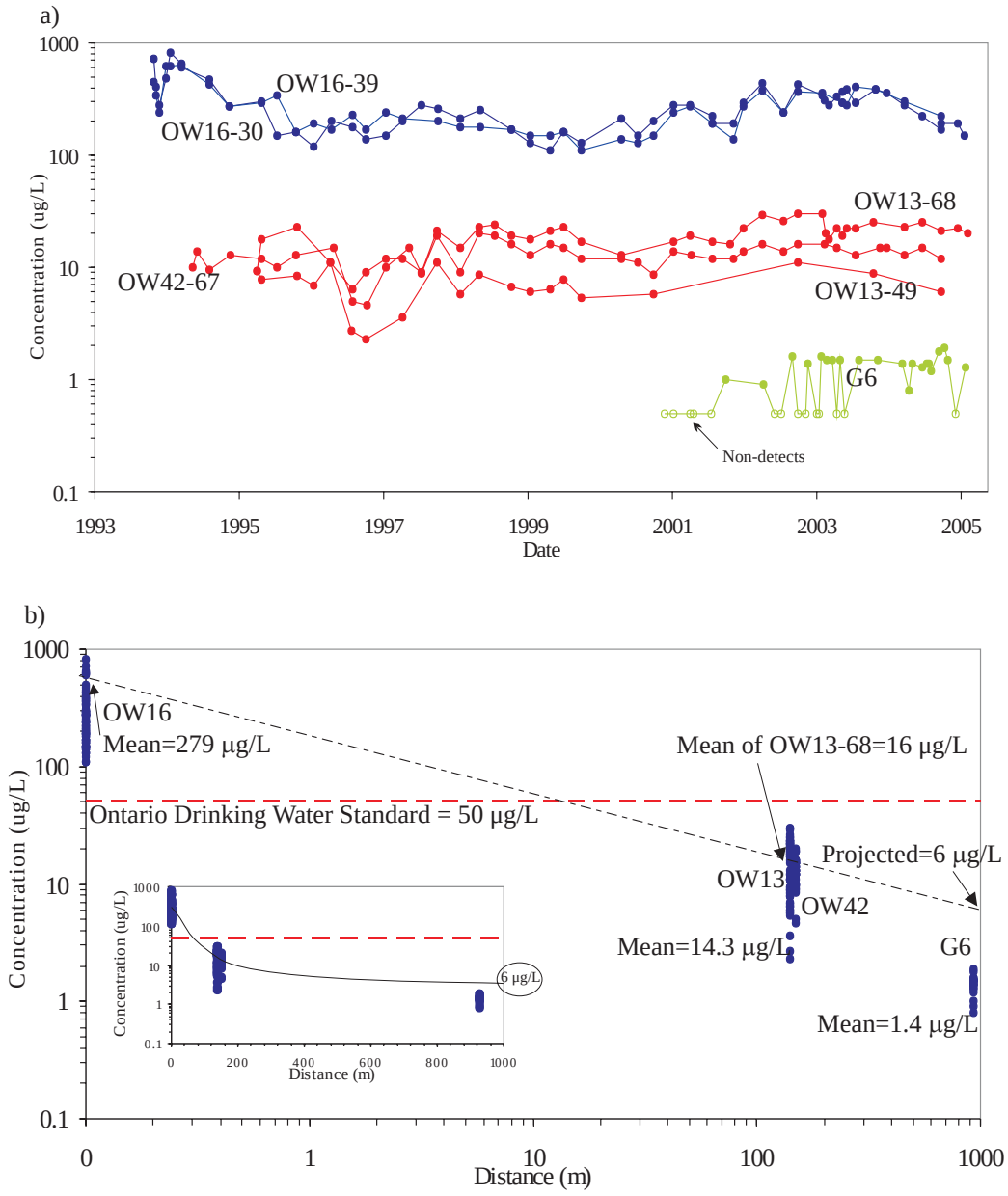


Figure 4.2: Metolachlor concentrations versus time in bedrock conventional wells along north-south line (a) and straight-line concentration projection to G6 based on mean concentration values. The projected concentration of metolachlor in G6 is 6 $\mu g/L$ which is higher than the actual maximum concentration of 1.9 $\mu g/L$. This concentration difference can occur due to well-bore mixing. Adapted from Burns (2005).

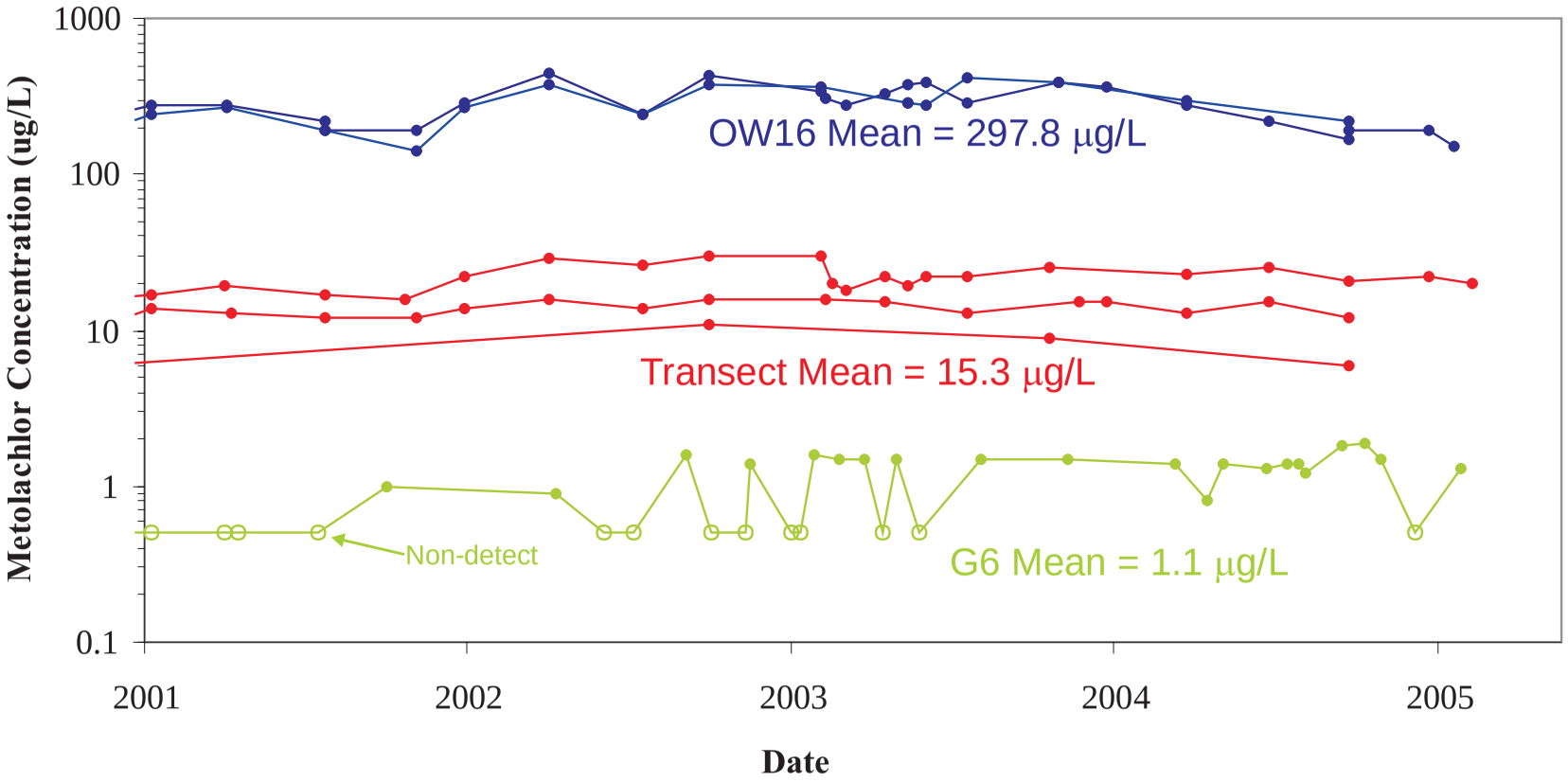


Figure 4.3: Metolachlor concentration data from conventional wells OW16 (source area), OW13 and OW42 (transect), and G6 from 2001-present (Since detection of metolachlor in G6). The concentration decreases by a factor of nearly 300 from the source area to G6.

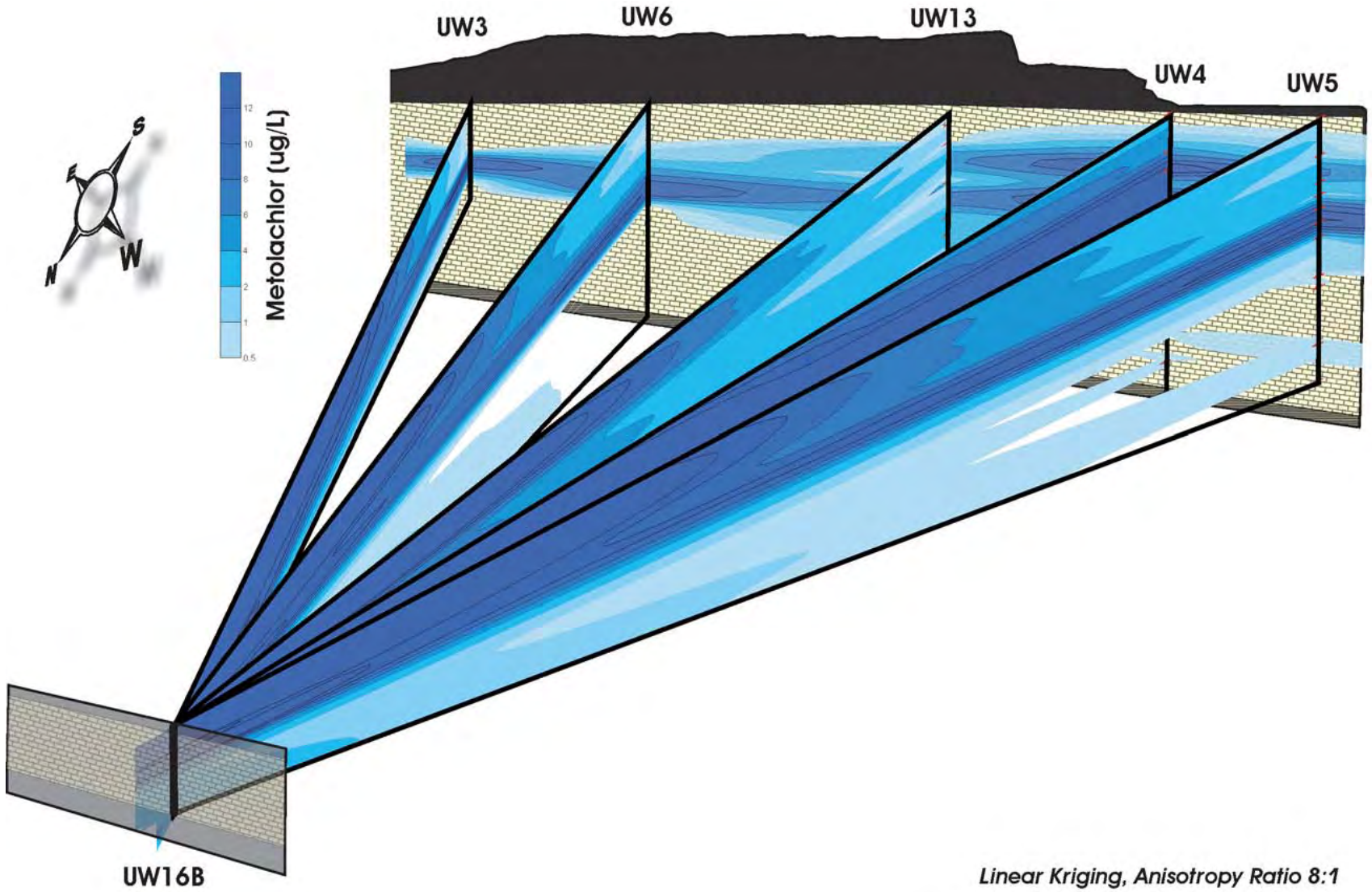


Figure 4.4: Metolachlor concentrations contoured from the source area (UW16B) to the multilevels along the transect. The plume is very wide along the transect and the full lateral extent is unknown. Most of the metolachlor contamination appears to be located in the upper half of the dolostone aquifer.

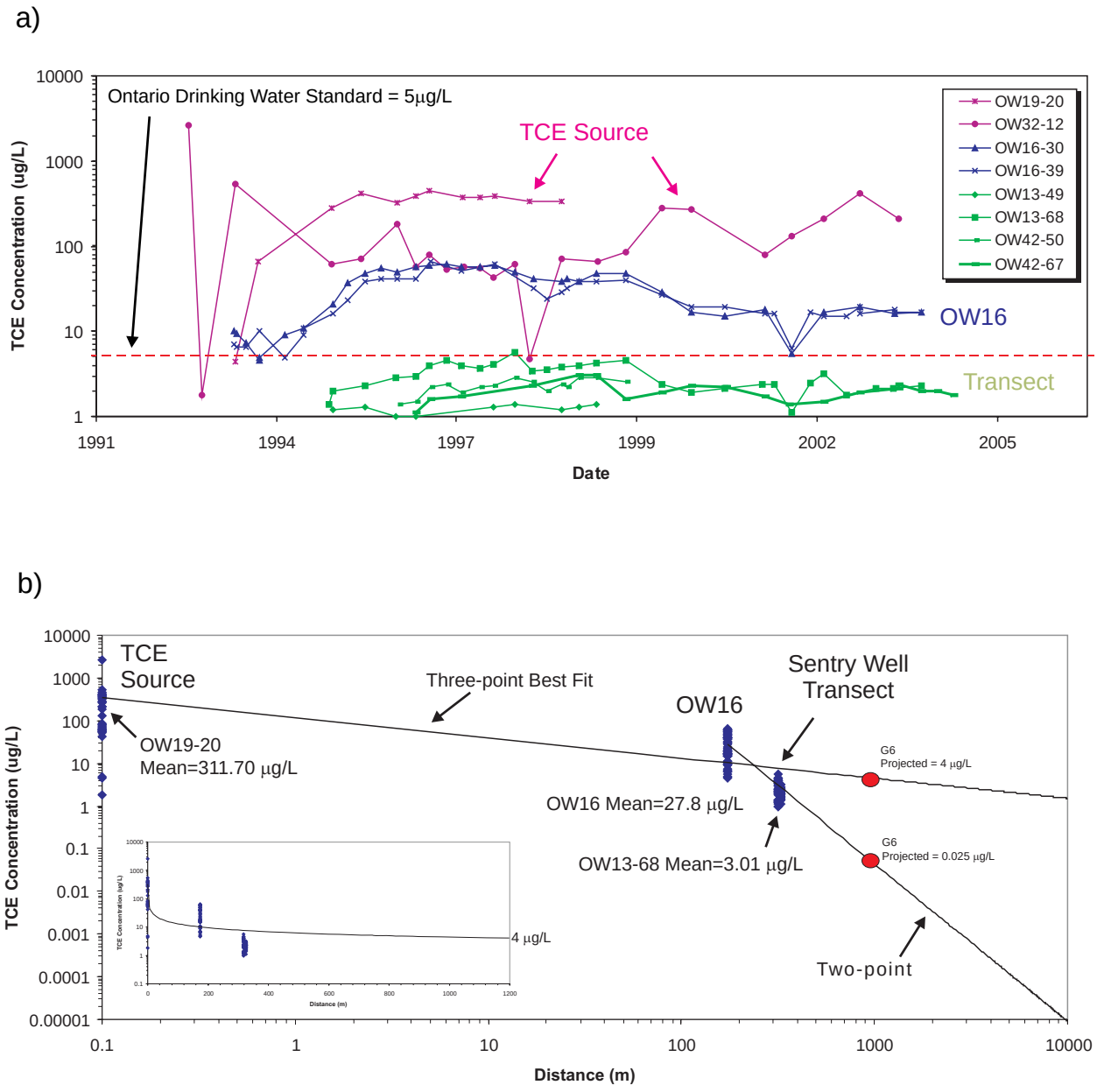


Figure 4.5: TCE concentrations versus time in bedrock conventional wells along north-south line (a) and Best fit line concentration projections to G6 based on mean concentrations values. Projected range of TCE concentration in G6 is between 0.025 and 4 $\mu g/L$ depending on three-point best fit line or a two point line.

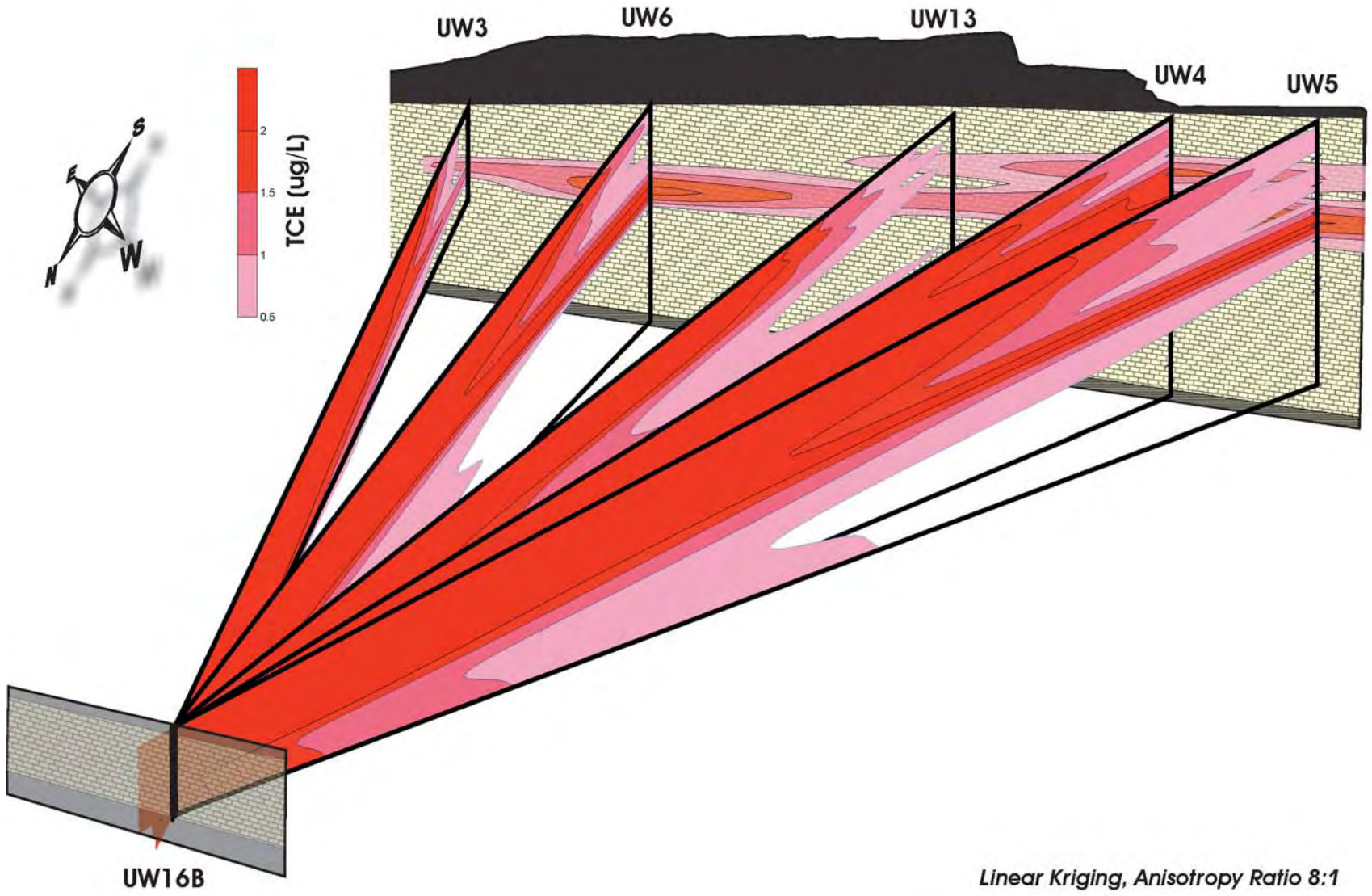


Figure 4.6: TCE concentrations contoured from the metolachlor source area (UW16B) to the multilevels along the transect. The plume is very wide along the transect and the full lateral extent is unknown. Most of the TCE contamination appears to be located in the upper half of the dolostone aquifer.

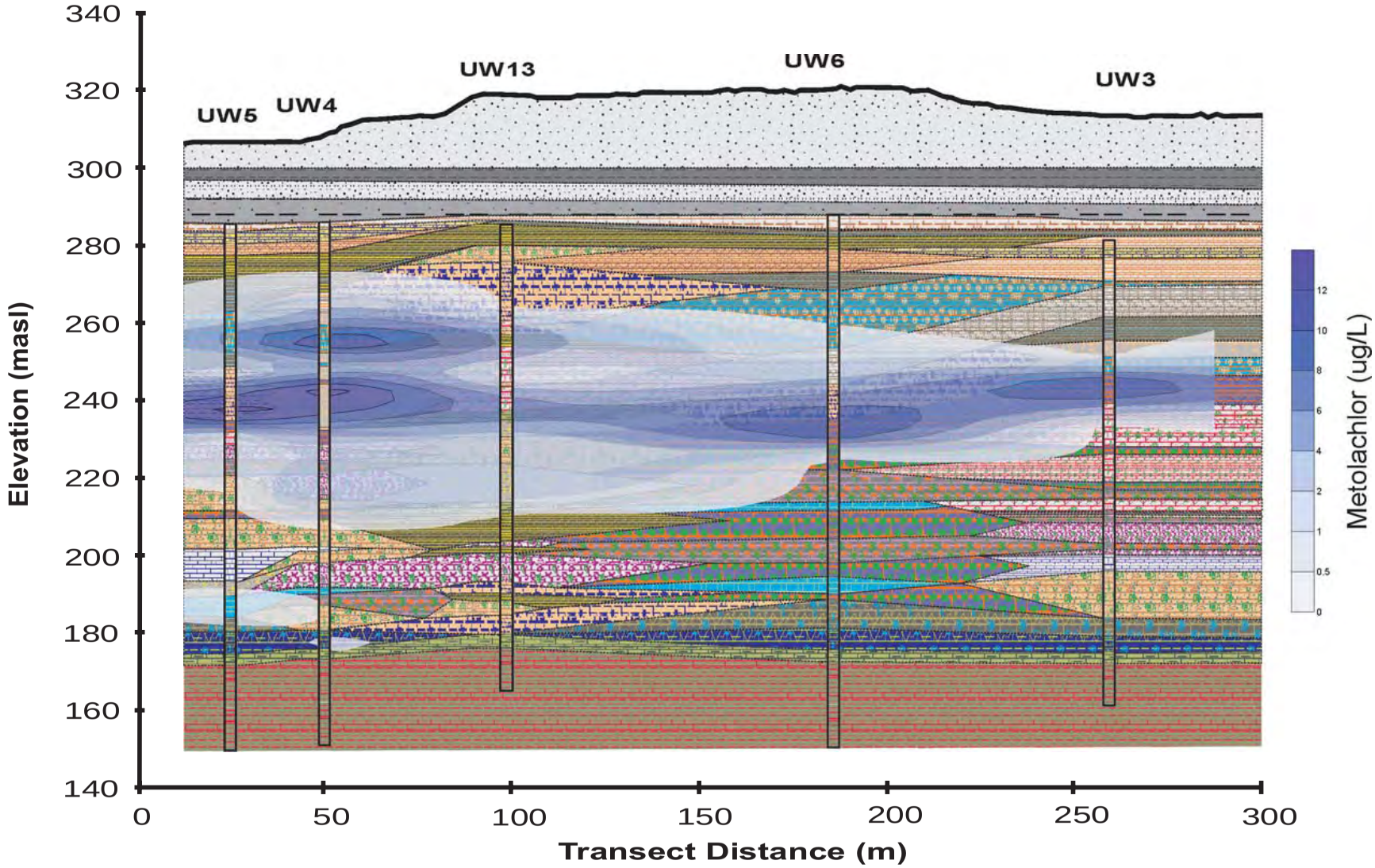


Figure 4.7: The metolachlor concentration contours from December 2005 are superimposed on the corelogs along the transect. This figure illustrates the influence of the Eramosa unit on the metolachlor plume. The highest metolachlor concentrations occur at, or mostly above the Eramosa unit.

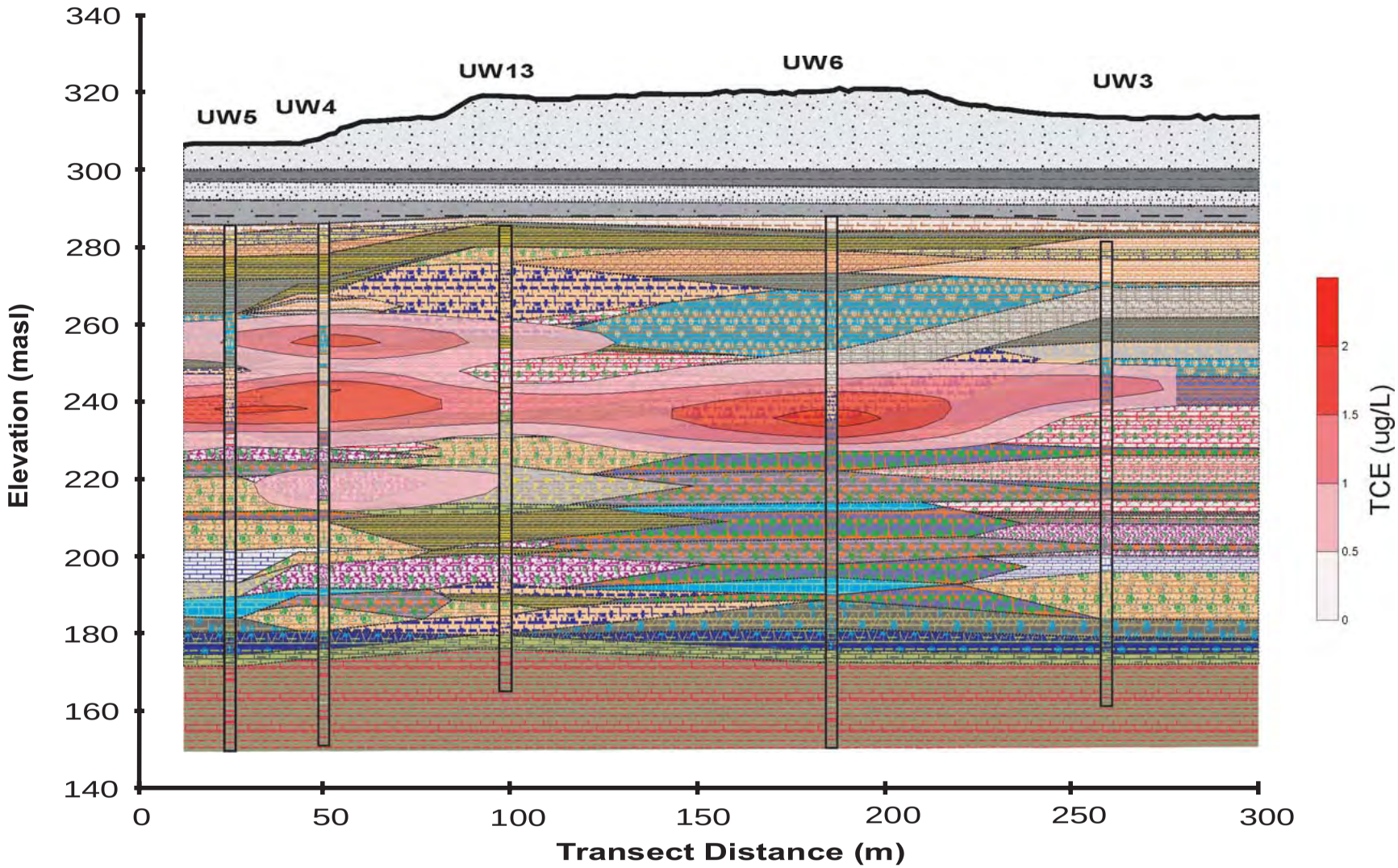


Figure 4.8: The TCE concentration contours from December 2005 are superimposed on the corelogs along the transect. This figure illustrates the influence of the Eramosa unit on the TCE plume. The highest metolachlor concentrations are coincident with the Eramosa unit and very low concentrations occur below that unit.

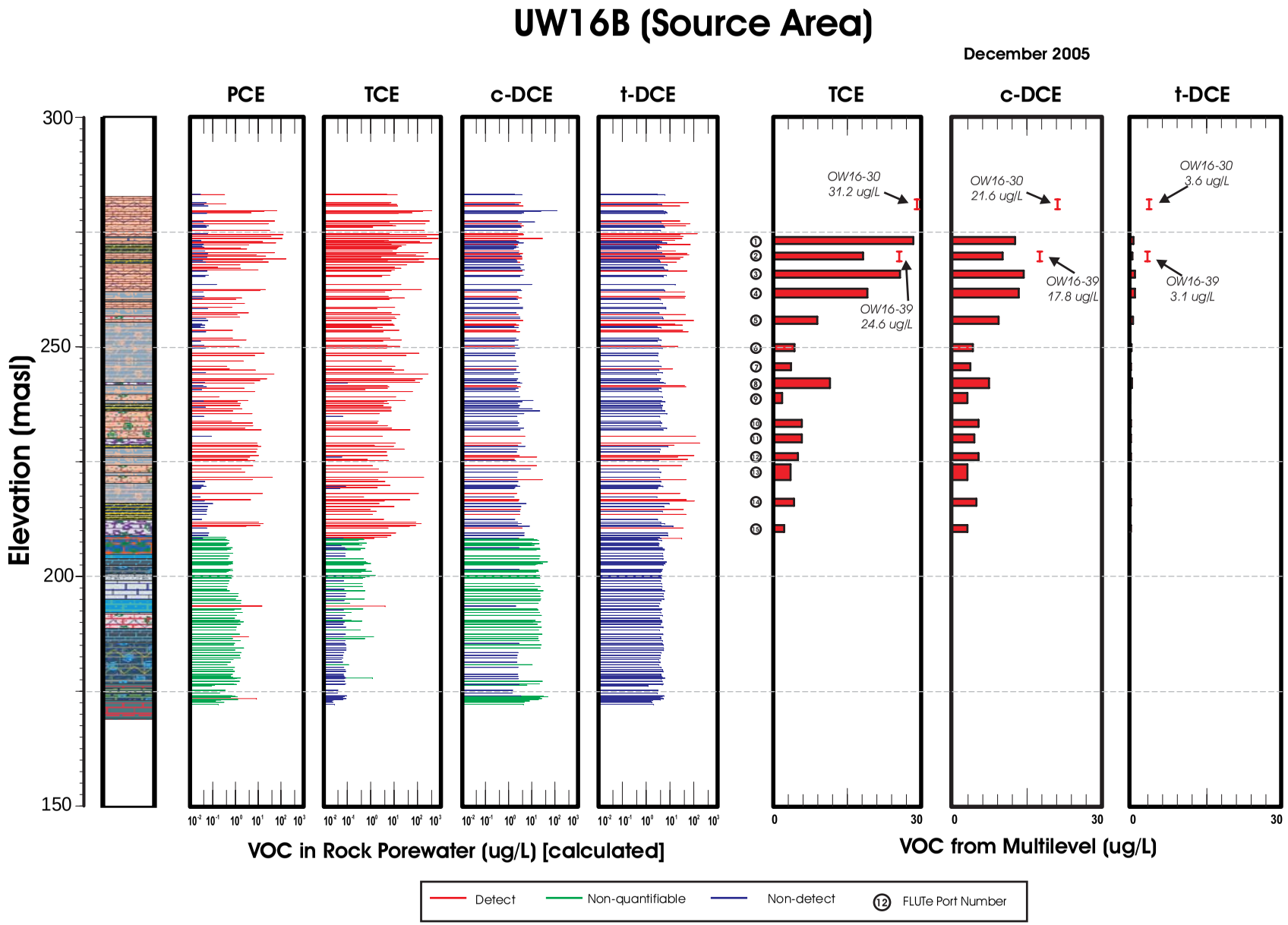


Figure 4.9: UW16B TCE degradation products in rock core and multilevel sampling results from December, 2005. c-DCE and t-DCE were both detected in multilevel samples however c-DCE occurred in much higher concentration than t-DCE. Conventional well results are provided for comparison and show very similar concentrations to UW16B

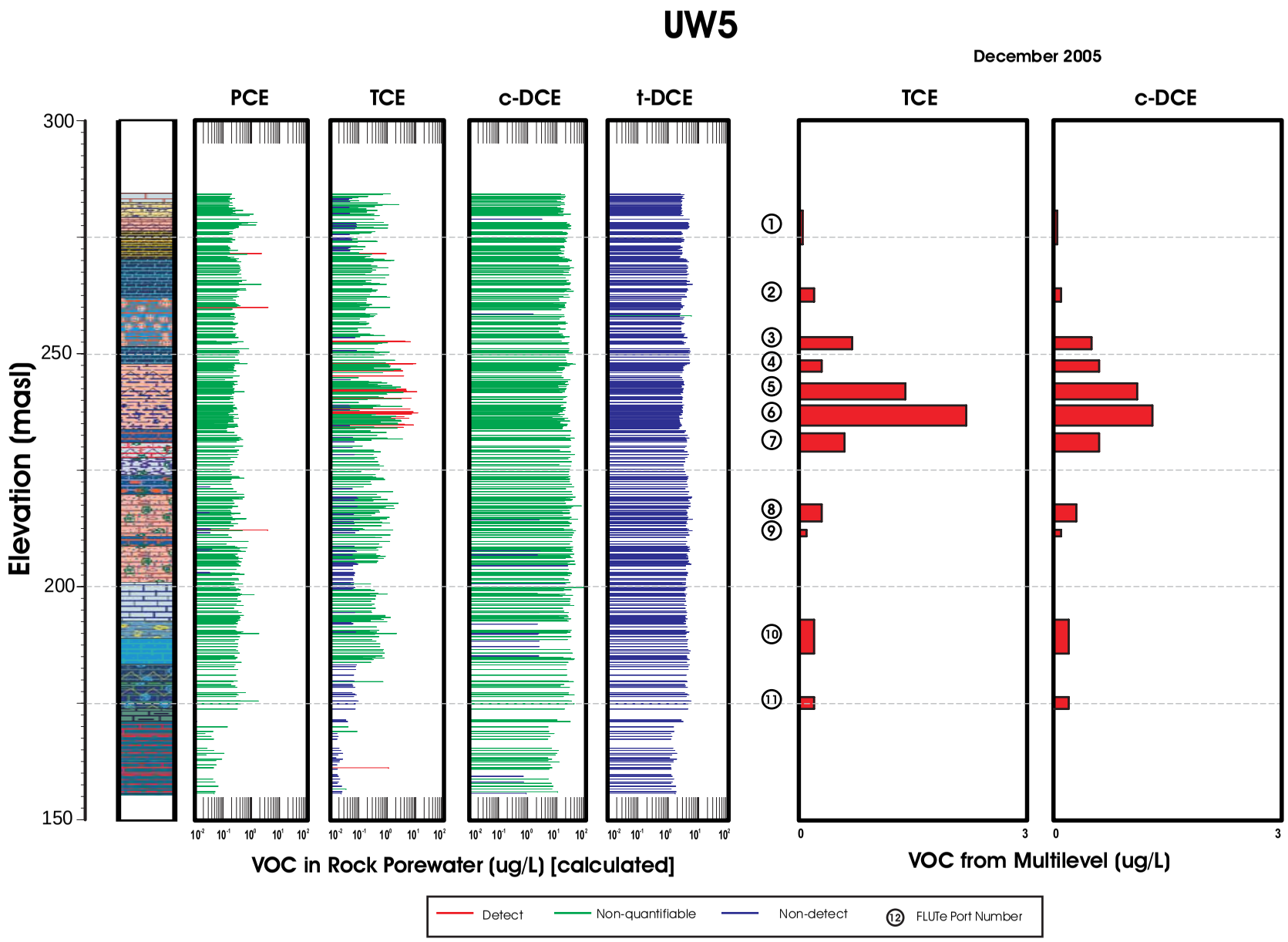


Figure 4.10: UW5 TCE degradation products in rock core and multilevel sampling results from December, 2005. c-DCE is the only degradation product detected in the multilevel in UW5, however both c-DCE and t-DCE were detected in the rock core.

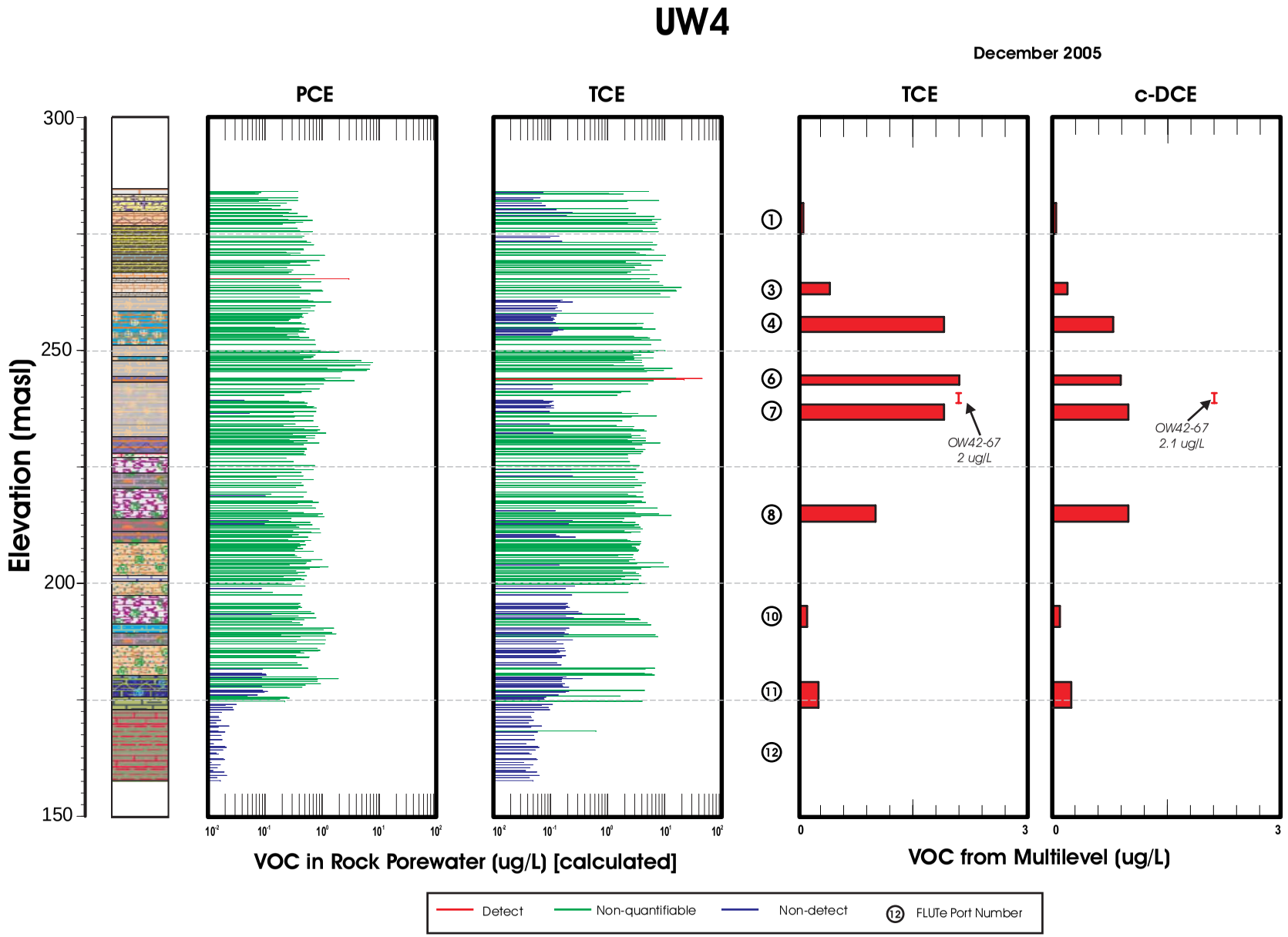


Figure 4.11: UW4 TCE degradation products in rock core and multilevel sampling results from December, 2005. c-DCE is the only degradation product detected in the multilevel in UW4. TCE degradation products were not analysed for in the rock core data. Sentry well OW42 shows similar concentrations of c-DCE to UW4.

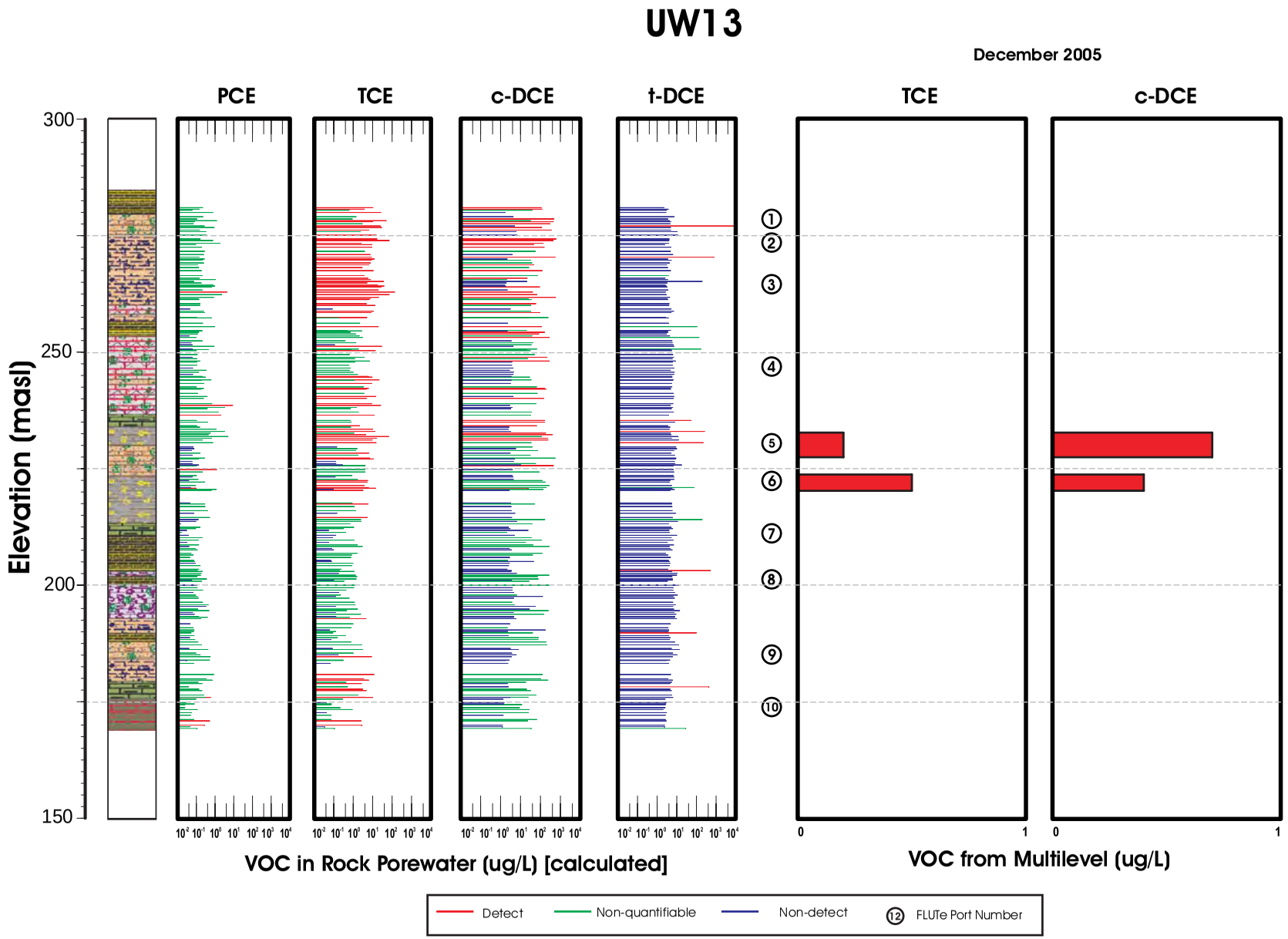


Figure 4.12: UW13 TCE degradation products in rock core and multilevel sampling results from December, 2005. c-DCE is the only degradation product detected in the multilevel in UW13, however both c-DCE and t-DCE were detected in rock core analyses; t-DCE has fewer detections but has much higher concentrations than c-DCE.

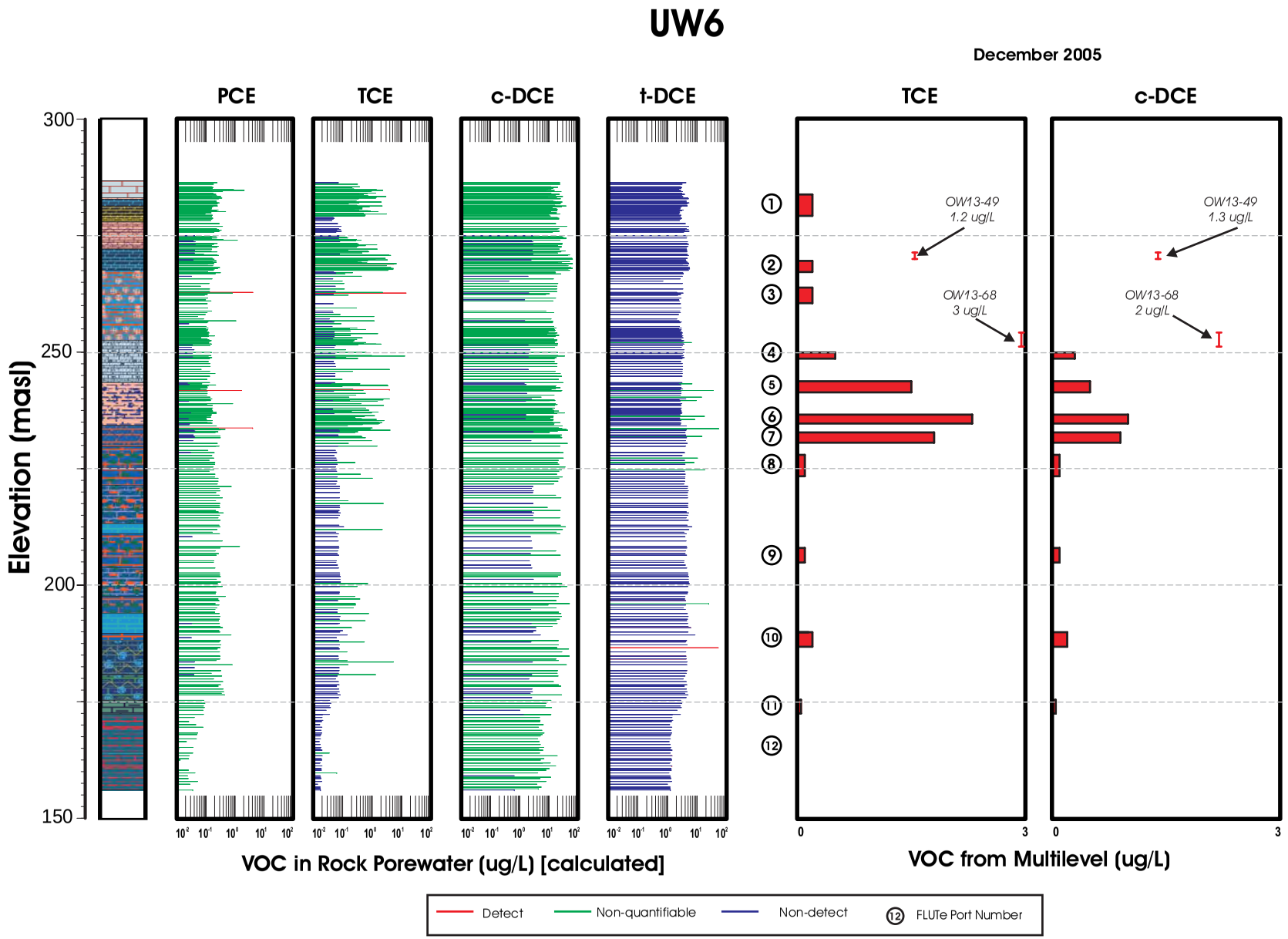


Figure 4.13: UW6 TCE degradation products in rock core and multilevel sampling results from December, 2005. c-DCE is the only degradation product detected in the multilevel in UW6, however both c-DCE and t-DCE were detected in rock core analyses. Sentry well OW13 concentration data is provided and show similar concentrations as UW6

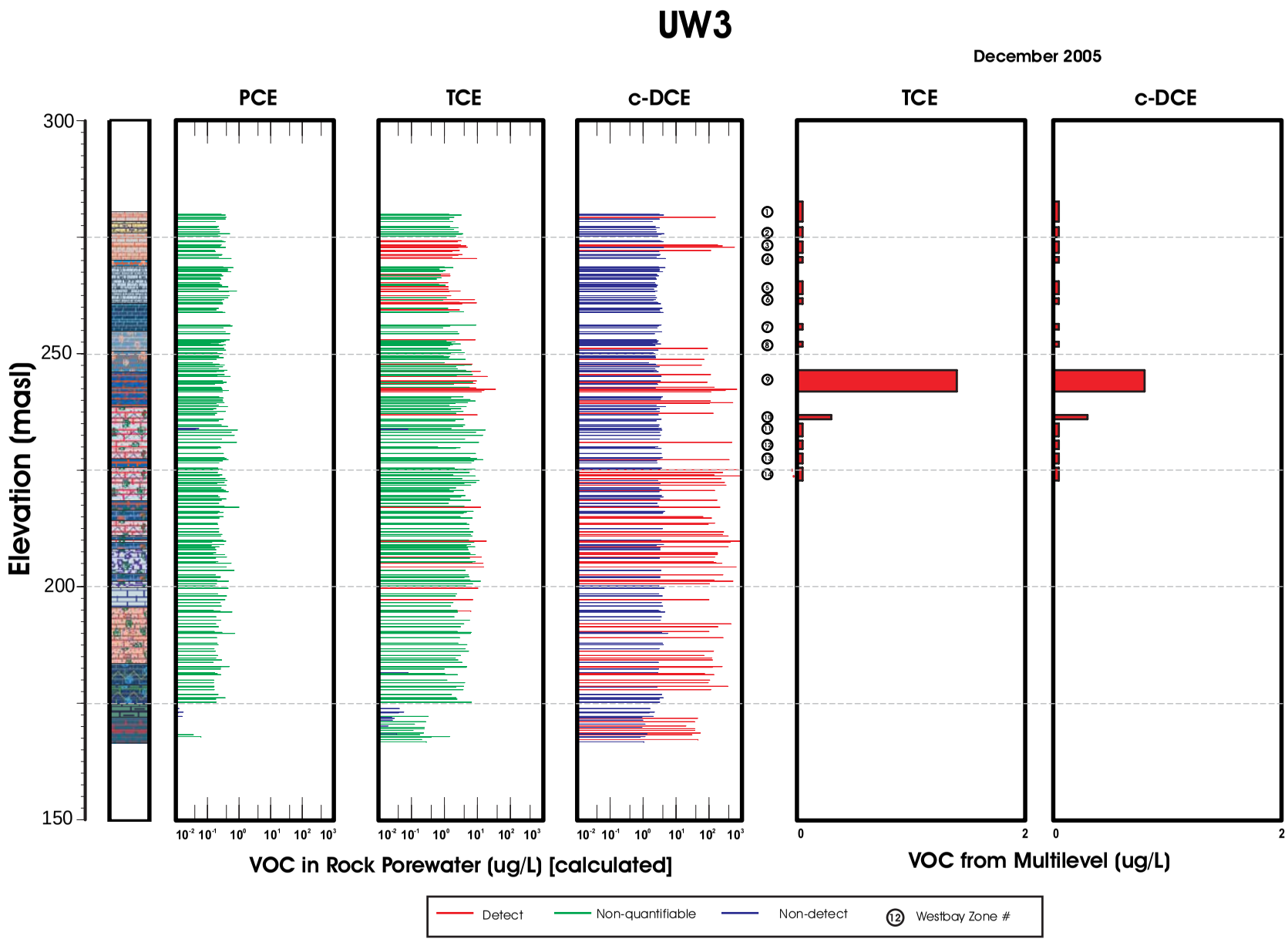


Figure 4.14: UW3 TCE degradation products in rock core and multilevel sampling results from December, 2005. c-DCE is the only degradation product detected in the multilevel in UW3. c-DCE was detected with very high concentrations in the rock core.

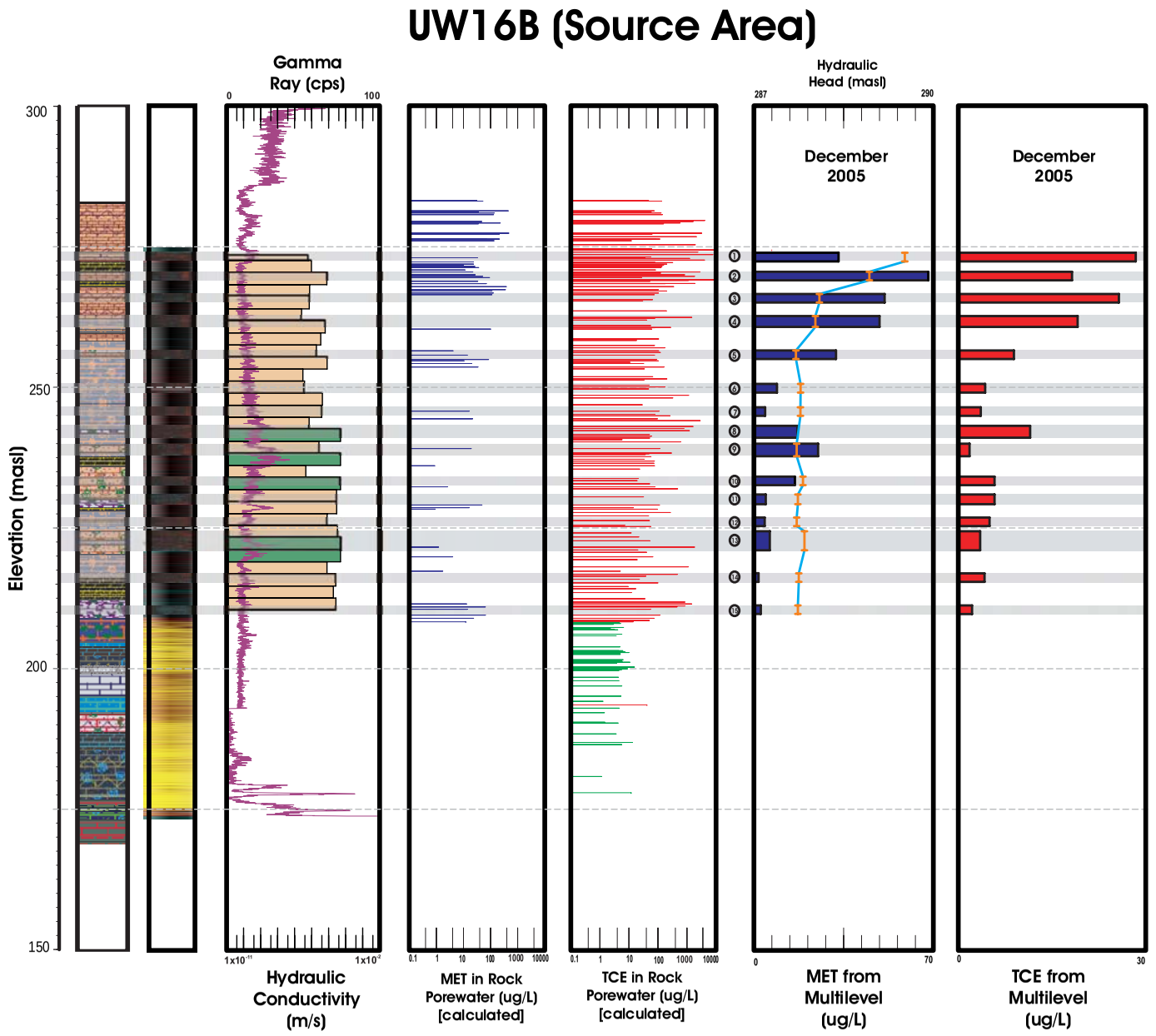


Figure 4.15: UW16B metolachlor and TCE concentrations obtained from both rock core and multilevel sampling. These data along with the vertical hydraulic head profile, hydraulic conductivity, gamma log, and corelog, provided detailed information on the nature of the dolostone aquifer and contaminant distribution at UW16B

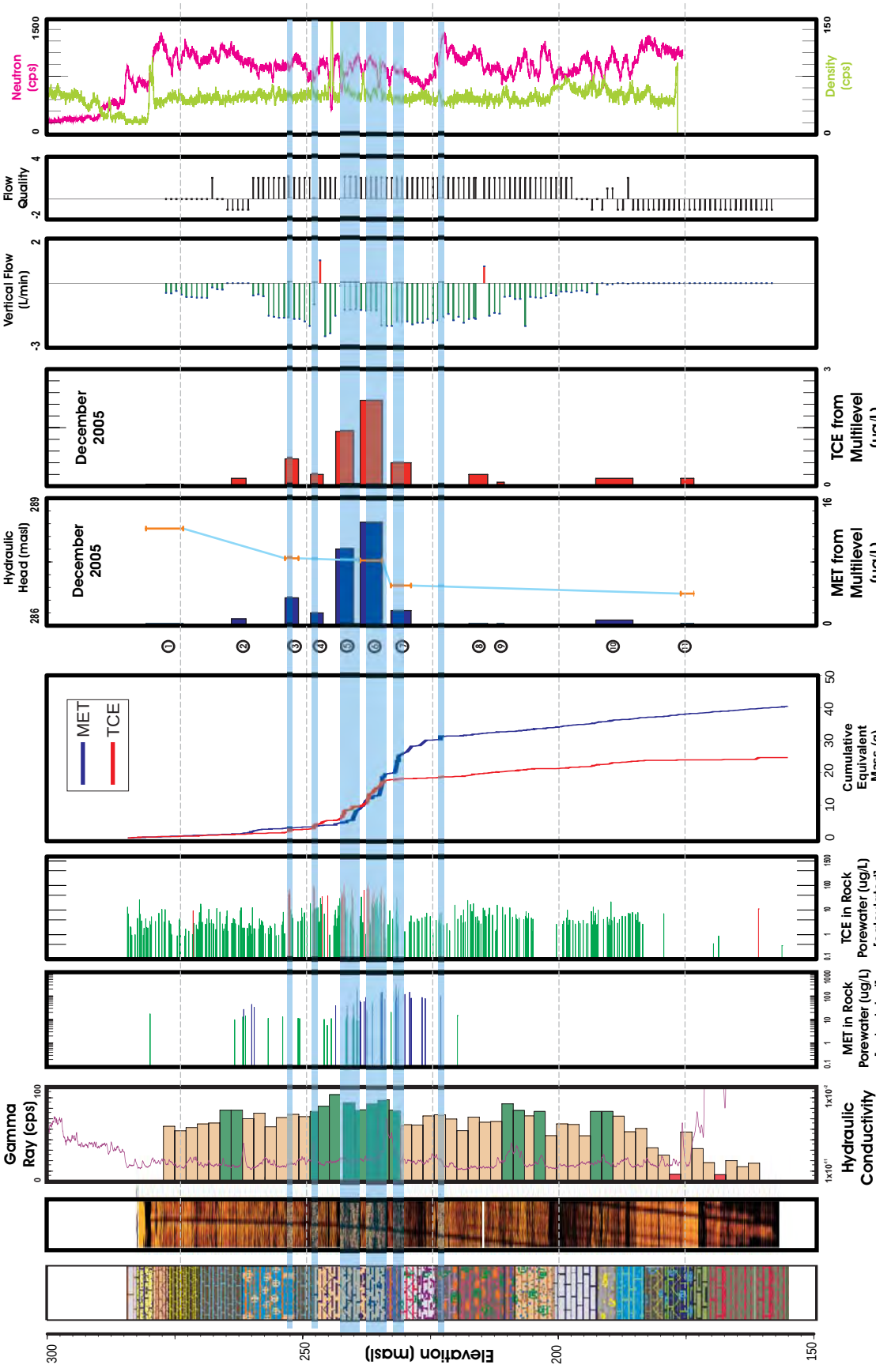


Figure 4.16: UW5 metolachlor and TCE concentrations obtained from both rock core and multilevel sampling. The cumulative equivalent metolachlor and TCE mass is also plotted to determine where the accumulation of contaminants with depth occurs. The highlighted areas indicate where contaminant mass accumulation most likely occurs. These data along with the vertical hydraulic head profile, hydraulic conductivity, gamma log, and corelog, provided detailed information on the nature of the dolostone aquifer and contaminant distribution at UW5

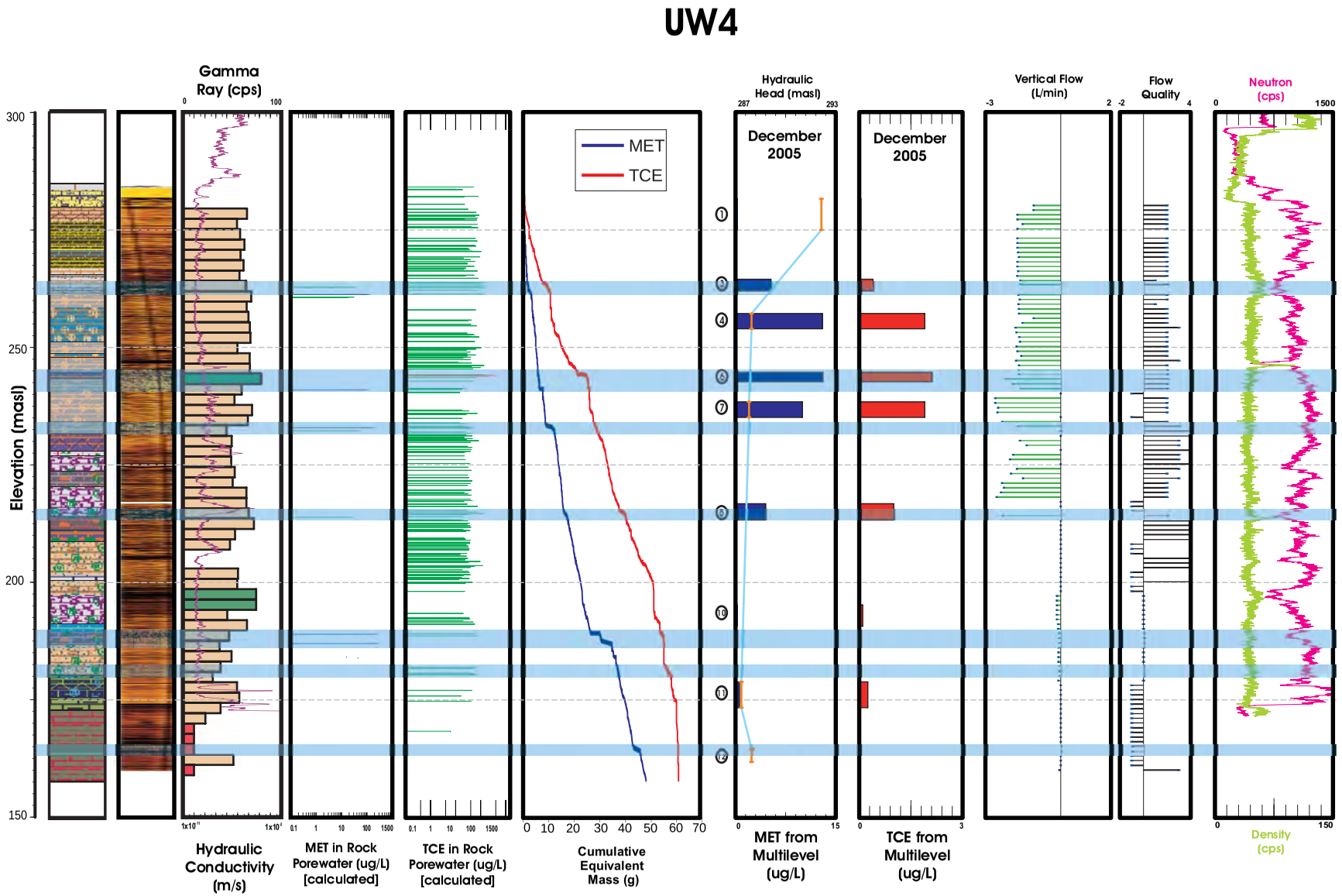


Figure 4.17: UW4 metolachlor and TCE concentrations obtained from both rock core and multilevel sampling. The cumulative equivalent metolachlor and TCE mass is also plotted to determine where the accumulation of contaminants with depth occurs. The highlighted areas indicate where contaminant mass accumulation most likely occurs. These data along with the vertical hydraulic head profile, hydraulic conductivity, gamma log, and corelog, provided detailed information on the nature of the dolostone aquifer and contaminant distribution at UW4

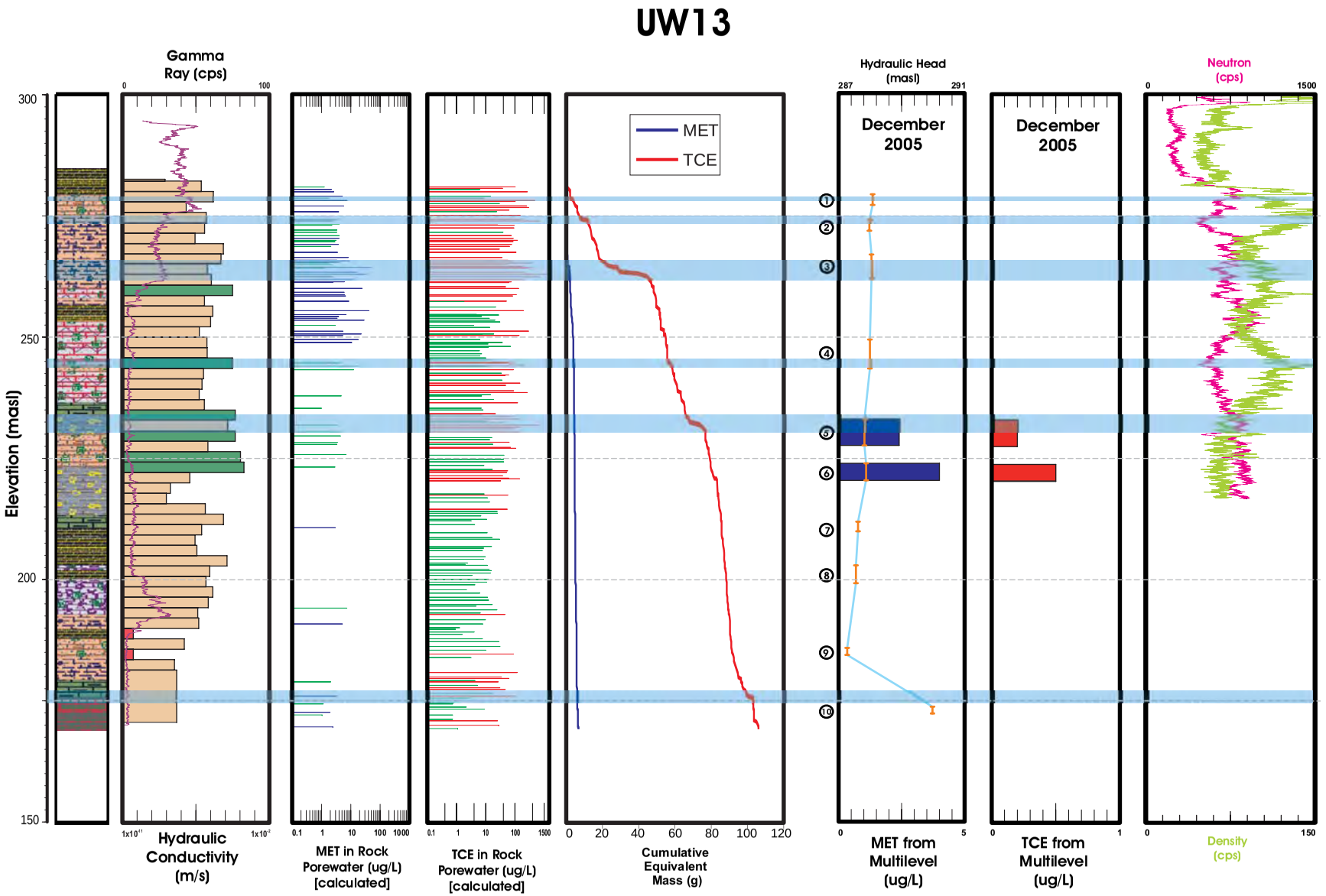


Figure 4.18: UW13 metolachlor and TCE concentrations obtained from both rock core and multilevel sampling. The cumulative equivalent metolachlor and TCE mass is also plotted to determine where the accumulation of contaminants with depth occurs. The highlighted areas indicate where contaminant mass accumulation most likely occurs. These data along with the vertical hydraulic head profile, hydraulic conductivity, gamma log, and corelog, provided detailed information on the nature of the dolostone aquifer and contaminant distribution at UW13

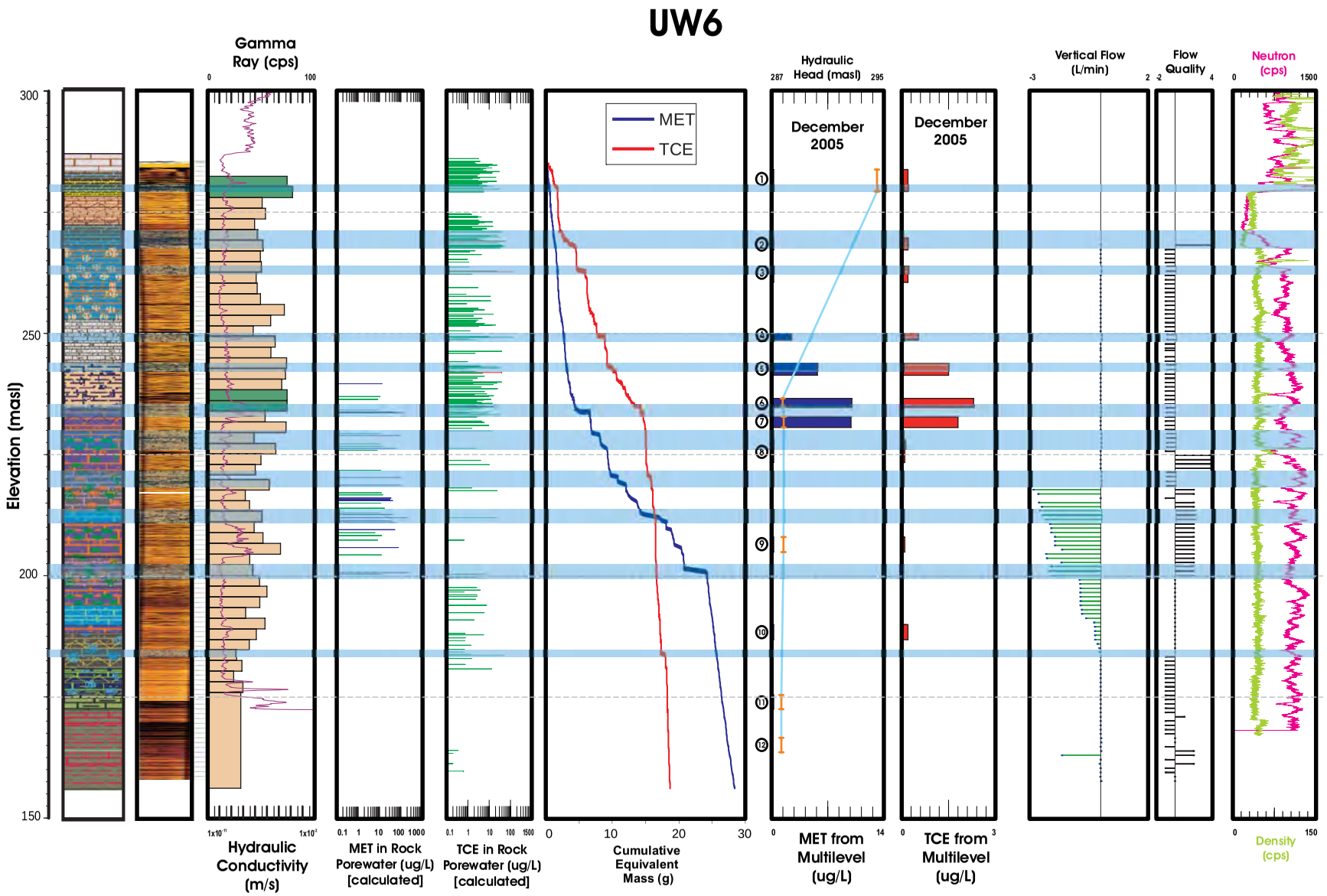


Figure 4.19: UW6 metolachlor and TCE concentrations obtained from both rock core and multilevel sampling. The cumulative equivalent metolachlor and TCE mass is also plotted to determine where the accumulation of contaminants with depth occurs. The highlighted areas indicate where contaminant mass accumulation most likely occurs. These data along with the vertical hydraulic head profile, hydraulic conductivity, gamma log, and corelog, provided detailed information on the nature of the dolostone aquifer and contaminant distribution at UW6

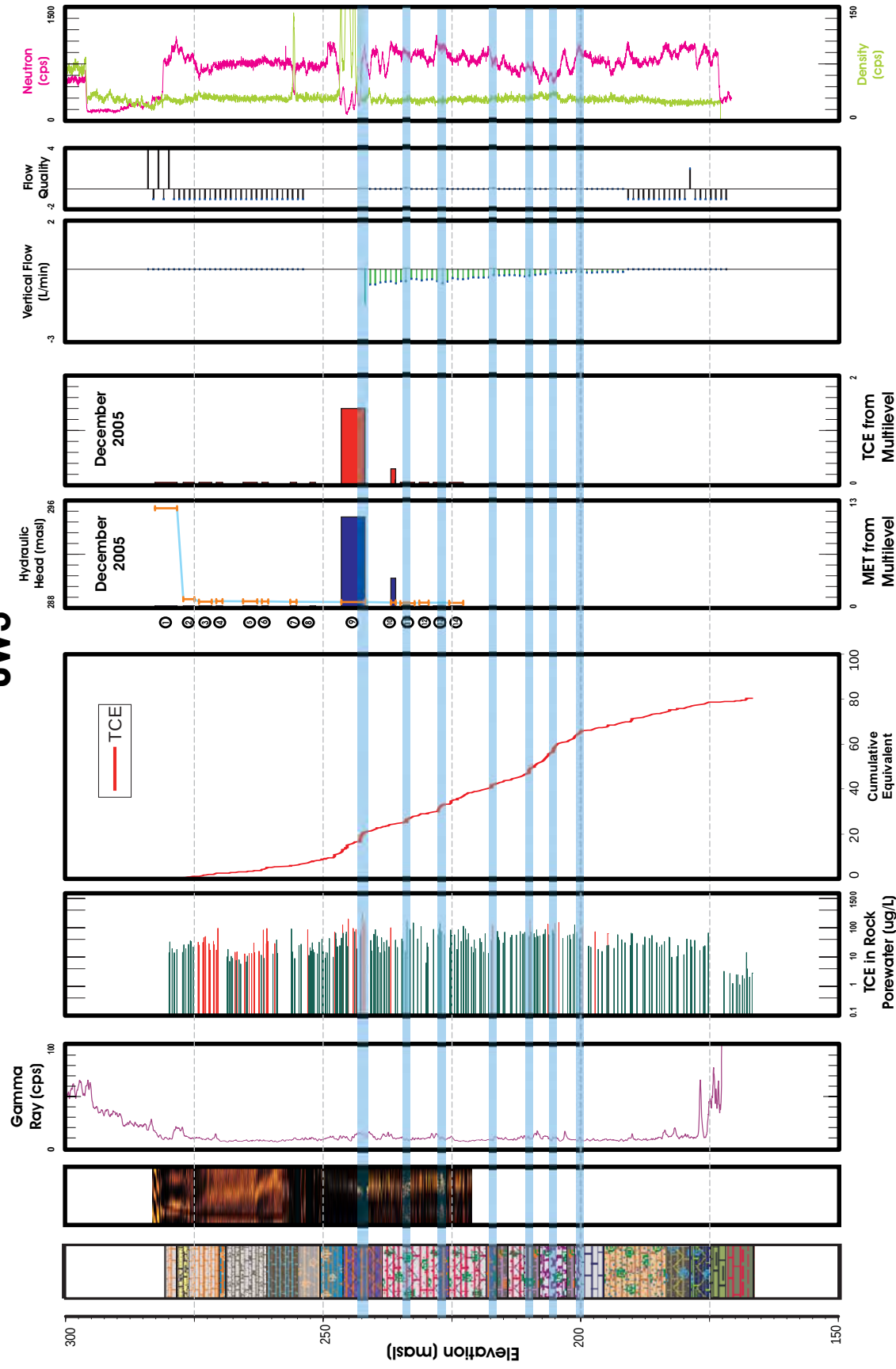


Figure 4.20: UW3 metolachlor and TCE concentrations obtained from multilevel sampling and TCE rock core concentrations. The cumulative equivalent metolachlor and TCE mass is also plotted to determine where the accumulation of contaminants with depth occurs. The highlighted areas indicate where contaminant mass accumulation most likely occurs. These data along with the vertical hydraulic head profile, gamma log, and corelog, provided detailed information on the nature of the dolostone aquifer and contaminant distribution at UW3

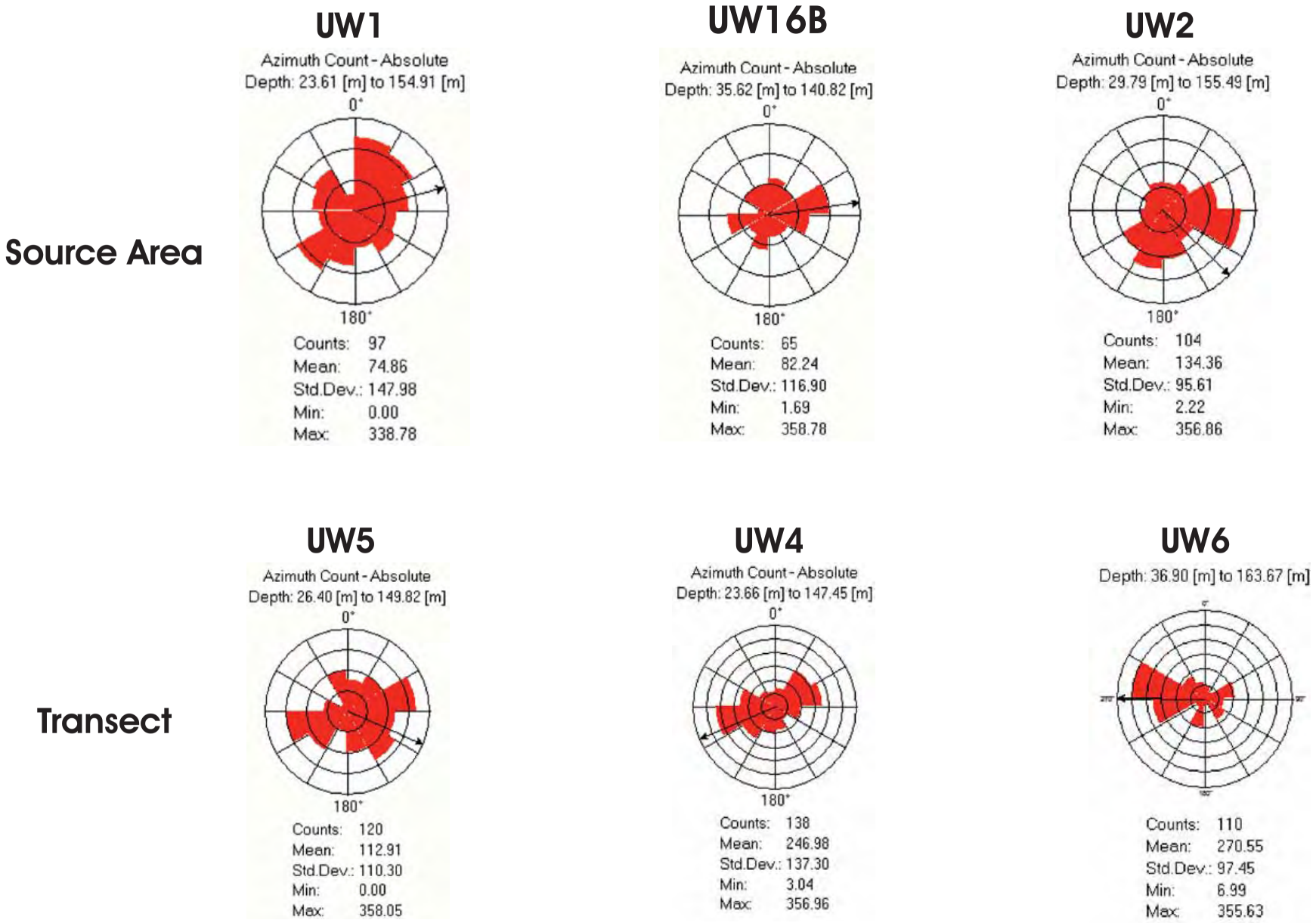


Figure 4.21: Fracture rose diagrams obtained from fracture analyses on acoustic televiewer logs showing the fracture direction. The majority of the fractures are aligned in an east-west orientation which is coincident with a westward hydraulic gradient. These data may suggest that a large scale anisotropy exists between the flow direction and the contaminant transport direction to the south towards municipal supply well G6. Source area data taken from Burns (2005).

Chapter 5

Conclusions

The detailed determination of the contaminant distributions from rock core and the multilevel systems show only low concentrations on the transect located 150 m downgradient from the metolachlor input area (i.e. source area) and approximately 300 m downgradient of the suspected TCE source area. This transect monitoring confirms that there is strong natural attenuation of metolachlor and TCE during groundwater transport southward towards municipal well G6 where metolachlor was first detected in 2001. The transect shows that the plume is very wide, even wider than the monitored portion of the transect. The transient nature of the hydraulic head distribution with time caused by variable pumping rates at the municipal well is likely a strong contributing factor to the large plume width. The concentration decline between the source area and the transect and then between the transect and municipal well G6 is greater for TCE than for metolachlor and this is likely due to TCE degradation. This conclusion is supported by the occurrence of degradation products typical of TCE microbial reductive degradation (cis-DCE and trans-DCE) which were found in the rock core.

The transient nature of the hydraulic head observed on the transect indicates that the fracture network has strong vertical connectivity in the dolostone aquifer. This strong vertical connectivity was also observed by Turner (2001) and Burns (2005) in the metolachlor input area. Straddle packer testing and FLUTe profiling indicates the shale beneath the dolostone has much lower hydraulic conductivity than the dolostone and at two of the three locations where multilevel monitoring extends into the shale, there is low vertical hydraulic connectivity between the shale and the overlying dolostone.

The Eramosa unit, described as Corelog Unit "J", has a characteristic gamma signature and this signature occurs in four of the five holes on the transect. Although the head profiles show a discontinuous zone of relatively low vertical hydraulic conductivity, the transient head monitoring at all locations shows strong vertical hydraulic connectivity across this zone. The gamma logs define the presence of the Eramosa Member, however, the core lithology and the hydraulic head profiles do not indicate occurrence of the Eramosa member as an influential zone of low vertical hydraulic conductivity in the study area, although it is considered an aquitard in areas of Cambridge-Guelph (Parker et al., 2006b).

The multilevel monitoring systems on the transect show the metolachlor plume positioned in the middle third of the dolostone aquifer and this also is the general position of the TCE plume but with more vertical spreading. In contrast, the zone of highest concentration upgradient in the metolachlor source zone is in the upper quarter of the dolostone. The vertical position on the transect of the metolachlor and TCE plumes coincides with a zone of relatively high hydraulic conductivity indicated by the straddle packer testing. This zone also includes abundant stylolites observed in core and where karst features are

observed using borehole TV and the acoustic televiewer. In the longitudinal perspective, the zone of highest metolachlor and TCE concentrations in the source area is likely continuous with the plume position in the middle of the dolostone on the transect and therefore the plume likely arrives at pumping well G6 as a thin zone with considerable well-bore dilution.

On the transect, the rock core metolachlor and TCE concentrations converted to groundwater concentrations are substantially higher than the groundwater concentrations obtained from the multilevel systems and this is also the situation in the source area indicated by Turner (2001) and Burns (2005). This relation between higher rock matrix concentrations and the lower groundwater concentrations in the hydraulically active fractures suggests that the plume persists because of back-diffusion from the rock matrix into the active groundwater flow system. Given that the plume is maintained by back diffusion decades after the DNAPLs entered the rock and that the transect everywhere shows only relatively low metolachlor and TCE concentrations in the groundwater, there is no reason to expect that there will be any substantial increases of metolachlor or TCE at municipal well G6 in the future.

One of the multilevel systems on the transect was sampled for inorganic constituents, tritium, oxygen-18 and deuterium. There is a zone of relatively low total dissolved solids, chloride and tritium that coincides with the metolachlor and TCE plume focused in the middle of the dolostone aquifer. The reason for this reverse relation between the organic contaminants and the inorganic species is not evident. Another outcome of the transect and other monitoring for which there is no clear explanation is the relation between the

hydraulic head distribution and the metolachlor and TCE plume. The hydraulic head distribution indicates gradients directed westward whereas the plume indicated on the transect and the metolachlor occurrence in municipal well G6 is directed southward. This inconsistency between plume orientation and hydraulic gradient directions may be caused by strong flow anisotropy which may be related to karst features.

References

Advanced Logic Technology (2002). *FAC40 Televiewer: Notes on use and operation*. Advanced Logic Technology.

Amirtharaj, S. (2003). Statistical synthesis of image analysis and mercury porosimetry for multiscale pore structure characteristics. Master's thesis, Department of Chemical Engineering, University of Waterloo, Waterloo, Ontario.

Back, W., Resenshein, J., and Seaber, P. (1988). *Hydrogeology: The Geology of North America*, volume 0-2. The Geological Society of America, Inc.

Bear, J., Tsang, C., and de Marsily, G. (1993). *Flow and contaminant transport in fractured rock*. Academic Press Inc.

Berkowitz, B. (2002). Characterizing flow and transport in fractured geologic media: a review. *Advances in Water Resources*, 25(8):861–884.

Bliss, J. and Rushton, K. (1984). The reliability of packer tests for estimating the hydraulic conductivity of aquifers. *Quarterly Journal of Engineering Geology*,

(17):88–91.

Burns, L. (2005). Fracture network characteristics and velocities of groundwater, heat and contaminants in a dolostone aquifer in Cambridge, Ontario. Master's thesis, Department of Earth Sciences, University of Waterloo.

Carter, R., Stiebel, W., Nalasco, P., and Pardieck, D. (1994). Investigation and remediation of pesticide contamination in a layered aquifer system. Edmonton, Alberta. International Association of Hydrogeologists XXVI Congress, Proceeding Solution '95.

Carter, R., Stiebel, W., Nalasco, P., and Pardieck, D. (1995). Investigation and remediation of groundwater contamination at a pesticide facility-a case study. *Water Quality Resources Journal Canada*, 30(3):469–491.

Chapelle, F. (2001). *Ground-Water Microbiology and Geochemistry*. John Wiley & Sons Inc., New York, USA.

Churcher, P. and Dickhout, R. (1987). Analysis of ancient sediments for total organic carbon-some new ideas. *Journal of Geochemical Exploration*, (29):235–246.

Clark, I. and Fritz, P. (1997). *Environmental Isotopes in Hydrogeology*. CRC Press LLC.

Coleman, M., Shepard, T., Durham, J., Rouse, J., and Moore, G. (1982). Reduction of water with zinc for hydrogen isotope analysis. *Analytical Chemistry*, 54:993–995.

Collins, R. (1961). *Flow of Fluids Through Porous Materials*. Reinhold Publishing, New York.

Craig, R. (1997). *Soil Mechanics*. E & FN Spon, 6th edition.

Dames and Moore (1993). Report on remedial investigation (period covered June 1991-July 1993) Ciba-Geigy Cambridge Plant. Technical report, Dames and Moore Canada.

Dames and Moore (1998). Reconnaissance TCE investigation 180 Sheldon Drive Cambridge, Ontario. Technical report, Dames and Moore Canada.

Drimmie, R. and Heemskerk, A. (1993). *Water ^{18}O by CO_2 Equilibration*. Environmental Isotope Laboratory, Department of Earth Sciences, University of Waterloo. Technical Procedure 13.0.

Drimmie, R., Heemskerk, A., and Johnson, J. (1991a). *Tritium Analysis*. Environmental Isotope Laboratory, Department of Earth Sciences, University of Waterloo. Technical Procedure 1, Revision 3.

Drimmie, R., Heemskerk, A., Mark, W., and Weber, R. (1991b). *Deuterium by Zinc Reduction*. Environmental Isotope Laboratory, Department of Earth Sciences, University of Waterloo. Technical Procedure 4.0.

Dullien, F. (1992). *Porous Media Fluid Transport and Pore Structure*. Academic Press, Inc., 2nd edition.

Einarson, M. and MacKay, D. (2001). Predicting the impacts of groundwater contamination. *Environmental Science and Technology*, 35(3):66A–73A.

Golder Associates (1991). Cambridge groundwater study, report no. 891-1582. Technical report, Golder Associates Ltd.

Gorecka, M. (2003). Report of VOC concentrations. Internal document, Department of Earth Sciences, University of Waterloo.

Gorecka, M., Gorecki, T., and Parker, B. (2001). Automated cool on-column injection for highly sensitive determination of chlorinated solvents in soils and rocks. In 24th International Symposium on Capillary Chromatography and Electrophoresis, Las Vegas, NV.

Greenhouse, J. and Pehme, P. (2002). Monitoring the temperature in a sleeved borehole: Implications for fracture detection. In Ground and Water: Theory to Practice, Proceedings of the 55th Canadian Geotechnical and 3rd Joint IAH-CNC and CGS Groundwater Specialty Conference, Niagara Falls, Ontario.

Guilbeault, M., Parker, B., and Cherry, J. (2005). Mass and flux distributions from DNAPL zones in sandy aquifers. *Ground Water*, 43(1):70–86.

Hadermann, J. and Heer, W. (1996). The Grimsel (Switzerland) migration experiment: integrating field experiments, laboratory investigations and modelling. *Journal of Contaminant Hydrology*, 21(1996):87–100.

Hurley, J. (2003). Rock core investigation of DNAPL penetration and persistance in fractured sandstone. Master's thesis, Department of Earth Sciences, University of Waterloo, Waterloo, Ontario.

Johnson, M., Armstrong, D., Sanford, B., Telford, P., and Rutka, M. (1992). *Geology of Ontario; Paleozoic and Mesozoic geology of Ontario.*, volume 4. Ontario Geological Survey.

Karrow, P. (1987). Surficial quaternary geology of the cambridge study area. Technical report, Ontario Geological Survey.

Kearey, P. and Brooks, M. (1991). *An Introduction to Geophysical Exploration*. Blackwell Science Ltd., 2nd edition.

Keller, C. (2005). FLUTe profiling results from Cambridge, Ontario. Personal Communication.

Keller, C., Cherry, J., and Parker, B. (2006). A new method for fracture identification and continuous hydraulic conductivity profiling in fractured rock boreholes. In Progress.

Langer, V., Novakowski, K., and Woodbury, A. (1999). Sorption of trichloroethene onto stylolites. *Journal of Contaminant Hydrology*, 40:1–23.

Langer, W. (1999). *Investigation of Trichloroethene TCE Transport in Fractured Porous Media with Emphasis on Sorption onto Stylolites and Matrix Diffusion*. PhD thesis, University of Manitoba. Dept. of Civil and Geological Engineering.

Lapcevic, P., Novakowski, K., and Sudicky, E. (1999a). *Handbook of Engineering*, chapter 17, Groundwater Flow and Solute Transport in Fractured Media, pages 17.1–17.39. CRC Press, Florida.

Lapcevic, P., Novakowski, K., and Sudicky, E. (1999b). The interpretation of a tracer experiment conducted in a single fracture under conditions of natural groundwater flow. *Water Resources Research*, 35(8):2301–2312.

LeBlanc, D., Garabedian, P., Hess, K., Gelhar, L., Quadri, R., Stollenwerk, K., and Wood, W. (1991). Large-scale natural gradient tracer test in sand and gravel, Cape Cod, Massachussetts. *Water Resources*, 27(5):895–910.

Lotowater Ltd. (1997). Study of the hydrogeology of the Cambridge area: Prepared for the Regional Municipality of Waterloo. Technical report, Lotowater Limited.

Mackay, D., Freyberg, D., Roberts, P., and Cherry, J. (1986). Natural gradient experiment on solute transport in a sand aquifer: 1. approach and overview of plume movement. *Water Resources Research*, 22(13):2017–2029.

McMaster, M. (1996). Fate and persistence of metolachlor and dinoseb in groundwater. Master's thesis, University of Waterloo.

Meyer, J. (2005). Migration of a mixed organic contaminant plume in a multilayer sedimentary rock aquifer system. Master's thesis, Department of Earth Sciences, University of Waterloo, Waterloo, Ontario.

MSI (2002). *HFP-2293 Heat Pulse Flow Meter*. Mount Sopris Instrument Co., Inc.

Najiya, H. (2003). Geological characterization of the middle Silurian dolomite aquifer in Cambridge, Ontario. Master's thesis, Department of Earth Sciences, University of Waterloo, Waterloo, Ontario.

National Research Council (2004). Contaminants in the subsurface: Source zone assessment and remediation. Technical report, National Academy Press, Washington DC.

Noble, W. (2004). Laboratory analysis for vinyl chloride and dichloroethene isomers. Technical report, Institute for Groundwater Research, University of Waterloo.

Olsen, R. and Davis, A. (1990). Predicting the fate and transport of organic compounds in groundwater. *Part 1: Hazardous Materials Control*, 3(3):38–64.

Pankow, J. and Cherry, J. (1996). *Dense Chlorinated Solvents and other DNAPLs in Groundwater*. Waterloo Press.

Parker, B. (2006). personal communication. Department of Earth Sciences, University of Waterloo, Waterloo, Ontario.

Parker, B., Cherry, J., and Swanson, B. (submitted 2006a). A multilevel system for high resolution monitoring in rotosonic boreholes. *Ground Water Monitoring and Remediation*. submitted March 10, 2006.

Parker, B., Turner, C., Burns, L., and Cherry, J. (submitted 2006b). DNAPL origin for deep metolachlor and TCE contamination in a dolostone aquifer. *Journal of Contaminant Hydrology*.

Perrin, J., Parker, B., and Cherry, J. (2006). Contaminated dolostone aquifers in southern Ontario: Are they fractured or karstic? page 6, Neuchatel, Switzerland. 8th Conference on Limestone Hydrogeology.

Pierce, A. (2005). Isotopic and hydrogeochemical investigation of major ion origin and trichloroethene degradation in fractured sandstone. Master's thesis, Department of Earth Sciences, University of Waterloo, Waterloo, Ontario.

Pierce, A., Parker, B., and Cherry, J. (in preparation 2006). Field evidence for trichloroethene degradation mechanisms in fractured sandstone. *Environmental Science and Technology*.

Plett, J. (2002). Comparison of depth-discrete hydraulic conductivity and hydraulic head measurement techniques in a fractured dolostone aquifer. Bachelor's Thesis, Department of Earth Sciences, University of Waterloo.

Sanford, P. (1969). Silurian of southwestern Ontario. page 44, Toronto. Ontario Petroleum Institute Inc., Eighth Annual Conference.

Schwarzenbach, R., Gschwend, P., and Imboden, D. (1993). *Environmental Organic Chemistry*. John Wiley & Sons, Inc.

Shurmer, B. (2005). Personal communication. Technical report, University of Guelph, Guelph, Ontario.

Snow, D. (1968). Rock fracture spacings, openings, and porosities. *Journal of the Soil Mechanics and Foundations Division*, Proceedings of the American Society of Civil Engineers(94):73–91.

Sterling, S. (1999). Comparison of discrete depth sampling using rock core and a removable multilevel system in a TCE-contaminated fractured sandstone. Master's thesis, Department of Earth Sciences, University of Waterloo.

Turner, C. (2001). Origin and behaviour of TCE and metolachlor contamination in a fractured dolostone water supply aquifer. Master's thesis, Department of Earth Sciences, University of Waterloo.

USEPA (1990). *Test Methods for evaluating solid waste, physical/chemical methods: method 8270B semivolatile compounds by Gas Chromatography/mass spectrometry, capillary column technique,Technical Report SW-846.*

USEPA (1991). *Method 0525.1 Organic compounds in drinking water by liquid-solid extraction and capillary column gas chromatography/mass spectrometry, Technical Report 821/R-93-010-B.*

USEPA (1996a). *Test Methods for evaluating solid waste, physical/chemical methods: method 3510C separatory funnel liquid-liquid extraction, Technical Report SW-846, Chapter 4.2.1.*

USEPA (1996b). *Test Methods for evaluating solid waste, physical/chemical methods: method 8260B volatile organic compounds by gas chromatography/mass spectrometry (GS/MS), Technical Report SW-846 Chapter 4.3.2.*

USEPA (1999). *USEPA Contract Laboratory Program: National Functional Guidelines for Organic Data Review, Method EPA540/R-99/008.*

USEPA (2003). *Method 0625 Acid and Base/neutrals including PCBs, 40 CFR Part 136, Appendix A*.

Vogel, T., Criddle, C., and McCarthy, P. (1987). Transformation of halogenated aliphatic compounds. *Environmental Science and Technology*, 23(8):722–736.

Westbay (2005). Completion report for MP38 monitoring well: UW3, Cambridge, Ontario. Technical report, Westbay Intruments Inc.

Wiedemeier, T., Rifai, H., Wilson, J., and Newell, C. (1999). *Natural Attenuation of Fuels and Chlorinated Solvents in the Subsurface*. John Wiley & Sons Inc.

Appendix A

Appendix A

Table A.1: UW5 Rockcore porewater and multilevel concentrations comparison

			TCE		Metolachlor	
UW5 Monitoring Zone	**Monitoring Zone Elevation (masl)**	**Rock Core Sample Elevation (masl)**	**Groundwater Concentrations (multilevel) ($\mu g/L$)**	**Rock Core Porewater Concentrations ($\mu g/L$)**	**Groundwater Concentrations (multilevel) ($\mu g/L$)**	**Rock Core Porewater Concentrations ($\mu g/L$)**
1	280.64-273.4	280.56	< 0.1	1.99	< 0.5	2.55
		280.41		1.85		2.70
		280.23		1.86		2.79
		280.03		0.48		2.80
		279.87		3.44		2.65
		279.72		2.50		2.48
		279.57		5.32		1.99
		278.81		3.42		4.60
		278.12		7.40		3.51
		277.94		0.77		2.71
		277.76		0.82		3.70
		277.56		10.71		3.87
		277.38		0.78		2.88
		277.23		0.83		1.55
		277.05		3.27		3.46
		276.90		10.39		17.43
		276.75		0.74		4.14
		276.14		3.67		2.62
		275.99		2.82		2.72
		275.83		2.64		2.79

Continued on next page

Table A.1 – continued from previous page

			TCE		Metolachlor	
UW5 Monitoring Zone	**Monitoring Zone Elevation (masl)**	**Rock Core Sample Elevation (masl)**	**Groundwater Concentrations (multilevel) ($\mu g/L$)**	**Rock Core Porewater Concentrations ($\mu g/L$)**	**Groundwater Concentrations (multilevel) ($\mu g/L$)**	**Rock Core Porewater Concentrations ($\mu g/L$)**
		275.68		1.03		2.12
		275.53		0.47		2.53
		274.79		0.53		2.88
		274.72		0.46		2.47
		274.56		0.89		1.80
		274.41		0.58		2.08
		274.16		3.89		2.96
		274.05		4.47		1.62
		273.90		0.92		3.14
		273.75				2.10
		263.92		2.87		3.92
		263.76		2.84		4.12
		263.61		4.54		3.40
		263.51		1.22		3.92
		263.36		4.05		4.31
2	264.00-261.15	263.21	0.2 - 0.51	2.73	0.85 - 2.1	4.02
		262.60		2.38		2.60
		262.24		9.42		4.51
		262.09		12.36		4.66
		261.94				2.95
		261.78		1.88		2.78
		261.63				26.87
		261.48		1.86		1.25
		253.42		0.73		3.40
		252.71		42.44		2.64
3	253.55-250.93	252.55	0.2 - 0.7	65.67	2.2 - 5.3	2.57
		252.34		10.36		3.16
		252.19		6.39		2.51
		252.04		4.60		3.00
		251.04		3.40		13.06
		248.04		8.69		11.33
		247.86		102.68		3.31
		247.73		78.70		10.95
		247.68		11.20		1.41
4	248.57-246.12	247.50	0.3 - 0.51	11.25	1.4 - 1.8	2.10
		247.39		12.98		2.19
		247.17		12.52		2.79

Continued on next page

Table A.1 – continued from previous page

			TCE		Metolachlor	
UW5 Monitoring Zone	**Monitoring Zone Elevation (masl)**	**Rock Core Sample Elevation (masl)**	**Groundwater Concentrations (multilevel) ($\mu g/L$)**	**Rock Core Porewater Concentrations ($\mu g/L$)**	**Groundwater Concentrations (multilevel) ($\mu g/L$)**	**Rock Core Porewater Concentrations ($\mu g/L$)**
		246.97		3.17		2.05
		246.78		3.37		2.69
		246.65		30.05		2.35
		246.46		16.54		2.50
		246.31		35.31		2.51
		243.54		2.14		2.60
		243.41		4.54		2.35
		243.26		3.45		2.43
		243.16		14.82		2.41
		242.96		5.78		10.15
		242.83		30.03		2.69
		242.50		20.71		2.71
		242.35		46.57		5.64
5	243.66-240.2	242.21	0.5 - 2.0	42.08	8.4 - 11	2.73
		242.03		47.85		2.18
		241.86		110.86		2.57
		241.71		36.77		2.80
		241.56		9.46		10.98
		241.28		9.83		39.51
		240.77		4.88		2.55
		240.64		7.26		2.16
		240.47		68.97		2.67
		240.30		30.61		2.65
		238.84		4.00		53.04
		238.69		33.58		2.62
		238.56		0.50		11.39
		238.41		3.11		12.63
		238.16		63.96		57.74
		237.98		0.48		2.66
		237.82		1.03		86.42
		237.55		82.25		24.80
		237.37		52.59		11.75
		237.34				2.28
		237.29		120.48		
6	238.91-234.57	237.09	0.7 - 2.3	72.84	9.5 - 15	12.58
		236.96		3.90		
		236.81		2.75		2.47

Continued on next page

Table A.1 – continued from previous page

			TCE		Metolachlor	
UW5 Monitoring Zone	**Monitoring Zone Elevation (masl)**	**Rock Core Sample Elevation (masl)**	**Groundwater Concentrations (multilevel) ($\mu g/L$)**	**Rock Core Porewater Concentrations ($\mu g/L$)**	**Groundwater Concentrations (multilevel) ($\mu g/L$)**	**Rock Core Porewater Concentrations ($\mu g/L$)**
		236.58		20.23		8.87
		236.48		39.02		52.70
		236.28		13.40		8.76
		236.15		58.15		3.03
		235.89		19.00		2.47
		235.74		29.70		3.08
		235.59		31.23		2.63
		235.39		5.74		2.91
		235.13		23.10		2.87
		234.88		40.71		144.54
		234.73		83.74		155.45
		234.57		0.48		158.27
		232.51		4.37		3.99
		232.06		0.61		67.02
		231.91		9.89		318.25
		231.73		34.67		89.35
7	232.92-229	231.59	0.2 - 0.6	2.68	1.9 - 6.0	3.53
		231.42		2.75		192.15
		231.12		0.69		
		230.20		1.33		117.18
		229.90		0.59		20.32
		229.29		3.37		144.92
		217.40		16.56		3.42
		217.30		0.87		3.55
		217.12		8.75		2.41
		216.97		7.32		14.74
		216.84		18.14		2.81
		216.41		5.09		2.37
		216.08		5.41		2.66
8	217.73-214.06	215.92	0.1 - 0.5	2.75	$<$ 0.5 - 1.7	3.42
		215.77		3.69		2.63
		215.67		0.67		3.57
		215.52		0.63		3.42
		215.37		2.71		3.10
		214.93		11.92		4.14
		214.65		9.71		3.28
		214.53		1.04		3.24

Continued on next page

Table A.1 – continued from previous page

			TCE		Metolachlor	
UW5 Monitoring Zone	**Monitoring Zone Elevation (masl)**	**Rock Core Sample Elevation (masl)**	**Groundwater Concentrations (multilevel) ($\mu g/L$)**	**Rock Core Porewater Concentrations ($\mu g/L$)**	**Groundwater Concentrations (multilevel) ($\mu g/L$)**	**Rock Core Porewater Concentrations ($\mu g/L$)**
		214.53		1.04		2.72
		214.37		5.49		3.39
		214.07		0.64		2.60
		212.22		15.80		1.52
9	212.24-210.86	212.06	$<$ 0.1 - 0.5	1.00	$<$ 0.5 - 0.8	2.66
		211.63		0.74		2.17
		211.15		12.82		3.41
		192.88		2.52		4.12
		192.70		2.57		3.86
		192.55		9.84		3.45
		192.37		0.53		3.40
		192.17		0.63		3.48
		192.04		0.60		2.75
		191.48		4.20		3.28
		190.75		5.16		3.48
		190.52		2.36		3.39
10	193.00-185.76	190.42	0.2 - 0.5	3.26	0.67 - 1.7	3.59
		190.37		4.22		3.47
		190.37		0.79		4.07
		190.19		2.36		3.46
		190.04		21.42		3.87
		189.88		3.69		3.82
		189.37		5.07		3.91
		188.74		2.91		3.71
		188.41		4.07		4.25
		187.85		5.61		4.44
		187.24		5.51		3.66
		186.63		7.39		4.38
		186.33		7.09		3.27
		185.84		8.02		3.37
		175.93		0.83		4.48
11	176.44-173.9	175.60	0.2 - 0.5	0.96	$<$ 0.5	4.07
		175.02		0.77		4.38
		174.56		0.74		4.05
		165.87				0.96
		165.45		0.20		0.99
		164.98		0.23		0.74

Continued on next page

Table A.1 – continued from previous page

			TCE		Metolachlor	
UW5 Monitoring Zone	**Monitoring Zone Elevation (masl)**	**Rock Core Sample Elevation (masl)**	**Groundwater Concentrations (multilevel)** ($\mu g/L$)	**Rock Core Porewater Concentrations** ($\mu g/L$)	**Groundwater Concentrations (multilevel)** ($\mu g/L$)	**Rock Core Porewater Concentrations** ($\mu g/L$)
12	166.21-160.92	164.37	NA	0.27	NA	0.59
		164.04		0.19		0.76
		163.43		0.16		0.84
		163.13		0.27		
		162.82		0.21		0.68
		162.52		0.20		0.68
		161.91		0.17		0.80
		161.30		11.14		0.67
		161.00		0.18		0.55

Table A.2: UW4 Rockcore porewater and multilevel concentrations comparison

			TCE		Metolachlor	
UW4 Monitoring Zone	**Monitoring Zone Elevation (masl)**	**Rock Core Sample Elevation (masl)**	**Groundwater Concentrations (multilevel) ($\mu g/L$)**	**Rock Core Porewater Concentrations ($\mu g/L$)**	**Groundwater Concentrations (multilevel) ($\mu g/L$)**	**Rock Core Porewater Concentrations ($\mu g/L$)**
1	281.56-274.96	281.54	< 0.1 - 0.5	0.70	< 0.5	5.07
		281.01		0.81		4.18
		280.40		22.82		3.85
		280.17		1.27		
		279.58		2.40		6.48
		279.35		31.21		4.26
		278.92		1.91		6.86
		278.68		65.46		13.23
		278.08		85.64		9.21
		277.84		59.43		12.84
		277.44		73.22		5.36
		277.27		22.28		5.90
		277.06		68.76		6.31
		276.15		74.14		10.20
		275.67		40.67		8.72
		275.42				4.93
2	270.50-267.43	270.45	NA	46.54	NA	9.58
		270.38		103.51		4.84
		269.22		92.32		3.94
		268.94		20.59		6.77
		268.64		38.52		4.13
		268.24		58.41		2.24
		267.89		28.69		7.20
		267.72		29.80		7.54
3	264.48-262.03	263.94	0.4 - 2.2	92.87	0.87 - 5.3	8.53
		263.48		197.02		10.82
		263.39		107.66		14.11
		262.93		156.55		17.76
		262.72		162.19		36.67
		262.12		82.95		10.22
4	257.18-	257.12	0.5 - 2.2	1.00	13 - 17	7.04
		256.91		1.13		
		256.65		1.17		8.52
		256.42		1.10		8.42
		255.94		1.23		10.76
		255.78		42.30		8.46

Continued on next page

Table A.2 – continued from previous page

			TCE		Metolachlor	
UW4 Monitoring Zone	**Monitoring Zone Elevation (masl)**	**Rock Core Sample Elevation (masl)**	**Groundwater Concentrations (multilevel) ($\mu g/L$)**	**Rock Core Porewater Concentrations ($\mu g/L$)**	**Groundwater Concentrations (multilevel) ($\mu g/L$)**	**Rock Core Porewater Concentrations ($\mu g/L$)**
	253.95	255.68		31.82		11.09
		254.89		40.70		8.84
		254.78		1.37		11.13
		254.58		68.53		9.16
		254.41		1.68		10.54
		254.18		1.32		10.63
		253.95		1.10		
		248.16		29.01		2.86
		247.90		39.25		4.41
		247.77		18.32		
5	248.17-246.08	247.71	NA	19.80	NA	8.27
		247.40		39.56		2.95
		246.87		12.69		2.23
		246.68		42.92		10.29
		246.13		135.55		
		244.09		157.09		4.80
		243.97		452.56		13.32
6	244.64-242.67	243.76	0.75 - 2.6	219.28	12 - 21	12.70
		243.49		63.84		10.60
		242.80		50.65		11.74
		238.18		1.13		7.57
		237.97		1.01		
		237.88		0.82		7.15
7	238.41-235.12	237.66	0.75 - 2.4	1.13	10 - 17	12.54
		236.90		0.96		3.35
		236.68		17.79		3.67
		236.48		34.25		7.25
		235.96		72.39		8.09
		235.77		26.21		4.30
		216.68		28.87		
		216.21		74.50		10.75
		215.63		1.21		9.92
		215.22		30.53		9.01
8	216.77-213.30	214.97	0.3 - 1.0	79.14	3.3 - 5.0	15.23
		214.64		129.91		10.02
		214.36		37.83		57.42
		213.97		19.54		26.87

Continued on next page

Table A.2 – continued from previous page

			TCE		Metolachlor	
UW4 Monitoring Zone	**Monitoring Zone Elevation (masl)**	**Rock Core Sample Elevation (masl)**	**Groundwater Concentrations (multilevel) ($\mu g/L$)**	**Rock Core Porewater Concentrations ($\mu g/L$)**	**Groundwater Concentrations (multilevel) ($\mu g/L$)**	**Rock Core Porewater Concentrations ($\mu g/L$)**
		213.56		2.41		13.31
		213.34		17.91		9.64
		206.20		27.98		11.19
		205.96		15.23		11.95
		205.63		26.95		11.38
		205.15		30.18		13.28
		204.86		23.58		8.64
9	206.46-202.08	204.49	NA	95.47	NA	5.85
		204.25		32.32		10.83
		204.02		1.41		11.28
		203.60		118.36		11.85
		203.51		56.59		12.13
		203.22		38.44		13.70
		202.76		18.37		14.41
		202.44		31.17		15.54
		202.15		35.38		11.29
		195.18		2.01		14.94
		194.91		2.15		14.89
		194.66		1.83		8.18
		194.04		3.06		15.71
		193.63		3.54		8.69
10	195.25-190.73	193.46	0.1 - 0.5	20.01	$<$ 0.5 - 2.0	9.14
		193.07		1.85		11.13
		192.66		2.54		14.58
		192.50		34.99		16.36
		192.26		37.38		14.15
		191.90		19.85		9.50
		191.62		50.08		11.43
		191.18		57.52		14.15
		178.57		1.77		
		178.28		1.59		
		178.06		1.63		7.88
		177.82		2.09		13.92
		177.12		44.49		13.96
		176.90		2.08		12.80
11	178.91-173.42	176.73	0.25 - 1.1	1.81	0.56 - 2.1	10.10
		176.14		1.38		8.94

Continued on next page

Table A.2 – continued from previous page

			TCE		Metolachlor	
UW4 Monitoring Zone	**Monitoring Zone Elevation (masl)**	**Rock Core Sample Elevation (masl)**	**Groundwater Concentrations (multilevel)** ($\mu g/L$)	**Rock Core Porewater Concentrations** ($\mu g/L$)	**Groundwater Concentrations (multilevel)** ($\mu g/L$)	**Rock Core Porewater Concentrations** ($\mu g/L$)
		175.91		16.76		3.75
		175.67		0.83		5.39
		175.47		0.76		6.12
		175.19		0.77		4.06
		174.82		40.62		4.70
		174.13		1.08		3.72
		173.94		0.69		3.51
		173.43				4.46
		164.36		0.54		30.24
		163.70		0.42		2.62
12	164.65-161.88	163.49	< 0.1	0.46	< 0.5	2.30
		162.46		0.56		2.69
		162.30		0.59		2.53

Table A.3: UW13 Rockcore porewater and multilevel concentrations comparison

			TCE		Metolachlor	
UW13 Monitoring Zone	**Monitoring Zone Elevation (masl)**	**Rock Core Sample Elevation (masl)**	**Groundwater Concentrations (multilevel) ($\mu g/L$)**	**Rock Core Porewater Concentrations ($\mu g/L$)**	**Groundwater Concentrations (multilevel) ($\mu g/L$)**	**Rock Core Porewater Concentrations ($\mu g/L$)**
1	279.17-276.97	278.99	< 0.1	14.33	< 0.5	5.18
		278.53		9.09		1.87
		278.15		502.08		7.63
		277.92		102.15		0.30
		277.49		29.41		0.35
		277.00		250.50		5.75
2	273.87-271.67	273.32	< 0.1	25.86	< 0.5	4.12
		273.02		92.66		2.27
		272.46		92.44		0.31
		272.03				3.37
3	266.77-261.67	266.39	< 0.1	36.12	< 0.5	8.17
		265.83		57.65		3.38
		265.52		78.37		9.41
		265.22				4.19
		265.14		367.95		1.84
		264.81		52.05		2.24
		264.41		178.27		0.44
		264.15		384.92		51.34
		263.97		279.53		1.41
		263.29		197.00		16.97
		262.86		1354.04		34.56
		262.32		718.12		2.56
		261.71		202.40		13.31
4	249.27-243.37	248.89	< 0.1 - 3.2	36.95	< 0.5	10.72
		248.58		11.97		
		248.07		70.36		
		247.87		12.36		0.54
		247.18		6.11		0.39
		246.57		7.23		0.41
		246.12		6.36		
		245.71		10.06		0.48
		245.20		16.82		0.41
		244.77		60.35		0.57
		244.64		94.31		4.72

Continued on next page

Table A.3 – continued from previous page

			TCE		Metolachlor	
UW13 Monitoring Zone	**Monitoring Zone Elevation (masl)**	**Rock Core Sample Elevation (masl)**	**Groundwater Concentrations (multilevel) ($\mu g/L$)**	**Rock Core Porewater Concentrations ($\mu g/L$)**	**Groundwater Concentrations (multilevel) ($\mu g/L$)**	**Rock Core Porewater Concentrations ($\mu g/L$)**
		244.03		213.95		5.34
		243.96		11.29		18.66
		232.63		11.02		
		232.32		44.70		
		231.89		673.28		3.71
		231.54		156.25		0.68
5	232.77-227.47	231.18	0.1 - 0.5	94.92	2.4 - 5.6	0.57
		230.57		150.63		4.24
		229.66		1.44		4.41
		229.30		16.11		0.74
		228.90		13.64		0.50
		228.34		63.53		3.48
		227.93		17.48		3.35
		223.56		8.70		0.41
		223.26		1.20		2.90
		222.75		16.85		0.33
		222.47		55.98		
6	223.77-220.27	222.14	0.4 - 0.6	52.12	2.5 - 7.6	0.65
		221.43		37.68		0.41
		220.97		60.65		0.54
		220.82		144.94		1.18
		220.56		0.95		
		220.39		32.27		0.42
		211.37		4.18		0.42
7	211.77-209.77	210.76	$<$ 0.1 - 0.75	1.29	$<$ 0.5	3.00
		210.23		0.89		0.40
		202.61		1.76		0.54
		202.23		13.12		0.72
		201.92		15.56		0.51
8	202.77-199.17	201.41	$<$ 0.1 - 0.6	14.55	$<$ 0.5	0.43
		201.13		1.00		0.57
		200.93		3.42		0.28
		200.09		12.48		1.03
		199.53		10.86		0.64
		185.54		10.07		0.67
9	185.77-184.27	185.16	$<$ 0.1 - 0.6	1.70	$<$ 0.5	0.72
		184.75		89.10		0.62

Continued on next page

Table A.3 – continued from previous page

			TCE		Metolachlor	
UW13 Monitoring Zone	**Monitoring Zone Elevation (masl)**	**Rock Core Sample Elevation (masl)**	**Groundwater Concentrations (multilevel) ($\mu g/L$)**	**Rock Core Porewater Concentrations ($\mu g/L$)**	**Groundwater Concentrations (multilevel) ($\mu g/L$)**	**Rock Core Porewater Concentrations ($\mu g/L$)**
10	173.67- 172.27	173.42 172.76	< 0.1	8.99 0.42	< 0.5	0.14 1.96

Table A.4: UW6 Rockcore porewater and multilevel concentrations comparison

			TCE		Metolachlor	
UW6 Monitoring Zone	**Monitoring Zone Elevation (masl)**	**Rock Core Sample Elevation (masl)**	**Groundwater Concentrations (multilevel) ($\mu g/L$)**	**Rock Core Porewater Concentrations ($\mu g/L$)**	**Groundwater Concentrations (multilevel) ($\mu g/L$)**	**Rock Core Porewater Concentrations ($\mu g/L$)**
		283.71		5.07		2.13
		283.45		7.31		2.25
		283.30		29.55		2.25
		283.15		13.84		1.40
		283.00		13.30		3.37
		282.84		3.43		4.86
		282.41		2.86		3.84
		282.26		2.57		
		282.13		20.55		4.44
		281.96		3.58		3.78
		281.80		1.58		4.54
1	283.74-279.18	281.45	0.2 - 0.5	3.00	< 0.5	4.27
		281.29		22.06		4.11
		281.17		8.17		2.41
		280.91		4.57		2.36
		280.69		4.59		
		280.58		2.45		2.37
		280.41		3.49		3.04
		280.27		7.19		
		280.23		8.57		2.79
		280.10		16.01		3.15
		279.87		9.25		2.73
		279.82		10.73		3.01
		279.74		5.14		
		279.59		30.71		
		279.31		5.88		2.66
		269.38		3.05		4.86
		269.23		4.30		3.31
		269.07		6.73		3.51
		268.95		67.01		4.77
		268.82		55.24		3.98
2	269.53-267.16	268.52	0.2 - 0.5	31.12	< 0.5	
		268.08		42.93		4.32
		268.03		43.55		3.32
		267.93		52.38		3.75
		267.80		33.81		3.60

Continued on next page

Table A.4 – continued from previous page

			TCE		Metolachlor	
UW6 Monitoring Zone	**Monitoring Zone Elevation (masl)**	**Rock Core Sample Elevation (masl)**	**Groundwater Concentrations (multilevel) ($\mu g/L$)**	**Rock Core Porewater Concentrations ($\mu g/L$)**	**Groundwater Concentrations (multilevel) ($\mu g/L$)**	**Rock Core Porewater Concentrations ($\mu g/L$)**
		267.70		51.24		4.11
		267.52		34.36		3.12
		267.17		0.49		2.01
		263.51		1.14		2.95
		262.98		0.57		2.16
		262.80		22.72		1.62
		262.65		142.38		0.63
3	263.82-260.48	262.49	0.2 - 0.5	15.37	< 0.5	1.96
		262.34		0.48		1.36
		262.19		1.56		1.67
		261.58		9.89		2.23
		261.21		17.52		1.90
		260.96		12.03		2.25
		249.68		0.55		2.85
		249.26		9.71		2.87
4	249.90-248.60	249.13	0.5 - 1.2	129.23	2.4 - 4.6	3.36
		248.94		0.57		
		248.80		1.29		2.49
		248.65		3.27		3.65
		243.48		0.54		2.72
		243.35		0.41		1.90
		243.20		3.86		1.59
		243.05		3.77		2.05
		242.93		33.59		1.45
5	243.76-241.36	242.78	0.5 - 1.7	34.96	5.7 - 13	1.32
		242.63		0.96		1.85
		242.37		10.98		2.44
		242.09		2.23		1.27
		241.94		38.42		2.60
		241.79		4.96		1.55
		241.64		0.49		1.81
		236.58				1.98
		236.40		12.19		8.24
		236.25		5.50		
		236.07		2.56		2.04
6	236.59-234.68	235.87	0.75 - 2.3	2.66	10 - 17	1.43
		235.74		4.37		2.41

Continued on next page

Table A.4 – continued from previous page

			TCE		Metolachlor	
UW6 Monitoring Zone	**Monitoring Zone Elevation (masl)**	**Rock Core Sample Elevation (masl)**	**Groundwater Concentrations (multilevel) ($\mu g/L$)**	**Rock Core Porewater Concentrations ($\mu g/L$)**	**Groundwater Concentrations (multilevel) ($\mu g/L$)**	**Rock Core Porewater Concentrations ($\mu g/L$)**
		235.56		13.99		1.65
		235.44		3.45		2.15
		235.31		25.43		
		234.93		2.88		2.32
		234.88		21.50		1.89
		234.78		18.46		1.33
		232.79		2.66		
		232.23		0.70		2.94
		232.08				2.68
7	232.79-230.60	232.01	0.1 - 1.8	0.73	9.9 - 14	
		231.93		4.35		2.86
		231.78		4.66		4.09
		231.65		5.93		
		231.04		9.56		2.69
		227.84		0.52		
		227.31		0.60		12.04
		226.80		0.63		14.38
8	227.97-223.39	226.34	0.1 - 0.5	2.65	< 0.5	59.25
		225.98		0.65		7.88
		225.38		0.57		2.80
		224.77		0.60		3.02
		224.46		0.63		2.12
		223.85		4.01		3.60
		208.02		0.75		2.29
		207.41		0.68		8.15
9	208.05-204.93	207.41	0.1 - 0.5	0.68	< 0.5	2.73
		206.83		0.66		1.75
		206.50		0.73		74.60
		205.28		0.60		2.49
		204.97		0.59		3.17
		189.73				2.70
		189.42		1.42		3.61
10	189.99-186.90	188.82	0.2 - 0.5	0.62	< 0.5	2.20
		188.21		0.74		3.62
		187.90		5.47		3.23
		187.29		0.77		
		175.40		0.36		1.35

Continued on next page

Table A.4 – continued from previous page

			TCE		Metolachlor	
UW6 Monitoring Zone	**Monitoring Zone Elevation (masl)**	**Rock Core Sample Elevation (masl)**	**Groundwater Concentrations (multilevel) ($\mu g/L$)**	**Rock Core Porewater Concentrations ($\mu g/L$)**	**Groundwater Concentrations (multilevel) ($\mu g/L$)**	**Rock Core Porewater Concentrations ($\mu g/L$)**
11	175.53-172.57	174.78	$<$ 0.1 - 1.5	0.40	$<$ 0.5	1.02
		174.18		0.36		0.77
		173.88		0.38		1.34
		173.27		0.27		1.17
		172.40		0.36		1.15
12	166.70-163.70	166.56	$<$ 0.1	0.16	$<$ 0.5	0.71
		165.95		0.17		0.59
		165.34		0.18		0.63
		165.03		0.18		0.71
		164.73		0.20		0.62
		164.12		0.35		0.36

Table A.5: UW3 Rockcore porewater and multilevel concentrations comparison

			TCE		Metolachlor	
UW3 Monitoring Zone	**Monitoring Zone Elevation (masl)**	**Rock Core Sample Elevation (masl)**	**Groundwater Concentrations (multilevel) ($\mu g/L$)**	**Rock Core Porewater Concentrations ($\mu g/L$)**	**Groundwater Concentrations (multilevel) ($\mu g/L$)**	**Rock Core Porewater Concentrations ($\mu g/L$)**
1	283.74-279.18	279.83 279.69 279.22 278.84 278.31	< 0.1	13.84 32.50 19.38 13.93 18.02	< 0.5	
2	269.53-267.16	276.97 276.59 276.09 275.70 275.58 275.17	< 0.1	26.11 19.16 26.90 35.84 33.80 22.05	< 0.5	
3	263.82-260.48	274.03 273.98 273.27 273.09 272.81 272.76 272.08 271.89	< 0.1 - 0.1	24.72 25.15 30.95 45.35 49.71 25.63 28.51 16.92	< 0.5	
4	270.69-269.48	270.67 270.38	< 0.1 - 0.1	17.10 94.94	< 0.5	
5	265.51-262.75	265.19 264.83 264.66 264.32 263.83 263.41 263.25	< 0.1 - 0.1	12.70 6.74 10.73 13.01 13.11 30.08 13.87	< 0.5	
6	261.85-260.64	261.58 261.43 260.98 260.87 260.70	< 0.1 - 0.1	82.84 8.92 28.49 94.09 34.08	< 0.5	
7	256.36-	256.15 256.12	< 0.1	9.87 90.69	< 0.5	

Continued on next page

Table A.5 – continued from previous page

			TCE		Metolachlor	
UW3 Monitoring Zone	**Monitoring Zone Elevation (masl)**	**Rock Core Sample Elevation (masl)**	**Groundwater Concentrations (multilevel) ($\mu g/L$)**	**Rock Core Porewater Concentrations ($\mu g/L$)**	**Groundwater Concentrations (multilevel) ($\mu g/L$)**	**Rock Core Porewater Concentrations ($\mu g/L$)**
	255.15	255.94		14.71		
		255.51		8.88		
8	254.23-251.49	252.96	< 0.1	85.29	< 0.5	
		252.74		11.29		
		252.51		20.73		
		252.44		13.59		
		252.28		15.94		
		252.08		30.42		
		251.90		17.55		
		251.72		14.32		
9	250.57-239.30	250.22	< 0.1 - 1.5	40.28	2.6 - 12	
		249.99		15.41		
		249.56		9.15		
		249.41		14.26		
		249.13		13.60		
		248.79		42.80		
		248.04		9.90		
		247.74		69.93		
		247.56		65.26		
		247.52		40.09		
		247.21		22.40		
		246.75		24.40		
		246.44		44.30		
		246.21		122.98		
		246.13		64.69		
		245.57		59.30		
		245.50		70.92		
		245.24		22.91		
		245.10		198.32		
		244.17		94.38		
		243.87		72.56		
		243.62		87.18		
		243.43		18.77		
		242.80		56.95		
		242.66		90.28		
		242.37		352.67		
		242.12		159.50		

Continued on next page

Table A.5 – continued from previous page

			TCE		Metolachlor	
UW3 Monitoring Zone	**Monitoring Zone Elevation (masl)**	**Rock Core Sample Elevation (masl)**	**Groundwater Concentrations (multilevel) ($\mu g/L$)**	**Rock Core Porewater Concentrations ($\mu g/L$)**	**Groundwater Concentrations (multilevel) ($\mu g/L$)**	**Rock Core Porewater Concentrations ($\mu g/L$)**
		241.81		133.10		
		240.74		36.66		
		240.54		15.67		
		240.15		59.91		
		239.86		86.05		
		239.50		50.84		
		239.36		20.97		
		238.20		31.77		
		238.05		15.28		
10	238.38-235.95	237.65	0.1 - 0.3	36.97	0.57 - 3.6	
		237.24		22.32		
		236.90		99.30		
		235.96		37.63		
		234.72		41.25		
		234.41		35.96		
		233.96		16.00		
11	235.02-232.26	233.78	< 0.1	0.79	< 0.5	
		233.62		173.20		
		233.14		89.18		
		232.49		145.23		
		230.99		109.56		
12	231.36-229.55	230.02	< 0.1	6.22	< 0.5	
		229.85		30.23		
		229.69		21.77		
		228.60		87.96		
		227.71		59.60		
13	228.62-226.50	227.55	< 0.1	95.34	< 0.5	
		227.30		146.96		
		227.04		78.22		
		226.61		63.99		
		225.48		20.33		
		225.27		83.77		
		225.13		53.97		
14	225.57-223.75	225.08	< 0.1	54.86	< 0.5	
		224.54		57.02		
		224.04		18.14		
		223.81		84.69		